



Australian Government  
Bureau of Meteorology

The Centre for Australian Weather and Climate Research  
A partnership between CSIRO and the Bureau of Meteorology



# 'High resolution modelling': extended abstracts of the second CAWCR Modelling Workshop, 25-28 November 2008, Melbourne, Australia

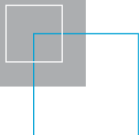
**CAWCR Technical Report No. 006**

A.J. Hollis (editor)

November 2008



[www.cawcr.gov.au](http://www.cawcr.gov.au)





ISSN: 1835-9884

ISBN: 978-1-921424-82-3

Series: Technical report (Centre for Australian Weather and Climate  
Research.) ; no. 6.

Enquiries should be addressed to:

Andrew Hollis  
Centre for Australian Weather and Climate Research:  
A Partnership between the Bureau of Meteorology and CSIRO  
GPO Box 1289  
Melbourne VIC 3001  
AUSTRALIA  
[a.hollis@bom.gov.au](mailto:a.hollis@bom.gov.au)  
Phone: 61 3 9669 4046  
Fax: 61 3 9669 4660

## Copyright and Disclaimer

© 2008 CSIRO and the Bureau of Meteorology. To the extent permitted by law, all rights are reserved and no part of this publication covered by copyright may be reproduced or copied in any form or by any means except with the written permission of CSIRO and the Bureau of Meteorology.

CSIRO and the Bureau of Meteorology advise that the information contained in this publication comprises general statements based on scientific research. The reader is advised and needs to be aware that such information may be incomplete or unable to be used in any specific situation. No reliance or actions must therefore be made on that information without seeking prior expert professional, scientific and technical advice. To the extent permitted by law, CSIRO and the Bureau of Meteorology (including each of its employees and consultants) excludes all liability to any person for any consequences, including but not limited to all losses, damages, costs, expenses and any other compensation, arising directly or indirectly from using this publication (in part or in whole) and any information or material contained in it.

# CONTENTS

---

<b>Foreword</b>	v
<b>Kevin Horsburgh</b>	
Current developments in operational storm surge modelling	1
<b>Siobhan O’Farrell</b>	
Regional sea level rise around the Australian coastline	5
<b>James Chittleborough</b>	
Tide models used at the National Tidal Centre	9
<b>John F. Middleton</b>	
Regional models for upwelling and shelf circulation: the importance of the backward boundary condition	13
<b>J. O’Callaghan, G. Rickard and S. Popinet</b>	
Adaptive, non-hydrostatic multi-scale modelling: application to coastal scale processes	15
<b>Marcus Thatcher, Debbie Abbs and John McGregor</b>	
Issues in regional climate modeling and future directions	19
<b>Frank Drost, Brett Mullan, Balakrishnan Bhaskaran, Jim Renwick and Sam Dean</b>	
On the effect of the domain size of New Zealand’s regional climate model on the modelled climatology	21
<b>Sam Dean, James Renwick and Brett Mullan</b>	
Regional climate modelling in New Zealand using the Unified Model	25
<b>John L. McGregor, Kim C. Nguyen and Jack J. Katzfey</b>	
A variety of tropical climate simulations using CCAM	29
<b>Debbie Abbs and Tony Rafter</b>	
Climate change and its impact on extreme rainfall in SE Australia	33
<b>Kim C. Nguyen and John L. McGregor</b>	
Simulation of rainfall and pan evaporation over Australia	37
<b>Carlos E.P. Teixeira and John F.F. Middleton</b>	
The effects of tides and wind forcing on the circulation within the Spencer Gulf	41
<b>Matthew Collopy</b>	
High resolution modelling of swell propagation in the near shore environment	43
<b>Chris Tingwell</b>	
Australian mesoscale data assimilation and numerical weather prediction in ACCESS	49
<b>Mohar Chattopadhyay, Peter Steinle, Yi Xiao, John Le Marshall, Tan Le and Chris Tingwell</b>	
Impact of using 4D-VAR assimilation of SSM/I data in the ACCESS modelling framework	53
<b>Holly Sims</b>	
Impact of remotely sensed wind data assimilation within a 4D-Var NWP system	57
<b>Elizabeth E. Ebert</b>	
Assessing the quality of high resolution precipitation forecasts using fuzzy (neighbourhood) verification	61
<b>Daisuke Miura</b>	
Operational mesoscale prediction model at JMA and its land surface process	67
<b>Vaughan J. I. Barras, Peter J. Hurley and Ashok K. Luhar</b>	
Modelling the atmospheric boundary layer in ACCESS: testing an alternate surface scaling	71
<b>Hongyan Zhu, Harry Hendon and Christian Jakob</b>	
MJO and convection behaviour in SP-CAM and CAM simulation.	75

<b>Isaac Ginis</b>	
New strategies for comprehensive coupled atmosphere-wave-ocean modeling in tropical cyclones	77
<b>Paul Sandery</b>	
Evaluation of a regional ocean-atmosphere coupled weather prediction system	85
<b>Kevin Walsh, Paul Sandery and Gary Brassington</b>	
Effects of air/sea interaction representations on ocean behaviour during tropical cyclones	87
<b>Alexander V. Babanin, Andrey Ganopolski and William R.C. Phillips</b>	
Wave-induced upper-ocean mixing and climate modeling	89
<b>Eric Schulz and Malek Ghantous</b>	
Two-way wind-wave coupling under tropical cyclone conditions	93
<b>Liu Chunxia, Yiquan Qi and Jianying Liang</b>	
The effect of sea waves on Typhoon <i>Imodu</i>	95
<b>Roger K. Smith</b>	
Axisymmetric dynamics of tropical-cyclone intensification	99
<b>Noel Davidson, Yimin Ma, Chi Mai Nguyen, Harry Weber, Yi Xiao and Marie-Dominique Leroux</b>	
Experiments with initialization and prediction of Tropical Cyclone structure and intensity	103
<b>Kathrin Wapler, Todd Lane, Peter May, Christian Jakob, Michael Manton and Steve Siems</b>	
The performance of nested cloud-scale simulations during TWP-ICE	109
<b>Michael J. Reeder and Philip Cunningham</b>	
Modelling pyro-cumulonimbi and tornadoes spawned by bushfires	113
<b>Kevin Cheung</b>	
Self-similarity in moisture processes and NWP models	117
<b>Jack Katzfey, John McGregor and Marcus Thatcher</b>	
Ensemble one kilometer resolution numerical weather forecasts for the America's Cup	119
<b>W.C. Arthur, R.P. Cechet and C. Thomas</b>	
High-resolution modelling for impact forecasting	123
<b>Jeff Kepert</b>	
Verification of high resolution NWP for wind energy prediction	127
<b>L.A. Sanabria &amp; R.P. Cechet</b>	
Assessing wind hazard in Australia's 'Region A' using a high resolution GCM approach	129
<b>R. Potts, Y. Miao, J. Bronsvort and G. McDonald</b>	
High resolution modelling for the aviation weather service	135
<b>John Nairn</b>	
Modelling priorities in South Australia	141
<b>B. Modra, S. Hesse, Peter Davidson and Edward Couriel</b>	
NSW tidal anomaly – a tidal epoch review	145

## FOREWORD

---

The scientific challenges that face Australia in the fields of weather and climate are significant and require the focused mobilisation of national-level resources. An important first step in this direction was the creation of the Australian Community Climate and Earth System Simulator (ACCESS) initiative. This process was accelerated further in 2007 when the Bureau of Meteorology and CSIRO jointly established the Centre for Australian Weather and Climate Research (CAWCR). This year's workshop '*High Resolution Modelling*' is the second Modelling Workshop under the auspices of the new Centre.

CAWCR has a very large breadth of responsibility and, whilst keeping true to its title, this year's workshop also acknowledges that "high resolution" means different things to different scientists. We have introduced a number of workshop themes to capture these different interests.

Numerical Weather Prediction, the topic of our first theme, deals with a number of difficult issues emerging as model resolutions move down towards the single kilometre range, including: assimilation of new types and volumes of data; design of scale-appropriate parameterisations (or indeed the move to resolving schemes); and predictability, representation and validation issues as we begin to resolve structures such as individual storms.

In the Coupled Weather Modelling theme we see how increases in computational power are enabling us to begin to unravel the dynamic interactions between the atmosphere and ocean; interactions that play a potentially important role in the nature of systems such as Tropical Cyclones.

Climate Modelling is one of the most computationally intensive tasks attempted and the earliest experiments were forced to use relatively coarse resolution as a result. There has been ever increasing demand for more accurate, and most importantly, more locally tailored, climate projections, however, which has seen the introduction of relatively high resolution "Regional Climate Models", the topic of our third workshop theme.

Ocean modelling is clearly important for an island continent and a great deal of important economic activity occurs relatively close to shore, where enhanced resolution is required to model features such as estuaries and to accurately capture high-impact events such as storm-surges. Work in this area is captured in the Ocean and Coastal Modelling theme of the workshop.

Our final theme, User Expectations of High Resolution Modelling, provides a forum in which we can discuss current and future user requirements in this area and how we might incorporate these into our ongoing system development.

The workshop includes participants from research groups around Australia. We also welcome a number of contributors from overseas institutes and national meteorological services to the workshop, with keynote presentations from Isaac Ginis (University of Rhode Island, USA), Kevin Horsburgh (Proudman Oceanographic Laboratory, UK) and Sue Ballard (UK Met Office). We are grateful for these expert contributions and to all the participants' contributions to the debate and discussions.

Finally, I would like to thank the Local Organising Committee for the workshop, comprising Gary Dietachmayer and Lawrie Rikus (Co-Chairs), Gary Brassington, Andrew Hollis, Val Jemmeson Jeff Kepert, John McBride, Kathy McInnes and Peter Steinle.

Bruce Mapstone

Director

Centre for Australian Weather and Climate Research:

A partnership between the Australian Bureau of Meteorology and CSIRO

November 2008

# Current developments in operational storm surge modelling

Kevin Horsburgh

*Proudman Oceanographic Laboratory, Liverpool, L3 5DA, U.K.*

Storm surges are the sea level response to wind stress and atmospheric pressure gradient, and they are a critical component of total sea level during coastal flood events. Numerical models for storm surge prediction most commonly solve the governing equations of fluid flow on regular grids. To achieve finer resolution around coastlines, it is possible to nest finer grids or use finite element techniques. Since the driving forces for storm surges are spatial fields that give rise to a free surface gradient then two-dimensional depth-averaged models of both surges and wind-driven currents have been very successful as predictive tools in shelf seas. A recent review of operational capabilities found that 75% of models used internationally were two-dimensional and depth-averaged, and that their forecast skill was comparable to 3D models that resolved the vertical structure of current.

The current UK operational surge model, CS3X, covers the entire northwest European continental shelf at 12 km horizontal resolution. Its surface boundary conditions are the sea level pressure and 10 m wind fields from the Met Office North Atlantic Extended (NAE) atmospheric model, at a similar spatial resolution ( $0.11^\circ$  longitude by  $0.11^\circ$  latitude). Tidal input at the model open boundaries consists of the largest 26 constituents. Finer resolution models of key channels and estuaries are nested within this outer domain. The model suite runs four times each day and simulations consist of a six hour hindcast portion (where the model is forced with meteorological reanalysis) followed by a 48 hour forecast. The modelled surge is derived by subtracting a tidal model run from one forced by both tide and atmosphere. Validation of the models is performed monthly by comparison with observed sea level data from the UK national tide gauge network. Typical monthly mean RMS errors in the model accuracy are of the order 10 cm.

This paper explores areas where operational storm surge modelling is amenable to improvement. Whilst always wishing to incorporate the very latest science and numerical sophistication, operational modelling has the additional challenge of delivering a reliable product at specific times, and must be tuned to the needs of the forecasting community who deliver public warning and initiate emergency response. Recent work in the UK has been directed at improved resolution, data assimilation, ensemble forecasting and a more explicit coupling with wave models. A systematic comparison of surge models of 12km and 3km horizontal resolution showed no significant differences when long time series were analysed. However significant differences were seen on smaller timescales during surge events at a local level (as in Figure 1). Clearly, improved resolution delivers a more accurate simulated surge where local effects (rather than traveling waves) are important. A corollary to this is that finer resolution surge models are likely to be more effective when coupled to finer resolution (e.g. 4 km) wind fields, when these become available operationally over the full hydrodynamic domain.

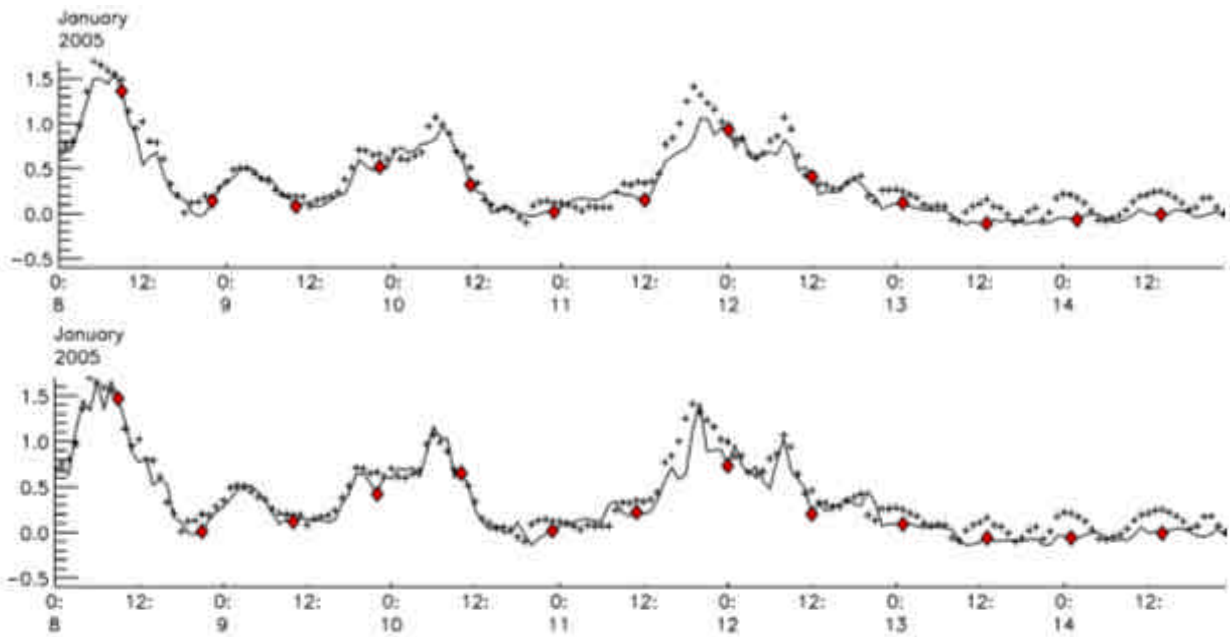


Figure 1. Improvement simulation of surge event at Liverpool with the 3km model (lower panel) compared to the operational 12km model (upper panel).

Sensitivity studies reveal the dependency of surge models on fairly small changes in the wind field. Closed marine basins effectively act as integrators for any sea level error. Ensemble forecasting quantifies the uncertainty by making many numerical simulations, using different choices of initial states and key parameters. It is a popular method for handling the uncertainty inherent in short-term weather prediction and climate models. A recently developed ensemble-based surge forecasting system has been validated over the period 2006-2008. The meteorological input to the surge model is taken from the Met Office Global and Regional Ensemble Prediction System (MOGREPS: Bowler et al., 2008). Each forecast cycle starts with a single meteorological analysis based on observations, to which perturbations are applied to generate 24 ensemble members (23 perturbed plus one unperturbed control). The meteorological perturbations are generated using the Ensemble Transform Kalman Filter (ETKF), which takes estimates of the observation error to scale and mix differences between the ensemble mean and the individual perturbations from the T+12 state of the previous forecast cycle (Bishop et al. 2001).

The ensemble surge model output can be processed to provide a variety of useful graphical products. Figure 2 shows the mean and spread (standard deviation) of the ensemble residual at midday, on 20 October 2008. Verification found that one of the most useful indicators of forecast accuracy was the ensemble spread (see Figure 3). The ensemble mean consistently had the lowest error, particularly at high spreads, which implies that the sampling of uncertainty provided by the system allows the mean to produce on average a better forecast than any perturbed member (or the control member).

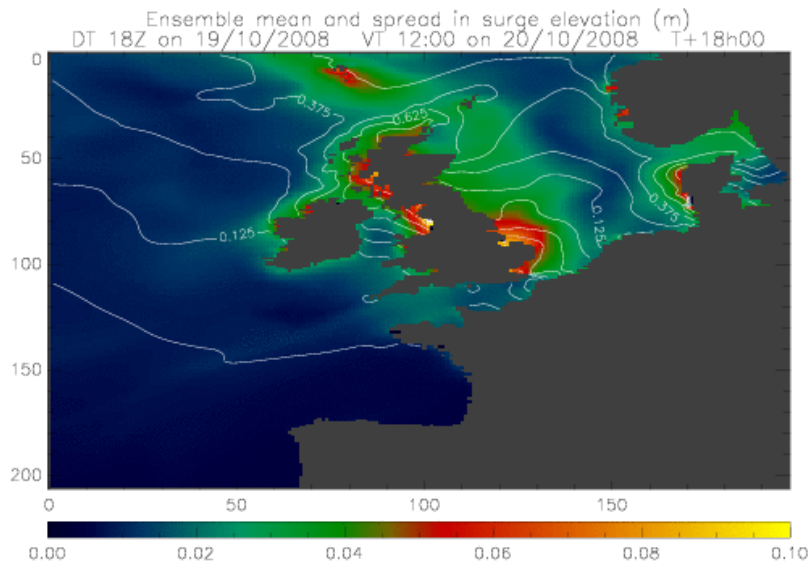


Figure 2. Ensemble mean and spread of sea level residual for 1200 on 20/10/08 from forecast on 1800 19/10/08.

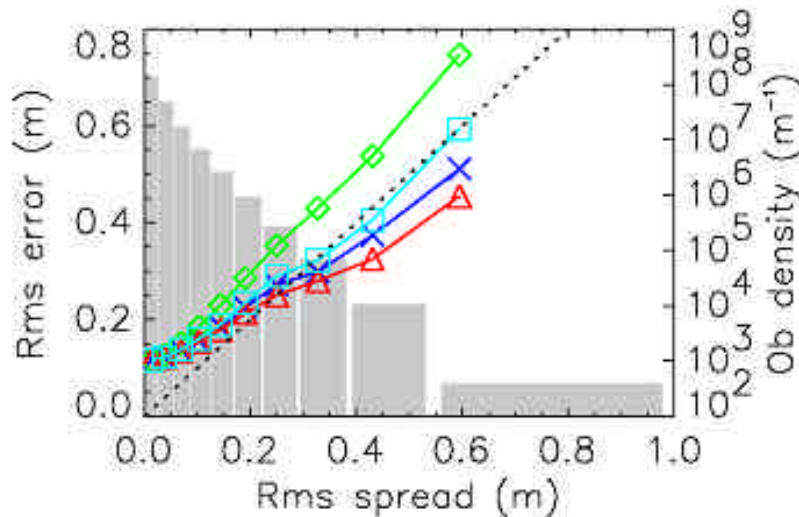


Figure 3. RMS error binned as a function of ensemble spread. Error-spread performance is shown for the ensemble mean (red), individual perturbations (green), the control member (dark blue) and deterministic model run (light blue).

A common application in forecasting is to make a yes/no decision (e.g. close a barrier, evacuate a district). We used the Brier Skill Score to measure the improvement of the probabilistic forecast relative to a reference forecast based on climatology. Figure 4 shows the ensemble scores slightly but consistently better than two climatological dressings, and far better than the undressed control. The improvement was larger at longer lead times, which hints at the usefulness of longer forecasts.

The other aspect of surge modelling systems most demanding of further study is the mutual influence of surge and short period waves. Wave-dependent stress at the sea surface and interactions in the bottom boundary layer are both important (e.g. Mastenbroek et al., 1993; Luettich and Westerink, 1999). It is also important for forecasting systems to explicitly include the wave set-up (due to radiation stress) in local predictions. However, the majority of model studies tend to focus on single events for their validation. Thus the global applicability of complex coupling has never been demonstrated. Work is currently directed towards demonstrating whether or not one can obtain consistently better surge predictions at all

locations with a fully coupled wave-surge, and whether higher order effects be sensibly parameterised in 2D surge models (e.g. via a variable Charnock parameter) in a manner that allows economic computation (so as to facilitate ensemble forecasts). Recent work has shown that a variable Charnock parameter is necessary if there are significant wave-age changes across a region. Any comprehensive program to study the utility of shelf-wide coupled wave-surge models would also benefit from an observational component.

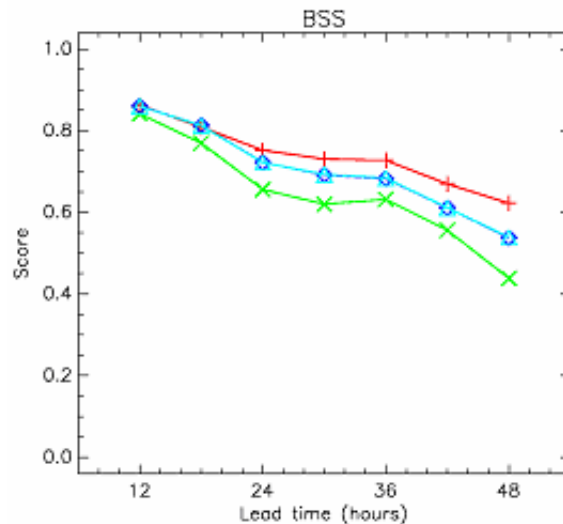


Figure 4. Brier skill score for ensemble prediction of total water level exceeding port-specific alert levels. Red – ensemble; green – control member only; blues – control member with statistical dressing.

As mean sea levels rise by 20-90 cm towards the end of this century, coastal flood managers will become more reliant on operational warning systems in order to protect lives and infrastructure. Forecasting systems must become more sophisticated in response to this challenge. Future improvements to all aspects of the modelling system will lead to better risk management and long-term decisions on coastal defence.

## References

- Bishop, C.H., Etherton, B.J., and Majumdar, S.J. (2001) Adaptive sampling with the ensemble transform Kalman filter. Part 1: Theoretical aspects. *Monthly Weather Review*, **129**, 420-436.
- Bowler, N.E., Arribas, A., Mylne, K.R., Robertson, K.B., and Beare, S.E. (2008) The MOGREPS short-range ensemble prediction system. Accepted for publication in *Quarterly Journal of the Royal Meteorological Society*. 46pp.
- Luetlich, R.A., and Westerink, J.J. (1999) *Implementation of wave radiation stress gradient as forcing for the ADCIRC hydrodynamic model*. Coastal Engineering Research Centre Report, May 1999. Dept. of the US Navy.
- Mastenbroek, C., Burgers, G., and Janssen, P.A.E.M. (1993) The dynamical coupling of a wave model and a storm surge model through the atmospheric boundary layer. *Journal of Physical Oceanography*, **23**, 1856-1865.

# Regional sea level rise around the Australian coastline

Siobhan O'Farrell  
*Antarctic Climate and Ecosystems CRC,  
CSIRO Marine and Atmospheric Research,  
CAWCR, WFO Flagship.  
Aspendale, Victoria, Australia*

The impact of sea level rise on the Australian coasts and coastal infrastructure needs a number of scientific disciplines to collaborate. Contributions to global sea level rise as seen arise from ocean thermal expansion and melting glaciers, ice caps and ice sheets. The best current estimate for the global sea level rise is 18-59 cm given by Meehl et al (2007). In the final analysis of sea level projections issued by IPCC AR4, they increased the upper limit for projected sea level rise by 10 to 20 cm to cover uncertainty on ice sheet discharge based on recent evidence of acceleration in Greenland and Antarctica. Hunter (2008) has drawn up tables of the AR4 and TAR estimates of 21<sup>st</sup> century global sea level rise for the IPCC SRES scenarios.

Regional sea level rise at the Australian coast also include local effects that differ for each coastline. There is local thermal expansion in the ocean from changes in ocean currents and positions of frontal regimes, driven by changes in regional wind forcing and atmospheric fluxes. The sea level at the coast is also impacted by short term extreme events such as storm surges and wave regimes which reflect distant storminess, both are predicted to increase in severity under climate change. The final regional component of the coastal impact is the local geology, with different effects on sandy and rocky shorelines, and the longer term geological response of the earths crust to reduced ice sheet loading (post-glacial rebound), vertical shifts in land following earthquakes and ground water extraction which can cause different parts of the coastline to rise or fall.

The focus of this presentation is on the regional sea level rise from the thermal expansion derived from 17 IPCC AR4 climate models where sea level data has been made available through the PCMDI CMIP3 archive. The analysis has centred on the SRESA1b scenario a mid level scenario that reaches 720 ppm CO<sub>2</sub> equivalent by 2100. The data for each model has been processed into decadal averages and the values for the control run simulation for the same decade subtracted to remove the drift. The models global mean sea level for each decade has been subtracted to provide regional anomalies and 20 year averages focussed on 2030, 2070 and 2100 extracted. Figure 1 shows the results for 2030 for the 17 models along with a mean field which was calculated by re-gridding all the models to a 1 degree x 1 degree grid and infilling to the coast from the nearest neighbour for models that had less detailed coastal geometry.

The results for 2030 show that greater than 70% of the models (BCCR, CSIRO Mk3.0, CSIRO Mk3.5, ECHO-G, GFDL2.0, GFDL2.1, GISS E-H, IPSL, Miroc-HIRES, MPI, MRI) have established the strongest aspect of pattern of sea level change seen in later decades, with a noticeable maximum of regional sea level rise on the East Coast of Australia and in particular in the Tasman Sea. This location of the maximum differs from what has been observed in the last couple of decades by the tide gauges of the National Tidal Centre and in the Topex/Poseidon and Jason satellite altimeter data set which showed maximum regional increase in Northern Australia. However, these observational time series were relatively short and have been biased by the tendency for ENSO conditions since the early 1990s.

The Tasman sea level rise signal (0-20cm) is linked to changes in East Australian current and the mirrors the increase seen in current flow and temperature observed along the NSW and Tasmanian coasts (Sutton et al, 2005, Ridgway et al, 2008). The change in the East Australian current is caused by the southward shift in winds and wind stress curl. The slightly different locations of the sea level maximum, in some of the models is due to the different position of the strongest gradient in the frontal systems, the structure of the currents which is model resolution dependent and the latitude of the strongest wind changes.

To the south of Australia, the sea level rise signal (0-10cm) is below the global average in nearly all the models. Earlier observational and modelling studies have shown that there is cooling in the ocean at mid depth 500-100m extending across the Indian ocean to south of Australia due to reduced ventilation. It is likely that this cooling is contributing to the reduced heat content changes over the water column but this needs further investigation.

To the west and north of the continent the models show a mixed picture but on average lower sea level rise than the global average. Several models show increased sea level rise in the Gulf of Carpentaria with one model having a very strong maximum. Detailed investigation of the oceanographic causes of this regional signal in these locations needs to be undertaken.

The model average created for Figure 1 has included all the models, and whilst it reflects the main features seen across the models, a more appropriate approach would be to form a weighted ensemble average. Criterion that would be prioritized in such a weighting would be realistic currents and salinity/temperature and density of water masses in the Australian region in the control and 20<sup>th</sup> Century simulations, and the ability of the models to represent the present trends in heat content in the late 20<sup>th</sup> and early 21<sup>st</sup> century.

Analyses of the trends in heat content globally have been prepared by Antonov et al, 2002, and Levitus et al 2005, and a new regional analysis is currently underway by CSIRO colleagues in Hobart (Wijffels, Domingues) that will be used to select the most appropriate models for our region. However, when using this approach one needs to consider how the pattern of regional heat content change develops above the noise with many multi-decadal variability signals impinging on the region at different ocean depths and integrated up into the sea level signal. Many of the models show clear differences in the regional sea level pattern between 2030, 2070 and 2100. Examination of the ensemble members of the 20<sup>th</sup> century simulations in the CSIRO Mk3.0 and Mk3.5 models show different patterns evolve in the sub-surface temperature fields in the different members. The 20<sup>th</sup> century ensemble ocean results exist for most of the AR4 models included in Figure 1 and a subset of the AR4 models (CSIRO Mk3.5 GISS\_AOM, GISS\_E-R, GISS\_E-H, FGOALS, MIROC\_MED, MPI, MRI) have 21<sup>st</sup> century ensembles that could be used in the analysis to derive a realistic weighted average of regional sea level rise.

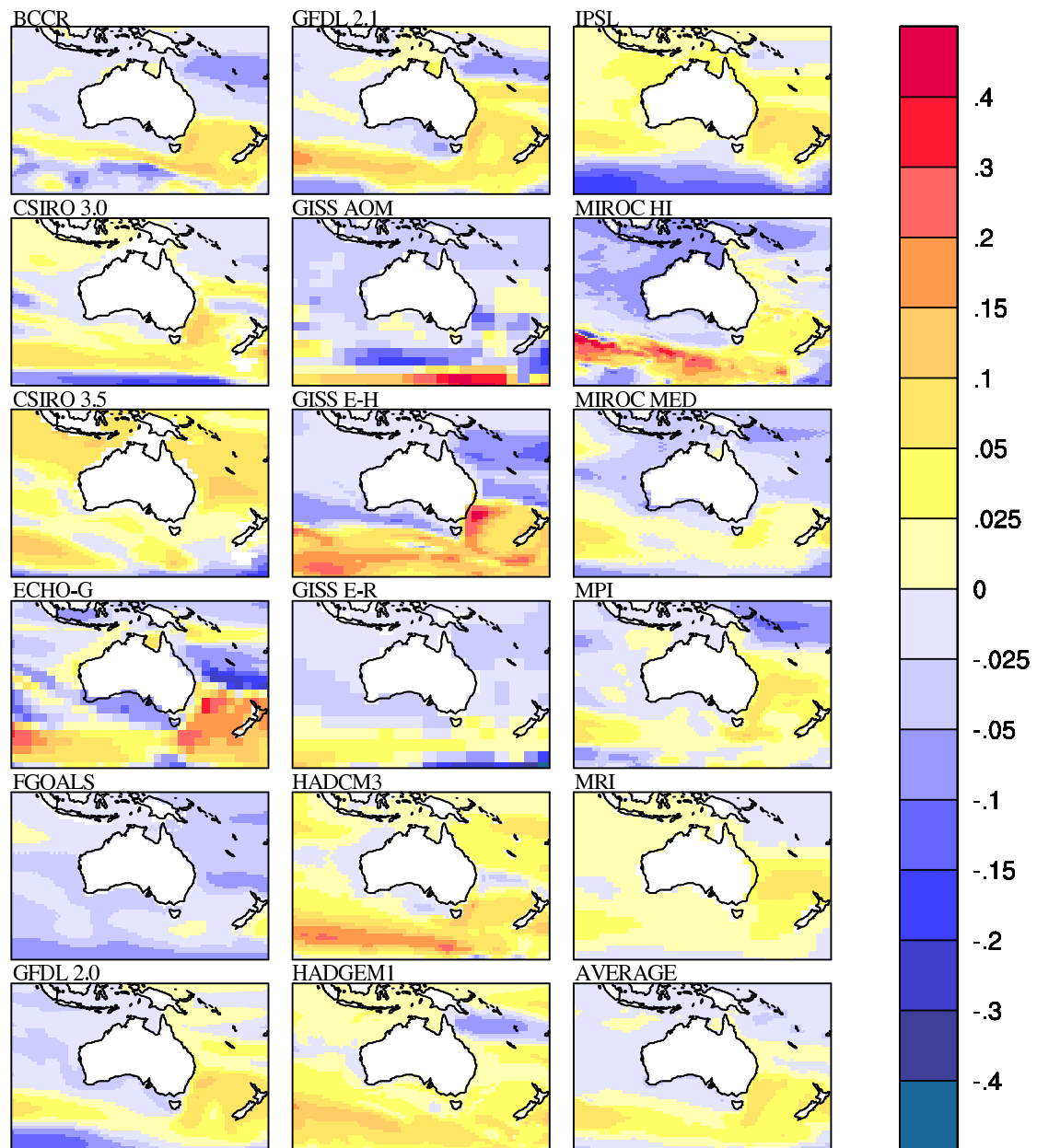


Figure 1. Regional sea level rise (in m) relative to global sea level rise for 17 AR4 models and an averaged field for a 20 year decadal average centred on 2030.

## References

- Antonov J. I., S. Levitus, and T. P. Boyer, 2002, Steric sea level variations during 1957–1994: Importance of salinity, *J. Geophys. Res.*, 107 (C12), 8013, doi:10.1029/2001JC000964.
- Hunter, J.R. 2008, Estimating Sea-Level Extremes Under Conditions of Uncertain Sea-Level Rise. Submitted to *Climatic Change*.
- Levitus, S. Boyer, T. P. and J. Antonov, 2005, Variability of heat content, freshwater content, and steric sea level for the world ocean- 1955-2002, Suki Manabe Symposium, San Diego, 2005, published by American Met. Soc.
- Meehl GA, Stocker TF, Collins WD, Friedlingstein P, Gaye AT, Gregory JM, Kitoh A, Knutti R, Murphy JM, Noda A, Raper SCB, Watterson IG, Weaver AJ and Zhao ZC, 2007, Global climate projections. In *Climate Change 2007: The Physical Science Basis. Contribution of Working Group 1 to the Fourth Assessment Report of the Intergovernmental Panel on Climate Change* (Eds S Solomon, D Qin, M Manning, Z Chen, M Marquis, KB Averyt, M Tignor and H Miller). Cambridge University Press, Cambridge, UK and New York.
- Ridgway KR, Coleman, RC, Bailey RJ and P Sutton, 2008, Decadal variability of East Australian Current transport inferred from repeated high-density XBT transects, a CTD survey and satellite altimetry, *Journal of Geophys. Res. C. Oceans*; 113(C8), doi:10.1029/2007JC004664.
- Sutton PJH, Bowen, M and D Roemmich, 2005, Decadal temperature changes in the Tasman Sea, *New Zealand Journal of Marine and Freshwater Research*; 39( 6) pg. 1321-1329.

# Tide models used at the National Tidal Centre

James Chittleborough  
*National Tidal Centre, Bureau of Meteorology, Australia*

A number of tidal models developed from and for Topex/Poseidon and Jason1 satellite altimetry have improved our knowledge of tides on the global scale. Tides can now be predicted with high accuracy over the deep oceans, but in shallow waters tides are more complex and the use of global tidal models for coastal sea level applications can be problematic. In order to provide better tidal services over the continental shelf an Australian regional tidal model has been developed. Aspects of various tidal models and their application in the Australian region and beyond will be discussed.

## Introduction

The National Tidal Centre provides tidal and sea level services for the Australian and South West Pacific, Indian Ocean, and Southern Ocean regions. Requests for sea level and tidal information extend worldwide and attract at least 1200 public enquiries per year. Tidal models are required to service requests in areas sparse of observations, for mapping of ocean tides and for information relating to tidal streams and tidal circulation.

## Global Tidal Models

The National Tidal Centre utilises a number of global tidal models, which have been developed for and from satellite altimetry. Global tidal models have evolved to an accuracy of several cm's over the deep ocean in parallel with precise altimetric measurements achieved by TOPEX/Poseidon and subsequent satellite altimeter missions.

The GOT00.2 global tide model, for example, is one of two used for operational tidal corrections to Jason-1 measurements (Jason User Handbook, 2008). Tidal predictions from GOT00.2 were used to verify measurements from the DART (Deep-Ocean Reporting of Tsunamis) buoy deployed in the Tasman Sea as part of the Australian Tsunami Warning System (Figure 1).

However, global tidal models, like satellite altimeters, tend to lack accuracy and resolution over shallow coastal regions. Many of the available global tidal models are also empirical models fit to sea-surface observations, rather than hydrodynamic models inclusive of tidal currents. The National Tidal Centre has therefore undertaken higher resolution tidal modelling for the Australian continental shelf region.

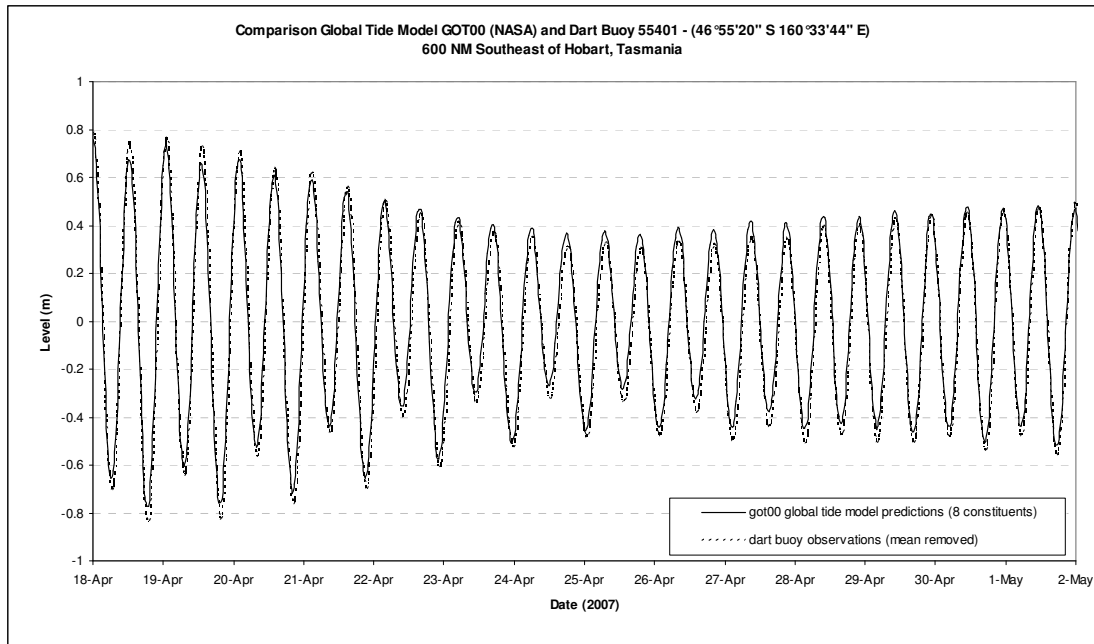


Figure 1: Comparison of tide predictions from GOT00.2 global tidal model and sea level measurements from the DART buoy deployed in Tasman Sea.

## Australian Continental Shelf Tidal Model

A tidal model of resolution 5 arcminutes of latitude and longitude over the region bounded by 111° E to 156° E and 9° S to 45° S has been developed, incorporating 8 tidal constituents Q1, O1, P1, K1, N2, M2, S2, and K2.

The underlying computer program (ORSOM) is a two-dimensional, barotropic model that solves the depth-integrated equations of mass and momentum on a finite-difference grid in either Cartesian or spherical coordinates. It accounts for Coriolis, non-linear advection, horizontal eddy viscosity, and quadratic bottom friction. An Orlanski-Sommefeld radiation condition is used on the open boundary. Other features available include spatially variable bottom friction, tidal potential, earth tides, and self-attraction and loading.

ORSOM is capable of simulation of tides and/or meteorological-driven motions over large domains. In this application it has been used to derive a database of tidal constants (u, v, and z components) over the entire Australian continental shelf at a resolution of 5 minutes in latitude and longitude.

The tidal constants for the 8 tidal frequencies have been compared with those observed at 81 standard ports that are suitably resolved by the model (Table1). For the principle lunar semidiurnal tide M2, the average amplitude error is around 9.4cm and average phase error is 8 degrees (~15 minutes). The corresponding errors for the GOT00.2 global ocean tide are 12.8cm and 14 degrees (~28 minutes).

Table 1: Average Absolute Errors of NTC Australian Tidal Model vs 81 standard ports.

Tidal Constituent	Average Amplitude Error (metres)	Average Phase Error (degrees)
Q1	0.004	8
O1	0.016	6
P1	0.011	6
K1	0.025	6
N2	0.017	12
M2	0.094	8
S2	0.036	6
K2	0.013	11

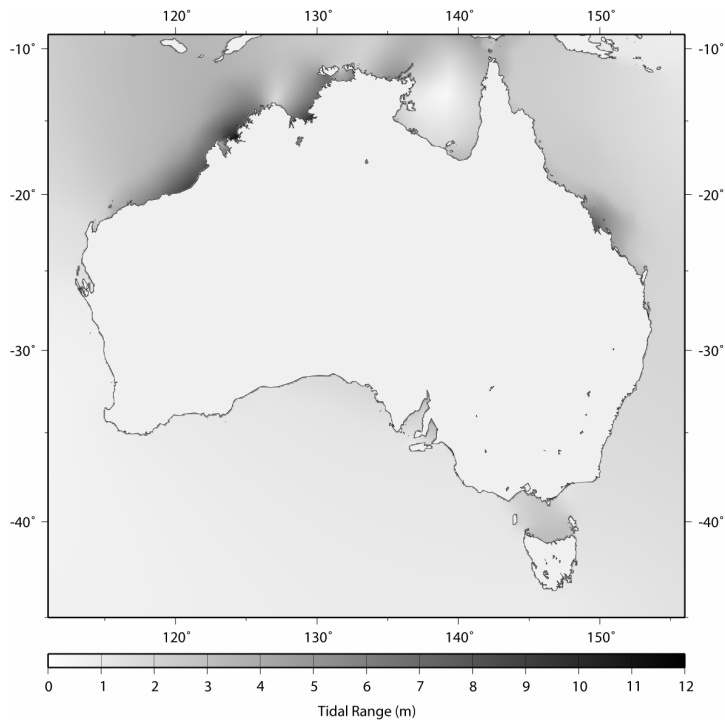


Figure 2: Tidal range within the Australian continental shelf model domain.

The available bathymetric databases all have their problems and efforts were made to ensure the coastal boundary area agreed in principle with the world vector shoreline and Australian hydrographic chart soundings. The demand for higher resolution modelling continues. The South Australian gulf systems have been modelled at 30arcsecond resolution. A number of other computer models provide the National Tidal Centre flexibility in modelling approach, including schema for 3-dimensional, wetting and drying, finite element and generalised inversion.

## Service delivery

Deployment of model-derived products and information is rapid with the use of a graphical user interface. Modelled tidal predictions can be produced for any location worldwide. 'Third party' ocean modellers require tidal parameterisation within their models (Li et al 2005) or along their open boundaries. Charts of ocean tides/currents are of interest for tidal power (Renewable Energy Atlas of Australia, 2008) and land-sea interface applications. Knowledge of tidal circulation and tidal streams are important for navigation, search and rescue, and fisheries management.

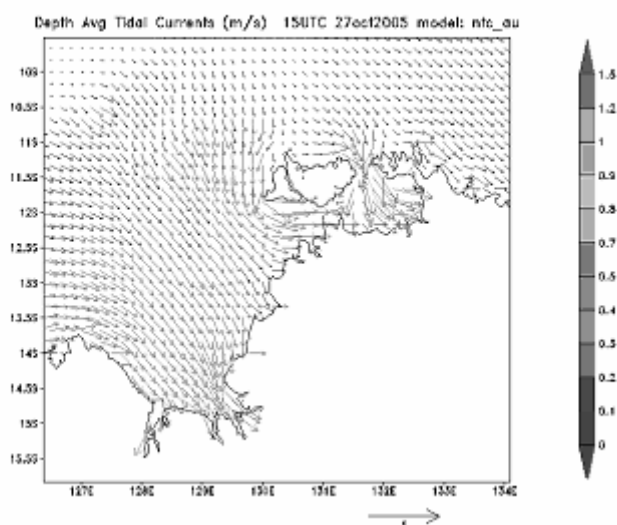


Figure 3: Snapshot of depth-averaged tidal currents around Darwin.

## References

Jason User Handbook (2008). AVISO and PODAAC User Handbook. IGDR and GDR Jason Products, SMM-MU-M5-OP-13184-CN (AVISO), JPL D-21352 (PODAAC).  
[ftp://podaac.jpl.nasa.gov/pub/sea\\_surface\\_height/jason/gdr/doc/Handbook\\_Jason\\_v4.1.pdf](ftp://podaac.jpl.nasa.gov/pub/sea_surface_height/jason/gdr/doc/Handbook_Jason_v4.1.pdf)

Li, F., Dyt, C., Griffiths, C.M., Jenkins, C., Rutherford, M., and Chittleborough, J. (2005). Seabed Sediment Transport and Offshore Pipeline Risks in the Australian Southeast. *APPEA Journal* **45**, 523-534.

Renewable Energy Atlas of Australia (2008). Online Resource. Department of the Environment, Water, Heritage and the Arts. Accessed 7 Nov 2008.  
<http://www.environment.gov.au/settlements/renewable/index.html>

# **Regional models for upwelling and shelf circulation: the importance of the backward boundary condition**

John F. Middleton

*South Australian Research and Development Institute, 2 Hamra Ave,  
West Beach, South Australia, Australia, 5024*

[Middleton.John@saugov.sa.gov.au](mailto:Middleton.John@saugov.sa.gov.au)

An analysis is made to determine the properties, scales and relationship between two and three-dimensional upwelling driven by an impulsively started, steady, uniform wind. For two dimensional upwelling, the alongshore velocity asymptotes to a constant value, (set by bottom drag) and over a time scale  $T(x)$  that increases with distance  $x$  offshore. As this viscous limit is achieved, the upwelling becomes increasingly confined to the bottom boundary layer and bottom stress balances wind stress. Interior upwelling is shutdown and upwelling occurs through the viscous boundary layers. This “viscous limit” of upwelling is related to three-dimensional upwelling that occurs where the backward “edge” of the wind field acts as a geographical origin for the generation of coastal-trapped waves (CTWs). Results are described that show that prior to the arrival of the first mode CTW, the upwelling is two-dimensional in nature and asymptotes towards the viscous limit. However, in three dimensions, this limit may not be achieved since after the arrival of the first CTW mode, a gradient in the alongshore velocity is set-up and its divergence acts to feed the offshore Ekman transport: upwelling is largely down even though the winds remain upwelling favourable. The importance of these results to numerical models of upwelling is illustrated through a case study of the Chilean shelf.

An analysis of the use of coastal sea level and a CTW paddle is also made in the context of closing backward boundary conditions for storm surge and shelf models.



# Adaptive, non-hydrostatic multi-scale modelling: application to coastal scale processes

O'Callaghan, J., Rickard, G., and Popinet, S.

*National Institute of Water and Atmosphere Research Ltd,  
Private Bag 14-901, Kilbirnie, Wellington, New Zealand.*

## Introduction

Simulating the full spectrum of spatial and temporal scales relevant to geophysical flows remains a formidable challenge. For coasts and oceans, capturing the interaction between small scale coastal mixing and its dependence on larger scales (such as tidal oscillations, and vice versa) is necessary for accurately representing ecosystem variability. Extending Gerris, an adaptive Navier-Stokes fluid solver, to multi-scale, non-hydrostatic, geophysical flows that characterise the coastal ocean is proving an exciting way forward.

Gerris is an open source code (Popinet, 2006), which is an adaptive, finite-volume, incompressible, Navier-Stokes fluid solver. Using either an oc-tree (3D) or quad-tree (2D) mesh structure, this model adapts dynamically in space and time to the evolving flow features. The governing equations are the incompressible, Navier-Stokes equations using the Boussinesq approximation (see Popinet & Rickard, 2007).

Available non-hydrostatic geophysical codes are typically modified hydrostatic codes (Marshall et al., 1997; Wadzuk et al., 2004; Bernsten et al., 2006) that split pressure into hydrostatic and non-hydrostatic components. Several geophysical codes are indeed fully non-hydrostatic and the pressure term is not split (Labeur & Pietrzak, 2005; Fringer et al., 2006). Regardless of approach, validation of the Boussinesq approximation in this new breed of models is typically done using two classic laboratory experiments: the lock-exchange and the internal solitary wave breaking on a sloping boundary. Here, the lock-exchange test case is presented, the latter to appear in Rickard et al., (2008). The behaviour of gravity currents were extended beyond the laboratory scale in order to understand plume dynamics that are frequent, yet event driven processes at the coast-ocean boundary. And lastly, using Cook Strait, New Zealand as an example we will evaluate barotropic processes at the coastal scale.

## Results: Non-hydrostatic lock-exchange

Here, we present results of a gravity current induced by the classic lock exchange using the initial conditions in Hartel et al. (1997). The domain length was  $12L$  where  $L$  is the vertical height of 0.2 m. Slip boundary conditions were used on all sides of the domain so that comparisons to plume intrusions into salt-stratified environments could be made (Hartel et al., 2000). Viscosity and diffusivity values were varied in each simulation to capture Reynolds numbers ranging from 2237 to  $1.8e^5$ . The benefits of using adaptivity for these simulations will be assessed. All simulations had a starting quad-tree level of 5 and cells could adapt, based on vorticity and tracer criteria, to a maximum of 10. Corresponding length scales of cells at these refinement levels were 0.0625 to  $1.95 e^{-3}$  m, respectively. Using 10 quad-tree levels met criteria outlined in Hartel et al.(2000) who justify that the full energy spectrum is resolved for cell sizes smaller than the smallest scales defined by  $Re$ . In the 2D lock exchange simulations the large scale features were preserved for the range of  $Re$  (Fig. 1). Prior to gravity current reflection at the right hand boundary, speeds of the head of the gravity current were remarkably similar at approx.  $2 \text{ ms}^{-1}$ . Not only are Gerris outputs similar to other high resolution simulations (Hartel et al., 2000; Ozgokmen et al., 2004; Bernsten et al., 2006), but

convergence of these solutions to the theoretical criteria of Benjamin (1968) indicate that these simulations also compare quantitatively.

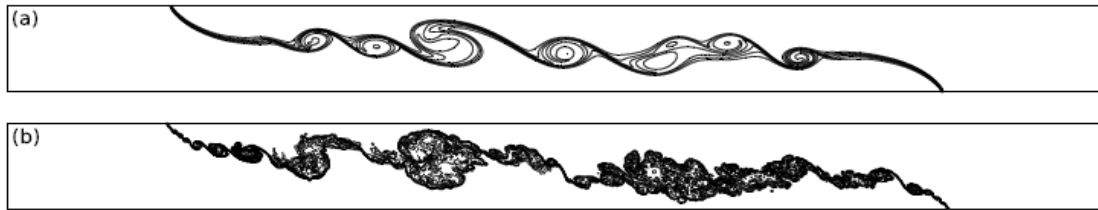


Fig. 1 Gravity currents for Reynolds numbers of (a) 2237, (b) 178500 at  $t = 14$  s.

To evaluate model efficiency, file sizes with and without adaptive mesh refinement are compared. For the lowest  $Re$  (2237) at time = 1.0 and 2.0 files were approximately 40 Mb and 100 Mb, corresponding to total cell numbers of  $8.6 \times 10^5$  and  $2.0 \times 10^6$ , respectively. For the highest  $Re$  of  $1.8 \times 10^5$  the maximum files size was 150 Mb. Several runs were done with adaptivity switched off, but with a uniform quad-tree level of 10 through the domain; for all time steps, the number of cells was  $1.25 \times 10^7$  and files were in excess of 600 Mb. A substantial saving is evident by using an adaptive mesh refinement with up to 2 orders of magnitude less cells per simulation, resulting in both a decrease in file sizes and substantially shorter run times.

## Results: Horizontal gravity currents at a coastal scale

Stratification implemented in the following simulations was chosen to replicate the strong near-surface gradients experienced in Doubtful Sound, Fiordland, New Zealand (Gibbs et al., 2000). In addition to rainfall being in excess of 7 m per year, there is a hydroelectric generation outflow which injects substantial low-salinity water into the head of the fjord at variable rates between  $350$  to  $500 \text{ m}^3\text{s}^{-1}$ . This substantial buoyancy and momentum flux forms a horizontal buoyant plume, or gravity current.

A rectangular domain of  $50 \times 400$  m with a rigid-lid was used to capture near-field dynamics. Although adaptivity (in time) was not used here, efficiency gains can still be made by specifying static quad-tree levels where required. As stratification is strongest near the surface (top 25 m) a quad-tree level of 9 was set, with a refinement level 6 in the lower 25 m. The minimum and maximum resolution is 0.05 and 0.4 m, respectively. A gaussian velocity profile injected almost fresh, cold water. Within 50 m of the source a gravity current was clearly established. Strong return flows below this current entrained material upwards into the gravity current head, doubling its thickness over another 200 m or so. Validation remains an outstanding issue.

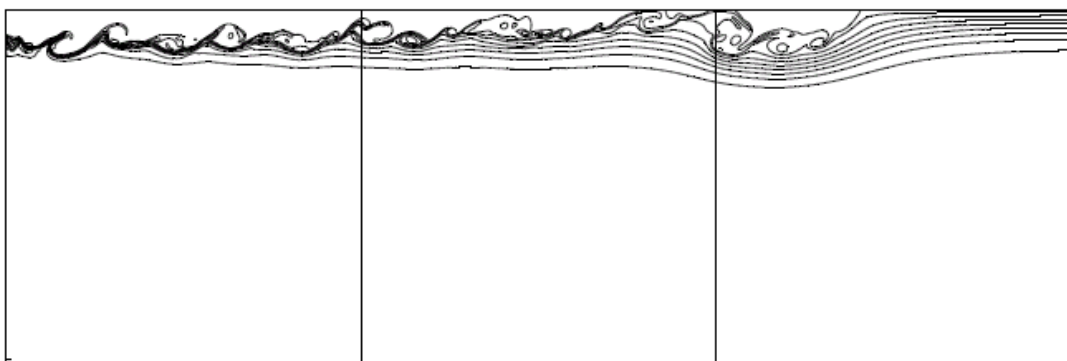


Fig. 2: Snapshot of horizontal gravity current at  $t = 124$  s. The vertical lines are 50 m intervals along the domain, with  $50 \times 150$  m shown here.

## Results: Tidally driven flow in Cook Strait, New Zealand

Cook Strait, New Zealand has a complex coastline and bathymetry, and experiences multi-scale process, which combine to provide a good coastal scale test. Barotropic flow is forced using 'Flather' boundary conditions on all four boundaries, using the  $M_2$  component of the tide (Walters and Goring, 2001). Competing tidal phases across the Strait result in strong currents between the north and south islands and in parts of Marlborough Sounds. Figure 3 shows the adaptive mesh grid for a sub-region of Cook Strait. Coastlines are statically refined at the finest quad-tree level, which was 12 in this example. However, the flow is dynamic with areas of high vorticity tracked as eddies are shed from headlands. Damping of eddies is evident away from the coast and validation of these high-resolution processes remains work in progress, but comparisons to eddy-like features observed in satellite images are highly encouraging.

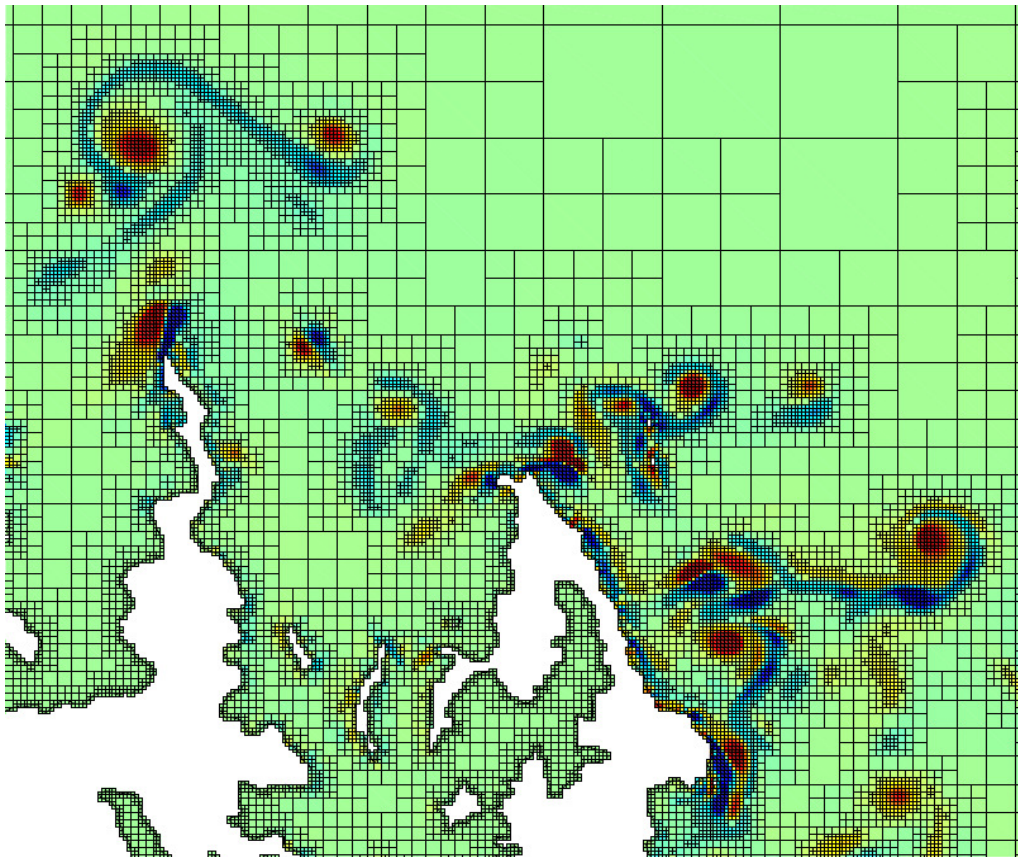


Fig. 3: Example of quad-tree mesh discretisation for a sub-region in Cook Strait, New Zealand. The domain extent was 36 x 29 km. The minimum cell resolution was 122 m.

## Summary

Model adaptivity in time and space represents a potential way to integrate complex, multi-scale geophysical flows efficiently. In this context we show examples of Gerris, a Navier-Stokes fluid solver, applied to geophysical coastal problems. So far, the model has shown itself capable of successfully handling small to near-coastal scale nonhydrostatic problems, and also shallow-water applications. The future challenge is to retain that efficiency in the face of significant aspect grid ratios allied to full non-linear equations of state.

## References

- Benjamin, T. B. 1968. Gravity currents and related phenomena. *Journal of Fluid Mechanics*, 31, 209-248.
- Berntsen, Xing, J.J., Alendal, G. 2006. Assessment of non-hydrostatic ocean models using laboratory scale problems. *Continental Shelf Research*, 26, 1433-1447.
- Fringer, O., Gerritsen, M., Street, R., 2006. An unstructured-grid, finite-volume, nonhydrostatic, parallel coastal ocean simulator. *Ocean Modelling*, 14, 139–173.
- Gibbs, M.T., Bowman, M.J., Dietrich, D.E., 2000. Maintenance of near-surface stratification in Doubtful Sound, a New Zealand fiord. *Estuarine, Coastal and Shelf Science*, 51 (6), 683- 704.
- Hartel, C., Kleiser, L., Michaud, M., Stein, C. F. 1997. A direct numerical simulation approach to the study of intrusion fronts. *Journal Engineering Maths*, 32, 103-120.
- Hartel, C., Meiburg, E., Necker, F., 2000. Analysis and direct numerical simulation of the flow at a gravity-current head. Part 1. Flow topology and front speed for slip and no-slip boundaries. *Journal of Fluid Mechanics*, 418, 189–212.
- Labeur, R.J., Pietrzak, J.D., 2005. A fully three dimensional unstructured grid non-hydrostatic finite element coastal model. *Ocean Modelling*, 51–67.
- Marshall, J., Hill, C., Perelman, L., Adcroft, A., 1997. Hydrostatic, quasi-hydrostatic, and nonhydrostatic ocean modeling. *Journal of Geophysical Research*, 102 (C3), 5733–5752.
- Ozgoekmen, T., Fischer, P., Duan, J., Iliescu, T., 2004. Three-dimensional turbulent bottom density currents from a high-order nonhydrostatic spectral element model. *Journal of Physical Oceanography*, 34, 2006– 2026.
- Popinet, S., 2006. The Gerris Flow Solver. <http://gfs.sourceforge.net>.
- Popinet, S., Rickard, G., 2007. A tree-based solver for adaptive ocean modelling. *Ocean Modelling*, 16, 224-249.
- Rickard, G. , O'Callaghan, J., Popinet, S. 2008. Adaptive modelling of internal solitary waves interacting with uniform slopes (in preparation).
- Wadzuk, M., Hodges, B.R., 2004. Hydrostatic and non-hydrostatic internal wave models. Final report to ONR. CRWR Online Report 04-09, U. Texas Austin, 77 pp. Available from: <<http://www.crwr.utexas.edu/online.shtml>>.
- Walters, R., Goring, D., Bell, R., 2001. Ocean tides around New Zealand. *New Zealand Journal of Marine and Freshwater Research*, 35, 567–579.

# Issues in regional climate modelling and future directions

Marcus J. Thatcher, Deborah Abbs, Jack J. Katzfey and John L. McGregor

*Centre for Australian Weather and Climate Research:  
a partnership between CSIRO and the Bureau of Meteorology  
PB1 Aspendale, Victoria 3195, Australia*

## Abstract

This talk reviews some of the objectives of regional climate modelling, describes the modelling techniques used and discusses some typical applications of regional climate projections.

Regional climate models (RCMs) are typically used to dynamically downscale the global climate predictions of General Circulation Models (GCMs) with spatial resolutions of 300-400 km, down to regional scales of the order of 50 km or less. RCMs enhance the climate predictions of the host GCM by modelling dynamical and physical atmospheric processes with increased resolution of weather systems as well as including local surface forcings that were not resolved in the host model (e.g., orographic, coastal effects, etc). A good RCM should be able to better simulate the regional atmospheric behaviour and weather systems than the host GCM dataset. Nevertheless, biases and errors in the GCM can distort a RCM projection, so care must be taken with the selection of the host GCM as well as the downscaling technique.

This presentation will describe the main numerical techniques and methods used to produce credible simulations of regional climates. The use of high-resolution global, variable-resolution and limited-area grids in RCMs, as well as one-way, two-way and multiple nesting approaches are considered and their strengths and weaknesses discussed in capturing the relevant drivers of a region's climate while still making the simulation computationally tractable. It is also usually necessary to employ the most efficient numerical schemes available which are also required to work robustly over a range of length scales (particularly important in models with variable resolution grids). Given the potential variety in host GCMs (or re-analyses), flexible techniques for including atmospheric information from the host have been devised including Davies lateral boundary conditions, nudging techniques, spectral filters and time-slice experiments. The optimisation of such techniques is a non-trivial problem since the greater the extent that the RCM is constrained by the atmospheric behaviour of the host at large length scales, the more likely the RCM will inherit the biases and systematic errors of the parent model.

There has been a significant amount of research devoted to extracting useful information from the output of RCM simulations. Typical applications include regional climate impact studies which often involve a hierarchy of models including off-line hydrology and

agricultural simulations. RCMs are also particularly useful for studying changes to extreme events and cyclones under different climate change scenarios; this requires relatively high resolution atmospheric simulations of selected events (i.e., of the order of kilometres) and ideally the inclusion of relevant microphysical processes in the model. Finally the complementary use of statistical and dynamical downscaling approaches can be particularly effective in extending the model predictions to even finer length scales while still accounting for dynamical changes in the regional climate.

Future directions of RCMs and applications of RCM datasets are discussed, including the development of multi-GCM and multi-RCM ensembles to better quantify the uncertainties when predicting future regional climates. The coupling of mixed layer or regional ocean models to regional atmospheric models by some groups has been found to produce a better representation of the regional climate and atmospheric phenomena. In addition, it has been argued that the interaction with the ocean is also beneficial for the modelling of cyclones over climate time scales. Recently, several groups have developed downscaling techniques to study changes in air quality over urban environments with global warming.

# On the effect of the domain size of New Zealand's regional climate model on the modelled climatology

Frank Drost<sup>1</sup>, Brett Mullan<sup>2</sup>, Balakrishnan Bhaskaran<sup>3</sup>, Jim Renwick<sup>2</sup> and Sam Dean<sup>2</sup>

<sup>1</sup> *University of Melbourne, Victoria, Australia*

<sup>2</sup> *National Institute of Water and Atmospheric Research, Wellington, New Zealand*

<sup>3</sup> *Met Office Hadley Centre, Exeter, United Kingdom*

## Introduction

To test the effect of domain size of a New Zealand regional climate model on the simulated climatology, three regional simulations were set up with identical dynamics, physics and initial boundary conditions but with different regional domain sizes. Simulations were carried out for a four-year period, 1986 to 1989. As well as studying the effect of domain size, this experiment was an opportunity to examine the model biases. The main biases in surface fields (precipitation, maximum and minimum temperature) were also investigated.

## Data

The study used the United Kingdom Unified Model (UM). The UM versions that were used were HadAM3P (GCM), which provided the lateral boundary conditions for all RCMs, and HadRM3P (RCM). The latter was the same for all three regional simulations and only the size of the regional domains differed for each simulation. The three regional domains are

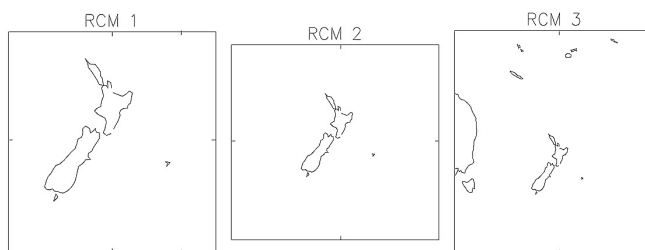


Fig 1. The three regional domains used in this study.

	RCM 1	RCM 2	RCM 3
Nr of columns	75	128	176
Nr of rows	75	113	178
Column spacing	0.27	0.27	0.27
Row spacing	0.27	0.27	0.27
First latitude	9.77	14.90	29.48
First longitude	170.00	161.90	155.15
Pole latitude	48.00	48.00	48.00
Pole longitude	176.00	176.00	176.00

Table 1. The characteristics of the three different regional domains.

presented in Fig. 1 and their domain characteristics are in Table 1. The GCM ran for 30 years for the years 1971-2000 with SST and sea ice forcing derived from hadISST1.1, and the RCMs ran over the four years of 1986-1989. This period was chosen so that both the summer of 1986/87 and 1988/89 were covered in the simulation. These particular periods were characterised by an El Niño and a La Niña respectively. HadISST SSTs and NCEP/NCAR reanalysis 500hPa geopotential heights were used in comparing the seasonal fields from the RCM simulations. Observed data from NIWA's Climate Database (CLIDB) were also used to examine biases in the model simulations. Daily data for precipitation and

maximum and minimum temperature for the 1986-1989 period were taken from the 0.05° by 0.05° gridded data set developed by Andrew Tait, NIWA.

For the purposes of intercomparison the smallest regional domain (RCM 1) was extracted from the two larger regional domains. The GCM was rotated along the same rotated pole as the RCMs and the regional domain of RCM 1 was then also extracted. The climatologies of the RCM 1 domain in the three different RCMs were compared against each other and against the GCM climatology of that area.

A number of fields were used to investigate any differences in the RCM simulations, examining both mean and variability. The seasonal mean fields assessed were: 500hPa geopotential height, skin temperature and precipitation. The daily fields assessed were: minimum and maximum surface air temperature (1.5 m), and precipitation.

## Results

For each regional domain, only the area the size of RCM 1 is presented. Differences between the RCM's mean seasonal 500hPa geopotential heights and the GCM are very small (Fig. 2). The differences are largest for the larger domain(s). The further a grid point is away from its regional boundary, the more it is affected by the regional dynamics, hence is more likely to

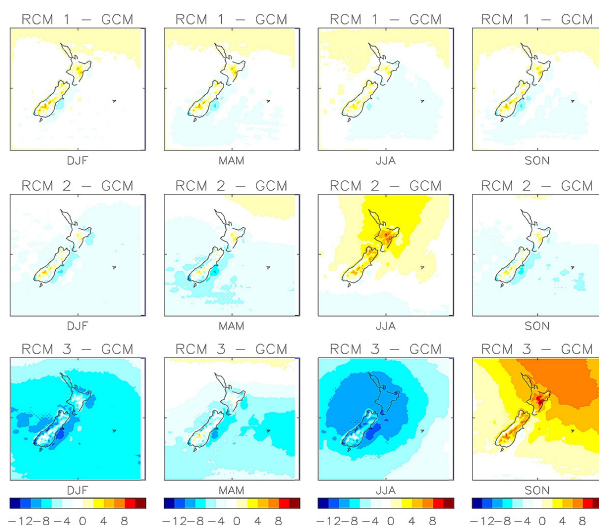


Fig. 2 Seasonal 500hPa geopotential height differences (m) between the GCM and RCMs .

deviate from the GCM's value. This is even more apparent when comparing the standard deviation of the monthly fields (not shown). However, applying student t-tests to the differences in the standard deviations between the GCM and the RCMs indicate that these differences are not significant at the 90% level (not shown).

Although the climatology of the middle troposphere as modelled by the regional models does not differ much from the one obtained by using the GCM, it is at the surface where we will notice enhanced detail, and hence the reason for the downscaling. The effect of the higher resolution of the orography is particularly apparent in both precipitation and surface temperature.

The mean seasonal precipitation does not differ much between the regional models and all seem to simulate the effect of the orography on precipitation correctly (not shown). The main differences between the mean seasonal precipitation patterns of the RCMs and the GCM can be found in the South Island. The RCMs show higher/lower precipitation to the west/east of the Southern Alps (not shown). Student t-test analysis shows that the differences between the monthly mean fields (grouped by season, Fig. 3) of the RCM and the GCM are significant at the 99.9% level for most of the South Island, and especially over those areas that are affected the most by the higher resolution of the orography. The larger variation in the differences between the standard deviation of the monthly mean fields (Fig. 3) of the RCMs with the GCM could possibly indicate the different modelled stormtracks for each regional domain. This is of concern. If the larger regional domains have a tendency to simulate more/stronger/deeper low pressure zones, it could result in different characteristics for precipitation over New Zealand. The abrupt "structures" at the boundaries of RCM 1 are related to the "smoothing" of the boundary conditions and have no real physical meaning.

All models produce a very similar pattern in the standard deviation of the daily precipitation to the pattern in the CLIDB (not shown). The largest variability is found over the Southern

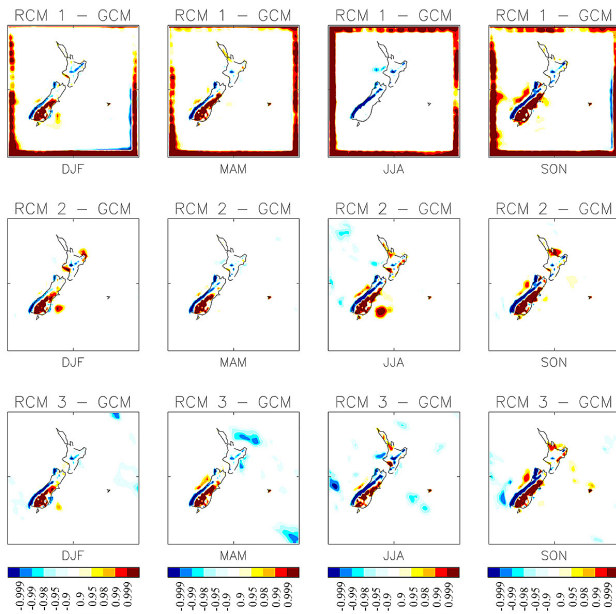


Fig. 3 Student t-test analysis for the differences in the standard deviation of the mean monthly precipitation (mm) for the RCMs and the GCM over the RCM 1 region.

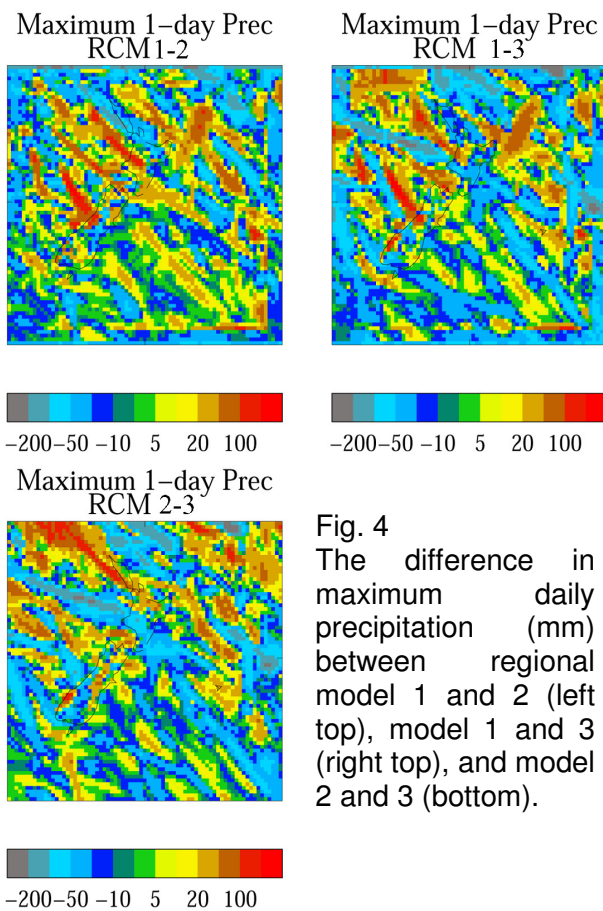


Fig. 4 The difference in maximum daily precipitation (mm) between regional model 1 and 2 (left top), model 1 and 3 (right top), and model 2 and 3 (bottom).

Alps, but minor maxima over the East Cape, Coromandel, Volcanic Plateau and the Tararuas show up as well, albeit that their extent and size do vary. The modelled variability along the coastal regions of Canterbury, as well as over most of Otago and Southland, is slightly too low. The largest anomalies are found over the Southern Alps, but are likely to be linked to the different heights and location of the interpolated data of the RCM and the recorded height of the data in the CLIDB. This is most apparent for the large anomaly over Mt Egmont (not shown).

Although the daily variability in precipitation in each simulation is very similar (not shown), there is the concern on how the internal dynamics of the larger regional domains could influence the stormtracks. Stormtracks, and the ensuing precipitation patterns in the smaller regional domain(s), are primarily introduced by the boundary conditions of the GCM. The dynamics of the larger regional domain(s) could have enough impact to alter the stormtracks and in doing so alter the landfall of the storms and the precipitation patterns over New Zealand. For that reason the maximum one-day precipitation and the average of the ten days of highest precipitation in the three regional simulations were analysed. Fig. 4 shows clearly the different “stormtracks” associated with the highest one-day precipitation events in each simulation. Each regional domain has its own pattern but since these simulations cannot be compared against observational data, it is not possible to conclude that any one model is better than another in reproducing these events. Comparing these patterns between each model does not indicate any obvious biases (not shown). Although it is obvious that on short time-scales each regional model has different precipitation patterns, when the average of the 10 highest precipitation events is taken (not shown), those differences have already become much less. On climatological time scales these differences are reduced even more and the size of the regional domain on the precipitation pattern in the New Zealand region will have little effect.

The differences in the mean seasonal skin temperature between the RCMs and the GCM are largest during the winter, and particularly over the Southern Alps and the north and south of the North Island (not shown). Compared to the GCM, the enhanced orography in the RCMs leads not only to lower skin temperatures in the mountain areas, but also to higher skin temperatures to the east of the mountain ranges (not shown). The latter is particularly clear during DJF. The largest differences between the standard deviation of the skin temperature of

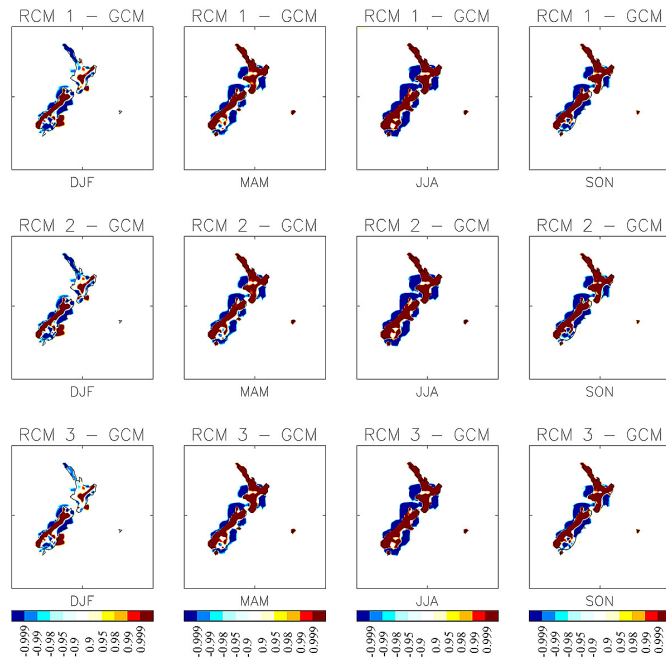


Fig. 5 Student t-test analysis for the differences in the standard deviation of the mean monthly skin temperature ( $^{\circ}\text{C}$ ) for the RCMs and the GCM over the RCM 1 region.

of the RCMs and the GCM occur during DJF and seem to increase for the larger regional domains (not shown). The differences between the monthly mean fields (grouped by season) of the RCM and the GCM are significant at the 99.9% level for almost the whole country (Fig. 5). Large significance values along the coast, particularly north of Taranaki and in north-west Nelson, are resolution and interpolation effects. Those points really compare warm SSTs of the RCM with cold landpoints in the GCM. Standard deviation patterns of daily maximum temperature are quite similar to those of the CLIDB data. However, Standard deviation patterns of daily minimum temperature are slightly too high over the South Island, in particular over the Southern Alps and Southland (not shown).

Although this study included both an El Nino and a La Nina year, due to the fact that the GCM did not simulate the westerly flow over the New Zealand correctly during those periods, the regional models were not able to correctly simulate the effect on precipitation over New Zealand during those ENSO periods (not shown).

# Regional climate modelling in New Zealand using the Unified Model

Sam Dean, James Renwick and Brett Mullan

*National Institute of Water and Atmospheric Research (NIWA),  
Wellington, New Zealand*

## Introduction

The National Institute of Water and Atmospheric Research (NIWA) has been using the Unified Model climate modelling system developed by the UK Met Office for over 10 years. This work has mostly focused on the development of a regional climate model (RCM) for current, future and paleo-climate simulations. The RCM is identical in its physics setup to the PRECIS modelling system (Jones et al., 2004). However, the global climate model (GCM) HadAM3P is also run locally at NIWA to generate boundary conditions for the RCM. The global model is analysed using many different techniques, including cyclone tracking, in order to better understand the simulated large scale Southern Hemisphere dynamics that drive the RCM.

In early simulations, Renwick et al. (1998) showed that the skill of simulating New Zealand's climate did increase noticeably when nesting an RCM inside a GCM. Subsequently, Drost et al. (2007) compared a preindustrial simulation of the RCM with regional observations averaged from station data. The largest anomalies occurred over the Southern Alps, where modelled temperatures were too low and where the amount of precipitation was too high. Many parts of the east coasts in both the North and South Island were simulated to be too warm and too dry.

In this paper we update the analysis of Drost et al. (2007), but using a current climate simulation (1970-2000) where the global atmospheric climate model is driven by observed SSTs. The observational dataset is on a  $0.27^\circ$  latitude/longitude grid covering all of New Zealand for a 29-year period (1972—2000). For temperature the data is interpolated using a fixed adiabatic lapse rate. The construction of the rainfall dataset is described in Tait et al. (2006). In brief, the daily rainfall surface (referred to as VClim in this paper) is estimated using a second order derivative trivariate thin plate smoothing spline interpolation model, incorporating the longitude and the latitude as location variables, and a mean annual rainfall variable. The interpolation is performed on a set of 128 climate stations with complete and reliable daily rainfall records. The disadvantage of this method is that it can often result in poor interpolation in areas with a low density network of climate stations, and can even miss an entire localized rainfall event. The data set has then been interpolated to the resolution of the regional climate model (~30 km) using a simple bilinear interpolation.

A number of future climate simulations have also been completed. Here we present results from future climate simulations of the RCM for a thirty year time slice from 2070 to 2100 for the A2 emissions scenario. Initial condition runs and a run under the B2 emissions scenario have also been completed, but are not considered in this extended abstract. Finally, we consider briefly the methodology used for creating the sea surface temperatures used in the future climate simulations.

## Results

### Control Simulations

Figure 1 compares the average daily maximum temperature between the CONTROL simulation of the RCM and the VClim gridded data. The model shows a negative bias of 1-3

degrees in most elevated regions. This may be partly due to the averaged topography of the RCM, but also may be partly due to the lack of high elevation station data and the fixed adiabatic lapse rate of used in generating VClim. Other studies have suggested that this value may be too low.

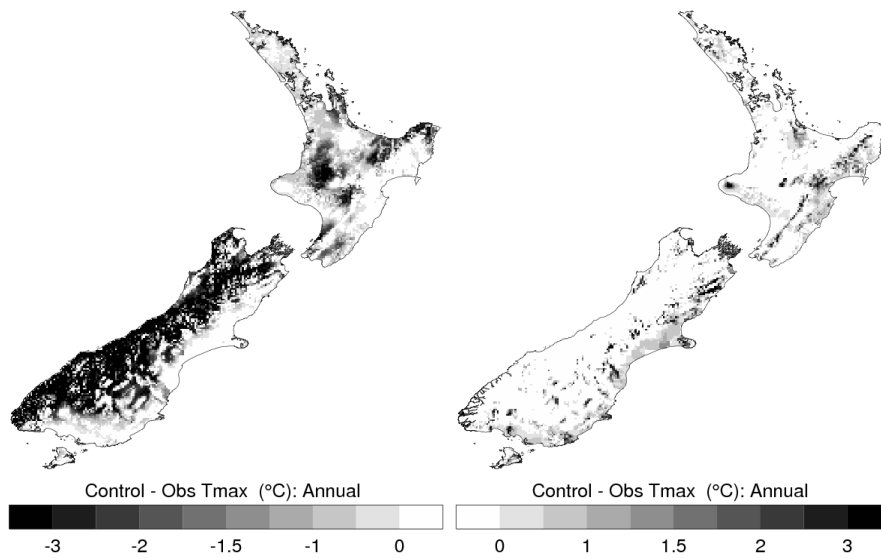


Fig 1: Difference in the average daily maximum temperature between the CONTROL simulation of the RCM and the VClim gridded data.

Precipitation biases shown in Fig 2 are more complex. The most significant difference is too little rainfall over almost all of the North Island. Given that the climatological rainfall in these areas is of the order of 10 mm per day this represents a deficit of 20-30%. In the South Island there is too much rain over the highest topography (beyond the scale of the figure) and too little at most lower elevations. Different methodologies have suggested that VClim underestimates rainfall at high altitudes (Tait et al., 2006).

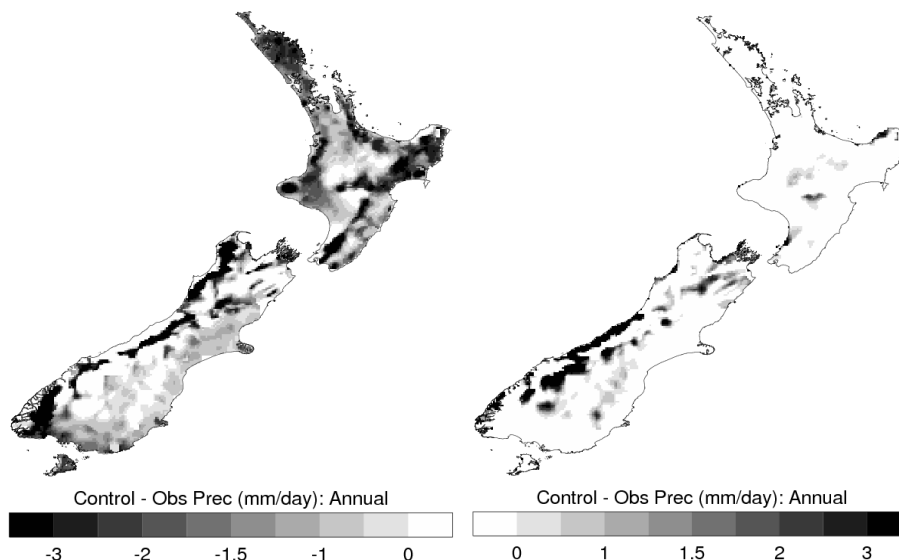


Fig 2: Difference in the average daily precipitation rate between the CONTROL simulation of the RCM and the VClim gridded data.

### Future simulations

A number of future climate simulations have been completed for two different emissions scenarios. Here we present changes in climate for the periods 2071-2100 relative to 1971-2000 for just one representative simulation under the A2 emissions scenario. In Fig 3 it is apparent that much of the country warms by between 2 and 5 degrees. This is higher and less

homogeneous than previous predictions made for New Zealand using a statistical downscaling methodology. The reasons for this are illustrated further in Fig 4. Here the daily maximum temperature change in summer is compared with the associated changes in soil moisture and snow amount. It is apparent that, for the North Island at least, the largest temperature increases are associated with significant reductions in soil moisture, while in the South Island the greatest warming is associated with a complete loss of snow cover. These feedbacks are not captured by the statistical downscaling approach.

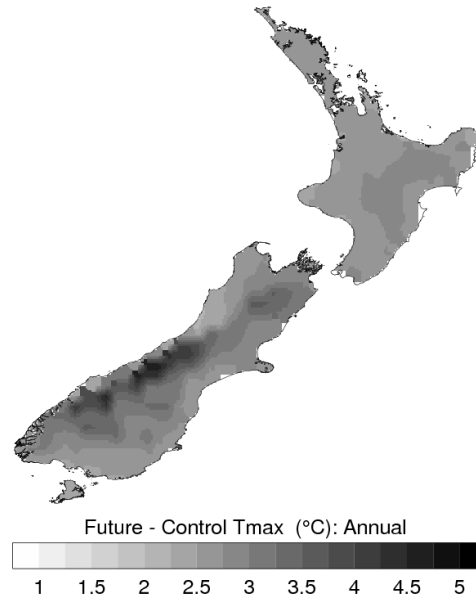


Fig 3: Change in the average daily maximum temperature simulated by the RCM for the 2080s compared to the 1980s under the A2 emissions scenario.

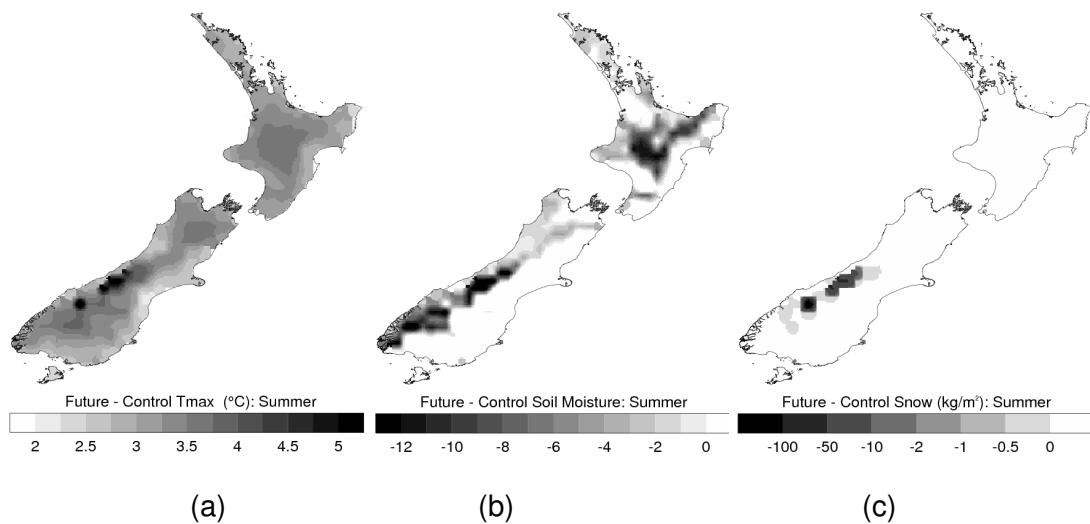


Fig 4: Change in the average maximum daily temperature for summer for the 2080s compare to the 1980s under the A2 emissions scenario (a) and the associated change in soil moisture (b) and snow amount (c).

In Fig 5 the change in precipitation is dominated by an increase on the west coast of the South Island. This increase is due to a significant increase in the westerly circulation in the winter season. Decreases are seen in the North Island due to decreased rainfall at all times of the year. A narrow band of decrease down the spine of the Southern Alps is associated with a large conversion of snowfall to rainfall and subsequently reduced transport of precipitation to the east.

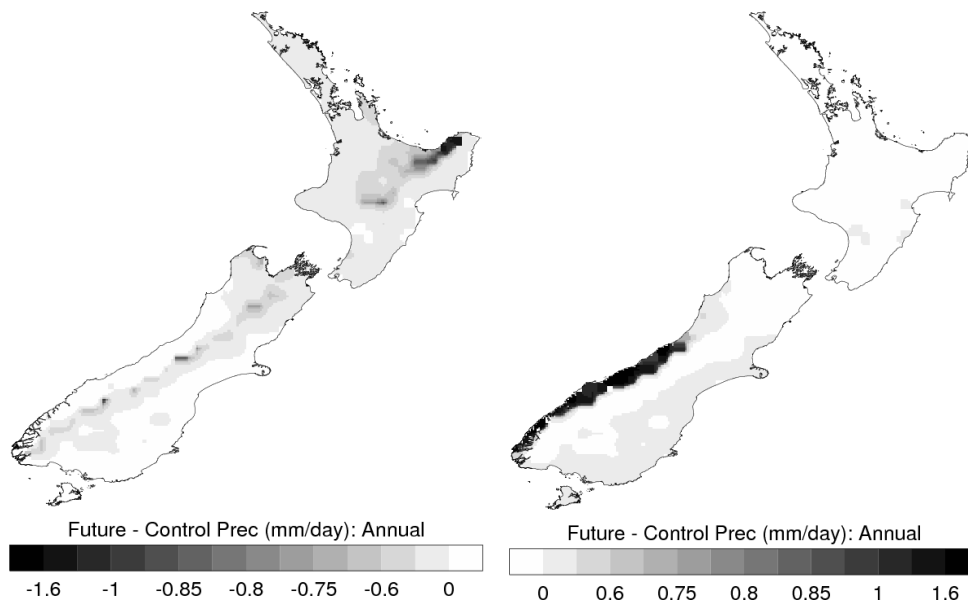


Fig 5: Change in the average daily precipitation rate simulated by the RCM for the 2080s compared to the 1980s under the A2 emissions scenario.

### Sea surface temperature biases

The ocean/atmosphere coupled climate model HadCM3 simulates a warm sea surface temperature (SST) bias in the New Zealand region. When an RCM of New Zealand is driven directly by HadCM3 SSTs there is a resultant warm bias in the RCM. The Met Office was aware of these regional biases in HadCM3 when developing the PRECIS regional modelling system and as such utilises a special SST and sea ice dataset for future climate simulations. Full details are given in Rowell (2005). In summary though, the dataset is constructed by first calculating the monthly climatological SST anomalies from the HadCM3 integrations and adding these to the observed HadISST1 data. Secondly the linear trend of the SSTs is adjusted to match that of the HadCM3 integration. This results in simulations with identical variability to the current climate, but with the warming relative to current climate as simulated by the GCM.

### Conclusion

In summary the regional climate model has been shown to offer new insight into climate processes that may be relevant to the impacts of climate change in this region. Work continues on investigating whether the simulated biases in the control simulation can be reduced.

### References

- Drost, F., J. Renwick, B. Bhaskaran, H. Oliver, and J. McGregor, 2007: Simulation of New Zealand's climate using a high-resolution nested regional climate model. *International Journal of Climatology*, **27**, 1153-1169.
- Jones, R.G., M. Noguera, D.C. Hassell, D. Hudson, S.S. Wilson, J. G.J., and J.F.B. Mitchell, 2004: Generating high resolution climate change scenarios using PRECIS, Met Office Hadley Centre, Exeter, UK, 40 pp.
- Renwick, J.A., J.J. Katzfey, K.C. Nguyen, and J.L. McGregor, 1998: Regional model simulations of New Zealand climate. *Journal of Geophysical Research D: Atmospheres*, **103**, 5973-5982.
- Rowell, D.P., 2005: A scenario of European climate change for the late twenty-first century: Seasonal means and interannual variability. *Climate Dynamics*, **25**, 837-849.
- Tait, A., R. Henderson, R. Turner, and X. Zheng, 2006: Thin plate smoothing spline interpolation of daily rainfall for New Zealand using a climatological rainfall surface. *International Journal of Climatology*, **26**, 2097-2115.

# A variety of tropical climate simulations using CCAM

John L. McGregor, Kim C. Nguyen and Jack J. Katzfey  
*Centre for Australian Weather and Climate Research  
PB1 Aspendale, Victoria 3195, Australia*

## Abstract

This presentation describes a number of climate simulations using CCAM, with an emphasis on tropical domains. The behaviour of tropical waves within CCAM is compared with that of other models by showing results from the aqua-planet intercomparison. Variable-resolution simulations of present-day climate over Asia and Indonesia are also presented, including some detailed diagnostics of the Asian monsoon. Finally, results are shown from a pilot simulation of climate change, performed over Fiji at 8 km resolution.

## Introduction

In recent years, it has become quite common to use limited-area models as regional climate models (RCMs), to downscale from GCM simulations (e.g. McGregor 1997, Wang et al. 2004), and this approach was used earlier at CSIRO with the DARLAM limited-area model. This is known as dynamical downscaling, and it can provide the detailed climate information needed for assessing a range of climate impacts.

A recent development is the use of variable-resolution GCMs as RCMs. An advantage is the avoidance of lateral boundary reflections, which can produce spurious vertical velocities and associated spurious rainfall near the boundaries of a limited-area model. This downscaling technique also avoids problems caused by the host and fine-scale climate models having different temperature or moisture biases.

This approach is currently used at CSIRO, downscaling with a variable-resolution global atmospheric model, the Conformal-Cubic Atmospheric Model (CCAM). CCAM may be run in stand-alone mode with modest stretching, or in a variety of nudged modes for stronger stretching (i.e. for small domains of interest).

The presentation will mainly show applications of the regional modelling system over the tropics. It is quite challenging to capture the behaviour of the Asian and equatorial monsoons, as they are strongly affected by both the treatment of convective parameterization and the

treatment of the high orography of the Tibetan plateau. The islands of the Maritime Continent also pose extra difficulties for simulating precipitation over the Indonesian region (Neale and Slingo 2003).

A brief description of the CCAM modelling system will be given, and then its tropical behaviour described in the context of the aquaplanet intercomparison. Next, the current CCAM downscaling methodologies are described. Results are then presented from a number of climate simulations performed over various tropical locations.

## Aquaplanet experiment

Because CCAM is a global atmospheric model, it is interesting to compare its tropical behaviour with that of other global models. Accordingly, we have participated for several years in the Aqua-Planet Experiment, as proposed by Neale and Hoskins (2000). This experiment compares about 10 GCMs employing their usual dynamics and physics, for 4-year simulations on an aquaplanet Earth, with prescribed sea surface temperature (SST) distributions. A selection of results will be shown from the intercomparison.

## Model description and downscaling

The Conformal-Cubic Atmospheric Model (CCAM) has been developed at CSIRO (McGregor 2005; McGregor and Dix 2001 2008), and includes a fairly comprehensive set of physical parameterizations, mostly similar to those of the Mk 3 GCM. The GFDL

parameterization for long-wave and short-wave radiation (Schwarzkopf and Fels 1991) is employed, with interactive cloud distributions determined by the liquid and ice-water scheme of Rotstain (1997). The model employs a stability-dependent boundary layer scheme based on Monin-Obukhov similarity theory (McGregor et al. 1993). A canopy scheme is included, as described by Kowalczyk et al. (1994), having six layers for soil temperatures, six layers for soil moisture (solving Richard's equation), and three layers for snow. The cumulus convection scheme uses mass-flux closure, as described by McGregor (2003), and includes both downdrafts and detrainment.

CCAM may be employed in quasi-uniform mode, or in stretched mode by utilising the Schmidt (1977) transformation. For modest grid stretching, e.g. to a 60 km grid, CCAM may be used to downscale directly from the sea-surface temperatures (SSTs) and sea-ice of a host coupled-atmosphere-ocean GCM (e.g., Engelbrecht et al. 2008). It should be noted that most current coupled GCMs do not employ flux corrections between atmosphere and ocean, and hence there are some biases of their present-day SSTs, up to 2 degrees near Australia, compared to observations. The CCAM simulations thus use the daily SSTs from the host GCM, but with the average monthly two-dimensional biases first subtracted.

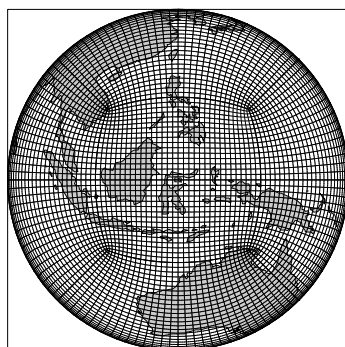


Fig. 1. The CCAM 60 km grid used for regional climate simulations over the Indonesian region, plotting every second grid point.

This moderately-stretched 60 km simulation may be further downscaled to say 15 km or 8 km resolution; for the finer

resolution simulations, broad-scale information is passed from the 60 km simulation, and this may be achieved by periodically (6- or 12-hourly) applying a scale-selective Gaussian digital filter (Thatcher and McGregor 2008).

### Some simulations

Many long climate-change simulations have been performed with CCAM over Australia at 60 km, 20 km and 14 km resolution, downscaling from the CSIRO Mk3 coupled GCM; results are shown during the presentation from several of these simulations. In addition, long simulations of present-day climate have been performed downscaling from NCEP reanalyses, to validate the methodology. CCAM has also taken part in other tropical projects: the regional model intercomparison project (RMIP) over Asia (Fu et al. 2005), tropical cyclone modelling (Nagata et al. 2000), and simulations at 14 km over the Mekong basin for an AIACC integrated assessment. The 60 km simulations over the RMIP domain provided a means of validating characteristics of the Asian monsoon within the model (Nguyen and McGregor 2008).

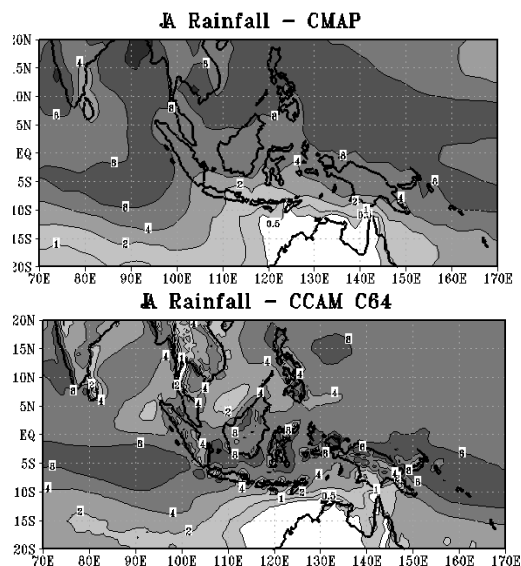


Fig. 2. Observed average rainfall for June-July-August (top, mm/day) and corresponding present-day simulated values from a trial CCAM simulation downscaling from the Mk3 GCM.

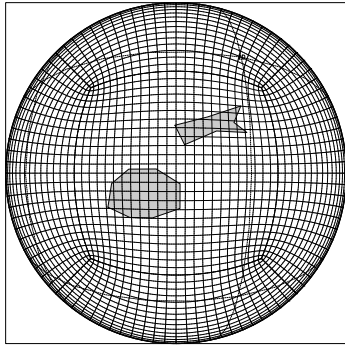


Fig. 3. The CCAM 8 km grid used for trial regional climate simulations over Fiji, plotting every second grid point.

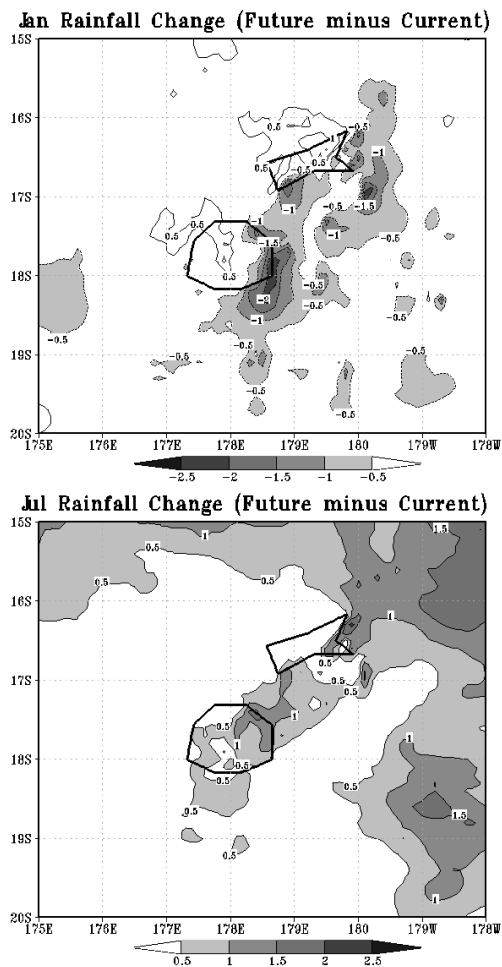


Fig. 4. Simulated average rainfall changes (2050 compared to present-day, mm/day) for Fiji from the trial climate-change simulations for January (top, decreases shaded) and July (bottom, increases shaded).

A separate set of 60 km resolution climate-change simulations is presently being performed over the Indonesian region, downscaling from six GCMs from

the IPCC Fourth Assessment. Figure 1 shows the grid being used for the simulations. A pilot simulation has been performed downscaling from the CSIRO Mk 3.5 coupled GCM. Preliminary results for the observed and simulated present-day June-July-August average seasonal rainfall are shown in Figure 2. Reasonable rainfall patterns are produced over Indonesia, although dry biases can be seen north of Indonesia.

CCAM has also been used in a 10-year simulation at 8 km resolution to downscale NCEP reanalyses over Fiji (Lal et al. 2008). Figure 3 shows the model grid. A preliminary climate-change simulation has also been performed over Fiji, downscaling from the Mk 3.5 GCM for 10 present-day Januarys and Julys and also for 10 future Januarys and Julys (centred on 2050). Note that coupled GCMs tend to have large directional errors in their simulated trade winds over the Pacific islands, related to the common “cold-tongue” SST bias over the equator in coupled GCMs. We consider that it is particularly important for these simulations, that a bias correction of the monthly SSTs be first performed. The simulated changes in rainfall are shown in Figure 4. The January reduction in rainfall on the east coast of the main island of Viti Levu is consistent with the trade winds becoming more northerly. The general increase in July rainfall is consistent with stronger easterly trade winds. Note that although these Fiji simulations are highly preliminary, they demonstrate the feasibility of simulating atmospheric climate change responses over small islands.

### Concluding comments

This presentation describes a methodology for dynamically downscaling coupled atmosphere-ocean GCMs to fine regional scale, including island domains. Examples of long climate-change simulations were provided over Australia, and preliminary results shown for simulations over Indonesia and Fiji. With advances in both computational power and downscaling techniques, it has now become feasible to provide downscaled ensembles from a range of coupled GCMs. This should

provide valuable insights into the range of likely climate-change scenarios.

### Acknowledgements

The authors acknowledge the assistance of Martin Dix, Eva Kowalczyk and Marcus Thatcher with various aspects of these simulations.

### References

- Engelbrecht, F.A., McGregor J.L. and Engelbrecht, C.J. 2008. Dynamics of the Conformal-Cubic Atmospheric Model projected climate change signal over southern Africa. To appear in *Int. J. Climatol.*
- Fu, C., Wang, S., Xiong, Z., Gutowski, W.J., Lee, D.-K., McGregor, J.L., Sato, Y., Kato, H., Kim, J.-W. and Suh, M.-S. 2005. Regional Climate Model Intercomparison Project for Asia. *Bull. Amer. Meteor. Soc.*, 86, 257-266.
- Kowalczyk E.A., Garratt, J.R. and Krummel, P.B. 1994. Implementation of a soil-canopy scheme into the CSIRO GCM - regional aspects of the model response. CSIRO Div. Atmospheric Research Tech Paper No. 32, 59 pp.
- Lal, M., McGregor, J.L. and Nguyen, K.C. 2008. Very high-resolution climate simulation over Fiji using a global variable-resolution model. *Climate Dynamics*, 30, 293-305.
- McGregor, J.L., Gordon, H.B. Watterson, I.G. Dix, M.R. and Rotstayn, L.D. 1993. The CSIRO 9-level atmospheric general circulation model. CSIRO Div. Atmospheric Research Tech. Paper No. 26, 89 pp.
- McGregor, J.L. 1997. Regional climate modelling. *Meteor. Atmos. Phys.*, 63, 105-117.
- McGregor, J.L. 2003. A new convection scheme using a simple closure. In "Current issues in the parameterization of convection", BMRC Research Report 93, 33-36.
- McGregor, J.L. 2005. C-CAM: Geometric aspects and dynamical formulation [electronic publication]. CSIRO Atmospheric Research Tech. Paper No. 70, 43 pp.
- McGregor, J.L. and Dix, M.R. 2001. The CSIRO conformal-cubic atmospheric GCM. In IUTAM Symposium on Advances in Mathematical Modelling of Atmosphere and Ocean Dynamics, P. F. Hodnett (Ed.), Kluwer, Dordrecht, 197-202.
- McGregor, J.L. and Dix, M.R. 2008. An updated description of the Conformal-Cubic Atmospheric Model. In High Resolution Simulation of the Atmosphere and Ocean, eds. K. Hamilton and W. Ohfuchi, Springer, 51-76.
- Nagata, M., Leslie, L., Kurihara, Y., et al. 2000. Third COMPARE Workshop: A model intercomparison experiment of tropical cyclone intensity and track prediction 13-15 December 1999, Tokyo, Japan. *Bull. Amer. Meteor. Soc.*, 82, 2007-2020.
- Neale, R.B. and Hoskins, B.J. 2000. A standard test for AGCMs including their physical parametrizations: I: The proposal. *Atmos. Sci. Let.*, 1, 101-107.
- Neale, R.B. and Slingo, J.M. 2003. The Maritime Continent and its role in the global climate: A GCM study. *J. Climate*, 16, 834-848.
- Nguyen, K.C. and McGregor, J.L. 2008. Modelling the East Asian summer monsoon using CCAM. To appear in *Climate Dynamics*.
- Rotstayn, L.D. 1997. A physically based scheme for the treatment of stratiform clouds and precipitation in large-scale models. I: Description and evaluation of the microphysical processes. *Q. J. R. Meteorol. Soc.*, 123, 1227-1282.
- Schmidt, F. 1977. Variable fine mesh in spectral global model. *Beitr. Phys. Atmos.*, 50, 211-217.
- Schwarzkopf, M.D. and Fels, S.B. 1991. The simplified exchange method revisited: An accurate, rapid method for computation of infrared cooling rates and fluxes. *J. Geophys. Res.*, 96, 9075-9096.
- Thatcher, M., and McGregor, J.L. 2008. Using a scale-selective filter for dynamical downscaling with the conformal cubic atmospheric model. Accepted by *Mon. Wea. Rev.*
- Wang, Y., Leung, L.R., McGregor, J.L., Lee, D.-K., Wang, W.-C., Ding, Y. and Kimura, F. 2004. Regional climate modeling: progress, challenges, and prospects. *J. Meteor. Soc. Japan*, 82, 1599-2004.

# Climate change and its impact on extreme rainfall in SE Australia

Debbie Abbs and Tony Rafter  
Centre for Australian Weather and Climate Research  
CSIRO Marine and Atmospheric Research,  
Private Bag 1, Aspendale, Victoria 3195  
Email: [Deborah.Abbs@csiro.au](mailto:Deborah.Abbs@csiro.au)

## Introduction

Each year extreme rainfall events cause significant flood damage in the highly urbanised regions along Australia's eastern coastline. This coastline is also subject to high population growth, with one-quarter of Australia's total increase in population between 1991 and 1996 accommodated within three kilometres of the coast. The Third Assessment Report of the IPCC states "*Precipitation extremes are projected to increase more than the mean and the intensity of precipitation events are projected to increase. The frequency of extreme precipitation events is projected to increase almost everywhere.*" This means that the community's exposure to extreme rainfall events is growing rapidly. In addition, flooding due to severe rainfall may be exacerbated if downstream water levels are elevated due to wind generated storm surge and wave set-up. Thus, there is a need to provide high-resolution extreme rainfall scenarios if projected climate change is to be factored into major infrastructure projects that are being designed to last for decades. These scenarios also require an understanding of the degree to which extreme rain and extreme sea level events overlap is required if effective flood plain modelling is to be undertaken. Furthermore, knowledge of the possible future changes in the nature of extreme rain and extreme sea levels and their coincidence is necessary for long-term flood plain management.

This paper presents results from recent CAWCR studies of climate change impacts on extreme rainfall and extreme sea levels and describes how stakeholders are using the results from our research to inform their long term planning for locations in Queensland, New South Wales and Victoria.

## Background

Information about extreme rainfall intensity and frequency for event-durations ranging from hours to multiple days is commonly needed for use in flood impact, design and mitigation applications. Flood impact models also rely upon information about how rapidly the average rainfall intensity increases with decreasing area, i.e. depth-area curves. These relationships are likely to be altered by climate change.

Quantifying likely changes in the behaviour of extreme rainfall events involves identifying possible changes in the weather systems that affect the region of interest and then downscaling these events using dynamical modelling with a very fine spatial resolution (4 km) and temporal resolution (sub-hourly) and the application of statistical methods. The downscaling method used for this study involves the use of a hierarchy of climate models ranging from global climate models (GCM) with a grid spacing of ~200km, to regional climate models (RCM) with a grid-spacing between 60 and 20km and finally to a high-resolution model with a grid spacing of 4km. The advantage of downscaling is that it allows realistic representation of coastal and terrain effects that play an important part in the spatial distribution of rainfall in extreme events and it provides an improved representation of weather systems such as fronts and east coast lows. Downscaling also assumes that climate models are able to represent the observed statistical characteristics of the main rainfall producing weather systems and that they represent the "ingredients" conducive to high rainfall: (1) high moisture and a rapid ascent

rate, (2) high time-averaged precipitation efficiency and (3) a long duration of the precipitation-producing system.

It is also valuable to use the outputs from multiple models as each model produces a unique time-series of weather patterns that results in a climatology that may differ from the climate of other models. More 'value' is placed on the outputs from models that skilfully simulate the observed climate. The models chosen in this study are models that have been shown to skilfully simulate Australia's average climate and represent the weather patterns that produce extreme rainfall over south eastern Australia.

## Methodology

The first step in this study has been to downscale the output from 2 realisations of the CSIRO Global Climate Model using the CSIRO Cubic Conformal Atmospheric Model (CCAM). The SRES A2 scenario was used to define the greenhouse gas emissions through to 2100. The results from this system are hereafter referred to as either CC-Mk2 or CC-Mk3. Following this step, extreme rainfall events identified from the CC-Mk2 and CC-Mk3 output have been downscaled, with a grid spacing of 4 km for various study regions, using the Regional Atmospheric Modelling System (RAMS). RAMS is a high-resolution, compressible, non-hydrostatic model. The physical processes represented by the model include an atmospheric boundary layer, soil and vegetation effects, long and short wave radiation, and the complex cloud processes that result in precipitation (ice, liquid and water vapour). RAMS is a suitable tool for the simulation of extreme rainfall events and has previously been used to model the extreme rainfall events described in Abbs (1999) and McInnes *et al.* (2002). In the simulations discussed here the numerical model has been initialised using output from CC-Mk2 and CC-Mk3. Three levels of interactive grid nesting were used; the outer grid had a resolution of 48km with the middle and finest resolution grids having a horizontal grid spacing of 16 km and 4 km respectively. The terrain used on all model grids was interpolated from the Geosciences Australia 9 second digital elevation model. The vegetation was obtained from a USGS 30 second dataset. The sea surface temperatures were interpolated from the CC-Mk3 output.

## Results

The results presented here are for a study focussed on southeast Queensland and northern New South Wales. Results for south eastern Australia will be presented during the workshop.

The downscaled results from the 2 high-resolution climate runs show a number of similarities. By 2030 (not shown), both sets of model results are showing increases in the intensity of extreme rainfall events in the McPherson Range. This increase is most evident for the shorter duration events, especially the 2-hour events. Both sets of results show a decrease in extreme rainfall for the coastal regions north of Brisbane for the 2030 climate. By 2070 (not shown) the regional extent of this decrease has either decreased (CC-Mk2) or changed sign (CC-Mk3). Both models show large increases in the intensity of the short duration, 2-hour events by 2070.

The different spatial patterns of rainfall change make it difficult to determine areas of increase or decrease identified by most models and so the 2 sets of results have been simply averaged to identify regions likely to experience an increase/decrease in the intensity of extreme rainfall – a robust statistical treatment is currently being developed. The results from the averaging are shown in Figure 1. They show a broad region of increase in the mountainous region straddling the Queensland-New South Wales border for the 24-hour and 72-hour events. With time, the spatial extent of this area of increase enlarges and the embedded maxima increase in magnitude to values greater than 1.4 (i.e. a 40% average increase in the intensity of the most extreme events). The 2-hour rainfall events show much larger projected changes with the largest changes in the high terrain inland from the Gold Coast. The 2-hour rainfall events have average increases in intensity of more than 70% in these regions. For the durations considered, the region of rainfall increase also increases in spatial extent with time.

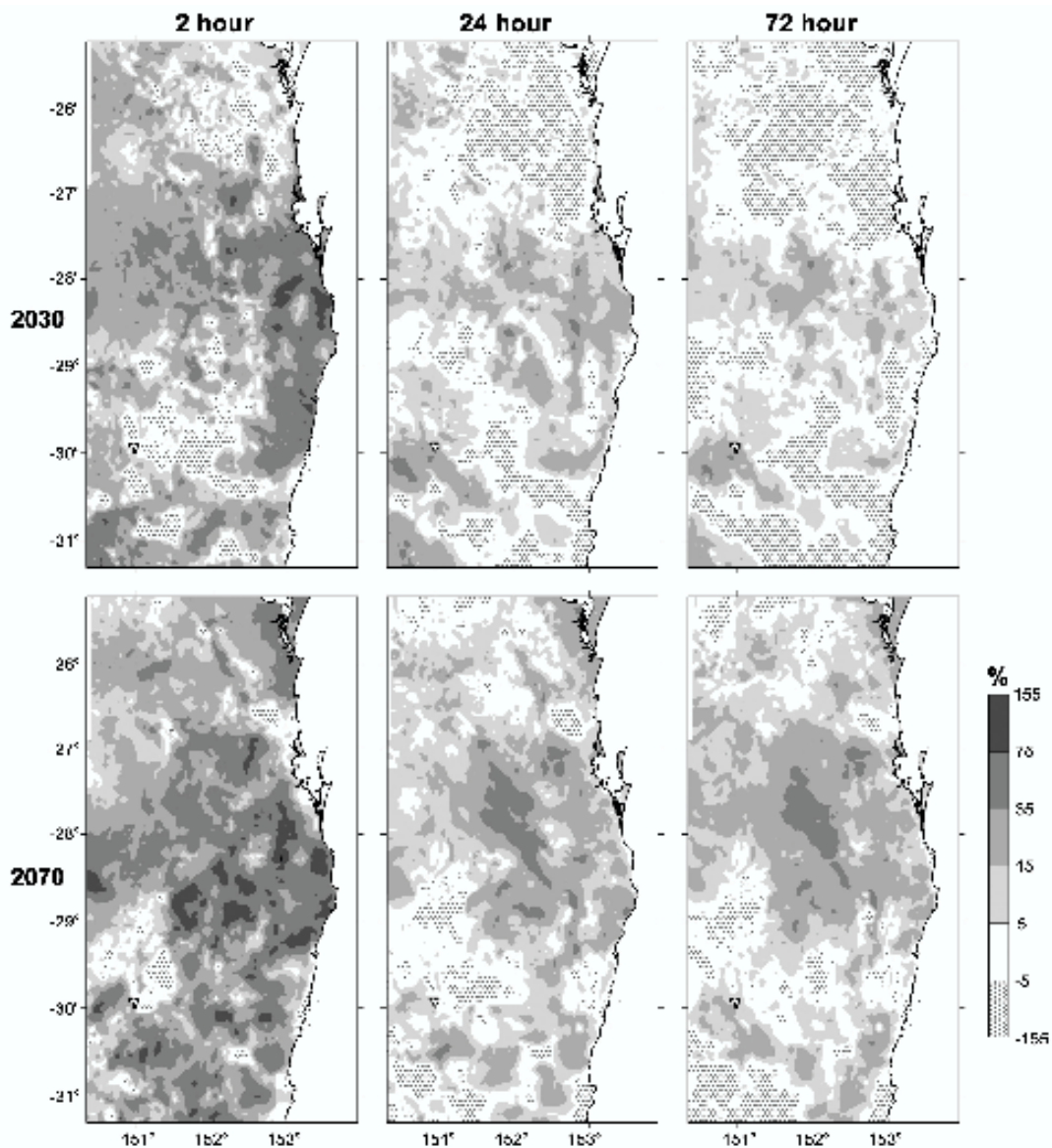


Figure 1: Mean projected change for 2030 and 2070 for the top 10% of modelled events (corresponding to a return period of 4 years or greater) for South-East Queensland and northern New South Wales. The results are based on a composite of the projected changes from CC-Mk2 and CC-Mk3 for extreme rainfall events of 2, 24 and 72 hours (vertical columns). Shading indicates regions of projected increases and stippling regions of decrease.

It is interesting to consider the value that the high-resolution downscaling adds to climate model projections. The average fractional change from the 65-km parent-model, CC-Mk2 and CC-MK3, simulations has been examined. These results show broad qualitative agreement with the results presented in Figure 3. They show a region of extreme rainfall decrease to the north of Brisbane and a tendency for extreme rainfall to increase in intensity with time. However, there are also some notable differences. The 65-km model results do not capture the increases in rainfall intensity projected for the McPherson Range nor the localized maxima that are projected for the Great Dividing Range west of Brisbane by 2070. These projected, localized maxima occur in the headwaters of the Brisbane and Albert-Logan River systems and are likely to result in significant increases in flooding for these rivers.

## Application

Various stakeholder groups are now starting to use the results from this research to inform decision making for planning and infrastructure projects into the future. The Gold Coast City has extensive flood plains and a large population that is exposed to the threat of flooding. The major exposure is in the Nerang River floodplain which contains almost 60,000 dwellings, 40% being flood prone. A GIS-based flood damage model has been developed by the Gold Coast City Council to assess the economic benefits of proposed flood mitigation options and to assess proposed flood plain developments (Betts 2002). Flood damage models estimate flood damage to building structures based on the depth of over-floor flooding, duration of the inundation, velocity of the floodwaters and the types of building material. The Council is now using this model coupled with CSIRO projections of changes in extreme rainfall to identify possible impacts of climate change on flood risk in the Nerang catchment (Rahman 2007). Their study found that for a 20% increase in rainfall, the number of properties affected by the 100-year flood event increased from the current 4500 residential properties to 7000 properties. The direct damage to properties from floodwaters entering the residences increased from \$160M to \$230M. A similar study for flooding of the Albert-Logan catchment (Abbs, McInnes and Trinidad, unpublished) found that damages due to flooding more than doubled when a 20% increase in rainfall was combined with sea-level rise of 20 cm or more. Awareness of the changed flood risk enables the council to implement new flood mitigation strategies, respond through land-use planning, minimise future risk in emergencies and to engage with and educate the community. Consideration of climate change based upon the best available information is a fundamental part of informed flood risk management and thus needs to be incorporated into management plans as they are developed or reviewed, as do strategic risk management decisions in relation to future developments and decisions on mitigation works. There are a number of ways (McLuckie *et al.* 2006) in which additional adaptive capacity can be built into these decisions. Studies such as that above suggest a possible need for changes in zoning, building regulations and evacuation procedures if the exposure of Australian communities to flood risk is not to be significantly increased in the future.

## References

- Abbs DJ (1999). A numerical modeling study to investigate the assumptions used in the calculation of probable maximum precipitation. *Water Resour. Res.*, **35**, 785-796.
- Betts H (2002). Flood damage analysis using GIS at Gold Coast City Council, *Australian Journal of Emergency Management* **17**, 33–37.
- McInness K, Hubbert G, Abbs D and Oliver S (2002). A Numerical Modelling Study of Coastal Flooding. *Meteorol. Atmos. Phys.*, **80**, 217-233.
- McLuckie D, Lord D & Gibbs J (2006). Climate change – the future is uncertain. 46<sup>th</sup> NSW Floodplain Management Authorities Conference, Lismore, 28 February-2 March, 2006.
- Rahman K (2007). Flood management initiatives in the Gold Coast. Presentation at the Coastal Cities Natural Disasters – Sydney Conference. 20–21 February 2007.  
<<http://www.conferenceworld.com.au/resources/other/7%20Khondker%20Rahman%20ppt.pdf>>

# Simulation of rainfall and pan evaporation over Australia

Kim C. Nguyen and John L. McGregor

*Centre for Australian Weather and Climate Research: a partnership between CSIRO and the Bureau of Meteorology, PB1 Aspendale, Victoria 3195, Australia*

## Abstract

A 55-year mean (1951-2005) climatology of Australia is studied using the CSIRO Conformal-Cubic Atmospheric Model (CCAM) to downscale the CSIRO NCEP Reanalysis 1. The skill of the model is investigated in simulating rainfall variability and pan evaporation over the Australian continent.

## Model simulation

A 55-year simulation from January 1951 to December 2005 was carried out with initial conditions, sea surface temperatures (SSTs) and winds provided by the NCEP-1 reanalyses (Kalnay et al., 1996). For the central high-resolution panel, weak global nudging of winds above 500 hPa from the large-scale reanalysis fields was employed, with an e-folding time of 24 h. Outside the central panel, gradually-increasing far-field nudging was employed for mean sea level pressures and for winds between 900 hPa and 500 hPa.

For calculating pan evaporation in the simulation, a pan water temperature is derived every model time step. This is determined by using the simulated latent heat flux from the surface of the pan, and sensible heat fluxes from the water surface, sides and bottom of the pan.

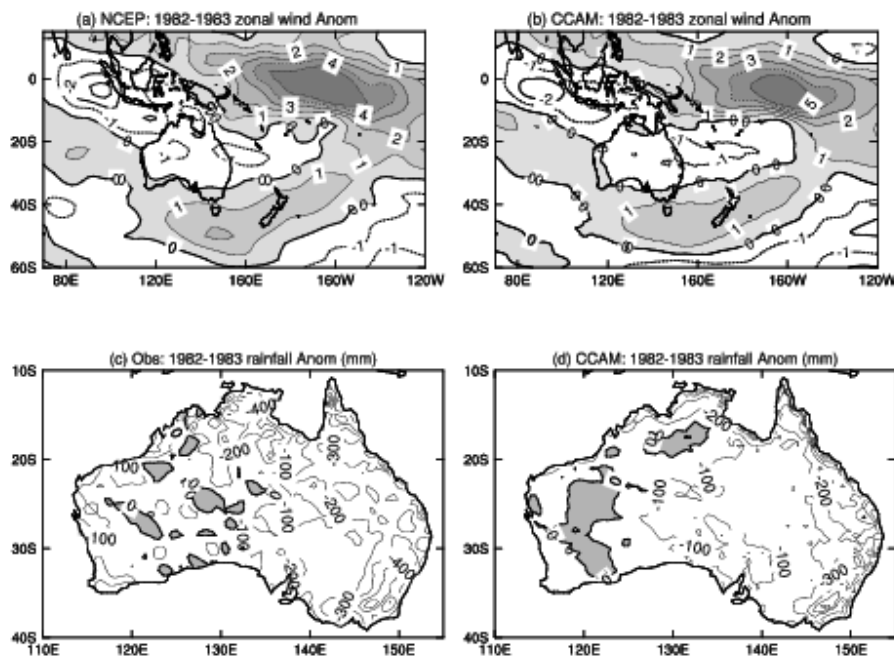


Fig 1: 850 hPa wind (m/s) and rainfall (mm/annum) anomalies for 1982/83 El Niño events: (a) NCEP wind, (b) CCAM wind, (c) observed rainfall and (d) CCAM rainfall, where positive anomalies are shaded.

## Relationship between ENSO and Australian rainfall

ENSO has direct influences on Australian rainfall (Suppiah 1993; Meehl and Arblaster 1998; Power et al. 1999). Under El Niño conditions, the wind over the western Pacific is weaker than normal due to the centre of

the convection cell or Walker circulation being shifted eastward towards the central or eastern Pacific (Vecchi et al. 2006). The warm/cold ENSO years chosen for the case study are 1982/83 and 2000/01, as shown in Figs 1 and 2. CCAM captures the strength and location of the wind anomaly and the rainfall pattern very well in both cases, where positive/negative anomalies depicts weakening/strengthening of the easterly trade winds. In the 2000/01 La Nina year (Figs 2c and 2d), CCAM successfully reproduces a dry region along the central south-east coast. However, there are some differences seen between the NCEP and CCAM winds in the 2000/01 La Nina event, where the CCAM winds are weaker than NCEP over the Australian tropics and over the western Pacific. Also, CCAM is unable to reproduce the dry conditions over the southwest and centre-south north of the Great Australian Bight and the intensification of dry (Figs 1c and 1d) and wet (Figs 2c and 2d) conditions in northern Australia.

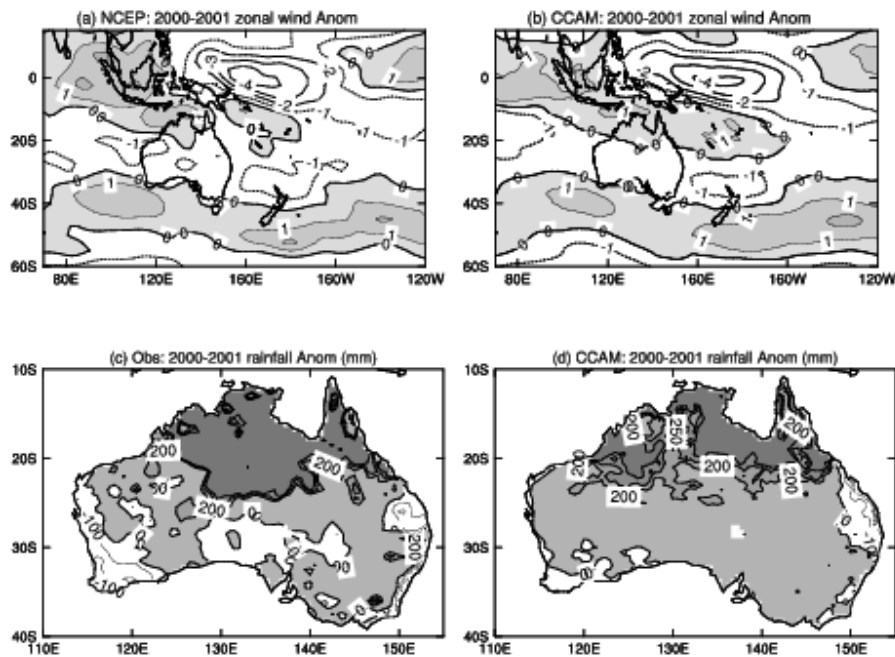


Fig 2: 850 hPa wind (m/s) and rainfall (mm/annum) anomalies for the 2000/01 La Nina event: (a) NCEP wind, (b) CCAM wind, (c) observed rainfall and (d) CCAM rainfall, where the positive anomalies are shaded.

## Pan evaporation

Roderick and Farquhar (2004) carried out a study of annual pan evaporation from 1975 to 2002 using 30 sites across Australia. They diagnosed an average decrease of annual pan evaporation of 3 mm/annum. They suggested that there was a decline in pan evaporation due to a decline in potential evaporation, as there has been an observed decrease in potential evaporation in many parts of the world. In terms of the surface energy balance, they suggested three possibilities to explain a decline in pan evaporation: decreases in one or more of vapour pressure deficit of air, net radiation, wind speed. Recently, Kirono et al. (2008) used 28 sites and monthly time scales across Australia from 1970 to 2004 to study the relationship of the trend between observed pan evaporation and point potential evaporation, as derived by the Morton method. Their study showed that there is a variation in trends from site to site and from month to month, and that the median trend is positive except in December. In another study, Jovanovic et al. (2008), used high-quality observations of monthly pan evaporation with appropriate inhomogeneity adjustment to study the long-term (1970-2005) trend of pan evaporation. Their findings showed that there is large interannual variability in Australian annual mean pan evaporation, but there was no trend over the study period.

Our current study describes an alternative evaluation, derived in the context of dynamically downscaling the Australian climate from the NCEP Reanalysis 1. We compare pan evaporation simulated by the model with the observed pan evaporation on annual time scales. The comparison is made at selected sites subject to observation availability. We try to explore all components that influence pan evaporation as mentioned above for the 1970-2005 periods.

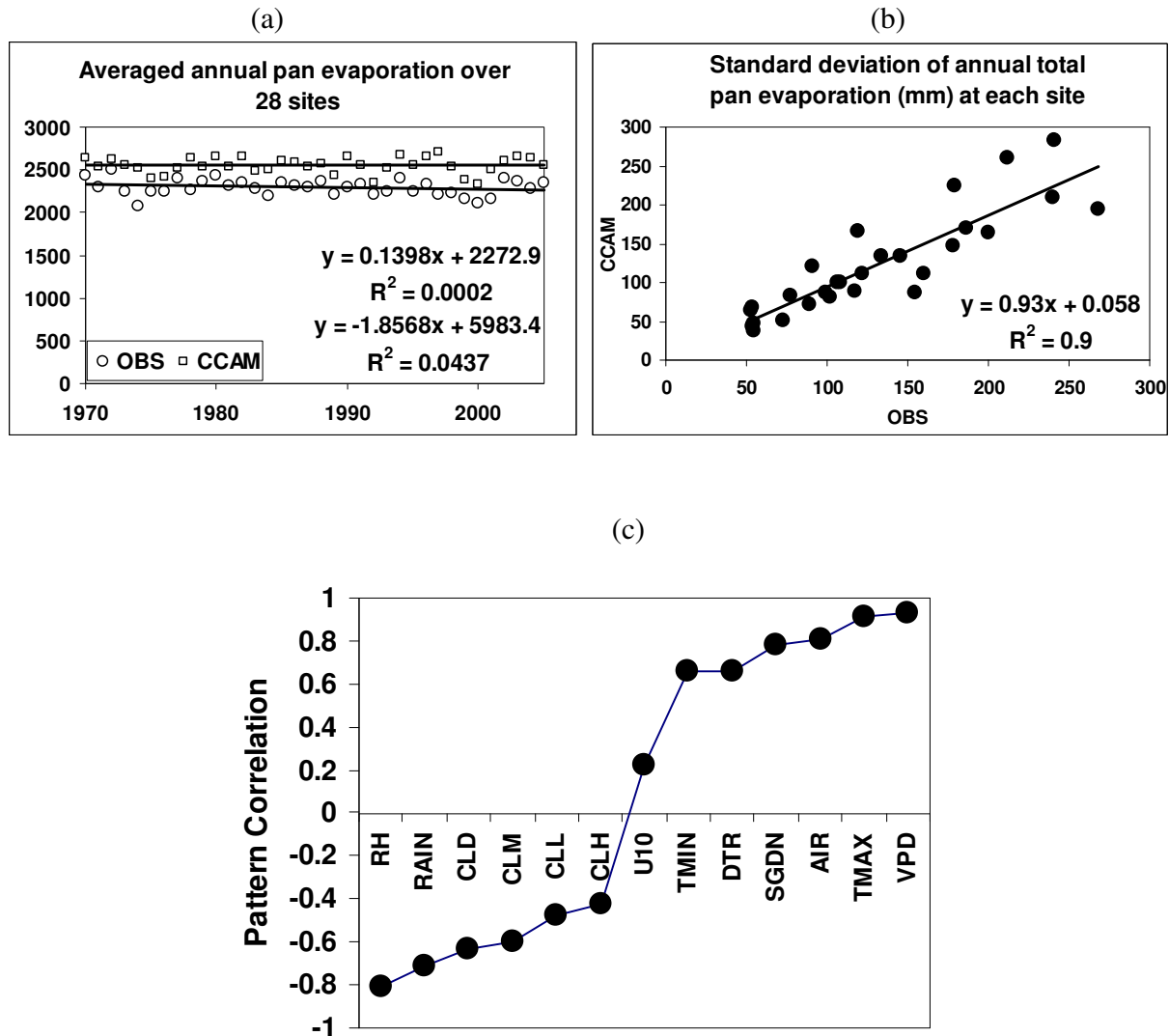


Fig 3. (a) Annual observed and CCAM pan evaporation (mm) averaged over 26 sites, (b) standard deviation of annual pan evaporation of CCAM against observations and (c) pattern correlation of annual pan evaporation with each of relative humidity (RH), total cloud cover (CLD), mid cloud (CLM), low cloud (CLL), high cloud (CLH), wind speed at 10 m (U10), screen minimum (TMIN) and maximum temperatures (TMAX), diurnal temperature range (DTR), net solar radiation at the surface (SGDN), air temperature at 2m (AIR) and vapour pressure deficit (VPD).

The model reproduces the observed pan evaporation reasonably well (Fig. 3a), although it slightly overestimates the observations. The observed pan evaporation shows a downward trend but it is insignificant ( $R^2$  is very small), while CCAM shows a very weak upward trend. Our conclusion is that there is no trend seen in either the observed or CCAM annual pan evaporation over the 26 sites used in this study. CCAM also

captures the interannual variability of pan evaporation well (Fig. 3b) with a correlation to the observations of about 0.95. Even though there is no trend in annual pan evaporation averaged over the 26 sites, there is some pattern of trend across the Australian continent (not shown). There is an upward trend of annual pan evaporation along the west coast and a downward trend over the north-east and central regions; this is mostly due to changes in the DJF and MAM seasons. The pattern correlation (Fig. 3c) shows that the trend in pan evaporation is mostly due to vapour pressure deficit (VPD) and net solar radiation (SGDN), both of which are related to screen temperatures and relative humidity (RH). The correlation of the pan evaporation and the diurnal temperature range (DTR) is about 0.65. The correlation with wind speed at 10m (U10) is about 0.2 which is lower than might be expected.

## References

- Allan R.J. and Haylock, M.R. 1993. Circulation features associated with the winter rainfall decrease in southwestern Australia. *J. Climate*, **6**, 1356-1367.
- Jovanovic, B., Jones, D. A. and Collins, D. 2008. A high-quality monthly pan evaporation dataset for Australia. *Climatic Change*, **87**, 517-535.
- Kirono, D.G.C., Jones, R.N. and Cleugh, H.A. 2008. Pan-evaporation measurements and Morton-point potential evaporation estimates in Australia: are their trends the same? *Int. J. Climatol.*, **28**, doi:[10.1002/joc.1731](https://doi.org/10.1002/joc.1731).
- Kalnay, E., Kanamitsu, M., Kistler, R., Collins, W., Deaven, D., Derber, J., Gandin, L., Iredell, M., Saha, S., White, G., Woollen, J., Zhu, Y., Chelliah, M., Ebisuzaki, W., Higgins, W., Janowiak, J., Mo, K.C., Ropelewski, C., Wang, J., Leetma, A., Reynolds, R., Jenne, R. and Joseph, D. 1996. The NCEP/NCAR 40-year reanalysis project. *Bull. Amer. Meteor. Soc.*, **77**, 437-471.
- Meehl, A.G. and Arblaster, J. 1998. The Asian-Australian monsoon and El Nino-Southern Oscillation in the NCAR Climate System Model., *J. Climate*, **11**, 1356-1385.
- Roderick, M.L. and Farquhar, G.L. 2004. Changes in Australian pan evaporation from 1970 to 2002. *Int. J. Climatol.*, **24**, 1077-1090.
- Suppiah, R. 1993. ENSO phenomenon and 30-50 day variability in the Australian summer monsoon rainfall. *Int. J. Climatol*, **13**, 837-851.

# **The effects of tides and wind forcing on the circulation within the Spencer Gulf**

Carlos E.P. Teixeira  
*SARDI Aquatic Sciences & University of New South Wales*

John F.F. Middleton  
*SARDI Aquatic Sciences*

We seek to determine the fundamental physics within Spencer Gulf (SG), Australia, of that driven by tides and local and remote ocean winds in the weather band (3-20 days). The remote effects are represented by Continental Shelf Waves (CSWs) entering the region. The problem is solved numerically using the ROMs model. The tidal model was forced using elevation and currents from the TPX06 global tidal model and the results compared with ANTT values. The wind experiments were forced with 10 days oscillatory zonal and meridional wind stress and the results compared with the analytical solutions following the analysis for a strait by Middleton (1991, JPO). With local winds forcing the model, the fundamental balance is between the wind stress and seal level gradient. Cross shore SW (NE) winds will generate a cyclonic (anti-cyclonic) circulation and raise (lower) water in the head of the gulf. Along shore NW (SE) winds will also results in a cyclonic (anti-cyclonic) circulation, but now the water will be raised in the east (west) side of the gulf. Even with strong winds (10 m/s), the currents are weak (less then 2 cm/s) in most part of the gulf when compared with tidal currents (20 cm/s). The remote forcing by CSWs from the GAB produces very weak currents (less than 1 cm/s) inside the gulf. The implications of the tides, wind and CSWs circulation on the dispersion of particles and nutrients will be discussed.

Carlos Teixeira - PhD Student



# High resolution modelling of swell propagation in the near shore environment

Matthew Collopy  
*Australian Bureau of Meteorology, South Australian Regional Office*

## Introduction

In this experiment SWAN (Simulating Waves Nearshore, developed by Delft Hydraulics) was used to simulate the propagation of swell from a boundary approximating the continental shelf into the complex coastal environment of the South Australian gulf system.

SWAN is a third-generation wave model for obtaining realistic estimates of wave parameters in coastal areas, lakes and estuaries from given wind, bottom and current conditions. SWAN functions by solving the spectral action balance equation without *a priori* restrictions on the spectrum for wave growth. This equation represents the effects of spatial propagation, refraction, shoaling, generation, dissipation and non-linear wave-wave interactions. SWAN uses formulations for source terms which are identical to WAM cycle 3 (WAMDI Group, 1998), however where WAM makes use of explicit propagation schemes in geographical and spectral space, SWAN (Booij *et al.*, 1999) employs implicit schemes, which are more robust and economic in shallow water.

SWAN was setup to run in stationary mode over a grid representing the SA Gulf system (Figure 1) with a resolution of 1 Nm, configured to account for relevant near shore physical processes including: shoaling, refraction, diffraction, bottom friction, currents and wave-wave interactions.

A range of incident swell sizes, directions and peak periods were modelled. Incident swell spectrum was set as a Gaussian distribution. Several physical processes were then included/excluded to investigate their effect on swell propagation over the model domain, these included: bottom friction (Hasselmann *et al.*, 1973, JONSWAP), tidal currents and varying water levels.

Model results for the SA Gulfs run were then compared with preliminary observational data from a bottom mounted wave recorder located in the near-shore environment of Gulf St Vincent (location shown in Figure 1). The other main data source for the experiment was the wave rider buoy located in deep water southwest of Cape du Couedic, Kangaroo Island.

## Results

SWAN results were obtained for a range of incident swell sizes, directions and periods, aiming to represent the spread of naturally occurring conditions over the domain. Incident ranges chosen were: height 1 to 6 meters, direction W, WSW, SW, SSW, S and periods from 10 to 18 seconds. A typical result for modelled significant wave height and direction is shown in Figure 1.

Model results from this range of incident swell conditions were obtained for the following parameters: significant wave heights, significant swell height (defined as the significant wave heights associated with the period greater than or equal to 10 seconds), mean wave period,

mean-wave direction, peak direction. Wind input was set to zero, and as such significant wave heights are representative of significant swell heights.

Model run performance in stationary-mode was satisfactory; convergence to approximately 98% of wet grid points was generally achieved in 10 to 12 iterations. This indicates some lack of convergence in the model solution, the reason for this is thought to be the complexity of the bathymetry over the domain.

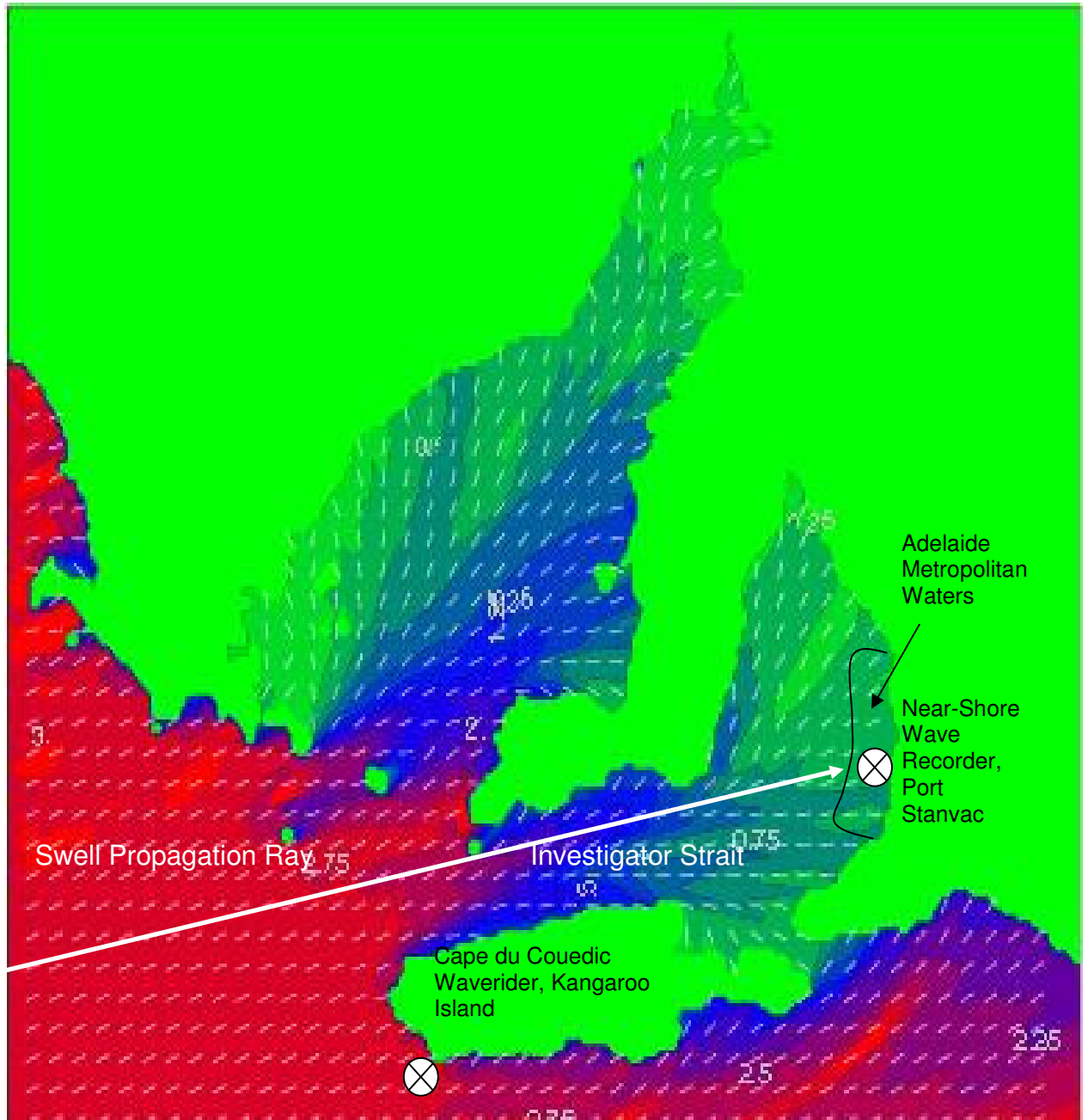


Figure 1: Map of model domain, with typical model 2D plot of wave height (m) and direction for 3 m WSW incident swell with 14-second period. Swell propagation ray also shown, along which model outputs parameters were obtained.

Preliminary results show a large variation in swell propagation to the near-shore area with incident swell direction and period, particularly for Gulf St Vincent. Figure 2 shows the variation of wave heights through Investigator Strait (along propagation ray) and into Gulf St Vincent for a range of incident swell direction. In the vicinity of the Adelaide Metropolitan

waters, the modelled difference in resultant wave heights between an incident westerly swell and a southerly case is approximately 85%.

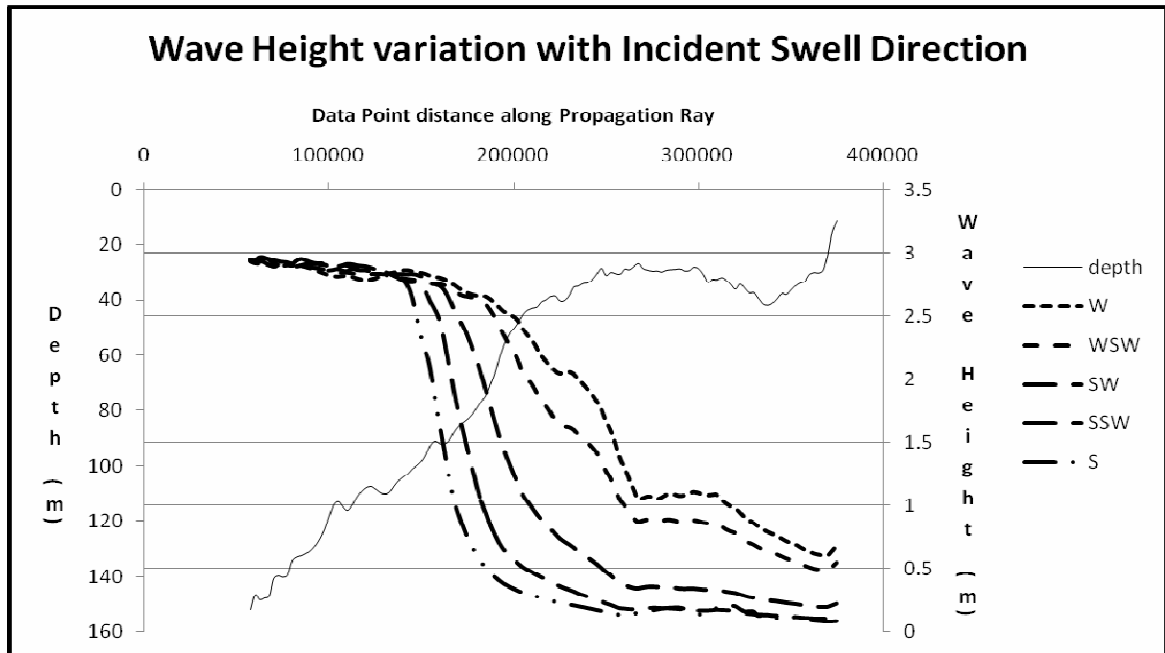


Figure 2: Modelled wave heights for W, WSW, SW, SSW and S incident swell directions, with 3 m 14 sec size and period.

Figure 3 shows modelled wave heights for a range of incident swell periods, with longer period swells resulting in lesser wave heights propagating through to the near-shore zone, than shorter period swells. It appears that the major reduction in modelled wave height due longer period incident swell occurs near the model boundary, i.e. at or near the continental shelf. This result requires further investigation and may be the result of model set-up conditions.

Figure 4 depicts model results for a range of physical processes which are thought to affect swell propagation through the model domain, including: water level (approximate 2 m tidal range of domain), dissipation due to bottom friction and currents (incoming/outgoing tidal currents). Water level over the entire domain was increased by 2 m to simulate the approximate difference between high and low tide, model results show a marginal increase in wave heights along the propagation ray, in the order of 5%. Typical tidal currents (derived from National Tidal Centre tide model) for large incoming/outgoing tides were input, figure 3 shows the percentage difference in wave heights along the propagation ray for incoming and outgoing tides. Model results indicate that wave heights in the near-shore area differ from the control case by approximately  $\pm 10\%$ , with higher wave heights for the incoming tide. Figure 4 also shows that the inclusion of bottom friction, with coefficient of friction set to the semi-empirically derived JONSWAP value of  $0.038 \text{ m}^2\text{s}^{-2}$  (Hasselmann et al., 1973, JONSWAP), has a significant effect on the propagation of wave energy through the domain, with approximately 40% lesser wave heights reaching the near-shore area.

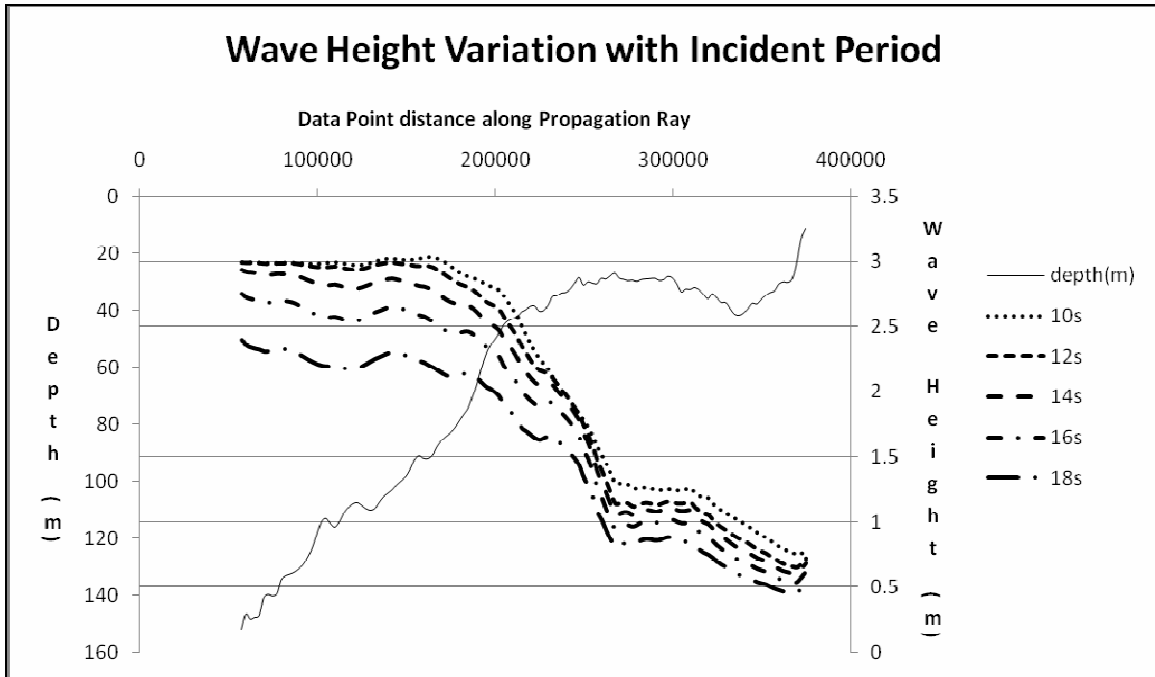


Figure 3: Modelled wave heights (along propagation ray) for range of incident swell periods.

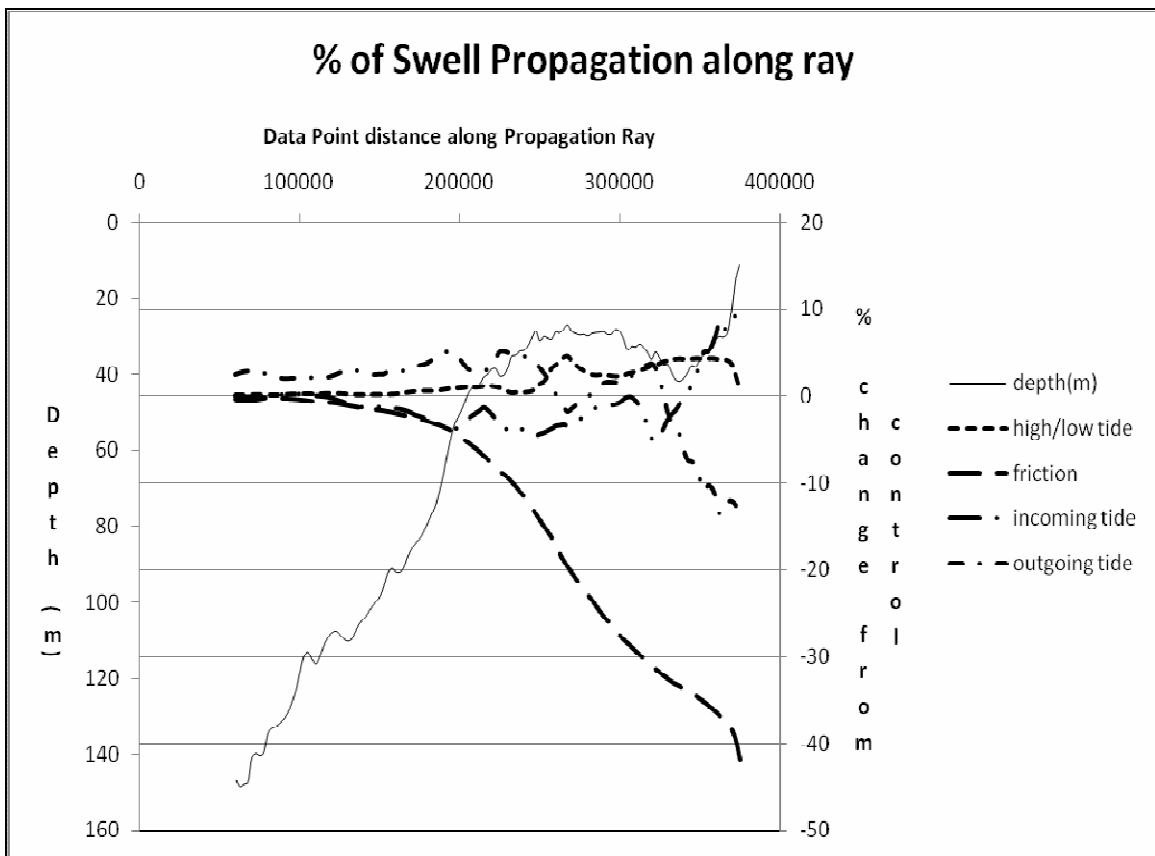


Figure 4: Percentage of wave height along propagation ray for a range of physical processes.

## Summary

Wave parameters for the South Australian gulf system were modelled using SWAN, run in stationary-mode with a grid resolution of 1 Nm. Wave parameters such as significant wave height, period and direction were output over the entire domain, as well as at selected points along a ray which approximated the passage of swell energy from the open ocean boundary, through Investigator Strait, into Gulf St Vincent, to the near-shore zone of the Adelaide metropolitan area.

Model outputs were then produced for a range of incident swell sizes, directions and periods. Results indicate a strong dependence on swell direction, with westerly swell propagating approximately 85% more energy to the near-shore area, than for a southerly direction. A lesser dependence on swell period, with longer period incident swell producing lesser resultant wave heights.

The inclusion/exclusion of physical processes including changing water levels and currents (derived from tidal components) and also bottom friction were investigated. Model results indicating that the inclusion of bottom friction has a significant effect on swell propagation, with approximately 40% lesser wave heights to the near-shore area. Tidal currents also produced a significant decrease/increase in near-shore wave heights, in the order of  $\pm 10\%$  for the outgoing/incoming (respectively) tidal currents. Tidal water level variations were found to have only a marginal (5%) effect on wave heights in the near-shore area.

## References

- Booij, N., L.H. Holthuijsen and J.A. Battjes, 2001: Ocean to near-shore wave modelling with SWAN, 4th International Conference on Coastal Dynamics 2001, Lund, Sweden, 335-344.
- Hasselmann, K., T.P. Barnett, E. Bouws, H. Carlson, D.E. Cartwright, K. Enke, J.A. Ewing, H. Gienapp, D.E. Hasselmann, P. Kruseman, A. Meerburg, P. Müller, D.J. Olbers, K. Richter, W. Sell and H. Walden, 1973: Measurements of wind-wave growth and swell decay during the Joint North Sea Wave Project (JONSWAP), *Dtsch. Hydrogr. Z. Suppl.*, 12, A8.
- SWAN – Technical documentation. Delft University of Technology, Environmental Fluid Mechanics Section, available from:  
<http://www.fluidmechanics.tudelft.nl/swan/index.htm> (Version 40.51AB, August 2007).
- WAMDI group, 1988: The WAM model – a third generation ocean wave prediction model, *J. Phys. Oceanogr.*, 18, 1775–1810.



# Australian mesoscale data assimilation and numerical weather prediction in ACCESS

Chris Tingwell, on behalf of the ACCESS research group.

*Centre for Australian Weather and Climate Research (CAWCR), a partnership between CSIRO and the Bureau of Meteorology, Melbourne, Victoria, Australia*

## Introduction

The Australian Community Climate and Earth System Simulator (ACCESS) will provide the Australian Bureau of Meteorology with a suite of NWP systems that incorporate state of the art data assimilation and forecast model components developed by the UK Met Office and adapted for local use by CAWCR staff. In the initial operational implementation of the ACCESS NWP suite, it is intended that every major component of the Bureau's legacy NWP systems will have an ACCESS replacement. In particular, the regional and mesoscale forecasting products generated by the Bureau's LAPS, MesoLAPS, MALAPS and city-LAPS systems will now be provided by ACCESS systems of similar horizontal domain and resolution.

The legacy limited area LAPS system is to be replaced by the ACCESS Regional Forecasting System (ARFS). ARFS features 4dVAR assimilation of conventional and remotely sensed observational data including some satellite data not available to LAPS: most importantly, radiance data from the hyper-spectral infrared sounder AIRS and moisture-sensitive microwave data from the SSM/I instrument. The Met Office Unified Model (UM) (Davies *et al.*, 2005) provides the ARFS forecast component. As well as providing its own forecast products, ARFS also provides the nesting conditions for the higher resolution mesoscale ACCESS Australian Forecasting System (AAFS), which replaces the legacy MesoLAPS and MALAPS systems. AAFS also features 4dVAR assimilation and UM forecasts.

Much work has been devoted to optimising both the data assimilation and forecast model components of ARFS and AAFS for the Australian region, with the success of this work being judged by comparisons of the system forecast skill with that of the LAPS suite. A particular focus of current work has been the optimal usage of satellite data, which will be discussed separately at this workshop. Here we will describe ARFS, AAFS and its nested systems and show some results indicating the expected forecast skill it will provide.

## Description of Limited Area ACCESS systems

For an overview of the whole ACCESS system, see Puri (2006). The ACCESS NWP suite consists of a hierarchy of systems nested within the ACCESS global NWP system. The global system currently consists of an N144 (~ 80km) configuration of the UM in conjunction with the Met Office 4dVAR data assimilation scheme (Rawlins *et al.*, 2007). Analyses are performed six hourly and long (240 hr) forecasts are run for base-times of 00UTC and 12UTC. The long forecasts provide the lateral boundary conditions (LBCs) for the regional 37km ARFS. This regional system also generates six hourly 4dVAR analyses which form the basis of twice-daily long (72 hr) forecasts. In turn the 12km AAFS system uses LBCs derived from regional ARFS forecast fields, performs 6 hourly 4dVAR analyses and 48hr long forecasts.

The nested regional and Australian systems are warm run: that is, the 4dVAR forecast loop is based on initial conditions generated from the previous analysis-forecast cycle of the same system.

The initial implementation of the ACCESS NWP suite will also include a number of higher resolution (3km or 5km) city/state-based forecast domains, where the initial condition for the 18hr forecasts is derived from a reconfigured “dump” file from the appropriate analysis cycle of the nesting AAFS system. In addition, a tropical 37km system extends further north and east but is otherwise similar to the regional 37 km system. The domains of the ACCESS systems (not including the tropical domain) are shown in Figure 1.

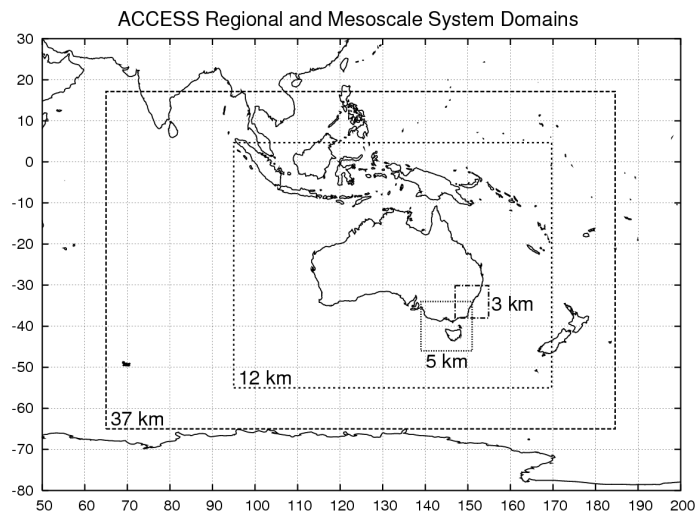


Fig 1: The ACCESS Regional and Mesoscale system domains.

The 37 and 12 km systems assimilate conventional surface and radiosonde observations, AIREPS, remotely sensed wind data (geostationary AMVs and scatterometer winds), SSM/I moisture retrievals and ATOVS and AIRS radiance data. Observations are retrieved from the Bureau’s Real Time Database or MARS archive to BUFR format and used to generate ECMWF Observation Data Bases (ODB) which are then processed by the Met Office Observation Processing System (OPS) for input to 4dVAR. To date, we have employed standard Met Office covariances and satellite data thinning distances, though some work has already been done to examine optimal thinning and selection strategies for both SSM/I moisture retrievals and AMV winds in ACCESS and will be reported at this workshop. Since the ACCESS regional and mesoscale systems differ from the corresponding Met Office system (NAE) in having 50 (versus 38) vertical levels, we have chosen to use the ATOVS channel selection employed by the Met Office global (N320) system. Radiance bias corrections generated from static Met Office global predictors are employed in the 12 and 37km systems, consistent with Met Office practice, although this strategy will be re-assessed in the future.

UM dynamics and physics settings have been based largely on global (N320) Met Office settings in the case of the 37 km system (whose horizontal resolution is very similar to N320), and NAE settings in the case of the 12 km and city/state systems. The ACCESS regional system grids do not employ a rotated pole, and this requires the use of 2D vector geometry in semi-Lagrangian trajectory evaluation, at a fairly minor computational cost. Early trials of the 37 km system without the use of 2D vector geometry exhibited severe forecast errors originating on the southern (most poleward) boundary of the domain. The use of a rotated-pole grid is currently being explored.

## Standard verification

Figure 2 shows standard MSLP forecast skill scores calculated for the trial version of the 12 km AAFS system compared with those calculated for the Bureau's legacy mesoscale MesoLAPS and MALAPS systems for the same forecast base date-times. Of the legacy systems, MALAPS is run on a 10 km Australian region grid and includes GenSI data assimilation (Steinle 2005), whereas MesoLAPS is a 12 km Australian region system whose forecast is run from an initial condition reconfigured from the nesting 37km LAPS system. The skill metrics, used as standard in the Bureau for evaluating NWP performance, are S1 skill score and root mean-squared error (RMSE). In this case they have been calculated on matching sub-domains of the model grids of each system being compared and averaged over a verification period of about six weeks. Each system is self-verified: the forecast is compared to the verifying analysis/initial-condition from the same system. In making the comparison it should be borne in mind that each MesoLAPS forecast has been verified against an initial condition interpolated from a lower resolution system, which will tend to produce a lower value of S1 than verification against an analysis at native resolution. The most appropriate S1 comparison is then between MALAPS and AAFS. The verification scores for the ARFS 37km system are also shown.

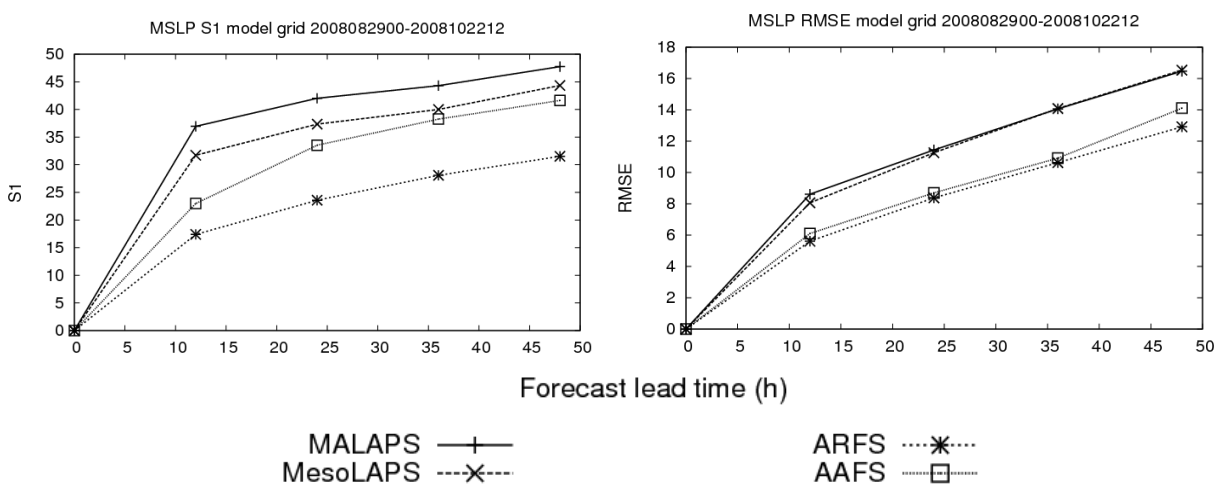


Fig 2: Averaged S1 skill score, RMSE and bias for MSLP forecasts produced by AAFS, ARFS and Bureau legacy MALAPS and MesoLAPS systems, as a function of forecast lead time. The units of RMSE are 0.1hPa.

It is clear from this comparison that, by existing standard measures, ACCESS-12km produces forecasts of considerably greater skill than those produced by MALAPS and MesoLAPS. In particular, the RMSE of the AAFS forecasts is substantially lower than for both legacy systems. This, however, raises the question of how best to evaluate the performance of mesoscale assimilation and prediction systems. While it is clear that the rather broad scale standard metrics are capturing a real and substantial improvement in forecast skill, the most useful evaluation of such systems should employ techniques appropriate to the classes of important meteorological events that they will be used to forecast.

For now, we mention a particular case to illustrate the expected improvement in forecasting guidance expected from the new ACCESS systems. Figure 3 shows two pairs of 48 hour MSLP forecasts based 12 hours apart for the east coast of Australia in early September 2008. Each pair compares the AAFS (12km) forecast with the corresponding MesoLAPS forecast. The verifying AAFS analyses are underneath each pair. The low pressure system that developed and caused severe flooding in Queensland and NSW was poorly forecast by the Bureau's legacy mesoscale systems – particularly in the early period of cyclogenesis; the ACCESS forecast of MSLP and rainfall (not shown), in contrast, is excellent.

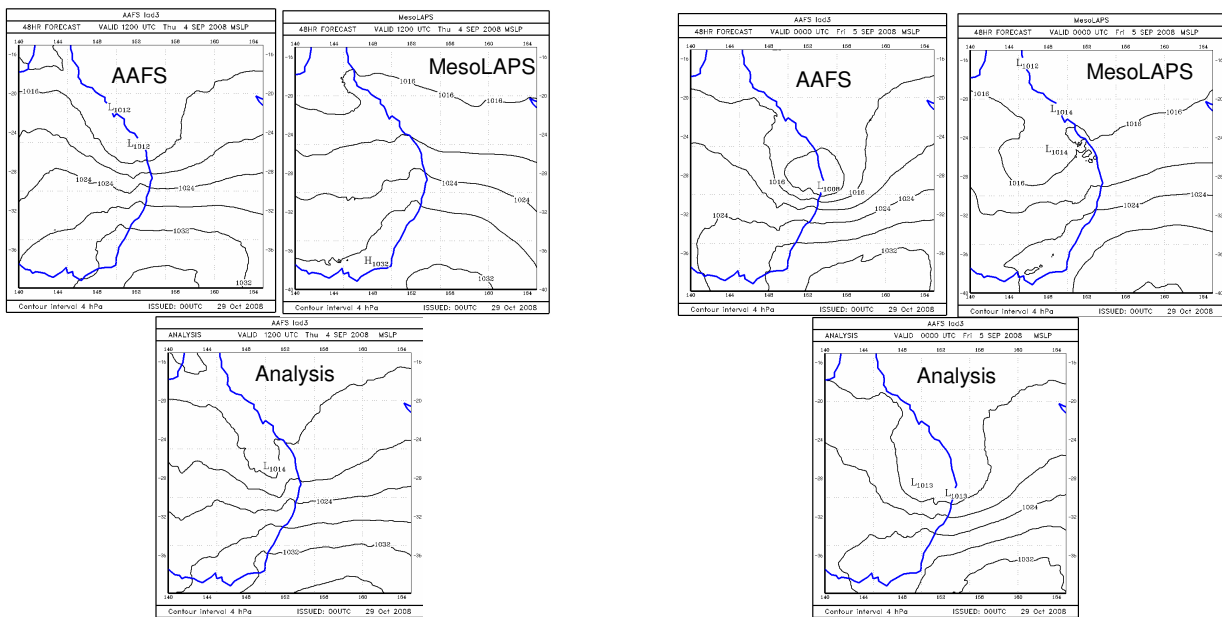


Fig 3: +48 hour MSLP forecasts from AAFS and MesoLAPS based at September 2<sup>nd</sup> 12Z (left hand pair) and September 3<sup>rd</sup> 00Z (right hand pair). The verifying AAFS analyses are underneath.

## Operational implementation and future work

At the time of writing, work is well underway in the National Meteorological and Oceanographic Centre to implement the first generation of ACCESS NWP systems as an operational suite. It is expected that operational forecast generation will commence in 1Q, 2009. Research and development work at the mesoscale will now focus on the implementation of data assimilation in a 5km system. The assimilation scheme will be 3dVAR in the first instance. A project to find and develop optimal methods of grid and observation based mesoscale verification is also underway.

This work will build on the very promising beginning of ACCESS NWP, with the aim of providing Bureau forecasters with state of the art forecast guidance at all applicable scales, including the mesoscale.

## References

- Davies T, Cullen M.J.P., Malcolm A.J., Mawson M.H., Staniforth A., White A.A., Wood N. 2005. A new dynamical core for the Met Office's global and regional modelling of the atmosphere. *Q.J.R.Meteorol. Soc.* **131**: 1759–1782.
- Puri, K., 2006: Overview of ACCESS, in A.J. Hollis and A.P. Kariko (eds), *BMRC Research Report No. 123. The Australian Community Climate and Earth System Simulator (ACCESS) - challenges and opportunities: extended abstracts of presentations at the eighteenth annual BMRC Modelling Workshop*, 1–4.
- Rawlins, F., S. P. Ballard, K. J. Bovis, A. M. Clayton, D. Li, G. W. Inverarity, A. C. Lorenc and T.J. Payne 2007: The Met Office global four-dimensional variational data assimilation system. *Q.J.R.Meteorol. Soc.* **133**: 347-362.
- Steinle, P.J., 2005: Generalized Statistical Interpolation. *Proceedings of the 4th World Meteorological Organization Symposium on Assimilation of Observations for Meteorology and Oceanography*, Prague, Czech Republic, 18 to 22 April 2005.

# Impact of using 4D-VAR assimilation of SSM/I data in the ACCESS modelling framework

Mohar Chattopadhyay, Peter Steinle, Yi Xiao,  
John Le Marshall, Tan Le and Chris Tingwell

*Centre for Australian Weather and Climate Research: a partnership between  
the Bureau of Meteorology and CSIRO, Melbourne, Australia*

## Introduction

The Special Sensor Microwave Imager (SSM/I) is a radiometer on board a Defense Meteorological Satellite Program (DMSP) satellite. These are sun-synchronous polar orbiting satellites. The DMSP satellites F13, F14 and F15 are used in this study. Detailed description of the instruments and retrieval of data is given in Phalippou (1996) and Deblonde and Wagneur (1997). Brightness temperatures from the SSM/I instrument are used to retrieve atmospheric parameters which include the near surface wind speed over the ocean, column integrated water vapour and liquid and ice water path. These retrieved parameters are part of the observation set analysed by the U.K. Met Office 4D-VAR data assimilation system (Rawlins et al. 2007, Lorenc et al. 2000) which provides the initial conditions for forecasts generated by the Australian Community Climate and Earth System Simulator (ACCESS) NWP suite.

Although many SSM/I observations are rejected because of cloud or rain contamination or failure to pass quality control checks, there are far more observations available to the assimilation system than can actually be analysed since it is computationally expensive and time consuming to process a large number of observations in a 4D-VAR system for operations. An important assumption for 4D-VAR methodology is that the observation errors are spatially uncorrelated. Hence, to use SSM/I observations effectively in 4D-VAR they need to be spatially thinned.

Different assimilation and model configurations require different thinning distances for each class of satellite observation depending upon the accuracy of the model, the satellite footprint and the accuracy of the observation operator. This is because forecast models differ from each other and the accuracy of observation operator depends upon the forecast model as well as weather conditions, but observation operators used in the assimilation systems are not changed with changing geographical locations or weather conditions. Thinning of satellite data generally improves forecasts, however in certain instances the information gained from using high density data may be greater than the errors due to ignoring observation error correlations. This means that the high resolution satellite data can still be useful for successful forecasting of special weather events, such as a tropical cyclone or a cold front (Dando et al. 2007).

Here we explore the different possibilities of using SSM/I data in the U.K. Met Office 4D-VAR assimilation system to get maximum positive impact on ACCESS NWP forecasts over the Australian region.

## Experiment

The thinning of SSM/I data in ACCESS global model (ACCESS-glb) is performed such that the observations are spatially thinned at 250km in the Northern Hemisphere and 125km in the Southern Hemisphere. A brief description of the model is given below. We conducted first part of the experiment in a global model framework where we have used uniform thinning

distances for SSM/I data at 250km (SSMI-250-glb) and 125km (SSMI-125-glb). The simulations were carried out for 15 days from 2008071512 UTC to 2008073112 UTC and the results were analysed against each other. It should be mentioned here that during the period chosen for the experiments, there was a strong convective event in northern Queensland and it was anticipated that assimilation of SSM/I data during that period may contribute to accurately predicting the event.

In the second part, we used the boundary conditions from our global experiments to run the Australian regional model (described below) over the same period of time. The experiments are run with 250km (SSMI-250-reg) thinning and 125km thinning (SSMI-125-reg) of SSM/I data. The results from these runs are compared with the standard pre-operational test version of the ACCESS regional system which currently does not assimilate SSM/I data.

Table 1: Model Description.

ACCESS-glb	ACCESS-reg
Model: Horizontal resolution : 90 km , Levels: 50 4D-VAR assimilation: Horizontal resolution : 120 km , Levels: 50	Model: Horizontal resolution : 37.5 km, Levels: 50 4D-VAR assimilation: Horizontal resolution : 70 km , Levels: 50

## Results

The observation coverage plots close to 2008070906 UTC for ACCESS-glb, SSMI-250-glb and SSMI-125-glb are shown in Figure1. The difference in thinning distances can be noticed especially for ACCESS-glb system where there is a split between the Northern and Southern Hemispheres.

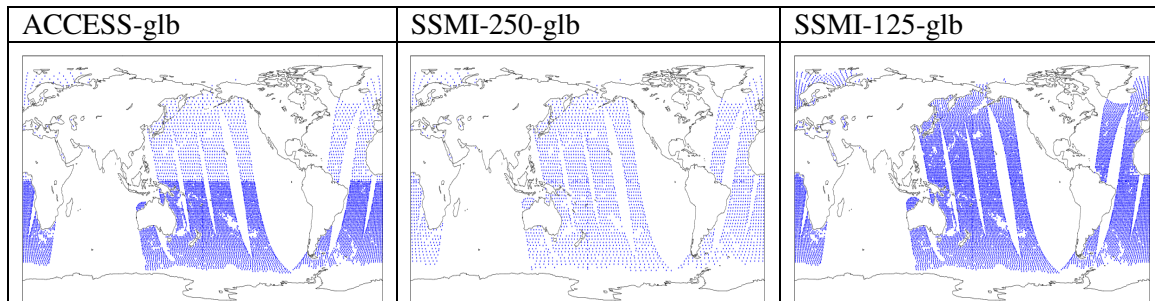


Figure 1. SSM/I observation coverage plots for ACCESS-glb(no. of obs. 6948), SSMI-250-glb(no. of obs. 2754) and SSMI-125-glb(no. of obs. 10281) at 2008070906 UTC.

Although it is recognized that the study conducted for 15 days provides only a small sample of results, 72 hour forecasts from the global runs ACCESS-glb, SSMI-250-glb and SSMI-125-glb were verified against their own analyses from 20080701600 UTC to 2008072700 UTC for S1 Skill score, root mean square error (RMSE), bias and anomaly correlation, shown in figure 2. Although there is negligible difference in S1 skill score and anomaly correlation for the three runs, there was a significant improvement in bias as well as in RMSE if a uniform thinning distance is used in both hemispheres.

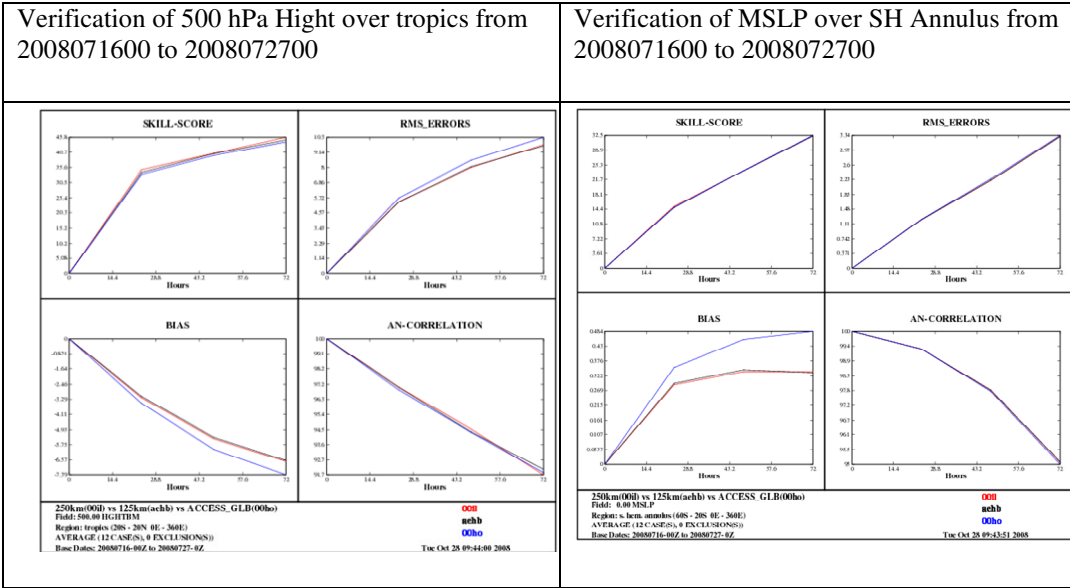


Figure 2. Verifications of S1 skill score, RMSE, bias and ANCOR at 500 hPa height over tropics and MSLP over Southern Annulus from 20080701600 to 2008072700 UTC.

As mentioned earlier, during the period of this experiment there was a strong convective event in Northern Queensland on the 2008072300 UTC. In order to diagnose if there was any impact in the moisture due to assimilation of SSM/I data at 250 km and 125 km thinning distances, Relative Humidity (RH) prediction from SSMI-250-glb and SSMI-125-glb were analysed. Figure 3 shows the difference in 12 hour zonal average RH forecast at 2008072300 UTC between 145°E and 165.5°E. A relatively high amount of RH is observed between 1000 to 850 hPa in SSMI-125-glb compared to SSMI-250-glb. This difference in moisture content in the lower atmosphere might contribute to a positive impact on rainfall forecast skill and will be the subject of further work.

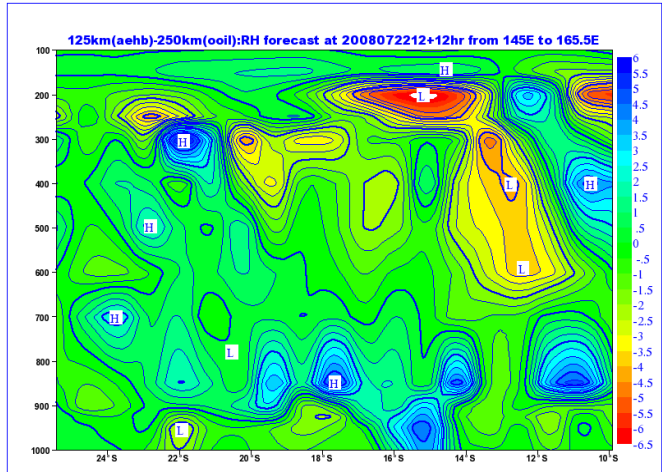


Figure 3. Difference in zonal average RH between 125km and 250km thinning of SSMI data: 12 hour forecast at 2008072212 from 145°E to 165.5°E.

Initial studies from the simulation of the ACCESS-reg model showed a significant improvement in the model's S1 skill score, RMSE and bias in MSLP up to 36 hour when SSM/I data were added in the assimilation system however, the impact was neutral to slightly negative for 48 hour forecast.

## Concluding remarks

The global model simulation using uniform thinning of SSM/I data has shown improvement in the model's S1 skill score, RMSE and bias over a 15 day period. Furthermore, improvement in the performance of the ACCESS-reg model has also been noted from very initial results. More studies using results from the ACCESS-reg domain are being undertaken and results will be presented in the workshop.

## References

- Dando, M.L., Thorpe, A.J., and Eyre, J.R., 2007. The optimal density of atmospheric sounder observations in the Met Office NWP system. *Quarterly Journal of the Royal Met. Soc.*, Vol. **133**, pp. 1933-1943.
- Deblonde, G. and Wagneur, N. Jr., 1997. Evaluation of global NWP analyses and forecasts using DMSP special sensor microwave imager retrieval: 1. Satellite retrieval intercomparison study. *Geophysical Research*, Vol. **102**, pp. 1833-1850.
- Lorenc, A.C., Ballard, S., Bell, R., Ingleby, N., Andrews, P., Barker, D., Bray, J., Clayton, A., Dalby, T., Payne, D., Saunders, F., 2000. The Met Office global three-dimensional variational data assimilation scheme. *Quarterly Journal of the Royal Met. Soc.*, Vol. **126**, pp. 2991-3012.
- Phalippou, L., 1996. Variational retrieval of humidity profile, wind speed and cloud liquid water path with SSM/I: Potential for NWP. *Quarterly Journal of the Royal Met. Soc.*, Vol. **122**, pp. 327-355.
- Rawlins, F., Ballard, S.P., Bovis, K.J., Clayton, A.M., Li, D., Inverarity, G.W., Lorenc, A.C. and Payne, T.J., 2006. The Met Office global four-dimensional variational data assimilation scheme. *Quarterly Journal of the Royal Met. Soc.*, Vol. **133**, pp. 347-362.

# Impact of remotely sensed wind data assimilation within a 4D-Var NWP system

Holly Sims, on behalf of the ACCESS research group

*Centre for Australian Weather and Climate Research: a partnership between CSIRO and the Bureau of Meteorology, Melbourne, Victoria, Australia*

## Introduction

Previous experience has shown that both remotely sensed Atmospheric Motion Vector (AMV) data derived from geostationary satellite imagery and surface wind data from polar-orbiting scatterometers have a significant influence on the accuracy of numerical weather prediction (NWP) forecasts during Australian severe weather events. As part of the preparation of the Australian Community Climate Earth-System Simulator (ACCESS) for use in the Australian Bureau of Meteorology's (ABM) operational NWP suite, it was necessary to assess that appropriate use was made of these remotely sensed data. Two experiments will be discussed in this presentation. The first experiment was conducted to optimise the quality control of QuikSCAT scatterometer data. The aim of the second experiment was to determine the optimal AMV thinning distance for the ACCESS region NWP configuration.

The ACCESS NWP system is based on the UK Met Office Unified Model and four dimensional variational (4d-Var) analysis system. There are several configurations of ACCESS which will become the components of the first operational ACCESS NWP system. These include regional and Australian mesoscale domains and a relocatable tropical cyclone region.

## The Data

### (1) Scatterometer

Currently the only scatterometer data used by ACCESS is from the QuikSCAT instrument. There are plans to begin assimilating Ascet data into ACCESS in the near future. Figure 1 shows QuikSCAT data accepted through quality control prior to assimilation in the global ACCESS model. The image on the left shows the current UK MetOffice practice of not including the central twenty pixel swath. This is done because the central pixels have a slightly higher observational error which peaks significantly at the central six pixels. Not including the central swath can lead to discontinuity problems in the presence of serious weather events such as tropical cyclones. An experiment was conducted to assess the impact of including inner swath apart from the central six pixels.

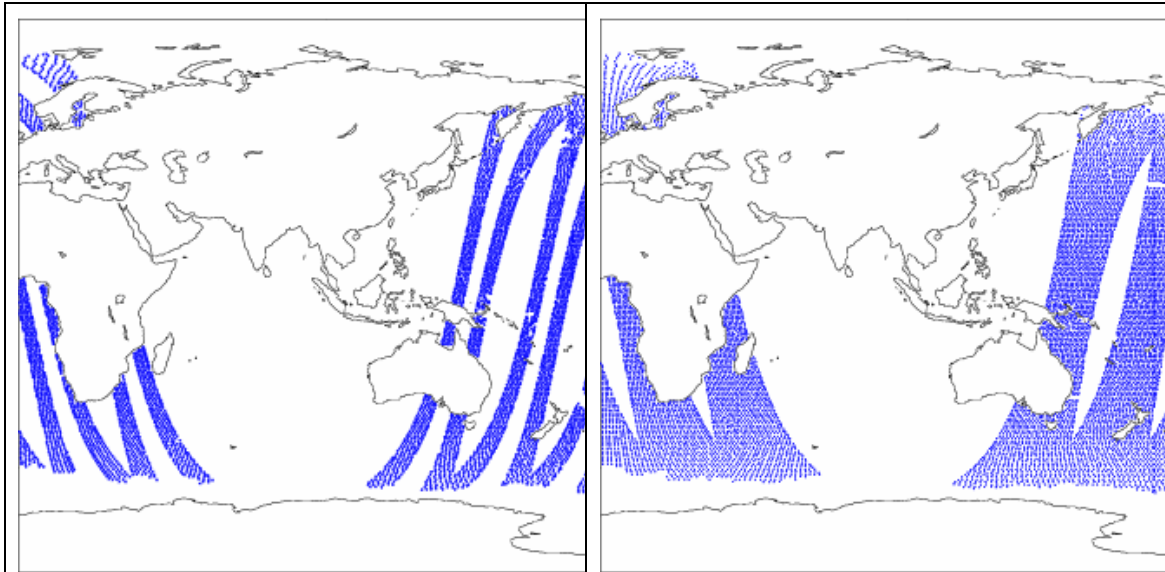


**Figure 1:** QuikSCAT Data accepted through quality control prior to assimilation in the global ACCESS model. The image on the right includes the central swath which is not used in the MetOffice data assimilation.

## (2) AMV

Figure 2 shows the AMV coverage, after quality control, available to the regional ACCESS assimilation system. The regional domain includes AMVs from three operational centres; EUMETSAT, JMA and BoM. EUMETSAT and JMA include visible, IR and water vapour AMVs. Locally generated ABM AMVs are calculated using MTSAT-1R IR imagery.

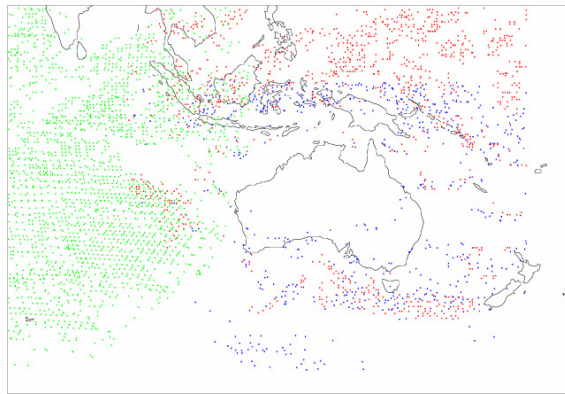


**Figure 2:** AMV data coverage accepted through quality control prior to assimilation in the ACCESS AUSLAM model. The green dots represent EUMETSAT AMVs. The blue dots represent locally produced AMVs derived from JMA satellite imagery. The red dots are JMA produced and processed AMVs.

## Scatterometer Experiment

The aim of this experiment was to determine the impact of QuikSCAT data on the forecast of tropical cyclone Fengshen which was incident upon the Philippines Sunday 22<sup>nd</sup> June 2008. The experiment involved three runs; a control run using no Scatterometer data, a run using Scatterometer data without the central swath and a run including the central swath. The preliminary experiment was conducted using the global configuration of the ACCESS NWP

system. The current global configuration has a horizontal resolution of N144 (~80km) and a vertical resolution of 50 levels. The experiment was conducted for the dates 15/06/08-23/06/08. This experiment indicated that assimilation of QuikSCAT data has an effect on the tropical cyclone forecast track. Comparing results from the simulation including the central swath and not including the central swath indicated that at N144 resolution the inclusion of the extra centre-swath data produced a slight difference in maximum speed.

While this result is encouraging, the N144 resolution of the preliminary experiment is insufficient to adequately resolve a tropical cyclone. An experiment using the mesoscale tropical cyclone configuration of the ACCESS code is currently being set up and results from this experiment will be presented.

## **AMV Thinning Experiment**

The aim of this experiment was to determine the optimal AMV thinning distance for the regional ACCESS configuration. The optimal thinning distance requires a balance between the error introduced by ignoring observation error correlation and the loss of information from ignoring observations. A preliminary seven-day experiment was conducted for 20/07/08-27/07/08. During these days a significant low pressure system developed off the coast of Queensland and was incident on the New Zealand north island following rapid intensification. Five different assimilation and forecast runs were conducted, including a control simulation without AMVs, and four simulations including AMVs with four different thinning box sizes:  $2.0^{\circ} \times 2.0^{\circ}$ ,  $1.5^{\circ} \times 1.5^{\circ}$ ,  $1.0^{\circ} \times 1.0^{\circ}$ ,  $0.5^{\circ} \times 0.5^{\circ}$ . Results from this experiment will also be presented

## **References**

Puri, K., 2006: Overview of ACCESS, in A.J. Hollis and A.P. Kariko (eds), *BMRC Research Report No. 123. The Australian Community Climate and Earth System Simulator (ACCESS) - challenges and opportunities: extended abstracts of presentations at the eighteenth annual BMRC Modelling Workshop*, 1-4.



# Assessing the quality of high resolution precipitation forecasts using fuzzy (neighbourhood) verification

Elizabeth E. Ebert

*Centre for Australian Weather and Climate Research, Melbourne, Australia*

## Introduction

High space and time resolution quantitative precipitation forecasts (QPFs) are now widely available and are used for a variety of applications from weather analysis and prediction, emergency management, flood and stream flow prediction, agriculture, etc. In order to make appropriate use of high resolution QPFs it is necessary to understand the nature of their errors. This is done by verifying against reference data such as rain gauge or radar analyses, where these are assumed to give a reasonable representation of the true precipitation distribution. The traditional verification approach is to compare the value of the forecast in each given grid box with the corresponding observation in that grid box. This matching strategy makes it very difficult for high resolution QPFs to demonstrate good skill, due not only to model errors but also to sampling and observation errors. Upscaling to coarser space and time resolution is a well known approach for reducing the sampling error, but this process loses information, much of which may be useful. For many applications it may not be essential to get the rainfall position and timing exactly right; instead, "close enough" may be good enough.

A new verification approach called "fuzzy verification" has been proposed by Ebert (2008). The term "fuzzy" is in keeping with the spirit of fuzzy logic as it describes the inexact nature of the verification – an estimate can be partially correct and partially incorrect. Instead of requiring an exact space/time match, all grid-scale values within a spatial and/or temporal neighbourhood of the observation are considered to be equally likely estimates of the "true" value, thus representing a probabilistic view of verification. Some fuzzy verification methods compare the estimated values within a neighbourhood to the observation in the center, while others compare the estimates to observed values within the same neighbourhood. The advantage is that good skill can be demonstrated even if perfect correspondence is not achieved at the grid scale. By varying the size of the neighbourhoods and performing the verification at multiple scales and for multiple intensity thresholds, it is possible to determine at which scales the QPFs have useful skill.

This paper focuses on four fuzzy verification methods that are particularly suited for evaluating precipitation mean values, precipitation frequency, occurrence of extreme values, and similarity of the intensity distribution. The methodology is demonstrated on precipitation forecasts from 0.05° mesoLAPS models using Australian Rainfields merged radar-gauge analyses as reference data (Seed and Duthie 2007). The information that can be gained from each of the methods is highlighted.

## Fuzzy verification methods

Fuzzy verification computes error metrics for the set of all neighbourhoods, or space/time windows, in a domain, rather than the set of all individual grid boxes. The size of the local spatial neighbourhood around a grid box is increased exponentially from 1x1, 3x3, ..., to  $(2^n+1) \times (2^n+1)$ , approximating the size of the domain. If a temporal domain is used then  $t$  time windows are increased in the same way. Since many fuzzy verification methods use the concept of an "event", i.e., the occurrence of a value greater than or equal to some threshold value, the rain intensity threshold for an event is also varied from small to large values,  $R_1, \dots, R_m$ . Thus, instead of the single score that is normally reported for grid box-scale validation using a rain/no rain threshold,

fuzzy verification provides an  $m \times n \times t$  array of scores for varying scales and thresholds. It is then possible to examine the array of scores to determine which space and time scales have useful skill for rain exceeding various intensities.

A well known verification approach that can be considered "fuzzy" is *upscaling*, in which the estimates and observations at grid scale are averaged to larger scales before being compared using the usual continuous and categorical verification metrics (e.g., Yates et al. 2006). In recent years many new techniques that verify neighbourhoods of grid boxes have been proposed in the meteorological literature. Each method is characterized by a decision model regarding what constitutes a useful forecast. For example, the upscaling method considers a useful estimate to be one that has the same average value as the observations. This is one criterion for judging whether precipitation estimates at the catchment scale are useful for hydrological purposes.

The *fractions skill score* (FSS) method of Roberts and Lean (2008) considers a perfect estimate to be one with the same frequency of events as was observed within a neighbourhood. This fuzzy method implicitly acknowledges that the observations are likely to contain random error at the grid scale, and asserts that a better approach to comparing QPFs with observations is to assess their similarity in terms of their fractional coverage of raining grid boxes. The fractions skill score is a variation of the Brier skill score used to verify probability forecasts:

$$FSS = 1 - \frac{\frac{1}{N} \sum (P_{fcst} - P_{obs})^2}{\frac{1}{N} \left[ \sum P_{fcst}^2 + \sum P_{obs}^2 \right]}$$

$P_{est}$  and  $P_{obs}$  are the fractional coverages of forecast and observed raining grid boxes, respectively, in each of the  $N$  neighbourhoods in the domain. The FSS varies between 0 for a complete mismatch and 1 for a perfect match. The target value of FSS above which the estimates are considered to have useful (better than random) skill is given by  $FSS_{useful} = 0.5 + f_{obs}/2$ , where  $f_{obs}$  is the fraction of observed raining grid boxes in the full domain. This leads to the concept of a "skillful scale", namely the smallest scale at which the FSS exceeds  $FSS_{useful}$ . This is a more meaningful concept for many users, and is now used at the Met Office to help forecasters understand the quality of mesoscale model QPFs (M. Mittermaier, personal communication).

The *multi-event contingency table* (MECT) method of Atger (2001) considers an estimate to be useful if at least one occurrence of an event is predicted close to an observed event. "Close" can refer to space, time, intensity, or any other important aspect. Closeness is an important criterion for weather forecasters using model output to prepare warnings of heavy rain, and for emergency managers and disaster relief agencies planning emergency response activities. The MECT method compares a neighbourhood of forecasts to an observation in the center using traditional categorical metrics such as frequency bias, probability of detection, false alarm ratio, and so on. Whenever rain is observed in the central grid box of the neighbourhood and also predicted by the model in at least one grid box in the neighbourhood, this counts as a hit. If there is no rain observed in the central grid box but one or more neighbourhood grid boxes with forecast rain, a false alarm is counted. As the neighbourhood increases in size, it is easier to get a hit, but also easier to get a false alarm. Although any categorical score can be computed, the one most relevant to accuracy assessment in this case is the Hanssen and Kuipers discriminant HK, which measures the difference between the probability of detection (rewarding hits) and the probability of false detection (penalizing false alarms).

Germann and Zawadzki (2004) proposed a fuzzy verification method that uses as its criterion for goodness, "A forecast is useful if it has a high probability of matching the observed value." Called the *conditional square root of RPS* (CSRR), it uses a probabilistic approach to compare forecasts to the observed rain in the center of each neighbourhood. The square root of the ranked probability

score (RPS) can be interpreted as the standard error of the probability estimates across the full range of rain intensities. Normalizing by the observed rain fraction in the domain enables performance to be compared for different cases:

$$CSRR = \frac{\sqrt{RPS}}{P_{obs}}$$

Likely users of CSRR information would include emergency managers and other decision makers concerned about the effects of local heavy rain.

The first two fuzzy methods described in this section, upscaling and FSS, compare neighbourhoods of QPFs against neighbourhoods of observations. Ebert (2008) calls this strategy "model oriented", meaning that the observations are manipulated to represent the scales resolved by the model. This gives a fair assessment of the QPFs in the sense that they are being evaluated only on scales that they claim to resolve. The last two fuzzy methods, MECT and CSRR, compare each neighbourhood of QPFs against the single observation in the center of the neighbourhood. Although this may seem "unfair", many users wish to know the accuracy of the QPF at a particular location. Note that this "user oriented" philosophy is more demanding than the model oriented one, but not as tough as the traditional grid box-to-grid box verification, since skill can still be demonstrated when the QPFs detect rain close to the observation.

## Fuzzy verification of mesoLAPS precipitation forecasts near Sydney

Figure 1 shows rainfall from the Rainfields analyses and the 0.05° mesoLAPS 12h forecast valid for the hour ending at 12 UTC on 13 October 2008. Both show a rain system near the coast at around 35°S, with the forecast field displaced slightly to the southeast of the observations.

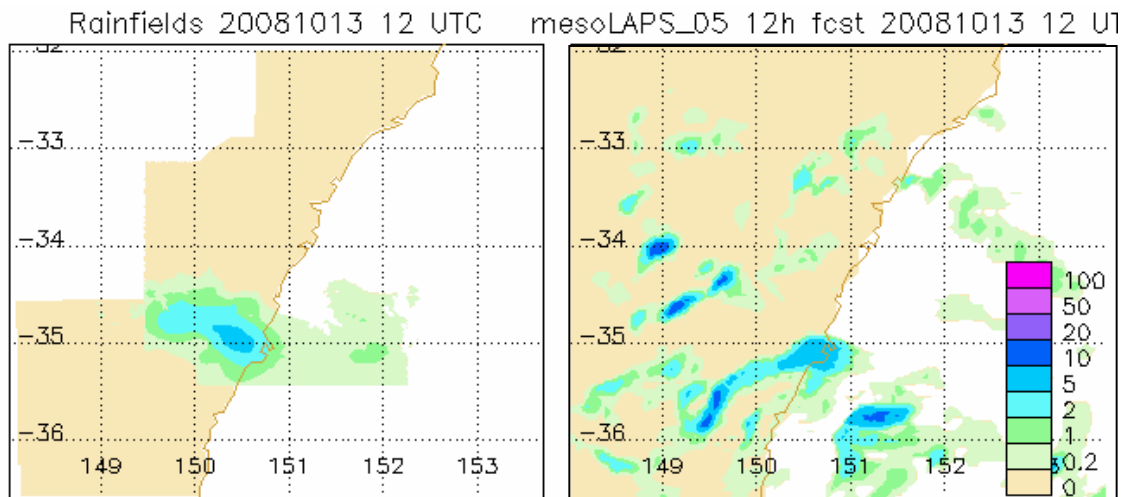


Fig 1: Hourly rainfall estimated from a radar-gauge analysis (left) and the 12h forecast from the 00 UTC run of the mesoLAPS 0.05° model (right), valid at 12 UTC on 13 October 2008.

To prepare the data for verification, the original 2 km resolution radar grid boxes were averaged to the 0.05° scale of the model. The fuzzy verification used six spatial scales increasing logarithmically from 1x1 to 33x33 grid boxes, the largest that the radar analysis could accommodate, and eight intensity thresholds ranging from 0.2 to 50 mm h<sup>-1</sup>. No time window was used. The results are shown in Figure 2 as a function of the rain intensity threshold (x-axis) and

spatial scale (y-axis). In these plots the shading and the number show the value of the score. The value in the lower left corner is the score that would be achieved using traditional grid box matching and a very low threshold, essential rain/no rain.

For the upscaling approach the equitable threat score was chosen as the error metric since it penalizes both misses and false alarms. MesoLAPS showed optimal skill at the largest spatial scale of  $1.65^\circ$  and an intensity threshold of  $0.5 \text{ mm h}^{-1}$ , indicating that the light rain was located more accurately than rain of other intensities (Fig. 2a). Although there were forecasts exceeding  $10 \text{ mm h}^{-1}$ , there were no corresponding grid scale observations, resulting in a score of 0 as seen in the right side of the diagram.

When comparing the estimated and observed fractional coverage of rain grid boxes using the fractions skill score a different picture emerges. Useful forecasts were made for intensities exceeding 1 or 2 mm at the largest scale (Fig. 2b). The FSS puts greater emphasis on the rain intensity *distribution* than does the upscaling approach and is more sensitive to bias. FSS generally improves with increasing spatial scale and decreasing rain intensity, and tends to be characterized by higher numerical values than the ETS.

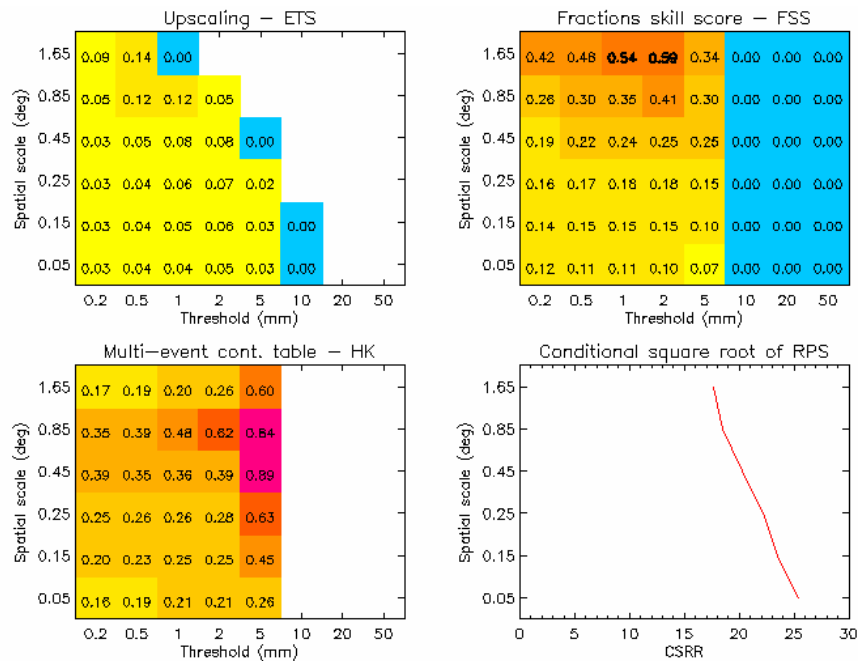


Fig 2: Fuzzy verification scores for the 12h mesoLAPS\_05 forecast of 1h accumulation valid at 12 UTC on 13 October 2008, verified against hourly radar-gauge analysis near Sydney. The bold numbers in the FSS plot indicate where useful skill was achieved.

The ability of mesoLAPS to predict rain of a given intensity close to where it was observed was measured using the MECT method (Fig. 2c). A good way to use the results from this method is to choose a threshold of interest, say  $5 \text{ mm h}^{-1}$ , and scan vertically to see which scales had a large HK score. In a warning context this would tell the user how large the neighbourhood surrounding the point of interest should be to provide a useful indication of rain, with some hits and not too many false alarms. In this case a neighbourhood of  $0.45^\circ$  to  $0.85^\circ$  (effective radius of about 25 to 50 km) gave quite useful detections of rain exceeding  $5 \text{ mm h}^{-1}$ .

The final evaluation of the mesoLAPS QPF was done using the probabilistic CSRR method, which has a low (good) value when the estimated intensity distribution peaks near the observed value. The focus of the CSRR on the rain rate distribution is similar to that of the FSS, but neighbourhood estimates are compared to point values rather than the neighbourhood distribution of observed rain rates. The CSRR showed better performance of mesoLAPS on the large scale, when there was little overall bias, than at small scales when the local forecasts contained significant bias error (Fig. 2d).

## Discussion

As the production and distribution of high resolution model-based precipitation products becomes increasingly common, the need to evaluate them appropriately becomes more important. Standard grid box-by-grid box verification can suggest that high resolution rainfall products are not as accurate as lower resolution products, yet most users intuitively feel that the high resolution products should be more useful. Fuzzy verification gives credit to estimates that are "close" to the observations, thus offering an alternative to traditional verification approaches. This is achieved by looking in space/time neighbourhoods surrounding the observations and evaluating the degree of "closeness" according to various criteria. By evaluating the accuracy of the QPFs as a function of both intensity and spatial scale, fuzzy verification gives information about which scales have useful skill. This helps users to decide whether to use the estimates at face value at full resolution, or spatially transform the values to give more accurate and useful information.

Most users of precipitation estimates are not very familiar with objective verification techniques and scores, and thus fuzzy verification may seem somewhat daunting. Two new metrics, namely the FSS and the CSRR, have only recently been introduced into the meteorological literature and are not yet found in standard textbooks on verification. Even those who are comfortable with verification methods and scores may find it overwhelming to interpret the results from several fuzzy methods, each of which produces a large array of scores. The key is to first identify which is the most important aspect of the estimated precipitation to get right – is it the spatial average, the precipitation area, the presence of one or more high intensity estimates nearby the location of interest, the rain rate distribution, etc.? Then choose the fuzzy verification method that addresses this aspect. Focusing on an intensity threshold of interest and condensing its scale-dependent performance into a single easily-interpreted value like the "skillful scale" can help make the verification results much more accessible. As fuzzy verification becomes more widely used, new approaches will certainly emerge for interpreting the results in ways that intuitively meet the needs of specific users.

## References

- Atger, F., 2001: Verification of intense precipitation forecasts from single models and ensemble prediction systems. *Nonlin. Proc. Geophys.*, **8**, 401-417.
- Ebert, E.E., 2008: Fuzzy verification of high resolution gridded forecasts: A review and proposed framework. *Meteorol. Appl.*, **15**, 51-64.
- Jolliffe, I.T., and D.B. Stephenson, 2003: *Forecast Verification. A Practitioner's Guide in Atmospheric Science*. Wiley and Sons Ltd, 240 pp.
- JWGV (Joint Working Group on Verification), 2008: Forecast verification: Issues, methods, and FAQ. [Available: [http://www.bom.gov.au/bmrc/wefor/staff/eee/verif/verif\\_web\\_page.html](http://www.bom.gov.au/bmrc/wefor/staff/eee/verif/verif_web_page.html) ]
- Roberts, N.M. and H.W. Lean, 2008: Scale-selective verification of rainfall accumulations from high-resolution forecasts of convective events. *Mon. Wea. Rev.*, **136**, 78-97.
- Seed A., and E. Duthie, 2007: Rainfields: A quantitative radar rainfall estimation scheme. *33rd Conf. Radar Meteorology, Amer. Met. Soc., Cairns, Australia, 6-10 August 2007*.
- Yates, E., S. Anquetin, V. Ducrocq, J.-D. Creutin, D. Ricard and K. Chancibault, 2006: Point and areal validation of forecast precipitation fields. *Meteorol. Appl.*, **13**, 1-20.



# Operational mesoscale prediction model at JMA and its land surface process

Daisuke Miura

Numerical Prediction Division, Japan Meteorological Agency

1-3-4 Otemachi, Chiyoda-ku, Tokyo 100-8122, JAPAN

E-mail: [d.miura@met.kishou.go.jp](mailto:d.miura@met.kishou.go.jp)

## Introduction

The Japan Meteorological Agency (JMA) has been operating a mesoscale prediction system (MSM) since March 2001. The main purpose of MSM is the prediction of severe weather. The system produces 33-hour forecast 4 times a day and 15-hour forecast 4 times a day. The forecast domain of the model covers a region of 3600km x 2880km over the Japan Islands and its surrounding areas with 50 vertical layers.

When MSM started in March 2001, it was composed of a 10km hydrostatic model and optimum interpolation at data assimilation. Thereafter, some big changes were done; the introduction of 4DVAR, the introduction of nonhydrostatic model (JMA-NHM), the enhancement the horizontal resolution from 10km to 5km, the forecast hours extended from 15 to 33 hours and improvement of many physical processes (Table 1).

In this paper, first of all, the specification of MSM and the history of precipitation prediction performance are described. Secondly, the improvement of land surface process at JMA-NHM is explained while referring the verification result of the 1.5m air temperature forecast. And then, the introduction of simple biosphere model (SiB) to JMA-NHM, which is developing now, is referred a little.

**Table 1** Main operational changes in MSM

Mar.2001		Hydrostatic model (10km, 4times, 18hour)
Mar.2002		4DVAR in MSM
Sep.2004	MSM0409	10km Nonhydrostatic model
Mar.2006	MSM0603	5km , 8times, 15hour
May.2007	MSM0705	5km, 4(4)times, 33(15)hour, physical process improved

## Specifications and Performance in MSM

Specifications in MSM are summarized in Table 2. Many processes (mainly physical processes) were improved in May 2007. Figure 1 shows QPF performance of MSM. In this figure, scores for 3-hour precipitation with a threshold value of 10mm at FT=00-15 are indicated. Bias score, which showed excessive forecast before, approaches gradually one. Along with it, the threat score has gotten higher. The performance of precipitation forecast has become better with big changes shown in Table 1.

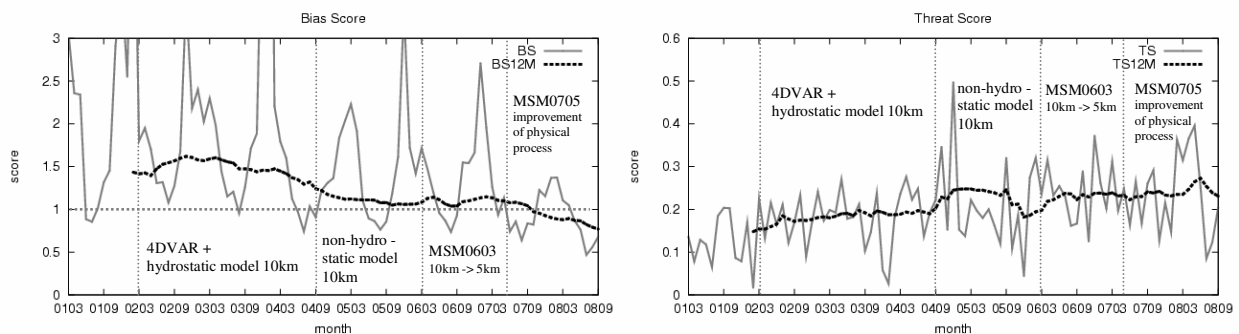


**Fig.1** QPF performance of MSM from Mar 2001 (0103) to Sep 2008 (0809). Bias score (left) and threat score (right) for 3hour precipitation at FT=00-03, 03-06, 06-09, 09-12, 12-15 with a threshold value of 10mm/3hour. Solid gray lines and broken black lines show scores on each month and scores averaged for 12 months respectively.

**Table 2** The specifications of JMA mesoscale model

Model	JMA-Nonhydrostatic model (JMA-NHM, Saito et al. 2006)
Number of grid points	721 x 577 x 50
Forecast period	15 hours (00,06,12,18UTC), 33 hours (03,09,15,21UTC)
Horizontal resolution	5km
Initial conditions	Meso4DVAR with 6-h assimilation window (integrating a latter half 3 hours of outer loop with NHM)
Boundary conditions	20km Global Spectral Model at JMA
Vertical Coordinates	hybrid terrain-following
Advection	flux form 4th order for horizontal, 2nd order for vertical with flux correction
Gravity / Sound Wave	split – explicit
Cloud microphysics	3-ice bulk + fall out of cloud ice
Convective parameterization	modified Kain-Fritsch (with perturbation depending on relative humidity)
Radiation	Two-stream with delta-Eddington approximation for shortwave Table look-up and k-distribution methods for longwave
Cloud water used in radiation	partial condensation scheme
Turbulent process	improved Mellor-Yamada Level 3 by Nakanishi and Niino Refer to Hara (2007)
Surface flux	Beljaars and Holtslag (1991)
Land Surface Process	Slab model, ground temperature predicted by 4 layer diffusive model. soil moisture: force restored method

## Forecast of surface temperature and land surface process

In this section, the history of 1.5m air temperature forecast performance and reason for the improvement are referred. Although 1.5m air temperature is influenced by various processes such as radiation, turbulence, and wet process, improvement of land surface process is mainly mentioned here.

The present land surface process is a slab model, which doesn't consider the influence of biosphere so much. The ground temperature is predicted by 4 layer diffusive model and the soil moisture is calculated by force restored method (Deardorff 1978). Surface flux scheme is based on Beljaars and Holtslag (1991).

Figure 2 shows the performance (Mean error and Root mean square error) of 1.5m air temperature forecast against observations at about 600 points in Japan. They show the scores at day time (15JST: Japanese Standard Local Time UTC + 9) and at night time (03JST). Although the predicted temperature at night has positive bias and one at daytime has negative bias in summer, ME and RMS decreased when the horizontal resolution was enhanced to 5km and some processes were improved in March 2006. And then

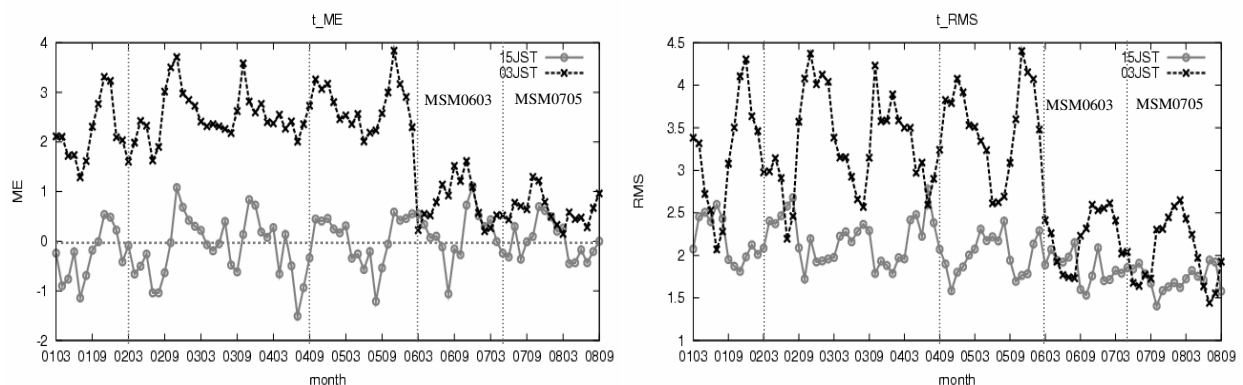


**Fig. 2** Mean error (left) and root mean square error (right) of surface (1.5m) air temperature forecast against observations at about 600 points in Japan from March 2001 to September 2008. Black lines and gray lines show scores at 03JST (Japanese Standard Time; UTC + 9) and scores at 15JST respectively.

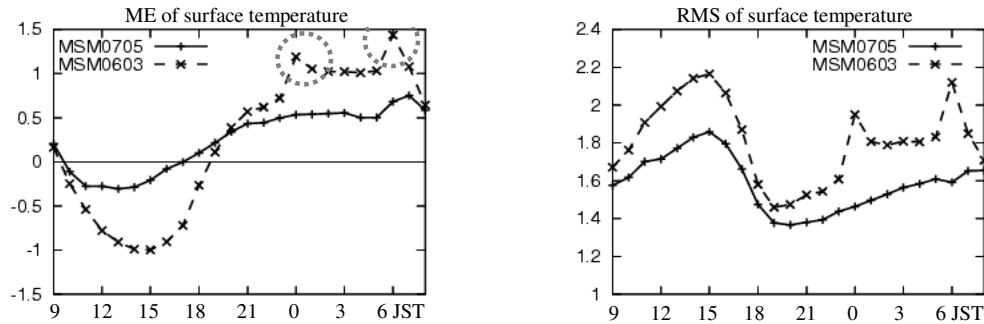


**Fig.3** Mean error (left) and root mean square error (right) of surface (1.5m) air temperature for each valid time compared with observations at about 600 points in Japan from July 2006 to September 2006. Solid line and broken line shows MSM0705 and MSM0603 shown in Table1 respectively. A horizontal axis indicates valid time in JST. Forecast data of FT = 00, 01..., 15 at 00, 06, 12, 18 JST initial time are used for verification.

many physical processes were updated in May 2007. The performance of temperature forecast before and after this update, mean error and root mean square error of surface (1.5m) air temperature for each valid time (JST), are shown in Figure 3. After this update, negative bias at daytime and positive bias at night time has reduced. Hereinafter main factors which make temperature forecasts more accurate are listed as follows.

(1-a, b, c) are related to land surface model.

### (1) Improvement at MSM0603

(a) The surface flux scheme used to diagnose surface temperature was changed from Louis et al. (1982) to Beljaars and Holtslag(1991). The temperature of 1.5m ( $T_a$ ) is averaged with temperature of the lowest level (20m) of the model ( $T_r$ ) and that of land surface ( $T_{sfc}$ ) using a weight ( $k$ ).

$$T_a = (1 - k) T_{sfc} + k T_r$$

This “ $k$ ” is calculated with the rate of bulk coefficients by a surface flux scheme. In the past Louis et al (1982) was used to calculate “ $k$ ”, which made “ $k$ ” consistent in stable case. Generally, the more stable, the smaller “ $k$ ” becomes. So, when Louis et al. (1982) was used, “ $k$ ” was excessive in stable case. This caused a positive bias of surface air temperature at night. On the other hand, the scheme by Beljaars and Holtslag(1991) makes “ $k$ ” become smaller when atmosphere becomes more stable, which suppresses positive bias at night.

(b) Some land surface parameters such as heat capacity, heat conductivity and roughness length were set using land cover data by digital national land information (KS-202) in Japan with the horizontal resolution of 1km. This made heat capacity smaller on the whole. So, the positive bias was improved.

(c) Soil moisture was consistent with climate value for the forecast period. So, on a hot day in summer, the temperature didn't rise because of excessive soil moisture. Therefore soil moisture is estimated with forcing restore method (Deadorff 1978). In the result, the temperature came to go up.

(d) Improvement of turbulence process, radiation process and wet process.

### (2)Improvement at MSM0705 (land surface process is not changed so much)

(a) Improved Mellor-Yamada level 3 by Nakanishi and Niino (MY3) are introduced (Hara 2007).

(b) Amount of cloud water is estimated by partial condensation scheme by MY3, which makes negative bias of short wave improved.

(c) Model is different between 4-DVAR (10km hydrostatic model) and forecast (5km non-hydrostatic model). This difference makes a gap at early time of forecast such as the spike circled in figure 3. Outer loop of 4-DVAR has the window of 6-hours. So, the latter half (3-hours) of this window is exchanged to Nhm. It makes these spikes fade out.

## Summary and future

JMA has been operating the mesoscale prediction model (MSM) since March 2001, and the performance has been gradually improved by the enhancement of resolution and improvement of various processes. And then, the modification of the land surface process suppressed positive bias of the surface air temperature forecast at night and negative bias at daytime.

But this bias still exists, and it is necessary to make the land surface process sophisticated. (A present process doesn't consider influence of transpiration or interception evaporation from vegetation and the way to predict soil moisture is simple. The snow process which estimates snow depth or amount is not considered. These can influence surface temperature and atmosphere.) Therefore, Simple Biosphere Model (SiB: Sellers et al. 1986) with 4-th layer snow model, which had been already introduced to GSM at JMA (Hirai et al. 2007), has been introduced to JMANHM. In my presentation, the result used this model, which has been adjusted and developed so far, would be referred.

## References

- Beljaars, A. C. M. and Holtslag, A. A. M., 1991: Flux parameterization over land surfaces for atmospheric models. *J. Appl. Meteor.*, 30,327.341.
- Deardorff, J.W., 1978: Efficient prediction of ground surface temperature and moisture, with inclusion of layer vegetation. *J. Geophys. Res.*, 83, 1889.1903.
- Hara, T., 2007: Implementation of improved Mellor-Yamada level 3 scheme and partial condensation scheme to jmanhm and their performance. CAS/JSC WGNE Res. Activ. Atmos. Oceanic Modell.,37.
- Hirai, M., T. Sakashita, H.Kitagawa, T.Tsuyuki, M.Hosaka and M.Oh'izumi, 2007: Development and validation of a new land surface model for JMA's operational Global Model using the CEOP observation dataset, *Journal of Meteorological Society of Japan*, 85A,1-24.
- Louis, J., M.Tiedtke, and J. Geleyn, 1982: A short history of the operational pbl parameterization at ECMWF. In Proc. Workshop on Planetary Boundary Layer Parameterization, pages 59.79, Reading, United Kingdom, 1982. ECMWF.
- Saito, K., T. Fujita, Y. Yamada, J. Ishida, Y. Kumagai, K. Aranami, S. Ohmori, R. Nagasawa, S. Kumagai, C. Muroi, T. Kato, H. Eito and Y. Yamazaki, 2006: The operational JMA Nonhydrostatic Mesoscale Model. *Mon. Wea. Rev.*, 134, 1266-1298.
- Sellers, P.J., Y. Mintz, Y.C. Sud, and A. Dalcher,1986: A Simple biosphere model (SiB) for use within general circulation models. *J. Atmos. Sci.*,43, 505.531.

# Modelling the atmospheric boundary layer in ACCESS: testing an alternate surface scaling

Vaughan J. I. Barras, Peter J. Hurley and Ashok K. Luhar  
*Centre for Australian Weather and Climate Research: a Partnership between  
the Bureau of Meteorology and CSIRO, Melbourne, Victoria, Australia*

## Introduction

A realistic representation of surface fluxes in the atmospheric boundary layer (ABL) is of considerable importance in numerical models for calculations of energy exchange between the surface and the atmosphere. The finite vertical resolution of the model atmosphere requires the use of flux-profile relationships to derive fluxes at the lowermost model level from known model variables. A commonly used flux-profile relationship in the surface layer (the lowest tens of metres of the atmosphere) is Monin-Obukhov Similarity Theory (MOST) that makes the assumption that fluxes are constant with height and that the mean wind follows a logarithmic profile, with an adjustment for diabatic flows. For the majority of stability conditions MOST has proven to be a satisfactory approximation for the calculation of surface fluxes of momentum, heat and moisture. However, there remains considerable uncertainty in the application of MOST to very stable boundary layers as many underlying assumptions of the theory may no longer apply (Mahrt, 1999; Cheng et al., 2005; Galperin et al., 2007; Zilitinkevich et al., 2007). For stable conditions, ACCESS presently uses the stability functions for the surface exchange of momentum and heat proposed by Beljaars and Holtslag (1991):

$$\begin{aligned}\phi_m(\zeta) &= 1 + \zeta [a - b(d\zeta - c - 1)\exp(-d\zeta)] \\ \phi_h(\zeta) &= 1 + \zeta \left[ a \left( 1 + \frac{2}{3} a\zeta \right)^{1/2} - b(d\zeta - c - 1)\exp(-d\zeta) \right]\end{aligned}$$

where  $a = 1$ ,  $b = 0.667$ ,  $c = 5$ ,  $d = 0.35$ ,  $\zeta = z/L$ ,  $z$  is height above the surface and  $L$  the Obukhov length. The above formulation displays the characteristic that  $\phi_m$  tends to increase at a slower rate than  $\phi_h$  at higher stabilities as observed by Forrer and Rotach (1997), but continues to rely upon the assumptions of MOST. We here describe the application of an alternative surface scaling function for momentum over land points for stable conditions for use within the framework of MOST. The function is derived from observations from the CASES-99 intensive observational period (Poulos et al., 2002) and the UK Met Office Cardington tower site.

## Observations

Data for the month-long CASES-99 intensive observational period and a three month subset of observations from the Cardington site were analysed to examine flux-gradient relationships under stable conditions. In their analysis, Luhar et al. (in press) examined the changes in isotropy of local turbulence (ratio of vertical to horizontal turbulent velocity variance) with increasing stability (Figure 1), finding that a transition occurred at  $\zeta \approx 0.4$  (corresponding to a bulk Richardson number  $Ri_b \approx 0.25$ ) between two distinct turbulent states, supporting the conclusions of Zilitinkevich et al. (2007) and Galperin et al. (2007) who assert that turbulence, albeit different in nature, continues to exist at Richardson numbers even greater than unity. This is contrary to the notion of the classical ‘critical Richardson number’ ( $\approx 0.2$ ) separating turbulent and laminar flow states, leading modellers to re-evaluate the paradigm of turbulence parameterisation at high stabilities. Using these observations, a new surface stability function for momentum was determined by relating the non-dimensional wind speed ( $\kappa\bar{U}/u_*$ ) to stability

in a similar approach to Cheng and Brutsaert (2005), where  $\kappa$  is the von Karman constant (= 0.4) and  $u_*$  is the friction velocity.

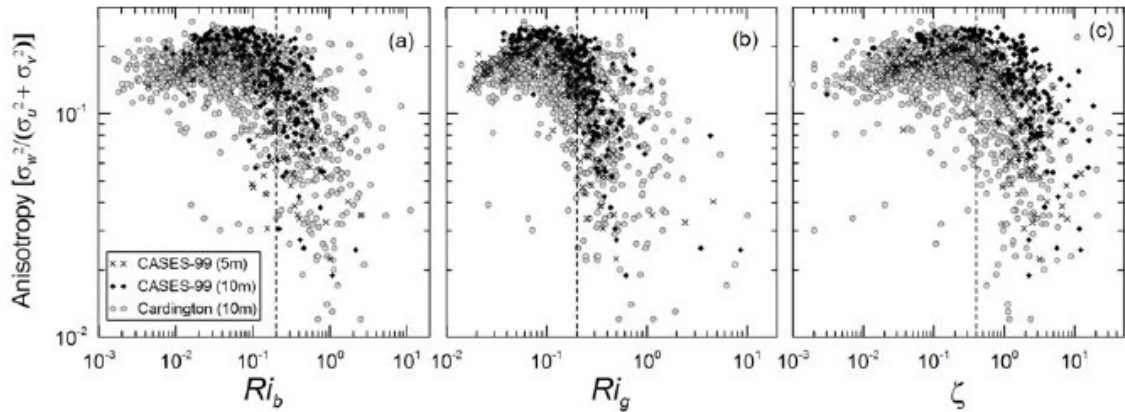


**Figure 1:** Observed variation of anisotropy with (a) bulk Richardson number ( $Ri_b$ ) (b) gradient Richardson number ( $Ri_g$ ) and (c) stability parameter ( $\zeta = z/L$ ) (Luhar et al., 2007)

## New parameterisation for $\phi_m$

In terms of variations of  $\phi_m$ , observations from the CASES-99 and Cardington datasets for stabilities greater than  $Ri_b \approx 0.25$  indicate that a discontinuity may exist for momentum as turbulence makes the transition to a different state. A parameterisation was developed to replicate such a transition by imposing an alternate stability function from stabilities greater than the threshold value (Figure 2). In addition, the new stability function for momentum does not contain any influence of the logarithmic profile dependence, instead following a power-law profile. The gradient function obtained from the non-dimensional wind speed parameterisation is:

$$\phi_m(\zeta) = \alpha\beta\zeta^\beta \left( 1 + \frac{\gamma}{\beta} \zeta^{1-\beta} \right)$$

where  $\alpha = 4$ ,  $\beta = 0.5$  and  $\gamma = 0.3$  for  $\zeta \geq 0.4$  chosen to fit the CASES-99 and Cardington observations. At stabilities below this threshold value, the Beljaars and Holtslag (1991) functions are retained.

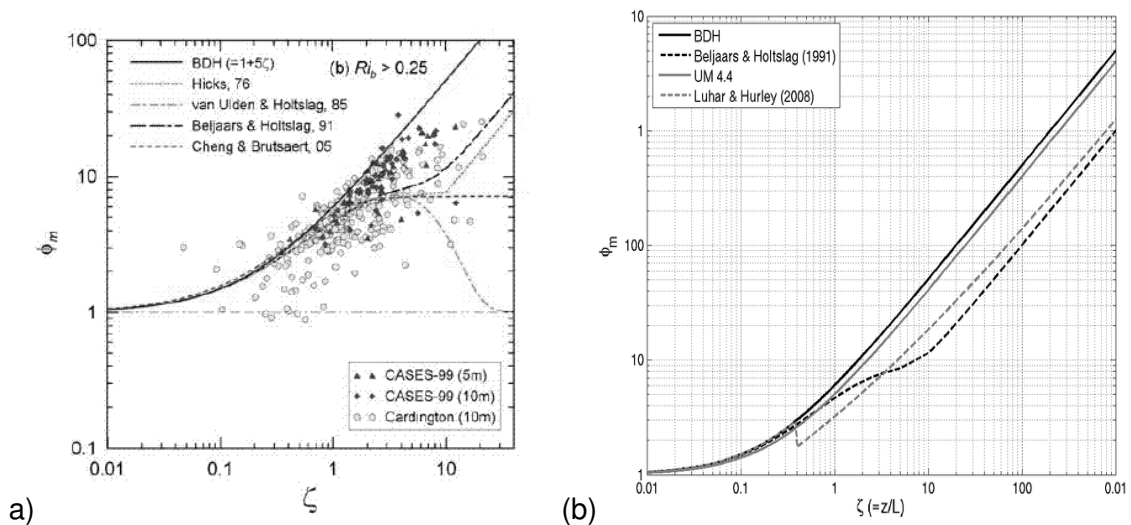


**Figure 2:** (a) Observed variation of  $\phi_m$  with  $\zeta$  for strongly stable conditions ( $Ri_b > 0.25$ ) with several reported parameterisation functions (from Luhar et al., in press) (b) functions used in the UM including new parameterisation function (grey, dashed line).

## Results

The initial testing phase of the surface scaling parameterisation was undertaken with the Single Column Model (SCM) version of ACCESS. The model was initially tested for the period of the CASES-99 observation period (October, 1999), periodically forced using profiles of temperature, wind and moisture from the numerical analyses of NCEP, ERA40, JRA and GASP. Although poorly constrained for the purposes of a direct comparison to observations, these simulations proved to be a useful test bed to examine the behaviour of the new surface scaling in a quasi-realistic framework. Figure 3a shows the difference in the calculations of bulk Richardson number over a range of stabilities using the alternate surface scaling parameterisation. There is also weak decrease in 10m wind speed evident in the simulations (Figure 3b), although the true extent of this is masked by the regular forcings of wind speed. The alternate surface scaling is now being tested in the full 3d model version.

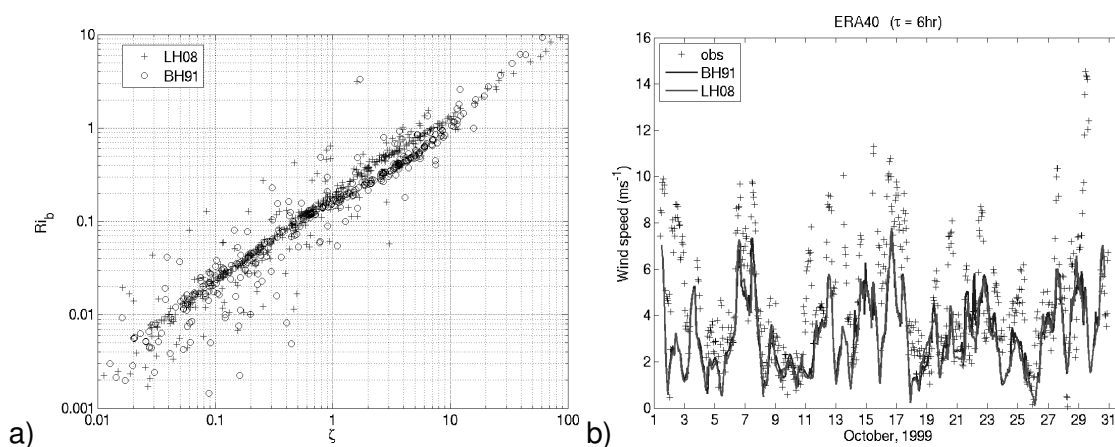


**Figure 3:** SCM simulation of CASES-99 using ERA40 forcing (a) variation of bulk Richardson number with stability parameter  $\zeta$  (b) 10m wind speed using momentum stability functions of Beljaars and Holtslag (black) and Luhar et al (gray).

## References

- Beljaars A.C.M. and Holtslag, A.A.M., 1991: Flux parameterization over land surfaces for atmospheric models. *J. Appl. Meteor.*, **30**, 327-341.
- Cheng, Y., and Brutsaert, W., 2005: Flux-profile relationships for wind speed and temperature in the stable atmospheric boundary layer. *Bound.-Layer Meteorol.*, **114**, 519-538.
- Cheng, Y., Parlange, M., and Brutsaert, W., 2005: Pathology of Monin-Obukhov similarity in the stable boundary layer. *Journ. Geophys. Res.*, **110**, doi:10.1029/2004JD004923.
- Forrer, J., and Rotach M.W., 1997: On the turbulence structure in the stable boundary layer over the Greenland ice sheet. *Bound.-Layer Meteorol.*, **85**, 111-136.
- Galperin, B., Sukoriansky, S., and Anderson, P.S., 2007: On the critical Richardson number in stably stratified turbulence. *Atmos. Sci. Lett.*, **8**, 65-69.
- Luhar, A., Hurley P.J., and Rayner K.N.: A modelling and observational study of near-surface winds over land under stable conditions. *Boundary-Layer Meteorol.* (under review).

- Luhar, A., Hurley P.J., and Rayner K.N., 2007: Modelling low wind-speed stable conditions in a prognostic meteorological model and comparison with field data. *Proc. 11th Int. Conf. Harmonisation within Atmospheric Dispersion Modelling for Regulatory Purposes*, Cambridge (UK), 2007.
- Mahrt, L., 1999: Stratified atmospheric boundary layers. *Bound.-Layer Meteorol.*, **90**, 375-396.
- Poulos, G.S., et al., 2002: CASES-99: A comprehensive investigation of the stable nocturnal boundary layer. *Bull. Amer. Met. Soc.*, **83**, 555-581.
- Zilitinkevich, S.S., Elperin, T., Kleerorin, N., and Rogachevskii, I., 2007: Energy- and flux-budget (EFB) turbulence closure model for stably stratified flows. Part I: steady state, homogeneous regimes. *Bound.-Layer Meteorol.*, **125**, 167-191.

# MJO and convection behaviour in SP-CAM and CAM simulation

Hongyan Zhu<sup>1</sup>, Harry Hendon<sup>1</sup> and Christian Jakob<sup>2</sup>

*1 Centre for Australian Weather and Climate Research: a partnership between the Bureau of Meteorology and CSIRO*

*2 Monash University*

The behaviour of convection and the MJO are investigated in two versions of the Community Atmospheric Model (CAM), the standard model with Zhang and McFarlane (1995) convection parameterization scheme (CAM), and a "multiscale modelling framework", in which the cumulus parameterization has been replaced with a cloud-resolving model (SP-CAM). Wavenumber-frequency spectrum analysis shows that there is a strong MJO, with pronounced spectral peaks in both precipitation and U850 fields, in the SP-CAM, but the MJO is completely absent in CAM simulation. In this study, we compare aspects of the different behaviour of convection in the two simulations with the aim of understanding what aspects of moist convection are important for simulation of the MJO.

We conclude that the following different features of convection are critical for the differences in MJO simulation in the two models:

1) In SP-CAM, rainfall exhibits an exponential increase with increasing column integrated relative humidity, consistent with gradual build up of shallow to deep convection, a "re-charge" process for governing the development of strong convection. In CAM, it tends to rain for low column relative humidity, indicating that the model can't sustain high column humidity and that the model rainfall does not depend on high column humidity. Instead, in the CAM it tends to rain prematurely. We infer this to be a limitation of CAPE closure in the CAM convection parameterization.

2) In SP-CAM, the precipitation is strongly related with tropospheric moisture anomaly, and humidity increases substantially over an increasingly deep layer with increasing rainfall. In CAM, there is relatively dry region in the lower troposphere that is strongly correlated with the boundary layer moisture anomaly.

The existence of a layer of dry air above the boundary layer for the deep convection in CAM also stems from the mass flux convective parameterization scheme: the CAM shows less adaptation to column relative humidity. The relative humidity of the environment plays a direct role in determining parcel buoyancy through entrainment. Derbyshire et al. (2004) suggest that relative humidity of the environment has an impact on cloud top height, hence on the large-scale circulation, on organized convection and on the MJO oscillation. A common problem in convective parameterizations based on mass flux models is the convective mass flux is insensitive to the environment relative humidity. For example, in a dry environment, deep convection can still occur. Lin et al. (2006) and Biasutti et al. (2006) also found that the sensitivity of deep convection to moisture in the lower troposphere above the boundary layer has not been well represented in many GCMs.

3) In SP-CAM, heavy precipitation is associated with a top heavy (stratiform) diabatic heating profile (as reflected by the associated vertical profile of the temperature perturbation), which should project onto slower horizontally propagating wave modes (e.g. Fulton and Schubert

1985). In the CAM simulation, the temperature profile is indicative of a convective-dominated heating profile that should project onto faster wave modes.

Lin et al. (2004) found that the observed profile of heating through the troposphere for the MJO is top heavy, and stratiform precipitation (heating the upper troposphere and cooling the lower troposphere) contributes more to the intraseasonal rainfall variations than it does to seasonal-mean rainfall. The role of the vertical heating profile for setting the strength and phase speed of intraseasonal oscillations has been studied in several works. For instance, a "stratiform instability" mechanism has been proposed by Mapes (2000). Yamasaki (1969) found in numerical modelling studies that some tropical systems are unstable only if the cumulus heating profile has a maximum in the upper troposphere. Lin et al. (2004) argued that a systematic lack of stratiform-like heating in models could be hypothesized to contribute to too-weak intraseasonal variability.

4) In SP-CAM, the latent heat flux increases the boundary layer entropy in phase with convection, and further decreases the value of CIN, therefore promoting sustained convection. In the CAM, the latent heat flux is reduced sharply during the development of deep convection, and thus acts to throttle deep convection.

All of these are not independent: built up convection is consistent with development of stratiform organization.

Wavenumber-frequency spectral analysis shows that the SP-CAM simulates a strong MJO while the CAM does not. We now attempt to relate this differing behaviour of convection in the two simulations to their differing simulations of the MJO.

Consistent with the recharge-discharge theory (e.g., Blade and Hartman 1993), there is a gradual moistening prior to the intense precipitation and afterward drying related to the MJO events for observations and in the SP-CAM. At the time of maximum MJO-rainfall, a stratiform heating profile is dominant for the SP-CAM and observations. In both SP-CAM and observations, shallow convection provides pre-condition for deep convection through a progressive moistening during the recharge (build-up) phase. However, the abrupt drying that accompanies the transition of the zonal wind as observed in Blade and Hartman (1993) are not captured by SP-CAM simulations.

The MJO-prec is mainly related to the rainfall events in the 5th quintile of rainfall rates, with precipitation in the lowest quintiles dominating during the MJO suppressed phase except in CAM simulation. There is a preceding shift from lower to upper quintiles prior to day 0 in both Sp-CAM and observation, but this feature is absent in CAM.

This analysis is not conclusive; however these sorts of analyses of convective behaviour could be performed with many different models, which all have different representation of the MJO but different treatment of convection. In this fashion, those aspects of convective behaviour (e.g. top heavy heating profile, re-charge of moisture, etc) which are critical for the MJO might be identified.

# **New strategies for comprehensive coupled atmosphere-wave-ocean modeling in tropical cyclones**

Isaac Ginis  
*Graduate School of Oceanography  
University of Rhode Island, Narragansett, RI USA*

## **1. Introduction**

The advent of numerical weather prediction tropical cyclone (TC) models has demonstrably improved the forecasts of TCs over the last decades. But to establish useful warning systems for TCs, it is necessary to accurately predict both storm track and intensity. Whereas TC tracks are determined almost exclusively by their large-scale atmospheric environment, storm intensity is influenced to a greater degree by smaller-scale features in both the atmosphere and ocean. The factors that control the intensity of TCs are still poorly understood, leading to limited reliability in forecasts of TC intensity evolution. Variability in TC intensity originates from two sources: internal variability and environmental interactions. There are three critical aspects of the environmental interactions: 1) the dynamical and microphysical processes near and at the sea surface that influence the turbulent exchange of heat and momentum between the ocean and atmosphere, 2) vertical and horizontal transport of momentum and heat in the atmospheric boundary layer and 3) the turbulent entrainment of relatively cold water through the seasonal thermocline, which affects the sea surface temperature and thereby influences storm intensity. Three-dimensional, coupled atmosphere-ocean research and operational models have been developed to simulate and predict the mutual response of a TC and the ocean (Bender and Ginis 2000, Bao et al., 2000, Bender et al., 2007, Chen et al., 2007, Surgi 2007). One such coupled model, the GFDL/URI hurricane-ocean prediction system, has been used operationally at the NOAA's National Centers for Environmental Prediction (NCEP) since 2001. The GFDL/URI model has demonstrated steady improvements in TC intensity prediction over the last several years (Bender et al. 2007). Another fully coupled model, the Hurricane Weather Research and Forecast (HWRF) model became operational at NCEP in 2007 (Surgi 2007).

Expert reports recently commissioned by NOAA, the U.S. National Science Board and the American Geophysical Union have concluded that further advances in TC intensity forecasts and impacts projection require novel theoretical concepts and the next generation very high resolution coupled atmosphere-wave-ocean numerical models with improved boundary layer and surface flux parameterizations, tested against high-quality observations.

Below I briefly summarize the results of the most recent efforts of our research group at URI and our collaborators and propose a future program of research to advance the understanding and parameterization of atmospheric boundary layer and surface fluxes in tropical cyclone conditions as a route toward skillful prediction of tropical cyclone intensity and structure.

## **2. Role of surface waves in air-sea momentum fluxes under tropical cyclones**

Recent observations from the Coupled Boundary Layer and Air-Sea Transfer (CBLAST) field program that was sponsored by the U.S. Office of Naval Research (Black et al., 2007) and the analysis of GPS drop sondes by Powell et al. (2003, 2007) have shown that the drag coefficient varies widely under TCs. However, even though this was one of the main foci of the CBLAST program, it was a daunting task to measure surface fluxes in wind speeds exceeding  $30 \text{ m s}^{-1}$ . Very few measurements exist for higher wind speeds and this remains an area of significant uncertainty.

Under the funding from the National Science Foundation and ONR CBLAST program our research group has developed a coupled air-sea interface model (ASIM) that explicitly resolves three key processes that are responsible for the wide variability of air-sea momentum flux: sea state dependence, air-sea flux budget and wind-wave-current interaction.

*a) Sea state dependence.* Proper evaluation of the sea state dependence of air-sea fluxes requires modeling the wave boundary layer (lower part of the atmospheric boundary layer that is affected by surface waves) and the equilibrium range of wave spectra. The effect of nonbreaking waves on the wave boundary layer was modeled using a variety of turbulence closure schemes (e.g., Chalikov and Makin, 1991, Makin and Mastenbroek, 1996, Makin and Kudryavtsev, 1999). Kudryavtsev and Makin (2001) investigated the impact of breaking waves on the wave boundary layer and the air-sea momentum flux.

Based on the equilibrium wave spectrum model by Hara and Belcher (2004) developed a new wave boundary layer model based on the conservation of momentum and energy by explicitly resolving the form drag due to non-breaking waves. Moon et al. (2004a,b,c) have coupled the NOAA's wave model (WAVEWATCH III or WW3), the equilibrium wave spectrum model, and the wave boundary layer model to predict the air-sea momentum fluxes over any given surface wave fields, including those under TCs. Fan et al. (2008a,b) extended this model to examine the turbulent kinetic energy (TKE) flux under growing seas and TCs.

Moon et al. (2004a,b,c) results have shown that the drag coefficient is spatially variable and is generally reduced at very high wind speeds under TCs, being consistent with the field observations. Another important finding is that the drag coefficient mainly depends on two parameters – wind speed and input wave age – regardless of the complexity of the wave field (even under TCs). Here, the input wave age is one of the standard output parameters of WW3 and is a measure of the development stage of locally wind forced waves, excluding the effects of long swell and waves that are misaligned with the local wind. Based on this finding Moon et al. (2007a) have developed a simplified parameterization of the drag coefficient in terms of the local wind speed and the local input wave age. This parameterization has been implemented into the GFDL/URI and HWRF operational coupled hurricane-wave models at NCEP (Bender et al. 2007) and the WAVEWATCH III wave model (Moon et al., 2008).

We have developed a new coupled wind and wave (CWW) model that includes the enhanced form drag of breaking waves. Breaking and non-breaking waves induce air-side fluxes of momentum and energy in a thin layer above the air-sea interface within the constant flux layer (the wave boundary layer). By imposing momentum and energy conservation in the wave boundary layer and wave energy conservation, we have derived coupled nonlinear advance-delay differential equations governing the wind speed, turbulent wind stress, wave height spectrum, and the length distribution of breaking wave crests. The system of equations is closed by introducing a relation between wave dissipation (due to breaking waves) and the wave height spectrum. Wave dissipation is proportional to nonlinear wave interactions if the wave curvature spectrum is below the threshold saturation level. Above this threshold, however, wave dissipation rapidly increases, thereby limiting the wave height spectrum.

The improved CWW model was first applied for fully-grown seas and then was applied for a wide range of wind wave conditions from laboratories to the open ocean. Kukulka and Hara (2008a,b) investigated the effect of air flow separation due to breaking waves on the air-sea momentum flux and concluded that the contribution of breaking waves is increasingly important for younger seas under higher wind speeds. The model results of the Charnock coefficient are similar to the results of non-breaking model (Hara and Belcher 2004, Moon et al., 2004a) for grown seas, but approach the breaking model results (Kukulka et al., 2007) for very young seas, highlighting the significant contribution of breaking waves under strongly forced conditions. This model provides the statistics of breaking wave events as a function of wave scales, and is a key component of the ASIM that includes the impact of sea sprays generated by breaking waves.

*b) Air-sea flux budget.* Traditionally, the momentum and TKE fluxes from wind to waves are assumed to be identical to the fluxes into subsurface currents due to wave breaking based on the assumption that no net momentum (or TKE) is gained (or lost) by surface waves. This assumption, however, is invalid when the surface wave field is not fully developed. Especially under TC conditions,

the surface wave field is complex and fast varying in space and time and may significantly affect the air-sea flux budget. Fan et al. (2008a,b) investigated the effect of surface gravity waves on the momentum and TKE transfer budget across the air-sea interface under growing seas and TC conditions. They found that the momentum and TKE fluxes into ocean currents may be significantly less than the fluxes from air when the wave field is growing and extracting momentum and TKE. The spatial variation of the TC-induced surface waves plays an important role in reducing the momentum and TKE fluxes into subsurface currents in the rear-right quadrant of the TC. In an idealized Category 3 TC moving with a forward speed of  $5 \text{ ms}^{-1}$ , this reduction is up to 7-8% for the momentum flux and 10% for the TKE flux on the right side of the storm. This difference highlights the significance of the air-sea flux budget analysis in coupled models.

*c) Wind-wave-current interaction.* Fan et al. (2008c) investigated the wind-wave-current interaction mechanisms in tropical cyclones and their effect on the surface wave and ocean responses a set of numerical experiments. The results show that the time and spatial variations in the surface wave field, as well as the wave-current interaction significantly reduce momentum flux into the currents. This reduction is the largest in the rear-right quadrant of the TC. In an idealized Category 3 TC moving with a forward speed of  $5 \text{ ms}^{-1}$ , wind-wave-current interaction can reduce the momentum flux into currents up to 10% relative to the flux from wind. The reduction in momentum flux into the ocean consequently reduces the magnitude of subsurface current and SST cooling to the right of the storm track and lessens mixed layer deepening in the wake of a TC. During wind-wave-current interaction, the momentum flux into the ocean is mainly affected by reducing the wind speed relative to currents, while the wave field is mostly affected by refraction due to the spatially varying currents. In the area where the current speed (in the wave propagation direction) has local maximum, the wave spectrum of longer waves is reduced, the peak frequency is shifted to a higher frequency, and the angular distribution of the wave energy is widened.

*d) Momentum flux parameterization in WAVEWATCH wave model.*

It has been known that the NCEP operational WAVEWATCH III (WW3) wave model overestimates the significant wave height under very high wind conditions in strong hurricanes (Tolman et al. 2005). Moon et al. (2008) applied the Moon et al. (2007) drag coefficient formulation with the reduced drag at high winds into the WW3 model. The results show significant improvements in the WW3 wave forecast during hurricanes. Fan et al. (2008d) continued this work and investigated the effects of wind-wave-current interaction on the wave predictions during Hurricane Ivan (2004) by coupling WW3 with the Princeton Ocean Model. The model results were compared with field observations of the surface wave spectra from a scanning radar altimeter (SAR), NDBC time series and satellite altimeter measurements. The results suggest that the WW3 model with the original drag coefficient parameterization tends to overestimate the significant wave height and the dominant wave length, and produces a wave spectrum that is higher in wave energy and narrower in directional spreading. When the improved drag parameterization of Moon et al. (2007) is introduced and the wave-current interaction is included, the model yields improved forecast of significant wave height and wave spectral energy. When the hurricane moves over pre-existing mesoscale ocean features (warm- and cold-core ring, Loop current), the short-term current response can be significantly modulated by the non-linear interaction of the storm-induced and pre-existing strong currents in the mixed layer. This modulation also affects surface gravity wave prediction.

### 3. Sea spray effects on tropical cyclones

During TC conditions, large amount of sea spray is produced by bursting air bubbles in whitecaps and by tearing spume from the wave crests. Consequently, both turbulence and sea spray provide routes by which moisture, heat and momentum cross the air-sea interface. Although the question as to whether or how sea spray affects the evolution of TCs has been around for a long time, the answer has remained elusive. All the modeling attempts to study the impact of sea spray evaporation on TCs have so far relied on simplified bulk parameterizations of the spray-mediated fluxes. They produced a wide range of contradictory effects on TC intensity, suggesting no impact (Wang et al., 1999), increased intensity

(Andreas and Emanuel, 2001; Bao et al., 2000), and reduced intensity (Lighthill et al., 1994; Henderson-Sellers et al., 1998).

There are several complex and not well understood aspects of sea spray dynamics in TC conditions. The first aspect is associated with spray generation processes. In nature, sea spray is the product of wave breaking. At present, all the spray-mediated flux schemes utilize very simple diagnostic relations to provide the wave-characteristic information based on the wind information only. In the current NOAA/ESRL air-sea heat flux parameterization scheme (Fairall et al., 2007) sea spray generation explicitly depends on two key wave parameters, namely, the total energy dissipation rate due to surface wave breaking, and the height of the droplet sources (i.e., the height of dominant breaking wave crests). These wave parameters are uniquely related to the wind speed if wave fields are fully developed. However, with young and complex wave fields under TCs these parameters are highly variable in space and time (e.g., Fan et al., 2008b). Therefore, a coupled TC-wave model is required to accurately simulate the sea spray generation and its impacts on TC forecasts.

The second aspect is the way in which spray effects are limited due to feedback processes within the marine boundary layer (MBL). That is, as spray exchanges heat and moisture with the atmosphere, it changes the temperature, humidity, and thermodynamic stability of the lower atmosphere, thereby changing the ability of additional spray droplets to conduct and evaporate. In the NOAA/ESRL air-sea heat flux parameterization scheme (Fairall et al., 1994), this effect is expressed in terms of the thermal feedback parameter  $\alpha$ . If spray droplets cool and moisten the layer in which they evaporate, they will thereby reduce sensible and latent heat fluxes carried by the droplets, and  $0 < \alpha < 1$ . The TC simulations in Kepert et al. (1999) and Bao et al. (2000) used an ad-hoc tuning that simply allowed  $\alpha$  to vary between 0 and 1 as a function of the total turbulent and droplet heat fluxes. There has been no data to justify this ad-hoc tuning. The work by Bao et al. (2000) and Wang et al. (1999) show that the results are very sensitive to the precise details of the spray flux.

The third aspect of sea spray is its direct effect on the surface stress where turbulence theory shows that surface drag can be reduced by heavy spray production. Theoretically, the concentration of sea spray droplets in the marine surface boundary layer can reach the level at which its associated air-flow density stratification will tend to suppress turbulence, reducing wind stress at the ocean surface and thus increase the surface wind speed (Kudryavtsev, 2006). However, in nature this process is much more complicated because this same turbulence is also responsible for maintaining the thermal air-fluxes. Reduction in wind stress will lead to reduction in thermal fluxes which in turn reduces the energy supply to the TC and ultimately limits the surface wind speed. It is important in the future to address the issue of how the stress reduction effect can be properly parameterized and incorporated into the TC model's physics at extreme high wind regimes.

The fourth aspect of sea spray is associated with the fate of the droplets after they have been thrown into the near-surface environment. This process is very complex and requires interactions on the MBL scale with full treatment of droplet microphysics and dynamics. If we picture sea spray droplets as being continuously thrown into the atmospheric surface layer, then their thermodynamic effect depends on their evaporation rate and their atmospheric suspension lifetime. The suspension lifetime in its turn depends on the fall velocity of large droplets and vertical transport by turbulence (which becomes more effective as wind speeds increase). However, the full evaporation of droplets is controlled by the sources of heat available to power the evaporation process and the interactions between droplets of different sizes. In dynamic equilibrium, there are only two heat sources: (1) upward turbulent transfer by sensible heat from the ocean, and (2) downward turbulent transfer of heat from the MBL above the droplet layer. Because evaporation of droplets cools and moistens both the MBL and the surface layer this problem cannot be investigated without realistic incorporation of full MBL-scale physics.

## 4. Roll vortices in tropical cyclones

The sensitivity of numerical models to MBL parameterization choice is fairly well-known (e.g. Braun and Tao, 2002). The boundary layer profiles and the surface wind factors are very sensitive to the details of

the turbulence parameterization. At present, little is known about boundary layer turbulence and its parameterization in TC conditions. As shown recently by Foster (2007), holding the surface flux parameterization constant, different MBL parameterization can generate very different boundary layer inflow and azimuthal flow profiles, vertical velocities, surface wind factors and inflow angles in TCs. However, improving the turbulence parameterization in TC models is still likely insufficient to capture the most elemental features of the TC MBL flow. A number of recent observational, numerical and theoretical studies have conclusively demonstrated that organized lineal coherent structures are prevalent in TC MBLs. These lineal features are the result of embedded secondary circulations in the TC MBL that consists of an overturning “roll” circulation in the plane roughly perpendicular to the mean flow direction. These rolls are spatially periodic with wavelengths that range from 100’s of meters to several km. The typical vertical and cross-roll velocities are  $>3$  to  $5 \text{ m s}^{-1}$  and the along-mean-wind perturbation velocities are  $>7$  to  $10 \text{ m s}^{-1}$ . The observational studies include analyses of satellite synthetic aperture radar (SAR) imagery (Katsaros et al., 2002; Zhang et al., 2006), land-based Doppler radar studies (Morrison et al., 2005; Lorsolo and Schroeder, 2006; Wurman and Winslow, 1998; Wurman et al., 2006) and aircraft penetrations into the boundary layer (Black et al., 2007).

As shown by theoretical analysis and numerical simulations in Foster (2005), Nolan (2005) and Ginis et al. (2004) boundary layer rolls have first-order effects on the fluxes within the TC MBL. The direct transfer of momentum, heat and water vapor by these structures across the MBL represents a potentially important contribution to the overall transport of momentum and enthalpy that is not currently included in TC models. Even in very high-resolution models roll vortices remain poorly represented as they require a horizontal resolution of  $\sim 50 \text{ m}$ . Better understanding of these processes and their parameterization in the MBL will enhance our ability to predict coupled ocean-atmosphere dynamics in TCs.

Under the ONR funding our research group has recently developed an efficient 2-D LES model which explicitly simulates roll vortices and their interaction with the 3-D mean flow in the MBL (Yu et al., 2008). This model is based on an approach that has been originally developed by Ginis et al. (2004) for an atmospheric boundary layer model in non-rotating fluid. The equation system of the model is deduced based on the results of a scale analysis allowing separation of the 3-D equation system into two coupled sub-systems: 2-D equations that resolve roll vortices explicitly (2-D LES model), imbedded into the 3-D equations of the large-scale atmospheric flow. The 2-D LES model has been calibrated using the results from 3-D LES model simulations. Yu et al. (2008) have conducted numerical experiments to study formation, orientation and scale selection of roll vortices in a prescribed mean sheared flow and identified key physical mechanisms important for development and decay of roll vortices in high wind conditions. At present, this model is being imbedded into a TC model.

## 5. New strategies for coupled TC-wave-ocean modeling

Our coupled TC-wave-ocean modeling strategies are predicated on two major assumptions:

- 1) Improved predictions of TC intensity, structure, and motion require a fully coupled ocean-wave-atmospheric model that explicitly resolves the effects of sea state on air-sea fluxes and spray generation.
- 2) The processes at the air-sea interface (e.g., wave breaking, fluxes, spray generation) and those in the MBL (e.g., roll vortices, sea spray transport and thermodynamics) in tropical cyclones are strongly coupled and have to be explicitly resolved.

Based on these assumptions we suggest to incorporate the following coupled modeling strategies:

- 1) In the TC and LES MBL models, the parameterizations of the air-sea heat and momentum fluxes and the spray source functions explicitly include the sea state dependence, ocean currents and SST; 2) the wave model is forced by the sea-state dependent momentum flux and includes the ocean current effects; 3) the ocean model is forced by the sea-state dependent momentum flux that accounts for the air-sea flux

budget; and 4) the TC and LES models are coupled by two-way interaction processes.

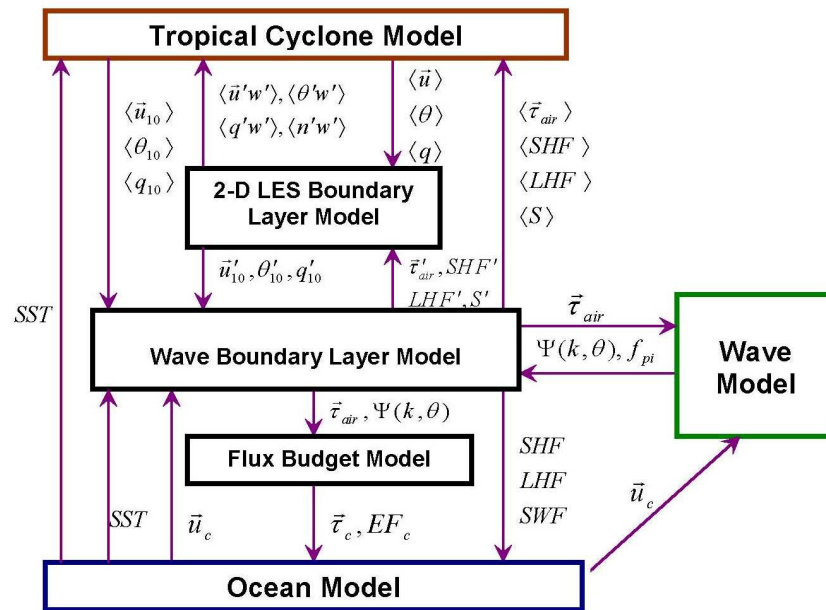


**Figure 1.** A schematic diagram of the coupled TC-LES-wave-ocean model being developed at URI. Here SST - sea surface temperature; SHF, LHF – sensible and latent heat fluxes and SWF – short-wave radiation flux.

Our research group at URI is presently working on implementation of these strategies into two hurricanes prediction models: GFDL and HWRF. The key element of our approach is the air-sea interface model (ASIM) developed by our research group at URI that consists of the wave boundary layer model of Moon et al (2004a,b) and the air-sea energy and momentum flux budget model of Fan et al (2008a,b,c). The ASIM is imbedded into the hurricane-wave-ocean coupled model and calculates all the flux boundary conditions for the atmospheric, wave and ocean components as shown in Figure 1. The ASIM is presently being augmented by including the effect of breaking waves on momentum and energy fluxes based on the theoretical studies of Kukulka et al. (2007) and Kukulka and Hara (2008a,b), and the sea-spray source function that explicitly depends on the breaking wave statistics. Another key element of our coupled model is a 2-D LES boundary layer model that is being embedded into the 3-D TC model to explicitly resolve roll vortices. The 2-D LES model and both GFDL and HWRF hurricane models will include the sea-spray dynamics based on the NOAA/ESRL sea-spray formulation (Kepert et al. 1999, Fairall et al. 2007).

## 6. References

- Andreas, E. L., and K. A. Emanuel, 2001: Effects of sea spray on tropical cyclone intensity. *J. Atmos. Sci.*, **58**, 3741-3751.
- Bao, J.-W., J. M. Wilczak, J.-K. Choi, and L. Kantha, 2000: Numerical simulations of air-sea interaction under high wind conditions using a coupled model: A study of hurricane development. *Mon. Wea. Rev.*, **128**, 2190-2210.
- Bender, M. A., and I. Ginis, 2000: Real-case simulations of hurricane-ocean interaction using a high-resolution coupled model: Effects on hurricane intensity. *Mon. Wea. Rev.*, **128**, 917-946.

- Bender, M.A., I. Ginis, R. Tuleya, B. Thomas, T. Marchok, 2007: The operational GFDL coupled hurricane-ocean prediction system and a summary of its performance. *Mon. Wea. Rev.* 135, 3965-3989.
- Black, P. G., and Coauthors, 2007: Air-sea exchange in hurricanes: Synthesis of observations from the Coupled Boundary Layer Air-Sea Transfer Experiment. *Bull. Amer. Meteor. Soc.*, **88**, 357-374.
- Braun, SA and WK Tao, 2002, Sensitivity of high-resolution simulations of hurricane Bob (1991) to planetary boundary layer parameterizations. *Mon Wea, Rev.* **130**, 39412-3961.
- Chalikov, D. V., and V. K. Makin, 1991: Models of the wave boundary layer, *Boundary Layer Meteorol.*, 56, 83-99.
- Chen, S. S., J. F. Price, W. Zhao, M. A. Donelan, and E. J. Walsh, 2007: The CBLAST-Hurricane Program and the next-generation fully coupled atmosphere-wave-ocean models for hurricane research and prediction. *Bull. Amer. Meteor. Soc.*, **88**, 311-317.
- Fairall, C. W., W. Asher, M. Banner, and W. Peirson, 2007: Investigation of the physical scaling of sea spray spume droplet production. *J. Geophys., Res.*, submitted.
- Fairall, C.W., J.D. Kepert and G.J. Holland, 1994: The effect of sea spray on surface energy transports over the ocean. *The Global Atmosphere and Ocean System*, **2**,121-142.
- Fan, Y., I. Ginis, T. Hara, and I. J. Moon, 2008a: Kinetic energy and momentum flux budget across air-sea interface: Part I: Steady uniform wind. *J. Geophys. Res.*, In review.
- Fan, Y., I. Ginis, T. Hara, and I. J. Moon, 2008b: Kinetic energy and momentum flux budget across air-sea interface: Part II: Tropical cyclones. *J. Geophys. Res.*, In review.
- Fan, Y., I. Ginis, and T. Hara, 2008c: The effect of wind-wave-current interaction on air-sea momentum fluxes and ocean response in tropical cyclones. *J. Phys. Oceanogr.*, 39, In press.
- Fan Y., I. Ginis, and T. Hara, C. W. Wright and E. J. Walsh, 2008d: Numerical simulations and observations of surface wave fields under an extreme tropical cyclone. Submitted to *J. Phys Oceanogr.*
- Foster, R.C., 2005: Why Rolls are Prevalent in the Hurricane Boundary Layer, *J. Atmos. Sci.*, 62, 2647-2661
- Foster, R.C., 2007 : Boundary Layer Similarity Under an Axisymmetric, Gradient Wind Vortex, 15<sup>th</sup> AMS Conference on Air-Sea Interaction. 20-24 August 2007, Portland, OR.
- Ginis, I., A. P. Khain, and E. Morozovsky, 2004: Effects of large eddies on the structure of the marine boundary layer under strong wind conditions. *J. Atmos. Sci.*, **61**, 3049-3064.
- Ginis, I., I-J. Moon, T. Hara, B. Thomas, M.A. Bender, 2006: Air-sea flux parameterization in a coupled tropical cyclone-wave-ocean model, *Eos Trans. AGU*, 87(36), Ocean Sci. Meet. Suppl. OS25C-01.
- Hara, T., and S. E. Belcher, 2004: Wind profile and drag coefficient over mature ocean surface wave spectra. *J. Phys. Oceanogr.*, 34, 2345-2358.
- Henderson-Sellers, A., G. Berz, R. Elsberry, K. Emanuel, W.M. Gray, C. Landsea, G. Holland, J. Lighthill, S.-L. Shieh, P. Webster, and H. Zhang, 1997: Tropical cyclones and global climate change: A post-FCC assessment. *Bull. Amer. Meteor. Soc.*, **79**,19-38.
- Katsaros, KB, P.W. Vachon, W.T. Liu, P.G. Black, 2002: Microwave remote sensing of tropical cyclones from space, *J. Oceanog.*, **58**, 137-151.
- Kepert, J. D., C. W. Fairall, and J.-W. Bao, 1999: Modeling the interaction between the atmospheric boundary layer and evaporating sea spray droplets. *Air-Sea Fluxes: Momentum, Heat, and Mass Exchange*, G. L. Geemaert, Editor, Kluwer, Dordrecht, 363-409.
- Kudryavtsev, V. N., 2006: On the effect of sea drops on the atmospheric boundary layer. *J. Geophys. Res.*, **111**, C07020, doi: 10.1029/2005/KC002970.
- Kudryavtsev, V. N., and V. K. Makin, 2001: The impact of air-flow separation on the drag of the sea surface, *Boundary Layer Meteorol.*, 98, 155-171.
- Kukulka T. and T. Hara, 2005. Momentum flux budget analysis of wind-driven air-water interfaces, *J. Geophys. Res.*, 110(C12020).
- Kukulka, T., T. Hara, and S. E. Belcher, 2007. A model of the air-sea momentum flux and breaking wave distribution for young, strongly forced wind-waves, *J. Phys. Oceanogr.*, 36(7), 1811-1828.

- Kukulka, T., and T. Hara, 2008a: The effect of breaking waves on a coupled model of wind and ocean surface waves. Part I: Mature seas, *J. Phys. Oceanogr.*, **38**, 2145-2163.
- Kukulka, T., and T. Hara, 2008b: The effect of breaking waves on a coupled model of wind and ocean surface waves. Part II: Growing seas, *J. Phys. Oceanogr.*, **38**, 2164-2184.
- Lighthill, J., G. Holland, W.M. Gray, C. Landsea, G. Craig, J. Evans, Y. Kurihara, and C. Guard, 1994: Global climate change and tropical cyclones. *Bull. Am. Met. Soc.*, **75**, 2147-2157.
- Makin, V. K., and V. N. Kudryavtsev, 1999: Coupled sea surface-atmosphere model 1. Wind over waves coupling, *J. Geophys. Res.*, 104 (C4), 7613–7624.
- Makin, V. K., and C. Mastenbroek (1996), Impact of waves on air-sea exchange of sensible heat and momentum, *Boundary Layer Meteorol.*, **79**, 279–300.
- Makin et al., 1995 Makin, V. K., V. N. Kudryavtsev, and C. Mastenbroek, 1995: Drag of the sea surface, *Boundary Layer Meteorol.*, **73**, 159–182.
- Moon, I. J., I. Ginis, T. Hara, H.L. Tolman, C. W. Wright, and E. J. Walsh, 2003. Numerical modeling of sea surface directional wave spectra under hurricane wind forcing. *J. Phys. Oceanogr.*, **33**(8), 1680-1706.
- Moon, I.-J., T. Hara, I. Ginis, S. E. Belcher, and H. Tolman, 2004a: Effect of surface waves on air–sea momentum exchange. Part I: Effect of mature and growing seas, *J. Atmos. Sci.*, **61**, 2321–2333.
- Moon, I.-J., I. Ginis, and T. Hara, 2004b: Effect of surface waves on air–sea momentum exchange. II: Behavior of drag coefficient under tropical cyclones, *J. Atmos. Sci.*, **61**, 2334–2348.
- Moon, I.-J., I. Ginis, and T. Hara, 2004c: Effect of surface waves on Charnock coefficient under tropical cyclones, *Geophys. Res. Lett.*, **31**, L20302.
- Moon, I.-J., I. Ginis, T. Hara, and B. Thomas, 2007: Physics-based parameterization of air-sea momentum flux at high wind speeds and its impact on hurricane intensity predictions. *Mon. Wea. Rev.* **135**, 2869-2878.
- Moon, I., I. Ginis, and T. Hara, 2008: Impact of reduced drag coefficient on ocean wave modeling under hurricane conditions, *Mon. Wea. Rev.*, **136**, 1217-1223.
- Morrison, I., S. Businger, I. F. Marks, P. Dodge, J. Businger, 2005: Observational evidence for the prevalence of roll vortices in hurricane boundary layers, *J. Atmos. Sci.*, **62**, 2662-2673
- Nolan, D.S., 2005 : Instabilities in hurricane-like boundary layers. *Dyn. Atmos. Oceans*, **40**, 209-236.
- Powell, M. D., P. J. Vickery, and T. A. Reinhold, 2003: Reduced drag coefficient for high wind speeds in tropical cyclones, *Nature*, **422**, 279 – 283, doi:doi:10.1038/nature01481.
- Powell, M. D, 2007: Drag coefficient distribution and wind speed dependence in tropical cyclones, JHT Final Report. April 2007.
- Surgj, N., 2007: Advanced hurricane prediction at NCEP’s Environmental Model Center: The operational implementation of the HWRF, 61<sup>st</sup> Interdepartmental Hurricane Conference, March 5-9, 2007, New Orleans, LA.
- Yu, Z., I. Ginis, and G.G Sutyryn, 2008: Roll vortices under high wind conditions and their impact on mean flow., *J. Atmos. Sci.* To be submitted.
- Tolman, H. L., J. H. G. M. Alves, Y. Y. and Chao, 2005: Operational forecasting of wind-generated waves by hurricane Isabel at NCEP, *Wea, Forecasting*, **20**, 544-557.
- Wang, Y., J. D. Kepert, and G. J. Holland, 1999: The impact of sea spray evaporation on tropical cyclone intensification. Preprints, 23d Conf. on Hurricanes and Tropical Meteorology, Dallas, TX, Amer. Meteor. Soc., 26–29.
- Wurman, J and J. Winslow, 1998: Intense sub-kilometer boundary layer rolls in Hurricane Fran, *Science*, **280**, 555-557.
- Wurman, J C. Alexander, P. Robinson, and F. Masters, 2006: Preliminary Comparison of DOW and In Situ Wind Measurements in Hurricane Rita. 27th AMS Conf. Hurricanes and Tropical Meteorology, 23-28 Apr., 2006, Monterey, CA.
- Zhang, J, W. M. Drennan, S. Lehner, K. B. Katsaros, and P. G. Black 2006: The effect of roll vortices on turbulent fluxes in the hurricane boundary layer, 27th AMS Conf. Hurricanes and Tropical Meteorology, 23-28 Apr., 2006, Monterey, CA.

# Evaluation of a regional ocean-atmosphere coupled weather prediction system

Paul Sandery and Gary Brassington

*p.sandery@bom.gov.au*

*CAWCR Centre for Australian Weather and Climate Research, Bureau of Meteorology, Melbourne, Australia*

## Abstract

A preliminary evaluation of a prototype coupled ocean-atmosphere limited-area weather prediction system configured for the northern Australian tropical region is presented. The coupled system uses an instance of the Bureau's tropical cyclone forecasting model *TCLAPS* that is run routinely for weather forecasts. The atmospheric model is coupled to a regional version of the *OceanMAPS-BLUElink* ocean forecasting system using *OASIS*. The system runs coupled forecasts in real-time taking input from the most recent ocean and atmosphere forecast information. We hypothesise that including a more complete and accurate representation of sea-state, sea-surface temperatures and feedback processes that influence the evolving oceanic and atmospheric boundary layers, will lead to improvement in coastal and marine weather forecasts in particular. A series of coupled forecasts are examined and the differences between these, original forecasts and observations are compared. Results are presented that demonstrate the impact of air-sea coupling on simulated tropical weather patterns in northern Australia and forecasts for local centres. The sensitivity of coupled weather simulations to SSTs modified by boundary layer dynamical processes and mesoscale oceanic features that in turn modify air-sea heat fluxes and structures in the atmospheric boundary layer is illustrated.



# Effects of air/sea interaction representations on ocean behaviour during tropical cyclones

Kevin Walsh<sup>1</sup>, Paul Sandery<sup>2</sup> and Gary Brassington<sup>2</sup>

*1 School of Earth Sciences, University of Melbourne*  
[kevin.walsh@unimelb.edu.au](mailto:kevin.walsh@unimelb.edu.au)

*2 Centre for Australian Weather and Climate Research: a partnership between the Bureau of Meteorology and CSIRO*

There remains considerable controversy regarding the dependence of drag and exchange coefficients on wind speed. The impact on ocean temperature profiles of various representations of these air/sea interaction processes is tested using a regional ocean model forced by idealized representations of tropical cyclone wind fields. The model used is CLAM (Coupled Limited Area Model), a regional configuration of the BLUElink global model. A number of severe tropical cyclone cases are simulated and the results compared with available SST observations. It is found that there is considerable sensitivity to the specification of drag and exchange coefficients and that this has implications for the parameterization of these processes in forecast models of tropical cyclones.



# Wave-Induced Upper-Ocean Mixing and Climate Modelling

Alexander V. Babanin<sup>1</sup>, Andrey Ganopolski<sup>2</sup> and William R.C. Phillips<sup>1</sup>

<sup>1</sup> Swinburne University of Technology, Melbourne, Australia, e-mail: [ababanin@swin.edu.au](mailto:ababanin@swin.edu.au), [wphillips@swin.edu.au](mailto:wphillips@swin.edu.au)

<sup>2</sup> Potsdam Institute for Climate Impact Research, Potsdam, Germany, e-mail: [andrey.ganopolski@pik-potsdam.de](mailto:andrey.ganopolski@pik-potsdam.de)

## Abstract

In air-sea interaction models, the wind stress is usually parameterised to directly drive the dynamics of the upper ocean, that is the wind stress provides a momentum flux to the ocean surface and the flux is then diffused down by means of turbulence. The dominant part of the wind stress, however, is supported by the flux of momentum from the wind to waves. This means that, before the momentum is received by the upper ocean in the form of turbulence and mean currents, it goes through a stage of surface wave motion. This motion can directly affect or influence the upper-ocean mixing and other processes, and thus disregarding the wave phase of momentum transformation may undermine accuracy of such parameterisations. There are at least two processes in the upper ocean which can deliver turbulence directly to the depths of the order of 100m instead of diffusing it from the top. First process is Langmuir circulation. Another mechanism is the wave-induced turbulence (in absence of breaking). The concept of this turbulence, its estimates and measurements, as well as implications of such turbulence for ocean circulation models, will be discussed.

## Introduction

Wind-generated waves and related phenomena are sub-grid processes from the point of view of climate models and therefore cannot be explicitly simulated by them. Nevertheless waves, at the very least, modulate all air-sea exchanges. Indeed surface waves play a primary role in upper-ocean mixing, a role which fast-tracks the thermodynamic balance between the atmosphere and the ocean. This role is often overlooked in large-scale models, where until now the wind has been parameterised to directly drive the dynamics of the upper ocean. That is, the wind stress is assumed to provide a flux of momentum to the ocean surface and that flux is then advected down by means of parameterised turbulence.

When viewed in more detail, however, it transpires that the dominant part of the wind stress is supported solely by the flux of momentum from the wind into the waves (e.g. Kudryavtsev and Makin 2002). This means that the momentum goes through an intermediate stage of wave motion prior to being transmitted into the upper ocean in the form of turbulence and mean currents. In fact, the waves accumulate only a small fraction, perhaps 3-4%, of the energy and momentum received (Donelan 1998), while the remainder is dissipated locally through wave breaking. Therefore, the prevailing approach would be acceptable were waves to transfer momentum into the ocean solely through wave breaking.

However, while wave breaking does inject turbulence kinetic energy into the ocean, the depths to which it penetrates are comparable only to the wave height, i.e. the order of meters, or in a major storm tens of meters (e.g. Terray et al. 1996, Babanin et al. 2005), whereas motions associated with the waves themselves penetrate to depths of the order of the wavelength of the dominant waves, which in the open ocean can be circa 100m. These motions can directly affect upper-ocean mixing to depths far below those achieved by wave breaking alone. In short, the prevailing approach likely grossly underestimates the mixed layer depth (MLD). If we further note that 2-3m of sea water has the same heat capacity as the

entire (dry) atmosphere (Gill, 1982, Soloviev and Lukas 2006), then we likewise see that gross underestimations of the MLD may undermine the accuracy of current climate models.

Here we explore two wave-related processes that can deliver turbulence kinetic energy to depths in excess of the surface wave amplitude. The first mechanism is a consequence of wave orbital motions, which acts to enhance turbulence kinetic energy and then transport it deeper into the layer (Babanin 2006). The presence of such motions is a wave property and is unrelated to wave breaking, although orbital motions will in addition act to transport turbulence kinetic energy antecedent to wave breaking. Moreover, turbulence production by such motions will persist to any depth where wave motion is significant. Potentially, it may even facilitate mixing across a thermocline. Thus including it, even within traditional  $k$ - $\epsilon$  mixing schemes, will provide an additional source of turbulence kinetic energy which is distributed over the mixed layer, whose depth is circa that of the wavelength of the dominant surface waves.

The second process is Langmuir circulation (e.g. Langmuir 1938, Phillips 2005). These circulations are a consequence of an instability resulting from the waves interacting with both themselves and a weak shear brought on by the wind (e.g. Craik and Levovich 1976, Phillips 1998). Their depth is determined by the wavelength of the dominant surface waves. Their rate of rotation is necessarily slow (of the order of cm/s); nevertheless, Langmuir circulation is a means to advect turbulence kinetic energy abundant in surface waters, deeper into the mixed layer. Smith (1992) provides strong observational evidence for the mixing prowess of Langmuir circulation, while Li et al. (1995) were the first to incorporate them in ocean models and question their role in deepening the mixed layer.

## Depth of wave-induced non-breaking mixing

Parameterisation of the wave-induced mixing depth due to turbulence generated by the wave orbital motion, unrelated to wave breaking, was done in Babanin (2006) and will not be reproduced here. For approximate estimates of such mixing in terms of the wind speed, shown in Figure 1, we employed the Pierson-Moscowitz limit and therefore it is an upper-limit value of such MLD.

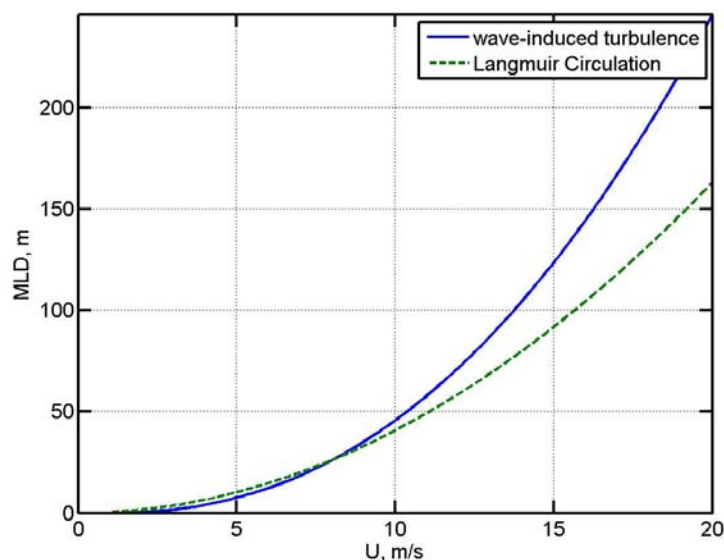


Figure 1. Prediction of MLD as a function of wind speed  $U$ , assuming that the mixing is driven either by the wave turbulence only (solid line) or by Langmuir circulation only (dashed line).

Parameterisation of the Langmuir-circulation mixing depth  $z$  in terms of the wind speed  $U$  are not available. Here, we will use relationship

$$z_{LC} = AU^2 / g \quad (1)$$

where  $g$  is the gravitational constant. The suggested expression is based on the observations by Smith (1992, 1998) that in each instance Langmuir-caused MLD scaled with the wavelength of the dominant-slope surface waves. To render (1) useful for our calculations, the constant  $A$  was chosen to match Smith's (1992) observations in which waves of 25m length are present in 8m/s winds, suggesting that  $A=4$ . Note that the depth of Langmuir cells not only determined, but is also restricted by the dominant wavelength, and therefore parameterisation (1) should not be used at scales greater than those wavelengths.

Parameterisations of MLD as a function of surface wind speed are compared in Figure 1 for the wave-induced turbulence and Langmuir-circulation mechanisms. Over the range of wind speeds shown, the latter is a weaker function of the wind speed and, if taken alone, is likely to underestimate the average MLD. For example, for wind speeds of 10m/s, which is close to average extra-tropical values, the wave-induced MLD parameterisation produces average depths just under 50m which is in reasonable agreement with observations (Carton et al. 2008) while Langmuir-circulation dependence suggests an MLD of about 40m. Therefore surface mixing as a consequence of wave-induced turbulence should, on average, dominate. And, although Langmuir circulation may act locally over smallish time scales, days or weeks say, to deepen the mixed layer, the long term average resulting solely from wave-induced turbulence is essential. Indeed, if, for example, the global winds were to grow to reach 15m/s, the mixing by wave-induced turbulence would realise a 125m-deep MLD and thus significantly alter the ocean-atmosphere thermodynamic balance. Therefore, estimates of the effect of the direct wave mixing below are done on the basis of the wave-induced turbulence parameterisation.

## Modelling pre-industrial climate

To study the effect of variable mixed layer depth on simulated equilibrium climate state and climate change, we use the climate model of intermediate complexity CLIMBER-2 (Ganopolski et al. 1998, Petoukhov et al. 2000). We compare simulations of the equilibrium preindustrial climate performed with the standard version (denoted as “STD”) of the CLIMBER-2 model (fixed 50m MLD) with the version (“VML”) which includes variable mixed layer depth as parameterised in the previous section. We performed two runs, each 3000 years long with constant preindustrial boundary conditions, by means of STD and VML versions. In both cases, qualitative patterns of the change of the environmental characteristics were similar, but wave-induced MLD parameterisation proved to be in a better agreement with the global atlas for monthly changes of the mixed-layer provided by the US Naval Research Laboratory (NRL) (<http://www7320.nrlssc.navy.mil/nmld/nmld.html>).

Impact of variable MLD on simulated climate characteristics is illustrated by Figure 2 which shows differences between VML and STD model versions for simulated summer (JJA) surface atmospheric temperature (top), sea-level pressure (middle) and precipitation (bottom). Local impacts are obviously significant, and, for instance, over the North Pacific the temperature differences between two model versions are as large as  $3^{\circ}C$  (Figure 2a). This further leads to changes in global sea-surface pressure patterns (Figure 2b) and atmospheric circulation. As a result, for example, differences in summer precipitations between VML and STD versions in South Eastern Asia region reach 3mm/day which is almost 50% of the absolute value of precipitation simulated in STD version.

## Conclusions

The results presented raise the issue of the importance of adequate modelling of MLD variations in climate models. In particular, emphasis is given to mixing driven directly by the waves. In this regard, although simulations are conducted by means of a model of intermediate complexity, the issue should be relevant for the general circulation ocean models (OGCMs) as well.

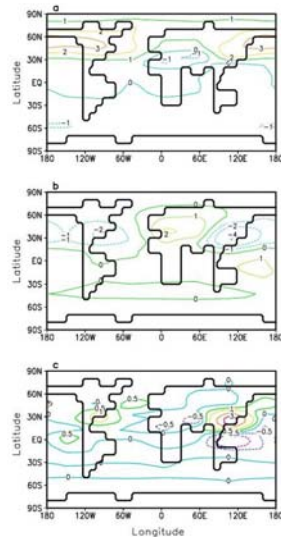


Figure 2. Differences between VDM and STD model simulation as described above.

## References

- Babanin, A.V., Young, I.R. and Mirfenderesk, H. 2005. Field and laboratory measurements of wave-bottom interaction. *Proc. 17th Australasian Coastal and Ocean Engineering Conf. and 10th Australasian Port and Harbour Conf., 20-23 September 2005, Adelaide, South Australia*, Eds. M.Townsend and D.Walker, The Institution of Engineers, Canberra, Australia, 293-298
- Babanin, A.V. 2006. On a wave-induced turbulence and a wave-mixed upper ocean layer. *Geophys. Res. Lett.*, 33, L20605, doi:10.1029/2006GL027308
- Carton, J.A., Grodsky, S.A. and Liu, H. 2008. Variability of the oceanic mixed layer. *J. Climate*, 21,1029-1047
- Craik, A.D.D. and Leibovich, S. 1976. A rational model for Langmuir circulations, *J. Fluid Mech.*, 73, 401-426
- Donelan, M.A. 1998. Air-water exchange processes. *Physical Processes in Lakes and Oceans*, 54, ed. J. Imberger, Coastal and Estuarine Studies, AGU, 19-36
- Ganopolski, A., Rahmstorf, S., Petoukhov, V. and Claussen, M. 1998. Simulation of modern and glacial climates with a coupled global model of intermediate complexity. *Nature*, 351,351-356
- Gill, A.E. 1982. *Atmosphere-Ocean Dynamics*. Elsevier, 662p
- Kudryavtsev, V.N. and Makin, V.K. 2002. Coupled dynamics of short waves and the airflow over long surface waves. *J. Geophys. Res.*, C107, 3209, doi:10.1029/2001JC001251
- Langmuir, I. 1938. Surface motion of water induced by the wind. *Science*, 87, 119-123
- Li, M., Zahariev, K. and Garrett, C. 1995. Role of Langmuir circulation in the deepening of the ocean surface mixed layer. *Science*, 270, 1955-1957
- Petoukhov, V., Ganopolski, A., Brovkin, V., Claussen, M., Elissev, A., Kubatzki, C. and Rahmstorf, S. 2000. LIMBER-2: a climate system model of intermediate complexity. Part I: model description and performance for present climate. *Clim. Dynam.*, 16, 1-17
- Phillips, W.R.C. 1998. Finite amplitude rotational waves in viscous shear flows. *Stud. Appl. Math.*, 101, 23-47
- Phillips, W.R.C. 2005. On the spacing of Langmuir circulation in strong shear. *J. Fluid Mech.*, 525, 215-236
- Smith, J. 1992. Observed growth of Langmuir circulation. *J. Geophys. Res.*, 97, 5651-5664
- Soloviev, A. and Lukas, R. 2006. The near-surface layer of the ocean: structure, dynamics and applications. *Springer*, 572p
- Terray, E.A., Donelan, M.A., Agrawal, Y.C., Drennan, W.M., Kahma, K.K., Williams III, A.J., Hwang, P.A. and Kitaigorodskii, S.A. 1996. Estimates of kinetic energy dissipation under breaking waves. *J. Phys. Oceanogr.*, 26, 792-807

# Two-way wind-wave coupling under tropical cyclone conditions

Eric Schulz<sup>1</sup> & Malek Ghantous<sup>2</sup>

<sup>1</sup>CAWRC-BoM, <sup>2</sup>School of Earth Sciences, University of Melbourne

Wave models provide reasonably accurate forecasts of the wave state under moderate conditions, but uncertainty increases rapidly under the extreme wind conditions observed in tropical cyclones (TC). One of the main barriers towards further research in this high wind regime has been the lack of *in situ* observations. This situation has changed in the past few years with the advent of drop sondes and wave buoys that provide observations of boundary layer winds and ocean waves under TCs. This has allowed the advancement of high wind speed boundary layer theory, and the interaction between TCs and the underlying waves to be investigated in a modelling framework. Here we present preliminary results of a 2-way coupling between the Bureau's wave model (WAM) and a simplified TC model. A number of traditional and new parameterisations of the surface roughness are also tested.



# The effect of sea waves on Typhoon *Imodu*

Liu Chunxia,<sup>1,2</sup> Yiquan Qi<sup>2</sup>, Jianying Liang<sup>1</sup>

1. Guangzhou Institute of Tropical and Marine Meteorology, CMA,  
Guangzhou, 510080

2. LED, South China Sea Institute of Oceanology, Chinese Academy of  
Sciences, Guangzhou 510301

## 1. Introduction

It is well known that the atmosphere-ocean interaction in typhoons is very complicated. In recent years, there have been many observational, numerical modeling and theoretical studies about the atmosphere-ocean interaction in high wind speed (e.g., Powell et al., 2003; Donelan et al., 2004; Emanuel, 2003). In particular, more scientists pay attention to the influence of sea state during tropical cyclone processes. For example, according to coupled atmosphere and wave model experiments, Desjardins et al. (2000) indicated that the effects of sea-state dependent surface roughness on the evolution and synoptic-scale aspects of the storm short-term forecasts are rather weak. Doyle (2002) investigated the impact of ocean waves on the structure and intensity of tropical cyclones using a coupled atmosphere-ocean wave modeling system. The main objective of this paper is to investigate the role of sea waves in the evolution of typhoon *Imodu* by coupling WRF and WAVEWATCH III wave model.

## 2. Typhoon process description

Typhoon *Imodu* formed in the western Pacific Ocean at 1800UTC 15 July 2003, and strengthened to typhoon force at 1800UTC 19 July 2003 when it was located at 10.9N 133.5E (Fig1). Then it crossed the Philippines into the Southern China Sea. *Imodu* continued towards the northwest reaching a maximum strength of  $45\text{ms}^{-1}$  and central pressure of 950hPa. Eventually, Typhoon *Imodu* made landfall between Yangxi and Dianbai, Guangdong Province China. The time period of interest in this study is from 0000UTC 23 July 2003 to 0000UTC 24 July 2003.

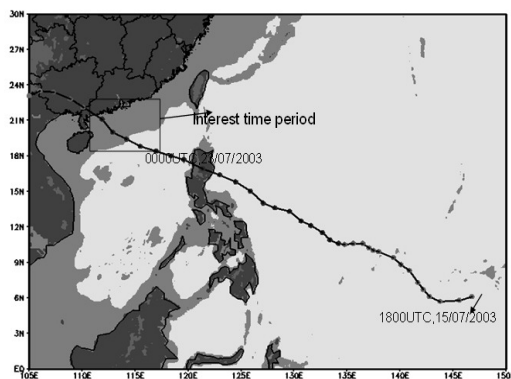


Fig. 1 Typhoon *Imodu* best track.

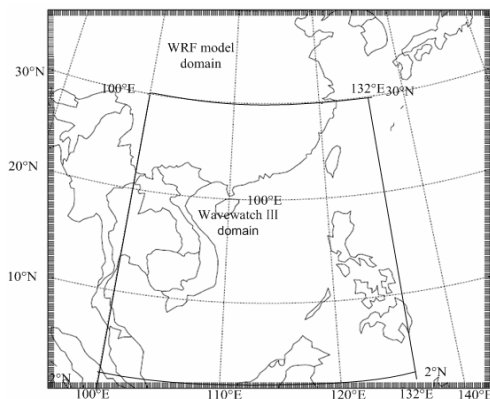


Fig.2 WRF and WAVEWATCH III domain.

### 3. Numerical model description

For this study, the coupled atmosphere-ocean wave model system is constructed with WRF V2.2 meteorological model (issued December 2006) and WAVEWATCH III. The coupling is bidirectional since the models influence each other throughout the integration. The sea surface temperature is kept fixed during the integration. The planetary boundary layer is based on the Yonsei University scheme, which includes non-local-K scheme with explicit entrainment layer and parabolic K profile in unstable mixed layer. The surface layer is based on similarity theory. The RRTM (Rapid Radiative Transfer Model) longwave and Dudhia Shortwave schemes are used. And a simple microphysics scheme, which accounted for vapor, cloud/ice, and rain/snow, is used. The land surface is 5-layer thermal diffusion scheme based on MM5 5-layer soil temperature model. The Cumulus parameterization scheme is based on Betts-Miller-Janjic convective adjustment scheme. WAVEWATCH III is the wave model from NCEP.

The domains of WRF model and WAVEWATCH III are described in Fig. 2. In this study, we only account for the impact of wave age on typhoon evolution. So, in the WRF model surface layer, we use the following formula (Smith et al., 1992) in place of the old one.

$$Z_0 = \alpha_c \left( \frac{u_*^2}{g} \right) , \quad \alpha_c = 0.48 \left( \frac{u_*}{C_p} \right)$$

$u_*/C_p$  is the inverse of wave age,  $C_p$  is the phase speed of the peak spectral frequency,  $u_*$  is the friction velocity and  $z_0$  is the roughness length. In our case, the coupling interval is 900s, and the WRF model time step is 90s so that the coupling takes place every ten time steps of WRF.

## 4. Results

### 4.1 Typhoon track and intensity

Figure 3 shows that the effect of sea waves on typhoon track is very small. The central pressure of the coupled simulation is lower than that of the uncoupled simulation, and the maximum wind speed of the coupled simulation is smaller than that of the uncoupled simulation. The maximum difference in pressure between the coupled simulation and the uncoupled simulation is 2hpa. Meanwhile the maximum difference in maximum wind speed between the coupled simulation and the uncoupled simulation is about 4.5 m/s. We also can find that the sea wave may affect the relationship between maximum wind speed and central pressure from Fig.3.

### 4.2 10m wind field

Figure 4 shows that the 10m wind speed of the coupled simulation in the inner area of the typhoon is larger than the wind speed of the uncoupled simulation where the wave age inverse is smaller. On the contrary, the 10m wind speed of the coupled simulation is smaller where the wave age inverse is larger. The older waves are in front of the typhoon along the direction of propagation, where the 10m wind speed intensifies. The young waves may cause the wind speed to decrease behind the typhoon.

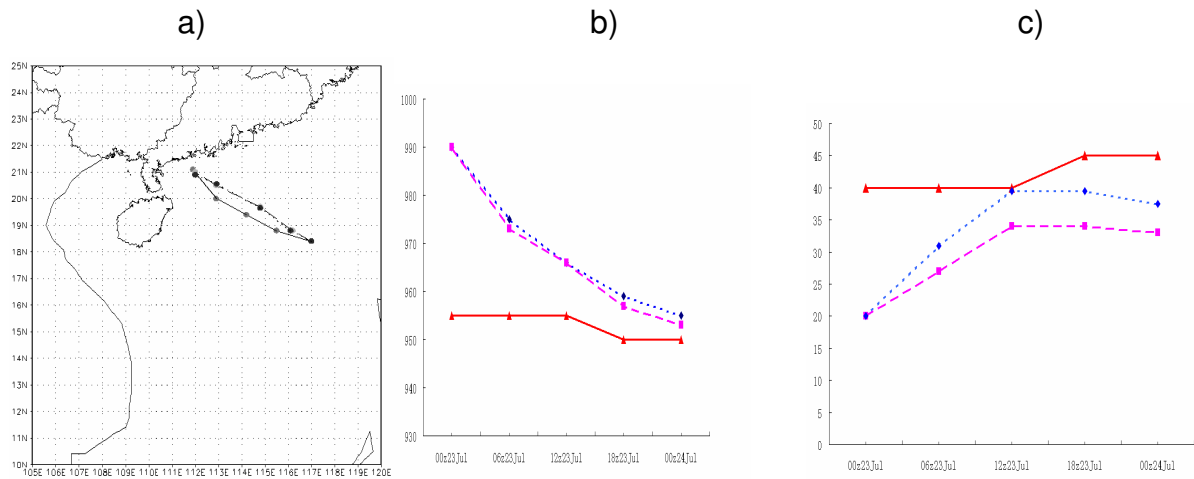


Fig.3 (a) Typhoon *Imodu* best track (solid line), the track of coupled simulation (dashed line) and the track of uncoupled simulation (dotted line). (b) The central sea level pressure of the best track (solid line), coupled simulation (dashed line) and uncoupled simulation (dotted line). (c) The maximum wind speed at 10m height of the best track (solid line), coupled simulation (dashed line) and uncoupled simulation (dotted line).

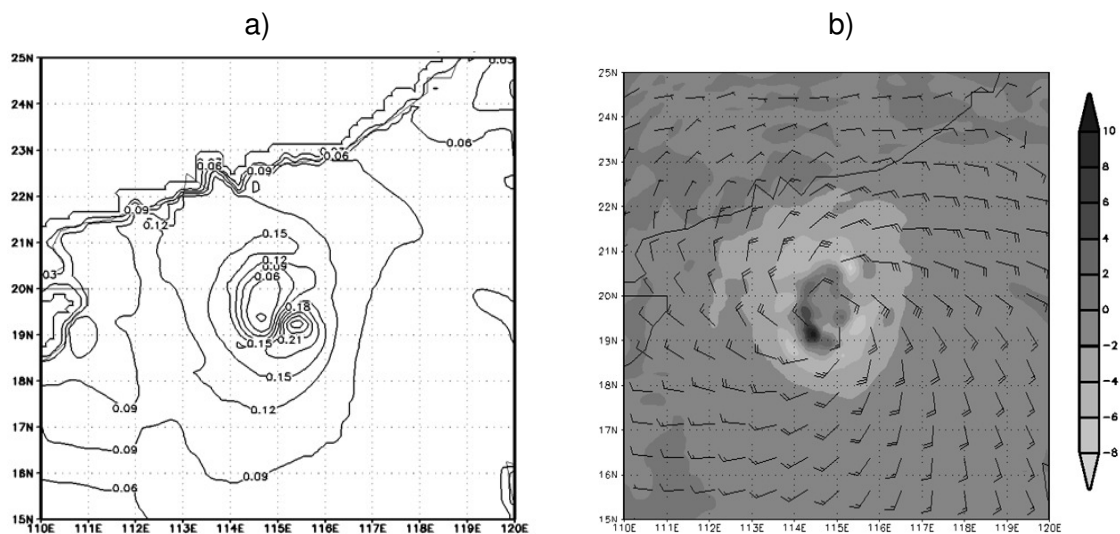


Fig.4 (a) Wave age inverse ( $u-/C_p$ ). (b) The 12-h forecast valid at 0000UTC 23 July 2003 of the 10m wind speed difference ( $\text{ms}^{-1}$ , grayscale) between coupled and uncoupled simulation and the coupled wind field.

### 4.3 Heat flux and rain of typhoon process

Figure 5a shows that the accumulated rain of the coupled simulation on the left of the typhoon along the direction of propagation is smaller than that of the uncoupled simulation, where the southwesterly wind is prevailing. But on the right of the typhoon, the accumulated rain of the coupled simulation is larger than that of the uncoupled simulation. We find the difference in latent heat flux between the coupled and uncoupled simulation reaches  $150\text{Wm}^{-2}$ , and the difference in sensible heat flux between the coupled and uncoupled simulations is under  $100\text{Wm}^{-2}$ . Therefore, the difference in heat flux is dominated by latent heat flux. Figures 5(a) and (b) show that the negative domain of accumulated rain

relates to a decrease of the latent heat flux by coupling wave. The mesoscale rain band structure of Typhoon *Imodu* may be showed detailed by the atmosphere-wave coupled model, and more information about the rain band structure can be obtained by comparing the rain between coupled and uncoupled simulations.

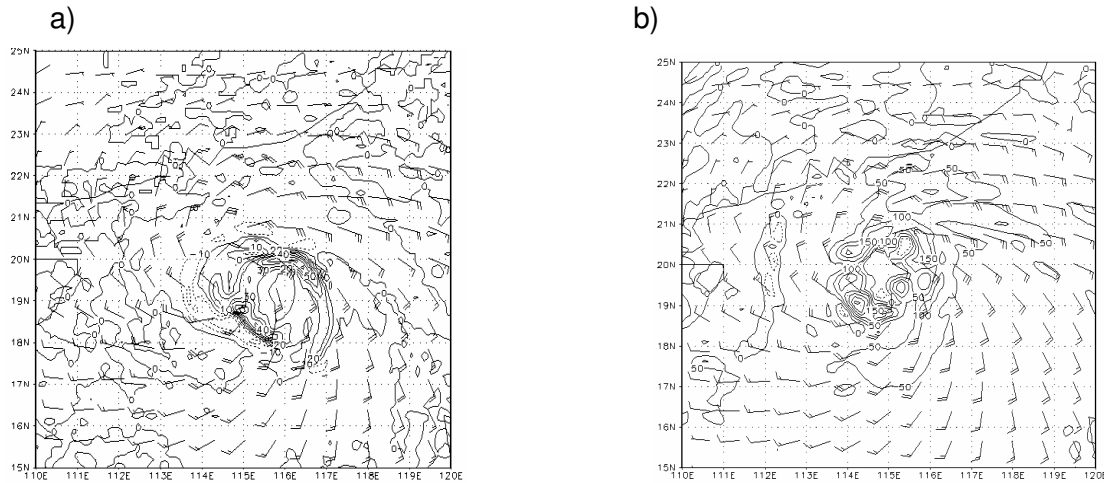


Fig 5. (a) The difference in the 12-h forecast valid at 0000UTC 23 July 2003 in accumulated rain between the coupled and uncoupled simulations, and the coupled wind field; (b) The difference in the 12-h forecast valid at 0000UTC 23 July 2003 in latent heat flux between the coupled and uncoupled simulations, and the coupled wind field.

## 5. References

- Desjardins, S., J. Mailhot, and R. Lalbeharry, 2000: Examination of the impact of a coupled atmospheric and ocean wave system. Part 1. Atmospheric aspects. *J. Phys. Oceanogr.*, 30, 385-401.
- Donelan, M.A., B.K. Haus, N. Reul, W. J. Plant, et al., 2004: On the limiting aerodynamic roughness of the ocean in very strong winds. *Geophys. Res. Lett.*, 31, L18306, doi:10.1029/2004GL019460.
- Doyle, J.D., 2002: Coupled atmosphere-ocean wave simulation under high wind condition. *Mon. Wea. Rev.*, 130, 3087-3099.
- Emanuel, K., 2003: A similarity hypothesis for air-sea exchange at extreme wind speeds. *J. Atmos. Sci.*, 60, 1420-1428.
- Powell, M. D., P.J. Vickery, and T. A. Reinhold, 2003: Reduced drag coefficient for high wind speeds in tropical cyclones. *Nature*, 422, 279-283.
- Smith, S.D., and Coauthors, 1992: Sea surface wind stress and drag coefficients: The HEXOS results. *Boundary-Layer Meteorol.*, 60, 109-142.

# Axisymmetric dynamics of tropical-cyclone intensification

Roger K. Smith

*Meteorological Institute, University of Munich, Germany*

**Preamble:** In this talk I will review some new research with my colleague, **Michael Montgomery** at the Naval Postgraduate School in Monterey, California, and my Ph. D. student, **Sang Nguyen**. The talk is a distillation of the results of two papers that are close to completion and which will be submitted to *Quart. J. Roy. Meteor. Soc.*.

(1) Montgomery, M. T., S. V. Nguyen and R. K. Smith. 2008: Do tropical cyclones intensify by WISHE? (Henceforth **M2**)

(2) Smith R. K., M. T. Montgomery and S. V. Nguyen. 2008: Axisymmetric dynamics of tropical-cyclone intensification in a three-dimensional model. (Henceforth **M3**)

These will be available soon at [http://www.meteo.physik.uni-muenchen.de/~roger/Roger/Rks\\_pubs.html](http://www.meteo.physik.uni-muenchen.de/~roger/Roger/Rks_pubs.html)

**Introduction:** Recently, Nguyen *et al.* (2008, *Quart. J. Roy. Meteor. Soc.*, **134**, 563-582; Henceforth **M1**) studied tropical cyclone intensification and predictability in the context of an idealized three-dimensional numerical model on an f-plane. The model has relatively simple physics including a bulk-aerodynamic formulation of the boundary layer and an explicit moisture scheme to represent deep convection. In the prototype amplification problem starting with a weak tropical storm strength vortex, the emergent flow becomes highly asymmetric and dominated by deep convective vortex structures, even though the problem as posed is essentially axisymmetric. The asymmetries that form are highly sensitive to the boundary-layer moisture distribution. When a small random moisture perturbation is added in the boundary layer at the initial time, the pattern of evolution of the flow asymmetries is dramatically changed and a non-negligible spread in the local and azimuthally-averaged intensity results. It was concluded that the intensification process is intrinsically asymmetric and small-scale features are random in nature. The local vertical rotation is amplified by deep convective towers growing in the rotation-rich environment of the incipient core. These so-called "vortical hot towers" (VHTs) are the basic coherent structures in the intensification process. In the numerical experiments it is the progressive segregation, merger and axisymmetrization of these VHTs and the low-level convergence they generate that is fundamental to the intensification process.

Prior to this study, most theoretical paradigms for tropical-cyclone intensification have been based on axisymmetric reasoning. One of these is the so-called wind-induced surface heat exchange, or WISHE-mechanism, a central feature of which is the relationship between fluctuations in subcloud-layer entropy and those in surface wind speed. The mechanism is summarized by Emanuel *et al.* (1994) and articulated in a revised form by Montgomery *et al.* (2008). It has become the accepted paradigm for explaining tropical-cyclone dynamics in university text books (e.g. Holton, 2004). It is central also to the theory for the potential intensity of tropical cyclones proposed by Emanuel (1988), which has been called upon by many researchers as a standard for comparison with the intensity attained in numerical models or assessments of possible changes in the intensity of hurricanes as a result of global warming.

Previous theoretical accounts of tropical-cyclone evolution have presumed that convergence above the boundary layer is a prerequisite for intensification and that this convergence must be large enough to oppose the frictionally-induced divergent outflow above the boundary layer (Ooyama 1969, 1982, Willoughby 1988, 1995, Smith 2000). In addition it has been supposed that friction generally reduces the winds in the boundary layer below the local gradient-wind value. For example, Willoughby (1995, p29) notes that "the swirling wind in the boundary layer is generally a little weaker than that just above" and Schubert and Alworth (1987, p157), in their theoretical study of tropical cyclone development using a Sawyer-Eliassen balanced vortex model, state that " ... one would expect that the inclusion of friction would reduce the low-level winds ... to bring closer agreement with observations". More recently, Raymond *et al.* (1998) assumes also that the boundary layer is generally responsible for spin-down, noting that " ... cyclone development occurs when the tendency of convergence to enhance the low-level circulation of a system defeats the tendency of surface friction to spin the system down".

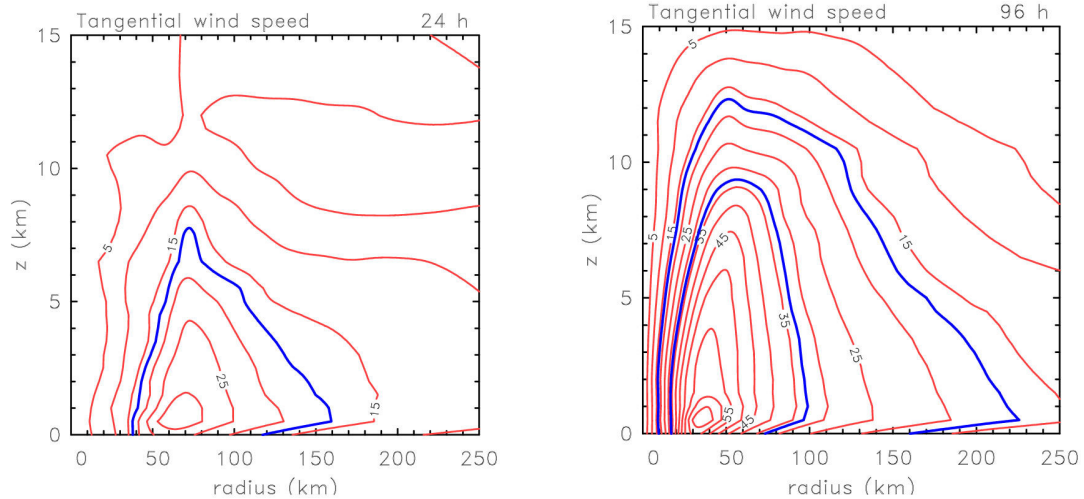


Figure 1. Radius-height cross-section of isotachs of azimuthal-mean tangential wind at 24 h (left) and 96 h (right). Contour interval  $5 \text{ m s}^{-1}$ . The thick blue contours indicate the location of gale-force ( $17 \text{ m s}^{-1}$ ) and hurricane-force ( $33 \text{ m s}^{-1}$ ) winds.

The idea that convergence above the boundary layer is a prerequisite for vortex spinup is that, in the absence of friction, the absolute angular momentum,  $M$ , is materially conserved. This quantity is related to the tangential wind speed,  $v$ , by the formula:  $v = M/r - fr/2$ , where  $f$  is the Coriolis parameter. For constant  $M$ , both terms in this expression lead to an increase in  $v$  as  $r$  decreases. An alternative, but equivalent interpretation for the acceleration of the mean tangential wind follows directly from Newton's second law in which the sole force is the generalized Coriolis force,  $-u(v/r + f)$ , associated with the mean radial component of inflow. In the boundary layer, absolute angular momentum is not materially conserved because of the frictional torque in the tangential direction, but if rings of air converge quickly enough, i.e. if the generalized Coriolis force exceeds the frictional torque, the tangential winds can increase with decreasing radius in the boundary layer as well. It is precisely for this reason that supergradient winds can arise in the boundary layer (Kepert, 2001; Smith and Vogl, 2008).

The development of supergradient winds in the boundary layer raises the possibility that the spinup of the inner core could proceed independently of the outer circulation. For example, in Emanuel's (1997) model of hurricane intensification as a frontogenetic process in equivalent potential temperature, core spin up arises entirely in the boundary layer, although the balanced boundary layer that forms the dynamical part of that model is forbidden from generating supergradient winds (Smith and Montgomery 2008). Thus the foregoing pathway to spinup is excluded from that model. Nevertheless, the importance of the boundary layer to vortex spin up finds support in unpublished calculations performed by my late colleague, Wolfgang Ulrich. Using a simple axisymmetric tropical-cyclone model and performing back trajectory calculations, he found that in all calculations examined, the ring of air associated with the maximum tangential wind speed invariably emanates from the boundary layer at some large radius from the storm axis. These findings naturally raise a fundamental question: *What are the relative roles of convergence in the boundary layer to convergence above the boundary layer in the spinup of the mean tangential winds, both in the inner core and in the region of gales?* In this talk I will seek to answer this question in terms of mean fields obtained from one of the three-dimensional numerical experiments performed by Nguyen *et al.* (2008). Further aspects of the dynamics and thermodynamics of tropical-cyclone intensification are discussed in M3 and M2, respectively. The latter paper challenges the foundations of the WISHE mechanism, itself.

## Results

Figure 1 shows radial-height plots of the azimuthal-mean tangential wind speed at 24 h and 96 h. It is noteworthy that the maximum tangential wind speed occurs at near the surface and that the vortex broadens with time as it intensifies. We have highlighted the latter feature by plotting the isotachs of gale-

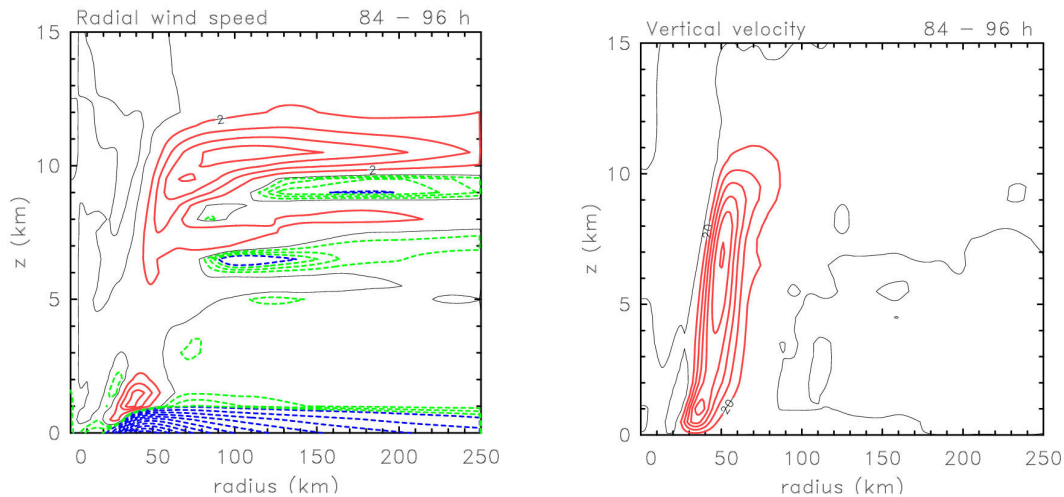


Figure 2. Radius-height cross-section of isotachs of the time-mean radial velocity (left, contour interval red and blue  $2 \text{ m s}^{-1}$ , green  $0.5 \text{ m s}^{-1}$ ) and vertical velocity (right, contour interval  $20 \text{ cm s}^{-1}$ ) during the period 84-96 h. Solid curves positive, dashed curves negative. Thin solid lines are zero contours.

force and hurricane-force winds. Note that the radius of gales moves outwards as the inner core strengthens. The reasons for this growth are discussed below.

The instantaneous fields of radial and vertical motion include the effects of inertia-gravity waves initiated by the VHTs and in order to filter these it is necessary to time average the fields. Figure 2 shows radius-height cross-section of the isotachs of the time-mean, azimuthal-mean, radial and vertical velocities during the period 84-96 h. A notable feature is that the strongest radial inflow takes place in a very shallow boundary layer. There is generally inflow in the lower troposphere, above the boundary layer, but it is much weaker with speeds mostly less than  $0.5 \text{ m s}^{-1}$ . There is a local region of strong outflow just above the inflow where it terminates. There is mostly outflow in the upper troposphere and this is spread over a much layer than the inflow, with maxima occurring at heights of around 10. Conspicuously there are one or two shallow regions of inflow in the upper troposphere with mean radial wind speeds reaching  $2 \text{ m s}^{-1}$ . There are two maxima in the vertical velocity, one is low down and marks the region where the boundary layer inflow rapidly terminates, erupting upwards and outwards. The other maximum is much higher and is presumably associated with the axisymmetric mean of deep convective updrafts and the local buoyancy within the VHTs as documented in Montgomery *et al.* (2008).

I examine now the relative roles of convergence in the boundary layer to that above the boundary layer in the spinup of the mean tangential winds, both in the inner core and in the region of gales. A well-known result from the inviscid axisymmetric balanced theory of vortex intensification is that the latent heat release in eye-wall convection produces a secondary circulation in which the tangential wind tendency is largest inside the radius of maximum tangential wind speed (Shapiro and Willoughby, 1982). Thus in this theory the vortex always contracts as it intensifies. The inherent assumption here is that the convergence takes place *above the boundary layer* and that the spinup occurs there. However, in the present calculations the largest tangential wind speeds and tendencies are found in the boundary layer, which owes its existence intrinsically to gradient wind imbalance. Thus a balanced theory cannot account for this feature (Smith and Montgomery, 2008).

Further insight into the foregoing question is provided by an analysis of the evolution of the mean absolute angular momentum fields. Figure 3 shows radial-height plots of these fields at the initial time and at 96 h. Some contours values have been coloured blue to highlight specific aspects of the evolution. This procedure is useful because in the absence of friction, absolute angular momentum is a materially-conserved property in an axisymmetric mean sense, provided at least that the eddy fluxes associated with asymmetric motions can be ignored. In regions where this condition is valid, the tangential wind speed will increase where the mean absolute angular momentum isopleths move inwards and decrease where they move outwards. Consider first the two inner blue contours in Fig. 3. These subsequently move

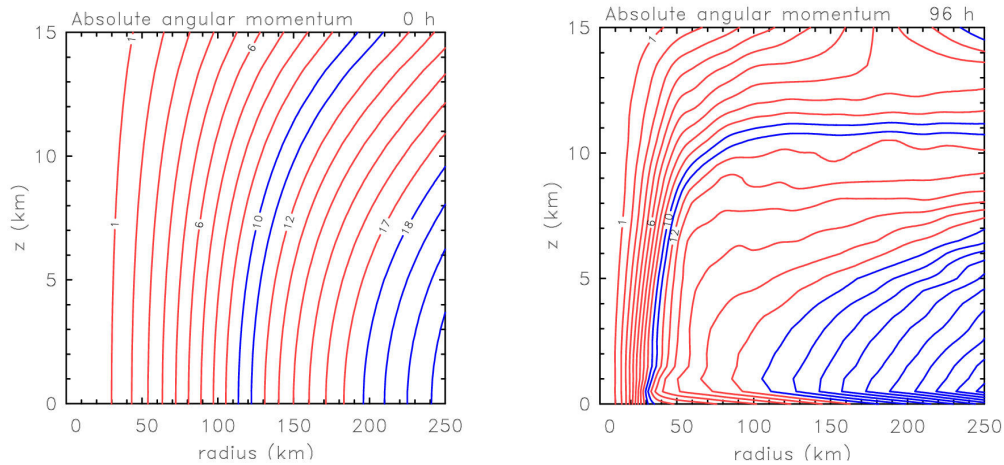


Figure 3. Radius-height cross-section of isopleths of absolute angular momentum at the initial time (left) and 96 h (right). (Contour interval  $5 \times 10^6 \text{ m}^2 \text{ s}^{-1}$ ).

inwards in the lower troposphere and outwards in the upper troposphere. Notably they emanate from the region where the boundary layer erupts into the vortex above and where the boundary layer winds are supergradient (see M3, Fig. 6). These results suggest an important modification of Shapiro and Willoughby's balanced picture as foreshadowed by Smith and Vogl (2008). If the boundary layer tends to generate supergradient winds inside the radius of maximum tangential wind speed, and if these winds are advected vertically out of the boundary layer, they would contribute in a similar way to a spin up of the core region in the free atmosphere. Nevertheless, since the strongest winds occur in the boundary layer, we would expect their evolution to be tied to the pressure gradients associated with the mass distribution aloft. In this view the intensification of the inner-core is a low-level process tied strongly to the dynamics of the boundary layer, which is intrinsically not in gradient-wind balance.

The foregoing ideas are supported by plots of the tangential wind tendency averaged during the periods 24-36 h and (b) 48-60 h (see M3, Fig. 8). During both time periods, the maximum tendency lies at low levels, especially during the period 48-60 h. This feature is consistent with the boundary layer playing the central role in the spin up of the inner core region.

Consider now the outer blue contours in Fig. 3. It is clear that these move inwards, but it can be shown that they lie above the region where the boundary layer winds are subgradient and where the flow is subsiding into the boundary layer. The inward motion is to be expected from the plot of mean radial motion shown in Fig. 2. The slow, but progressive inward motion explains the spinup of the outer circulation. As the radial motion and spinup occur in a region above the boundary layer where the tangential flow is close to gradient wind balance, it may be interpreted as resulting from the balanced response of the flow to gradual changes in the azimuthally-averaged heating rate in the convective region of the vortex. Such a response is described approximately by the Sawyer-Eliassen equation.

The foregoing results provide a physical explanation for certain long-standing observations of typhoons by Weatherford and Gray (1988), which indicate that inner-core changes in the azimuthal-mean tangential wind speed often occur independently from those in the outer-core. We have shown that there are two independent mechanisms for bringing about such changes, one that serves to intensify the core as soon as the boundary-layer winds become supergradient and the other that acts to spin up the outer circulation.

**References:** A full set of references is contained in M1, M2 and M3.

# Experiments with initialization and prediction of Tropical Cyclone structure and intensity

Noel Davidson<sup>1</sup>, Yimin Ma<sup>1</sup>, Chi Mai Nguyen<sup>2</sup>, Harry Weber<sup>3</sup>, Yi Xiao<sup>1</sup>  
and Marie-Dominique Leroux<sup>4</sup>  
[n.davidson@bom.gov.au](mailto:n.davidson@bom.gov.au)

<sup>1</sup> *Centre for Australian Weather and Climate Research:  
A partnership between CSIRO and the Bureau of Meteorology*

<sup>2</sup> *School of Mathematical Sciences, Monash University*

<sup>3</sup> *Meteorological Institute, University of Munich*

<sup>4</sup> *Permanent Affiliation: Meteo-France*

## Introduction

Objective verification of intensity forecasts from the Bureau's operational Tropical Cyclone Limited Area Forecast System, TC-LAPS (Davidson and Weber, 2000) indicates a level of skill slightly greater than climatology-persistence at 48 hours (Sampson and Knaff, 2009). These encouraging results indicate that skilful prediction of intensity and structure is indeed possible. Improved skill in structure forecasting will have major benefits for operational forecasting and nowhere more so than in detailed predictions of landfall (rain and wind) and storm surge.

Two key aspects of intensity and structure forecasting are: (a) Prediction of the large scale environment (LSE), and (b) Initial specification of storm structure. Objective verification of forecasts from the Australian Community Climate and Earth System Simulator (ACCESS, Puri et al., 2008, personal communication) has been most encouraging. ACCESS, based on the UK Met Office's 4DVAR and Unified Model, will provide major improvements in prediction of the LSE relative to that which is available to TC-LAPS.

Further, increased understanding of intensity change and vortex structure will continue to provide insights into methods for more skilful prediction.

## Estimated storm structure

Because of the paucity of observations available to initialize realistic TC circulations, a synthetic vortex is needed to construct the inner-core of storms for prediction. Figure 1 shows the fit of 7 such synthetic profiles to quality-controlled estimates of storm structure for 154 base times for storms over the North Atlantic and Gulf of Mexico (Ma et al., 2009). The parameters available to define storm structure are: central pressure (CP), maximum wind (VMAX), radius of maximum wind (RMW), radius of 34, 50 and 64 knot winds (R34, R50, R64), and radius of outer closed isobar (ROCI). Most idealized profiles use only a subset of these parameters. The left panel highlights the inner-core structure and the right panel is for the structure at outer radii. Note that the profiles differ both inside the RMW (so-called "U" and "V" profiles) and outside the RMW, where some profiles have a broader region of strong winds and others have winds which decrease rapidly with radius.

Even with the uncertainties in the estimation of some vortex parameters, we suggest that by utilising a more complete set of parameters for the vortex specification, it is possible to initialize TC structures which are more consistent with actual TCs and with the LSE.

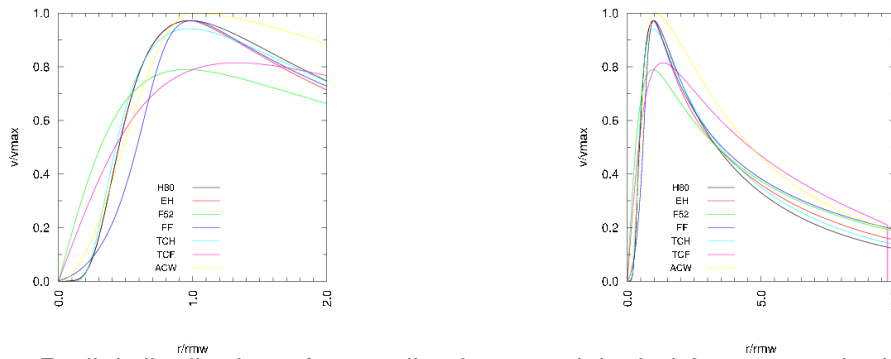


**Figure 1:** Radial distribution of normalized tangential wind from 7 synthetic profiles from 154 base time estimates of storm structure.



**Figure 2:** Radial distribution of mean 850 hPa PV (dashed lines) and its radial gradient (solid lines) during two asymmetric phases (A1,A2; left panel) and two symmetric phases (S1, S2; right panel).

## Forecast storm structure

The variability in storm structure, particularly of the inner-core is illustrated in Fig. 2, taken from Nguyen et al. (2008). In this study, internal structure change during the rapid intensification of Katrina (2005) was investigated. The simulated storm goes through asymmetric and symmetric cycles. Mesoscale convective vortices develop in the inner-core and then are axisymmetrized. During these phases the storm is characterized by a monopole potential vorticity (PV) structure (asymmetric phase, left panel) and a PV ring structure (symmetric phase, right panel), which is barotropically unstable.

Based on the consistent findings between the observational study of Kossin and Eastin (2001) and the high-resolution modelling study of Nguyen et al. (2008), the transition from symmetric to asymmetric state is rather rapid, while that from asymmetric to symmetric state is quite slow. This may imply that specification of a symmetric state may be more desirable during initialization. Experiments are planned to test this hypothesis.

## Impact of storm structure on forecasts

We have tested and validated the structures from 7 profiles for 3 storms (Bonnie (1998), Ivan (2004) and Katrina (2005)) over the North Atlantic and Gulf of Mexico where, because of available reconnaissance and dropsonde data, we might expect that vortex estimates are more reliable. These experiments (Davidson and Ma, 2009) were run using an enhanced TC-LAPS configuration at a resolution of  $0.05^\circ$ .

For these cases, the impact on forecast track is small (not illustrated), possibly because environmental control is so strong that the motion of nearly any vortex is determined by the environment.

For structure and intensity however, and particularly for Katrina, the forecasts are sensitive to the initial vortex specification. Figure 3 shows for Katrina from the 7 profiles, initialized (left panel) and 48 hour forecast values (right panel) of the radial profile of tangential wind. Also shown are estimated values of VMAX (and hence RMW), R34, R50 and R64. A very encouraging aspect of the forecasts is the ability of the model to preserve the relatively small RMW (~ 40km).

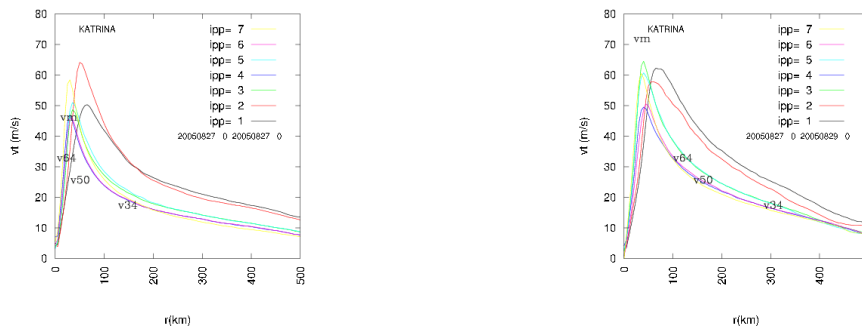


**Figure 3:** Radial distribution of initialized and 48-hour forecasts of tangential wind from 7 synthetic profiles for Hurricane Katrina. Base time is 00UTC, 20050827. Estimated values of VMAX (and hence RMW), R64, R50 and R34 are indicated.

For two profiles the RMW does not give a close fit to the estimated initial value. For two profiles, the timing of the intensification is rather poor and has commenced even during the initialization. For two profiles, the strengthening is poorly forecast with the predicted intensification much weaker than observed. For two of the profiles, in fact those that best fit the estimated structure, the forecast intensification is quite skilful. Note also that forecasts from all profiles predict the observed large increase in storm size during the forecast period. However storms initialized to be large are forecast to grow even larger, while storms initialized nearer to the correct size are forecast to grow to a more realistic size.

Another example of the impact of storm structure on prediction, this time on track, is illustrated in Fig. 4. It shows observed and forecast tracks and intensities from two forecasts of Typhoon Sinlaku, initialized with markedly different initial vortex sizes. In this case, the large initial vortex size has produced a superior forecast. For this event, we suggest that during the forecast period the storm became slow-moving and isolated from environmental influences on its motion. The  $\beta$ -effect began to play a relatively more important role in the motion of the storm. This effect, which produces slow westward and poleward motion, becomes increasingly important for large storms. Thus for Sinlaku we suggest that the larger initial vortex produced a more accurate forecast because of the increasing influence of  $\beta$ -propagation on the storm motion.

## The ACCESS Tropical Cyclone Forecast System, ATCFS

Early results from using an enhanced vortex specification (Weber, 2008, personal communication) with 4DVAR assimilation in the Unified Model is illustrated in Fig. 5. It shows observed and forecast tracks and intensities from forecasts with and without vortex specification, and using nested grids down to a resolution of  $0.11^\circ$  with 50 levels. The large

impact on prediction of both track and intensity from this NWP configuration is clearly evident.

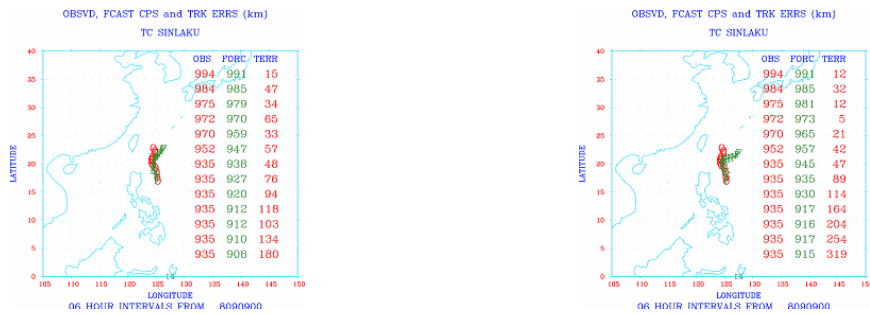


**Figure 4:** Estimated and forecast tracks and intensities for Typhoon Sinlaku from base time 00UTC, 20080909. Left panel is for forecast from a large initial vortex. Right panel is for a small storm.

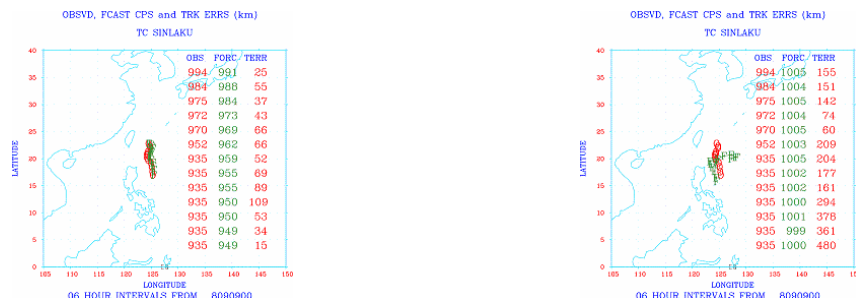


**Figure 5:** Estimated and forecast tracks and intensities for Typhoon Sinlaku from base time 00UTC, 20080909. Left panel is from the ACCESS TCFS with vortex specification and using 4DVAR and the UM. Right panel is with no vortex specification.

## Summary

With improved prediction of the LSE of storms and enhanced specification of vortex structure, more closely tied to observed structures, we suggest that there is a real possibility of true skill in prediction of structure and intensity. The operational benefits, particularly for prediction of landfall and storm surge where VMAX, the RMW and storm size appear to play crucial roles, are potentially very large.

Preliminary results from the ACCESS TCFS are rather encouraging. Much more work is required to validate initial and forecast storm structures. It is still unclear whether the 4DVAR can correctly initialize both the primary and secondary circulations of TCs, particularly for very intense storms.

## References

- Davidson, N.E. and Y.M. Ma, 2009: Surface Pressure Profiles and Initialization for Hurricane Prediction. Part II: Numerical Simulations of Track, Structure and Intensity. For submission to *Mon. Wea. Rev.*
- Davidson, N.E. and H.C. Weber, 2000: The BMRC high resolution tropical cyclone prediction system : TC-LAPS. *Mon. Wea. Rev.*, 128, 1245-1265
- Kossin, J.P., and M.D. Eastin, 2001: Two Distinct Regimes in the Kinematic and Thermodynamic Structure of the Hurricane Eye and Eyewall. *J. Atmos. Sci.*, **58**, 1079–1090.
- Ma, Y.M., M. Kafatos and N.E. Davidson, 2009: Surface Pressure Profiles and Initialization for Hurricane Prediction. Part I: Analysis of Observed and Synthetic Structures. For submission to *Mon. Wea. Rev.*
- Nguyen, C.M., M.J. Reeder and N. Davidson, 2008: Intensity Forecasts for Hurricane Katrina (2005) from TCLAPS: Vortex and Structure Evolution and Forecast Sensitivity. Extended Abstracts. 28<sup>th</sup> AMS Conference on Hurricanes and Tropical Meteorology. 28 April – 2 May, 2008. Orlando, FL, USA.
- Sampson, C.R. and J.A. Knaff, 2009: Southern Hemisphere Tropical Cyclone intensity forecast methods used at the Joint Typhoon Warning Center, Part III: Forecasts based on a multi-model consensus approach. Submitted to *Aust. Meteor. Mag.*



# The performance of nested cloud-scale simulations during TWP-ICE

Kathrin Wapler<sup>1,2</sup>, Todd Lane<sup>1</sup>, Peter May<sup>3</sup>, Christian Jakob<sup>4</sup>, Michael Manton<sup>4</sup>, and Steve Siems<sup>4</sup>

1. *School of Earth Sciences, The University of Melbourne, Australia*

2. *German Weather Service, Germany*

3. *Centre for Australian Weather and Climate Research, Melbourne, Australia*

4. *Monash University, Clayton, Australia*

## Introduction

The Tropical Warm Pool-International Cloud Experiment (TWP-ICE, May et al. 2008) took place in Darwin, Australia during January and February 2006. It provides an extensive data set describing tropical cloud systems, their evolution and interaction with the larger-scale environment. The experiment included a relatively dense network of ground-based observational systems including a polarimetric weather radar, cloud radar, wind profilers, radiation measurements, a lightning network and a balloon-borne sounding network. Additionally, five research aircraft measured cloud properties and the state of the atmosphere.

During the experiment four different convective regimes were sampled; these regimes were an active monsoon, a relatively suppressed monsoon, some clear days, and a monsoon break period. During the active monsoon a great variety of convective organization occurred, including isolated storms as well as convective lines. This period showed the highest cloud occurrence of the TWP-ICE experiment, and the area-averaged rain rate during the active monsoon period was around 17mm/day. Towards the end of this period a large mesoscale convective system (MCS) developed, which produced an area averaged accumulated rainfall of more than 70mm/day. In contrast, the monsoon break period was characterized by intense afternoon thunderstorms as well as several squall lines passing through the TWP-ICE domain during the evening and early morning. Due to the relatively transient and localized nature of the convection during the monsoon break period, the area averaged rain rate was only 8 mm/day.

The measurements of these different regimes during TWP-ICE provide a valuable resource for the validation of cloud-scale model simulations under different tropical meteorological situations. In particular, this study focuses on the performance of the Weather Research and Forecasting (WRF) model, and its ability to reproduce the observed cloud structures as well as the model's performance in terms of precipitation.

## WRF model simulations

The WRF model is a compressible nonhydrostatic finite difference model that has a variety of physics options, including explicit moisture processes (see Skamarock, 2005 for details). In this study, WRF is configured to explicitly simulate tropical cloud systems observed during TWP-ICE. The WRF simulations were performed with multi-nested domains with 4 different horizontal resolutions (34, 11.3, 3.78, and 1.26 km) all having 64 vertical levels (see Fig. 1); the innermost

nest, which is centred on Darwin encompasses an area of  $307 \times 307$  km; this innermost nest can be considered cloud resolving. The initial and boundary conditions were derived from the NCEP  $1^\circ \times 1^\circ$  global operational analysis. In all simulations, the model was configured using the longwave rapid radiative transfer model (Mlawer et al., 1997), the shortwave MM5 (Dudhia, 1989) radiation, thermal diffusion surface scheme, the Purdue Lin microphysical scheme (Chen and Sun, 2002), and the Mellor-Yamada-Janjic boundary layer scheme (Janjic, 2002).

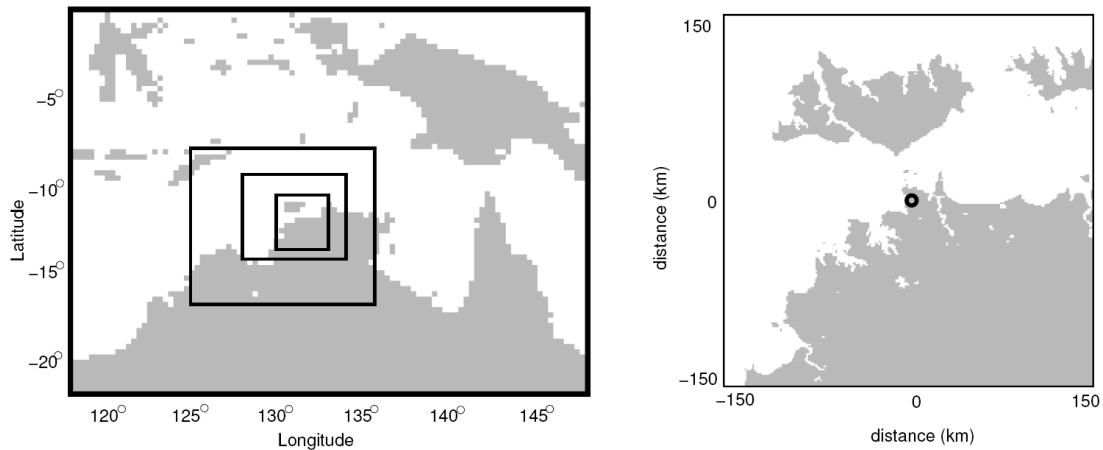


Fig. 1: Locations of WRF model domains (left) and the innermost domain (right).

Simulations for two different periods have been performed using version 2.2 of the Advanced Research WRF (WRF-ARW). The period from 21-24 January 2006 represents the active monsoon. The second simulation period, 6-9 February 2006, is part of the monsoon break period. The simulations and the available observations enable detailed assessments of the WRF model performance in simulating tropical convection and its regime dependence.

## Results

Figure 2 presents example time series of area-averaged precipitation rate for the two different simulation periods. The area-averaged rates are calculated over a circular area of radius 150 km surrounding the radar. For both periods, the WRF simulations show relatively good agreement with the observations. First, for both periods, the four-day simulated rainfall accumulations are very similar to the observations (not shown). Second, during both the active monsoon and monsoon break periods, the model mostly reproduces the timing and intensity of significant rainfall events. This agreement includes the large MCS on day 4 of the active monsoon simulation (Fig. 2a) and the strong afternoon convection on day 1, 2, and 4 of the monsoon break period (Fig. 2b). However, during the active monsoon period, a strong rainfall event on the evening of day 2 is poorly reproduced. Furthermore, in the early morning on day 3 of the monsoon break period, the simulation produces erroneous convective initiation. This initiation is the result of a simulated land breeze circulation between the Tiwi Islands and the mainland that was not present in the observations. Further simulations with shorter lead-time do not produce this initiation on day 3, and better reproduce the lack of precipitation on this day (not shown).

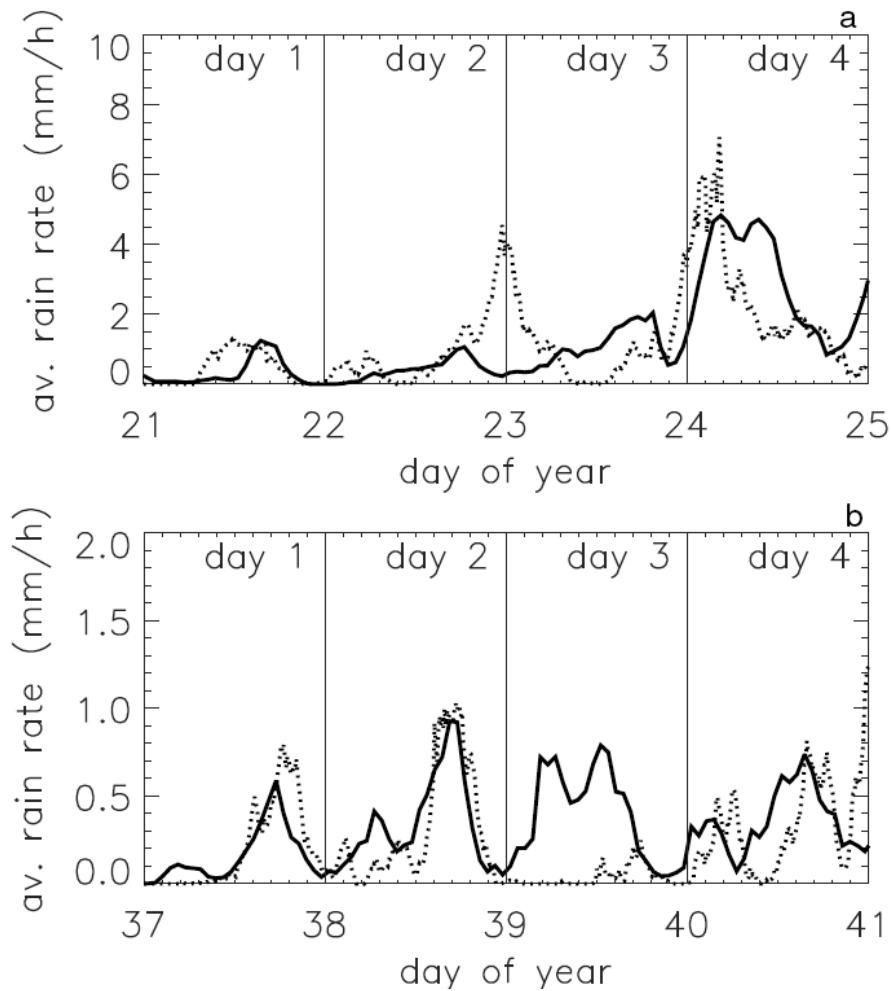


Fig. 2: Time series of area-averaged precipitation from the WRF simulations (solid) and the radar observations (dashed). (a) is for the active monsoon simulation and (b) is for the monsoon break simulation.

The results shown in Fig. 2, however, are for two different model configurations that produce the best simulations in terms of precipitation in the innermost domain. The active monsoon simulation uses cumulus parameterisation on Domains 1 and 2 (the 34 and 11.3 km domains) but the monsoon break simulation does not. If cumulus parameterisation is used in Domains 1 and 2 of the monsoon break simulation, the diurnal cycle of convection is poorly reproduced. The reason for this detrimental influence of the cumulus parameterisation is related to simulated mean descent over the TWP-ICE domain during the day. This descent is the response to large-scale contiguous regions of modeled ascent over regions remote from Darwin. This mechanism will be described in more detail at the workshop.

## Summary

The WRF model simulations have demonstrated the relatively good performance of the cloud-resolving model grids during two different convective regimes. This performance illustrates the utility of high-resolution numerical weather prediction at cloud-resolving scales and the use of

such domains for downscaling applications. The simulations have, however, highlighted a number of difficulties in producing robust simulations. The first difficulty is associated with the regime dependent model performance, where judicious choices of model settings were required to obtain the optimum results. The second difficulty is related to the predictability of small-scale features like land breezes; as demonstrated here the erroneous convective initiation in the early morning of day 3 of the monsoon break simulation has significant consequences for the simulated precipitation for the remainder of that day.

Further investigations of the performance of the WRF simulations and their sensitivity to initiation time and model configurations will be presented at the workshop.

## References

- Chen, S.-H., and W.-Y. Sun, 2002: A one-dimensional time dependent cloud model. *J. Meteor. Soc. Japan*, **80**, 99-118.
- Dudhia, J., 1989: Numerical study of convection observed during the winter monsoon experiment using a mesoscale two-dimensional model, *J. Atmos. Sci.*, **46**, 3077-3107.
- Janjic, Z. I., 2002: Nonsingular Implementation of the Mellor-Yamada Level 2.5 Scheme in the NCEP Meso model, *NCEP Office Note*, No. 437, 61pp.
- May, P. T., J. H. Mather, G. Vaughan, C. Jakob, G. M. McFarquar, K. N. Bower and G. G. Mace, 2008: The Tropical Warm Pool International Cloud Experiment (TWP-ICE), *Bull. Amer. Meteor. Soc.*, **89**, 629-645
- Mlawer, E. J., S. J. Taubman, P. D. Brown, M. J. Iacono, and S. A. Clough, 1997: Radiative transfer for inhomogeneous atmosphere: RRTM, a validated correlated-k model for the longwave. *J. Geophys. Res.*, **102 (D14)**, 16663-16682.
- Skamarock, W.C., J.B. Klemp, J. Dudhia, D.O. Gill, D.M. Barker, W. Wang, J.G. Powers, 2005: A Description of the Advanced Research WRF Version 2. NCAR Tech Note, NCAR/TN 468+STR, 88 pp. [Available from UCAR Communications, P.O. Box 3000, Boulder, CO 80307].

# Modelling Pyro-Cumulonimbi and Tornadoes Spawned by Bushfires

Michael J. Reeder

School of Mathematical Sciences, Monash University, Victoria  
Email michael.reeder@sci.monash.edu.au

Philip Cunningham

Department of Meteorology, The Florida State University, USA

## Introduction

As bushfires raced through several outer suburbs of Canberra on the afternoon of 18 January 2003, a series of large pyro-cumulonimbus cells developed to the west of Canberra Airport, as documented by Fromm et al. (2005). These authors report that the complex of pyro-cumulonimbi lasted for about 3 h, with each individual cell being about 10 km in diameter and forming near the leading edge of the fire and subsequently propagating eastward. Webb et al. (2004) report that the weather radar showed pyro-cumulonimbus cells reaching heights of 14 km, although Fromm et al. (2005) report the maximum height to be closer to 15 km. Sooty black hail was reported to have fallen from the one of the pyro-cumulonimbi about 300 km to the east of Canberra. One of the pyroCbs spawned several intense tornado-like vortices (Webb et al. 2004, Fromm et al. 2005). The path of one of these vortices was about 20 km long, 450 m wide, oriented northwest to southeast, and appeared to extend outside of the burning area. According to Fromm et al. (2005) the damage associated with this feature was consistent with an F2 tornado.

The work presented uses the Canberra bushfires to explore the dynamics pyro-cumulonimbi and the tornadoes they occasionally spawn. In particular, the work seeks to answer the two questions: How important is the heat of combustion in initiating the convection? How important is the water produced during combustion to the development of convection and the associated tornadogenesis?

## Model

The calculations described here are made with the Weather Research and Forecasting (WRF) model (Skamarock et al. 2005) configured for Large Eddy Simulations. The computational domain has  $160 \times 160$  grid points with a horizontal resolution of 200 m and 150 points in the vertical with a resolution of 150 m. The turbulent kinetic energy is calculated each time step and used to parameterize the subgrid-scale turbulence. The lateral boundaries are open, the upper part of the model domain includes Rayleigh damping, and a simple drag law is used at the lower boundary. For simplicity, the rotation of the earth is neglected. The model is initialized with the upper air sounding made at Wagga Wagga on 2300 UTC 17 January 2003 (0900 EST 18 January 2003) modified slightly in the lowest 100 mb to better reflect the afternoon conditions observed at Canberra Airport. The Convective Available Potential Energy is  $117 \text{ J kg}^{-1}$ , which is relatively low giving the development of severe convection later in the day, while the Convective Inhibition is  $36 \text{ J kg}^{-1}$ .

A prototype fire is incorporated into the model as described by Cunningham et al. (2005). The rate at which water is produced by the fire is calculated using the chemical reaction for the combustion of cellulose. Assuming complete combustion, this reaction implies that for

each kg of fuel consumed, about 0.55 kg of water is produced. As shown below, the production of water by the fire has a huge effect on the development of pyro-cumulonimbus cells and the associated tornadogenesis.

## Results

Figure 1 shows four views of the convection that develops in the model. The solid surface encloses the cloud hydrometeors, and hence defines the pyro-cumulonimbus cloud, while the translucent surface encloses the precipitating region. At this time the cloud top is located at about 14 km, having overshoot the tropopause and mixed part of the convective plume into the stratosphere. The temperature is plotted on the solid plane marking the lower boundary of the numerical model, with the circular region being the prototype fire. Although the fire is parameterised as a uniform heat source, the temperature in the heated region is highly variable as indicated by the speckled appearance. This variability reflects the transport by the individual eddies.

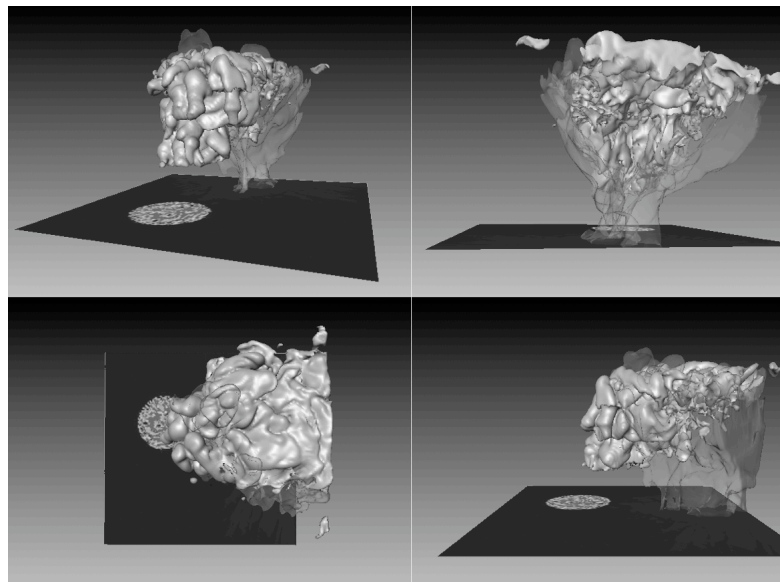


**Figure 1.** Pyro-cumulonimbus convection initiated by the prototype fire and moisture source. Top-left: view from the southwest. Top-right: view from the east. Bottom-left: view from above. Bottom-right – view from the south. Surface temperature (plane surface), cloud hydrometeors (solid shading) and precipitation (translucent shading).

The streamlines and surfaces of the magnitude of the total vorticity are shown in Fig. 2. As the vortex tubes are advected in the updraught of the cloud, they are stretched and twisted. At this time, there is a very strong, relatively upright tornado-like vortex close to the surface near the edge of the fire.

A plan section through the model at 375 m (Fig. 3a) shows the magnitude of the total vorticity, contours of the vertical component of vorticity and the horizontal wind vectors. Budget calculations show that tilting horizontal vorticity, which is then amplified by stretching, produces vertically oriented vortex tubes.

Although the low-level environmental winds are northwesterly, locally the flow is highly convergent and directed towards the prototype fire and convective updraught. On the western side of the fire, vortex tubes are aligned with the low-level winds, which is also the direction of the low level shear. These vortex tubes mark boundary layer rolls. On the eastern side of the fire, the low-level winds are weaker, but still point towards the fire.

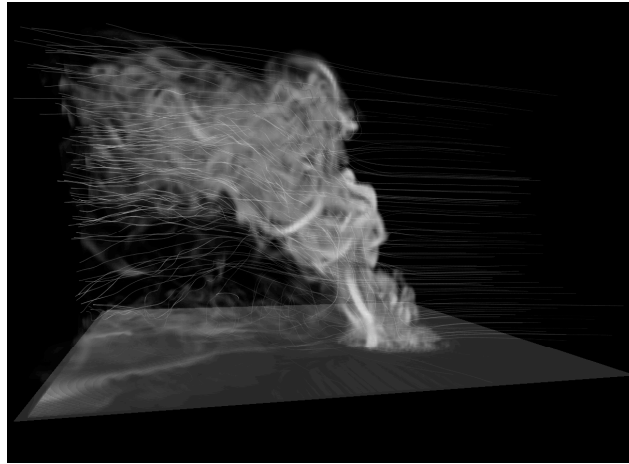


**Figure 2.** Pyro-cumulonimbus convection initiated by the prototype fire and moisture source. View from the northeast. Streamlines and surfaces of the magnitude of the total vorticity. The tornadic vortex is oriented vertically and located on the northeastern side of the fire.

An east-west, vertical cross section through the centre of the tornado-like vortex shows the vorticity and the vector velocity in the plane of the section (Fig. 4b). There is a concentrated tornado-like vortex below cloud base, which is located at a height of 4 km (not shown). The updraught speed within the vortex exceeds  $60 \text{ ms}^{-1}$ .

Although not shown here, the prototype fire and moisture source are essential in producing the deep pyro-cumulonimbus convection and tornado-like vortex. For example, no convection develops in model runs without the heat source and moisture source. Moreover, with the heat source alone, the convective cloud reaches a height of 8 km only and does not develop a tornado-like vortex.

## Conclusions

The simulations capture the main characteristics of the observed pyro-cumulonimbi, including the formation of a tornado close to where one was reported. The work addresses: the role played by the heat of combustion in the development of the convection and the importance of the water produced during combustion in deepening the convection. Further work includes investigations of the back-reaction of the convection on the fire and the dynamics and predictability of pyro-tornadogenesis.

## References

- Cunningham, P., S. L. Goodrick, M. Y. Hussaini, and R. R. Linn. 2005. Coherent vortical structures in numerical simulations of buoyant plumes from wildland fires, *Int. J. Wildland Fire*, 14, 61-75.

- Fromm, M., A. Tupper, D. Rosenfeld, R. Servranckx and R. McRae. 2006. Violent pyroconvective storm devastates Australia's capital and pollutes the stratosphere, *Geophys. Res. Lett.*, 33, L05815, doi:10.1029/2005GL025161.
- Skamarock, W. C., J. B. Klemp, J. Dudhia, D. O. Gill, D. M. Barker, M. G. Duda, X.-Y. Huang, W. Wang and J. G. Powers. 2008. A description of the Advanced Research WRF Version 3, NCAR Technical Note NCAR/TN-475, 113 pp., Natl. Cent. for Atmos. Res., Boulder, Colo.
- Webb, R., C. J. Davis and S. Lellyett. 2004. Meteorological aspects of the ACT bushfires of January 2003, paper presented at 2004 Bushfires Conference: Earth, Wind and Fire - Fusing the Elements, S. Aust. Dep. for Environ. and Heritage, Adelaide, S. Aust., Australia.

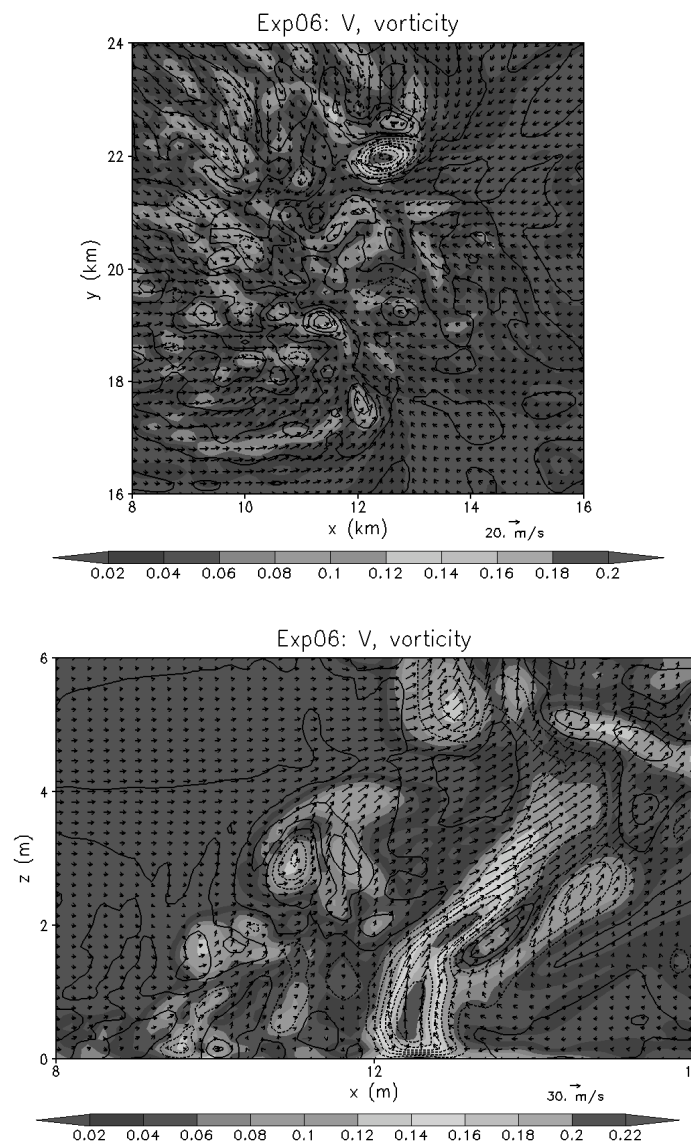


**Figure 3.** Pyro-cumulonimbus convection initiated by the prototype fire and moisture source. (a) Horizontal cross section at  $z = 375$  m showing the horizontal wind vectors, the magnitude of the total vorticity (shaded) and the vertical component of vorticity (contours with negative dashed). (b) Vertical cross section at  $x = 21.8$  km showing wind vectors in the plane of the section and the magnitude of the relative vorticity.

# Self-similarity in moisture processes and NWP Models

Kevin K. W. Cheung

*Department of Physical Geography, Macquarie University, Sydney, Australia*

*(kcheung@els.mq.edu.au)*

It has long been recognized that self-similarity or scale invariance exists in both temporal and spatial distributions of precipitation. Analysis of precipitation time series in previous studies showed embedded low correlation dimension that is often associated with chaotic dynamics of the atmosphere and existence of climate attractors. Spatial distribution of rainfall has also been analyzed and simulated by random cascade models and multifractal models that have intrinsic scaling behaviour. More interestingly, recent studies identified scaling relationship not only in the precipitation field but also in other parameters such as cloud-top irradiance and radar reflectivity data, which indicate that we may be able to describe the multiscale nature of moisture processes in the atmosphere with a unified framework. However, little is known about relationships between self-similarity and environmental conditions from synoptic setting to those specific for the precipitating systems.

In this presentation several questions will be discussed:

- (1) What are the implications of these findings about scaling behavior in moisture fields?
- (2) Do current numerical weather prediction (NWP) models simulate the correct scaling relationships in the moisture fields and what are the impacts to regional weather and climate forecasts?
- (3) What are the likely requirements in the NWP models that enable them to improve in terms of scaling aspects?



# Ensemble One-kilometer Resolution Numerical Weather Forecasts for the America's Cup

Jack Katzfey, John McGregor and Marcus Thatcher

*Centre for Australian Weather and Climate Research: a Partnership between CSIRO and the Bureau of Meteorology, Aspendale, Vic, Australia*

[jack.katzfey@csiro.au](mailto:jack.katzfey@csiro.au)

## Introduction

The America's Cup sailboat race is the oldest active trophy event in international sport, and is viewed as the peak of the sailing sport. The match is a two boat race between the previous Cup winner and the team which wins the challenge series. The race course is approximately 5 km long with two laps. Since sailboats cannot sail directly into the wind, on the legs going into the wind, they have to tack (zig-zag up the course with headings typically 40 degrees off the wind.) The races typical last about 2.5 hours.

The Swiss team Alinghi won the America's Cup in Auckland in February, 2003 and chose Valencia, Spain for the America's Cup held in June-July 2007. CSIRO was contracted to provide forecasts for both Cups. Forecasting for an America's Cup team primarily involves forecasting the wind, both speed and direction. Waves and other weather events also play a lesser part in the forecast. Key aspects of the forecast are: 1) which side of the start line is favorable and 2) wind speed and direction variations and trends for both the first leg and for the whole race. Knowing (and utilizing) the expected wind changes can give a sailboat an advantage over the other boat. Once in the lead, it is usually easier to keep the lead.

## Model setup

A important aspect of the agreement with Alinghi was to provide wind forecasts at 1 km resolution over the 5 km race course. Alinghi provided a Linux cluster in order to run the model. The setup involved forecasts using different initial conditions, different models and different large-scale forecasts. The two main initial conditions were the GFS analysis from NCEP in the US and the Canadian CMC analysis. Partial data was also available from ECMWF, though it was not as complete as the other analyses. In order to assess the confidence of the forecasts, an ensemble of high-resolution forecasts were run each day and presented to the team, along with our 'best' forecast.

The stretched-grid Conformal-Cubic Atmospheric Model (CCAM) was run at 60 km, 8 km and 1 km resolution (McGregor and Dix 2008, Katzfey 2003). The representations of the regions covered and resolution of the topography and coastline is shown in Fig. 1. In these forecasts, the 60 km resolution forecast was first initialised with the global analysis and a 5-day forecast was run. This output was then used as far-field nudging for the 8 km resolution forecast, run out for 3 days. The 8 km output was then used as far-field nudging for the 1 km resolution, 2 days forecasts. Global forecasts

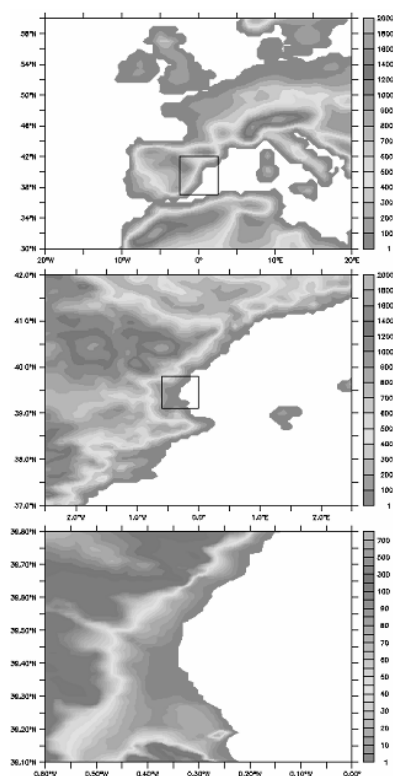


Fig. 1: Topography and approximate high resolution domains for CCAM 60 km (top), 8 km (middle) and 1 km (bottom) grids.

from both NCEP and CMC were also used to drive additional CCAM 8 km forecasts. In addition, RAMS was run with multiple nests down to 1 km and the WRF-ARF model was run with multiple nests down to 4 km, both driven by the GFS global forecast. The Spanish Met. Service also provided 5 km HIRLAM model forecasts. Finally, a few additional runs were completed with alternative settings in CCAM.

## Observations

Available observations included buoys, weather boats, land-based stations, a vertical wind-profiler, and publically available satellite and radar images. Locations of the various surface observations are indicated in Fig. 2. Most observations were updated every 15 seconds, but they were typically averaged over 1-2 minutes to remove the small-scale oscillations. The buoys gave good indications of current trends in wind and its variations across the race course. Teams also used historical data (about 2 years) in order to develop statistical relationships between observed data and future changes. Weather boats could be placed where needed, but typically their observations were noisier due to boat motion. Land-based stations were also relatively noisy.

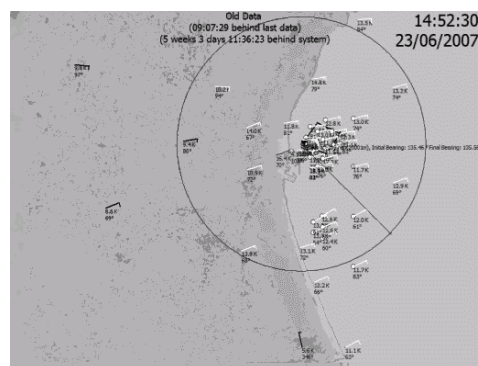


Fig. 2: Location of surface observations in Valencia. The circle is 10 km in diameter. The Diamond in the centre is the race course.

## Forecast requirements and procedure

Daily forecasts were required by the team in the morning to prepare the boat, with updates until the start of race to determine the final race call. The morning forecast presented the overall weather expected during the day, followed by the expected wind speed in the afternoon (for sail selection/boat setup), and the main trends expected in wind direction. This was the only briefing for the team as a whole, since the updates later in the day were only given to a few sailors in the boat.

After the briefing, the weather team headed out onto the water to get into position, ensured that the communication systems were working properly, and started studying the observations and comparing them against the forecast. Once the race boat came out, updates were given about every 15-30 minutes. The last communication to the race boat was about 6 minutes before start of race. Rules prevent any communication with the sailors from 5 minutes before the start of, and during, the race. All communication gear must be off the boat by the 5 minute mark (sometimes, an extra sailor jumped off boat at 5 minutes with the gear and was picked up by the follow boat).

The last weather call attempted to predict: 1) the favored end of the line due to expected wind direction at the start, 2) mean wind speed for the first leg (~30 minutes), 3) any expected wind speed/direction variations across the course for the next 30 minutes (and if they were expected to persist), and 4) any expected wind speed/direction trends during the first leg and during the race. In general, reading the small-scale shifts was left to the race boat using their on-board wind measurements and watching for variations on the water. The buoys were not sufficient to capture the small-scale-shifts reliably.

## Example forecast

The last (7<sup>th</sup>) race of the America's Cup was on 3 July 2007. The general synoptic situation was a trough aligned with the east coast of Spain with strong southerly winds over the water to the east and weaker westerly flow over the land. The CCAM 8 km forecast for 1700 LT is shown in Fig. 3. At this time, note the stronger winds to the south and lighter winds to the north. Also note the ridging along the coast to the north related to the lighter winds. The time series of the ensemble of high-resolution forecasts for the race area is presented in Fig. 4. Light (offshore) winds are evident in the morning, with the sea breeze developing around 1100 LT, building to 16-18 knots from the southeast. The forecast for the race was for a southeast wind building to 18 knots from 135°. Most model forecasts agreed with the direction very



before the 1400-1500 LT race start). In practice the 00 UTC forecast tended to be better than the 06 UTC forecasts, possibly because more data was available for the data assimilation. In addition, only limited computer resources were available for the model runs, which constrained what could be accomplished.

In general, though not exclusively, the forecasts were for afternoon sea breeze development. The strength and character of the sea breeze was largely determined by the large-scale pattern over Spain and the western Mediterranean. However, there were also significant coastal and orographic influences. Northeast winds tended to either persist, if strong enough, or weaken and shift more easterly. Easterly winds tended to be the weakest and the direction trends were harder to predict. Southeast sea breezes tended to develop most strongly, with stronger winds further south, and which either 1) were advected from the south, sometimes with rapid increases in strength, 2) developed throughout the day, or 3) developed then weakened rapidly and trended more easterly as in the example presented. Precipitation and clouds were mostly confined to inland mountains most days and did not directly influence the local winds.

Several interesting questions arise from this work:

- 1) **The relative importance of the model resolution versus data assimilation in the accuracy of the forecasts.** Here, no data assimilation was performed. However, the global analyses did use data assimilation at coarse resolution. The lack of sufficient upper air data and surface observations over water likely precludes benefit from mesoscale data assimilation.
- 2) **The role of forced versus unforced mesoscale winds.** What can models predict versus what is inherently unpredictable? Land/sea contrasts, shape of coastline, orographic effects should all be better predicted as resolution increases, given reasonably accurate large scale patterns. However, small-scale time and space variations over unforced regions are likely to be unpredictable.
- 3) **The influence of model formulation/dynamics on high resolution forecasts.** The relative performance of various models used in these forecasts, all with basically the same initial state, suggests some influence of model on the quality of the forecast. It would be interesting to investigate the error growth within the various models to determine the cause.
- 4) **The value of high-resolution data ensemble forecasts.** Here, the ensembles were based upon initial conditions, large-scale predictions and different models. At the short time scale of these forecasts (less than 18 hours), is there scope for an ensemble-based scheme which will help better capture the range of uncertainty in the forecast? Usage of the global ensemble members from NCEP did not provide any useful information, since the ensemble members tended to provide significantly worse forecasts than the control.

Finally, the CCAM technology has been licensed to a private company to provide recreational boating forecasts. Using similar setup as used here, 60 km, 8 km and 1 km wind forecasts for 320 regions around the world are available from [www.predictwind.com](http://www.predictwind.com). The forecasts are generated twice per day, using both the NCEP and CMC analyses and are free until end of 2008.

## References

- McGregor, J. L., and M. R. Dix, 2008: An updated description of the Conformal-Cubic Atmospheric Model. In *High Resolution Simulation of the Atmosphere and Ocean*, eds. K. Hamilton and W. Ohfuchi, Springer, 51-76.
- Katzfey, J. J. (2003). Wind forecasting makes sailing to victory a breeze. *Bulletin of the Australian Meteorological and Oceanographic Society*, 16 (2): 26-28.

# High-resolution modelling for impact forecasting

W.C. Arthur, R.P. Cechet and C. Thomas  
*Risk and Impact Analysis Group*  
*Geoscience Australia, Canberra, ACT, Australia*

## Abstract

The impact of major tropical cyclones in recent years has highlighted the benefits high-resolution atmosphere and ocean modelling can provide to emergency managers and the wider public (e.g. Hurricane *Ike*). When combined with geospatially enabled information on population and infrastructure, high-resolution wind fields from 3D atmospheric models could be used to operationally estimate the impacts of a tropical cyclone on an Australian community (similar to the successful implementation in the U.S. serving Government and Emergency Management). Presently, Geoscience Australia uses parametric wind fields, but with time would ideally like to incorporate wind fields from the same models forecasters use to issue warnings, ensuring consistent messages on the impacts of an impending tropical cyclone reach emergency managers and the broader community.

To demonstrate the utility of impact forecasting, a scenario involving a category 3 tropical cyclone impacting on the Gold Coast region is considered. The spatial extent of wind-related and flooding damage is displayed as well as likely impacts to critical infrastructure. The use of community GIS information is highlighted with regard to prioritising evacuations.

## Introduction

Impact forecasting, which emphasises social and economic impacts of severe weather, is becoming more prominent in the US and EU (Bush and Ivey, 2006; Dauelsberg *et al.*, 2007; Fernandez *et al.*, 2007). The spatial enablement of both Emergency Services and Government has been most evident through the coastal impact of severe tropical cyclones in the Caribbean. Research in severe weather prediction has been closely coupled with research in both structural and social vulnerability, preparedness (resources), and response. The ability to display and interact with information in both a 2D and 3D environment has been a strong driver for the acceptance of this new technology. There is a general recognition (within the emergency management community) that linking infrastructure-impact research more closely to extreme weather models has the potential to reduce vulnerability.

The combined effects of severe winds, heavy rainfall and coastal inundation mean tropical cyclones are one of the most destructive weather phenomena. Each year we see the devastating impacts of tropical cyclones on communities around the world. One can look to the recent impact of Hurricane *Ike* and the (very well documented) devastation wrought on the Texas coastline. From an emergency management point-of-view, combining meteorological information with spatial infrastructure information is invaluable in prioritising actions both before and after impact.

Geoscience Australia is proposing to exercise its skills in providing geospatial information to the nation by developing an impact forecasting tool for a wide range of rapid-onset natural hazards – e.g. earthquake, tsunami or tropical cyclone. Here we present a ‘desktop exercise’, designed to highlight the benefits of such a system. It is a vision for a decision support system for use by emergency managers and planners that we believe can become a reality within 5 years. The tool, nicknamed ‘WHIM’ (for ‘WHat-If Machine’), would incorporate and assimilate a range of datasets and models, covering all scales from local to national. Many of the individual elements already exist from the results of mitigation grant schemes, spatial data acquisition efforts at State and local levels and a number of modelling programs.

## Motivation

Our motivation for considering impact forecasting for the Australian region is twofold:

- 1) experience gained while working on the Cyclone *Larry* impact assessment convinced Geoscience Australia of the utility of spatial information for both Emergency Management and Local Government; and
- 2) the estimate of the Federal Government's exposure to Cyclone *Larry* damage costs resulted in a budget underspend of \$A0.5 Billion. Post-event budgetary forecasting assistance could be provided to both Federal and State Government to illustrate/inform their exposure to extreme events.

In addition, overseas experience with impact forecasting as detailed by the "Recommendations for Research on Extreme Weather Impacts on Infrastructure", a synthesized set of outcomes from the *Workshop on Weather Extremes Impacts on Infrastructure* held in Santa Fe, New Mexico (27-28 February 2007), states that "*Over the past year, a number of agencies have been positioning themselves to make major investments in the science needed to address the impacts of severe weather, e.g., by developing cross-agency working groups and funding mechanisms. NOAA, DOE, USACE, ONR, DHS, DOD, NASA, and FEMA are actively discussing ways to collaborate more effectively*". Collaboration with some of these agencies to fast-track development in Australia needs to be considered.

## The scenario: TC *Rufus*

The scenario analysed is that of a high category 3 tropical cyclone approaching southeast Queensland. Maximum wind gusts at landfall are 60 m/s (115 knots). We start analysis when *Rufus* is still well off the coastline, but on a south-southwest track towards southeast Queensland. Forecasts provided by ensemble forecast systems indicate that *Rufus* will turn towards the coast, the most likely crossing point being the southern end of South Stradbroke Island.

## The impacts

TC *Rufus* generates significant winds along the coastline, but due to shielding and terrain, winds drop off rapidly behind the foreshore. Over the hinterland, topographic accelerations result in significant (read damaging) wind speeds for many areas. The topographic accelerations in some areas push local wind speeds in excess of 70 m/s (135 knots) – bear in mind the design wind speed (for residential structures) in this area is 57 m/s. Because of this, the most severely damaged buildings are in the hinterland, over 25 km inland.

For storm tide inundation, we have used a simplistic approach (excluding riverine and/or flash flooding). This results in much of the low-lying areas behind the beachfront being at risk from inundation. Parametric storm tide modelling can provide estimates of the peak, while more detailed hydrodynamic modelling may be used to determine inundation extents (similar to tsunami inundation modelling activities already achieved at Geoscience Australia).

Geoscience Australia has the capacity to model the damage caused by severe winds to residential, commercial, industrial and critical infrastructure such as power transmission and generation facilities. These are empirical models, relating site wind speed to a mean damage level and can be rapidly calculated using site wind speed estimates. This provides the capacity to estimate the overall damage inflicted on a community due to a tropical cyclone. Using information on electrical transmission assets, WHIM could define areas without power, and estimate the downtime for power transmission. Spatially-enabled databases of infrastructure such as hospitals, nursing homes and schools can be incorporated to allow emergency managers to evaluate evacuation timing and routes.

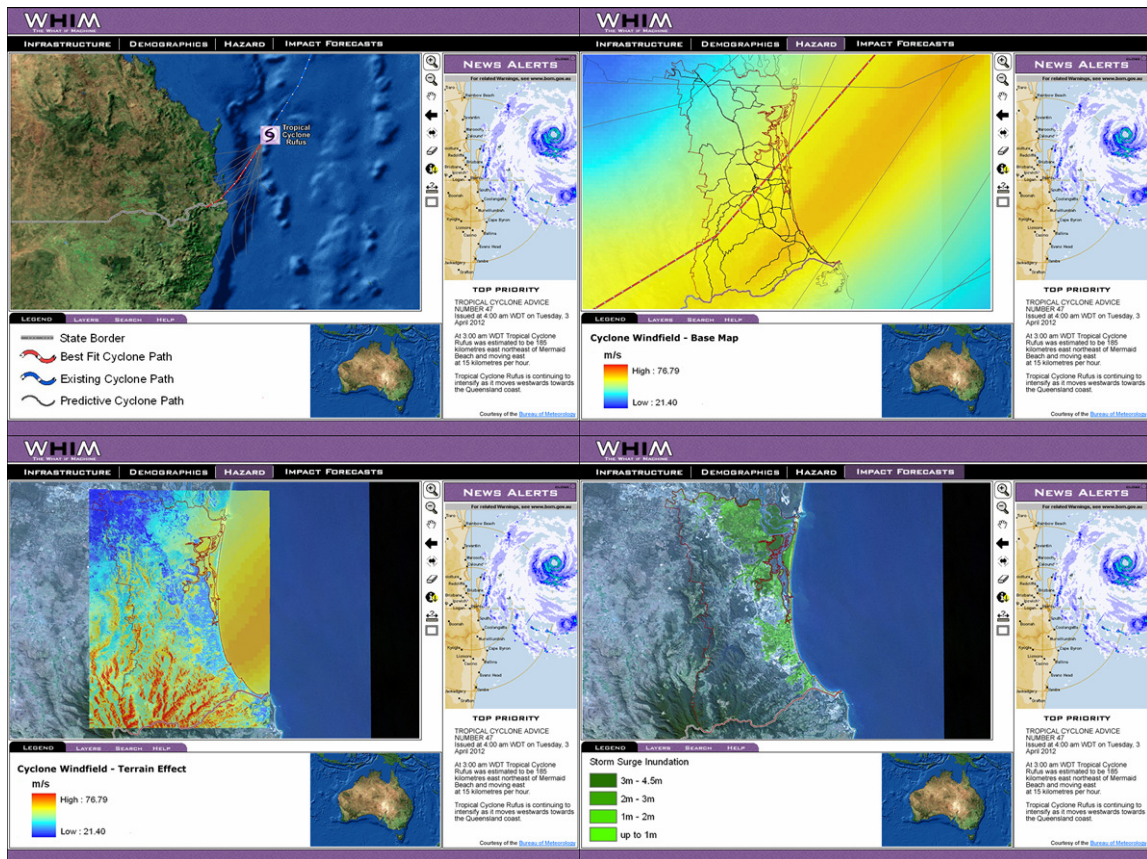


Figure 1: Sample screenshots from WHIM showing (clockwise from top left) estimated track of the cyclone; wind field associated with most likely track; wind field incorporating terrain, topographic and shielding effects; and inundation.

## Future high-resolution modelling requirements

There are several significant components of this tool that rely on high resolution modelling products. First and foremost would be ensemble forecasts of tropical cyclone tracks and intensity. These would be used to provide emergency managers with a range of potential outcomes given the current position and movement of an approaching tropical cyclone. Associated with each of the ensemble track forecasts could be a wind swath, albeit not at the highest resolution required for impact modelling. This again would provide for probabilistic estimates of the impact, and could in turn provide input to storm surge modelling. Geoscience Australia's ANUGA inundation model is being adapted to riverine flooding applications and, when combined with quantitative precipitation forecasts, could provide an inundation prediction capability.

Geoscience Australia currently uses a parametric wind field to estimate the regional wind field (1 km horizontal resolution). We then use wind field multipliers (based on AS/NZS 1170.2:2002) to incorporate the effects of terrain, topography and shielding from upwind structures at 25 metre resolution. Geoscience Australia has only developed these multipliers for capital cities and a limited number of regional centres, so many parts of the coastline remain unmapped. To complete the national picture, we plan to systematically calculate the required fields using an LES modelling approach to capture the full 3-D effects of flow around topography at a resolution of 100 metres or better.

The key to WHIM would be that much of this information is available to emergency managers in near-real time. We envisage a staged development program, with pre-calculated scenarios (similar to the approach used for the Joint Australian Tsunami Warning Centre)

used before the whole system is operational in real time. WHIM would also provide invaluable information – as a risk assessment tool – to planning agencies.

Wind, precipitation, storm surge, and flood risk can be represented geospatially and seasonally in terms of multi-dimensional risk maps (at the street or household level), quantifying consequence estimates tailored to needs of specific stakeholder categories, and that are based on historical or, in the context of climate change, prospective climatology.

## Discussion

*“Time and technology are ripe to develop and deploy an integrated decision-support system enabling rapid forecasting of the critical infrastructure, economic, and societal effects of high impact weather such as extreme wind and precipitation”* (Bent et al., 2007). Unprecedented opportunities exist today in Australia for rapid-response decision support tools, coordinated multi-domain visualisation and weather-impacts research. Weather-impacts decision support will advance once it embraces a broader consideration of economic, social, and cultural consequences. Directly and adaptively coupling atmospheric observations, numeric-weather-prediction models, hydrographic models, and infrastructure-impact simulations using modern, standards-based, service-oriented architectures and knowledge-management systems will open new opportunities for weather-based information delivery. These new decision-support tools need to be coupled with enhanced uncertainty quantification, risk analysis, and an understanding of the limits of predictability. Leveraging state-of-the-art data-assimilation and ensemble-model techniques within a rigorous statistical framework and combined with impact modelling will facilitate rapid uptake within stakeholder communities.

Scientists and engineers working on infrastructure impact modelling need to come together with atmospheric and social scientists, and engineers working on weather extremes to focus on the consequences of extreme weather (severe wind, extreme precipitation, fire weather, heatwaves, etc). They need to identify the research challenges and document gaps between existing and desired analytic capabilities, and assist the science and impact communities better develop joint requirements and form multidisciplinary collaborations.

## References

- Bent, R. and others (2007) Recommendations for Research on Extreme Weather Impacts on Infrastructure, Proceedings of the *Workshop on Weather Extremes Impacts on Infrastructure*, Santa Fe, New Mexico, USA, 27-28 February 2007.
- Bush, B. and A. Ivey (2006) Numerical Hurricane Model Outputs for GIS-Based Infrastructure Damage Estimation, Proceedings of *2006 ESRI Federal User Conference*, Washington, D.C., 31 January–2 February 2006.
- Dauelsberg, L.R., D.R. Powell, R.J. LeClaire, B.W. Bush, S.M. DeLand and M.E. Samsa (2007) Critical Infrastructure Protection Decision Support System Overview, Proceedings of *Risk Analysis for Homeland Security and Defense Theory and Application*, Santa Fe, New Mexico, 26–28 March 2007.
- Fernandez, S., B. Bush, G. L. Toole, L. Dauelsberg, S. Flaim, G.R. Thayer and A. Ivey (2007) Predicting Hurricane Impacts on the Nation’s Infrastructure: Lessons Learned from the 2005 Hurricane Season, Proceedings of the *Second International Conference on Global Warming*, Santa Fe, New Mexico, 17–21 July 2006.

# **Verification of high-resolution NWP for wind energy prediction**

Jeff Kepert

*Centre for Australian Weather and Climate Research:  
a partnership between the Bureau of Meteorology and CSIRO*

Incorporating significant amounts of wind energy into the national electricity grid is difficult since the output of wind farms varies dramatically over short time scales. Integrating wind energy with other forms of generation thus requires reliable forecasts of wind energy production, to ensure that the electricity system operates in a reliable and economical manner. Such forecasts place significant demands on the accuracy of numerical weather prediction (NWP) forecasts of wind, which implies a need to verify the accuracy of these wind forecasts at small spatial and temporal scales. This talk will describe past and present work to this end.

This work has been supported by the Dept of Resources and Energy, and carried out in consultation with electricity industry stakeholders.



# Assessing Wind Hazard in Australia's 'Region A' using a high resolution GCM approach

L.A. Sanabria & R.P. Cechet  
*Risk and Impact Analysis Group, Geoscience Australia*

## Introduction

The Risk and Impact Analysis Group of Geoscience Australia (RIAG) is assessing the risk posed by sudden impact natural hazards in the Australian region. At the moment there are teams developing models to study earthquake, tsunami, landslides, floods, volcanic and severe wind hazards.

Severe wind is one of the major hazards facing the Australian continent. While cyclonic winds are chiefly a northern Australian phenomenon, winds driven by thunderstorms and tornadoes also inflict serious damage and sometimes cause loss of life in southern states. Severe winds are responsible for about 40% of damage to Australian residential buildings. Their impact on Australian houses is significantly higher than other natural hazards such as floods (22%), bushfires (19%), and earthquakes (6%) (Chen, 2004).

In recent years RIAG has developed a statistical model to assess severe wind hazard in the non-cyclonic regions of Australia ('Region A' as defined in the Australian/NZ Standards for Wind Loading of Structures (AS/NZS 1170.2, 2002)). The model has been tested using observational data from wind stations located in South Eastern Australia. The statistical model matched the results of the Australian/NZ standard for wind loading of structures utilising a more efficient, fully computational method (Sanabria & Cechet, 2007a).

We present a methodology to assess severe wind hazard in Australia for regions where there are no observations. The methodology uses simulation data produced by a high resolution regional climate model in association with empirical gust factors. It compares wind speeds produced by the climate model with observations (mean wind speeds) and develops functions which allow wind engineers to correct the simulated data in order to match the observed mean wind speed data. The approach has been validated in a number of locations where observed records are available. In addition a Monte-Carlo modelling approach is utilised to relate extreme mean wind speeds to extreme peak gust wind speeds (Sanabria & Cechet, 2007b).

## High Resolution Climate Simulations

The climate simulation data used for this project was obtained from CSIRO's Conformal-Cubic Atmospheric Model (CCAM). Two runs of 50 years were simulated for the period 1951 to 2000, one for the Eastern states and the other one for the Western states of Australia. Hourly maximum wind speed (four lowest levels in the atmosphere) was saved for this study. Here we present results relating to the CCAM 10-metre height maximum hourly wind speed (maximum of time-step values within each hour) for the 50-year simulation period. The observed wind speeds used for this project were acquired from the Bureau of Meteorology (BoM) in 2006. Half-hourly datasets from a number of wind stations in southern NSW were used for algorithm development and testing. These datasets provide maximum wind gust and mean wind speeds in half-hourly intervals (the actual record has the mean speed and the 3 second maximum gust of the last 10 minutes of the half-hourly interval). For comparison with CCAM-modelled data, maximum daily mean wind speeds were calculated from the half-hourly mean observed wind speeds.

## Statistical Model

The core of the Statistical model calculates return periods of maximum wind speed using extreme value distributions. These types of distributions allow the wind analyst to extrapolate wind speed return periods well beyond the range of available data. Two types of extreme value distributions can be used: Generalised Extreme Value distributions (GEV), which work well with yearly observations, and the Generalised Pareto Distribution (GPD) which uses all data exceeding a given threshold. The problem with GEV is that only a few samples of the records available are used. A typical GEV application uses yearly maximum wind speeds (i.e. one observation per year); the other observations are discarded. This is problematic as it is possible that the highest values below the maximum in a single year exceed the maximum of another year and yet they are not included in the model. The GPD can be fitted using a greater proportion of the extreme wind speed data. On the other hand by setting the threshold high enough, the data will be better distributed in time, so it is likely that the data samples are independent from each other, one of the conditions of extreme value distributions. For this reason the GPD is becoming the preferred distribution for wind hazard analysis, see for instance Hecker *et al.*(1998), Holmes & Moriarty (1999) and Brabson & Palutikof (2000).

Figure 1a, produced by the Statistical model, show returns periods (RP) of Sydney Airport maximum *mean* daily wind speeds. The dataset covers the range 1952-2005 (53 years). The circles are the observed RP, the full line is the RP given by the GPD. Notice that using the GPD is possible to extrapolate RP values to 10,000 years. The dotted lines are the 95% confidence interval. There is a 95% chance that RP located within this interval are correct. Figure 1b shows the RP of Sydney Region wind speeds. The Sydney Region is a super-station made up by joining the wind speed datasets of Sydney Airport, Bankstown Airport and Richmond RAAF (Holmes, 2002).

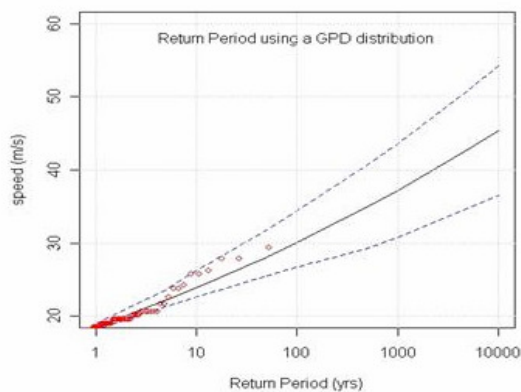


Figure 1a. Sydney Airport max daily mean wind speeds.

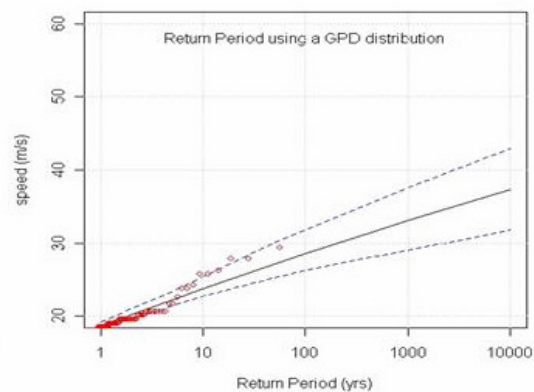


Figure 1b. Sydney Region max daily mean wind speeds

## Results

The Statistical model was used to generate RP of CCAM-modelled wind speeds. Four cases were considered based on the way wind speeds were extracted from CCAM simulations:

- Case 1 (nearest gridpoint or 0 km case);
- Case 2 (2x2 gridpoints or 40 km case);
- Case 3 (3x3 gridpoints or 60 km case);
- Case 4 (5x5 gridpoints or 100 km case).

For the Sydney Region super-station, the 4 cases were defined by joining the corresponding speed datasets of the 4 cases of Sydney, Bankstown and Richmond respectively. Figure 2a shows the observed RP of Sydney Airport max daily *mean* speed and the CCAM wind speeds around the recording station as explained above. The same results for the Sydney Region are presented in Figure 3b, the full line is the observed RP of wind speeds.

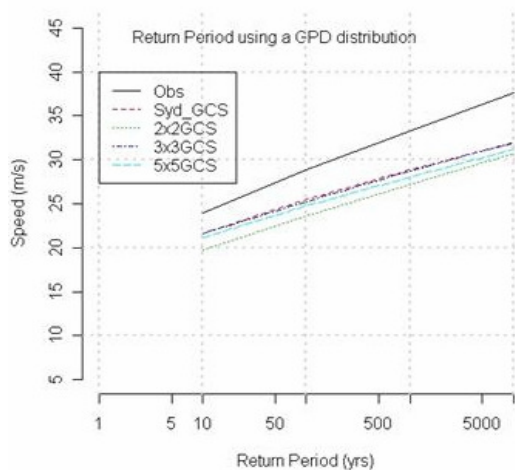


Figure 2a. Sydney Airport  
CCAM and observed RP of wind speeds.

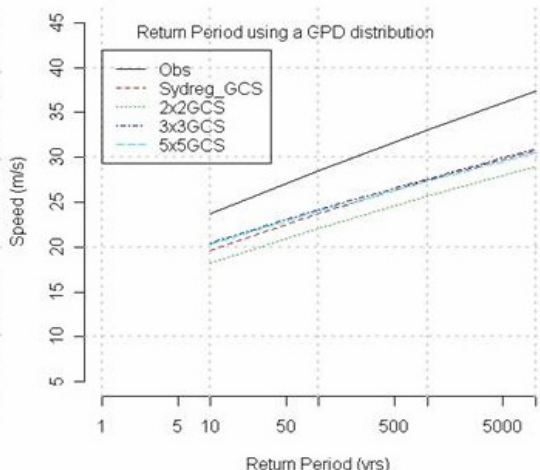


Figure 2b. Sydney Region  
CCAM and observed RP of wind speeds.

Figures 2a and 2b show that CCAM underestimates the RP for wind speeds in both the Sydney Region and the Sydney Airport cases. The bias is best considered in Figure 3 which presents a plot of CCAM RP for the 100 km case of the Sydney Region (Case 4 above) and the observed max daily *mean* speeds. The black points are the corresponding RP of wind speeds for 10, 100, 1000 and 10000 years. It is clear that there is a strong linear correlation – in the semi logarithmic scale – between the RP of CCAM speeds and the RP of observed speeds. The same strong linear correlation was observed between CCAM-modelled speeds and observed speeds in the Sydney Airport and in Bankstown and Richmond stations. This characteristic of the modelled wind speeds will be used to develop an expression to correct the bias of the CCAM-modelled speeds.

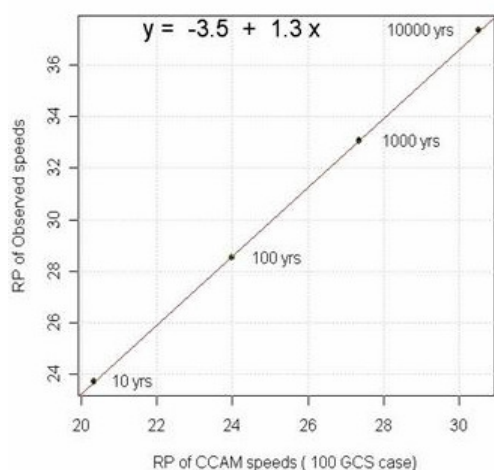


Figure 3. Linear Regression  
between CCAM and observed speeds

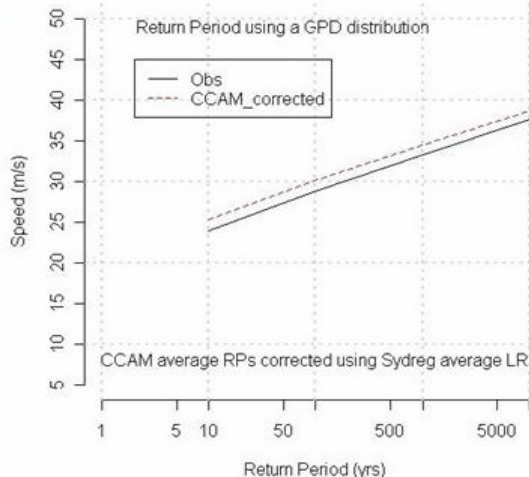


Figure 4. Sydney Airport corrected CCAM  
and observed wind speeds.

A linear regression (LR) between CCAM modelled mean wind speeds and observed mean wind speeds was calculated for each one of the 4 cases explained above. Figure 3 shows one of the LR for the Sydney Region example (Case 4 above). The regression expression is shown at the top of Figure 3. We were a little surprised at the relative insensitivity of the results with regard to the sampling area (Case 1-4; Figures 2a & b). This may be an indication that the horizontal resolution of the simulation may not be sufficient for this application. We

have decided to use an average of these regression lines that were calculated for the sampling areas (cases). The average of the Sydney Region regression lines operating on the average of the RP of the 4 CCAM cases was used to correct CCAM wind speed bias.

**(a) Comparing observed and CCAM-modelled wind speeds.**

Figure 4 compares the observed RP of wind speeds with the corrected CCAM-modelled RP of wind speeds for the Sydney Airport example; for this case the average of the LR expressions of the Sydney Region were used to correct the average RP of CCAM-modelled Sydney Airport speeds. Comparing Figures 2a and 4, it is possible to see that the correction has substantially improved CCAM results.

Table 1 presents a summary of the results. CCAM average refers to the average of CCAM RP for the 4 standard cases discussed above. The error between the observed and the CCAM corrected RP is defined as:

$$\text{Error (\%)} = \text{Abs}[(\text{Obs} - \text{CCAM})/\text{Obs}] * 100$$

The error is small, and in the worst case it amounts to less than 1.5 m/s on a 10 year return period. Notice that in all cases CCAM corrected RP are within the 95% confidence limit (CI).

Table 1. Wind hazard using CCAM-modelled speeds.

RP	Observed	95% CI	Corrected CCAM	Error (%)
10	23.9	(22.8,25.7)	25.3	5.9
100	28.8	(26.4,32.4)	30.1	4.5
1000	33.3	(29.1,38.2)	34.5	3.6
10000	37.6	(31.5,43.5)	38.6	2.7

Figures 5a and 5b compares the observed and CCAM-modelled wind speeds for Bankstown and Richmond stations. The average of the 4 standard cases of wind speed RP of each station was corrected using the average of the LR expressions of the Sydney Region as explained previously. Table 2 presents a summary of the results.

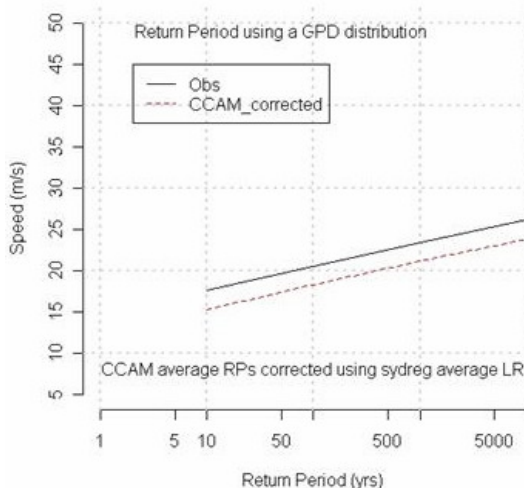


Figure 5a. Bankstown obs. and CCAM (corrected) wind speeds.

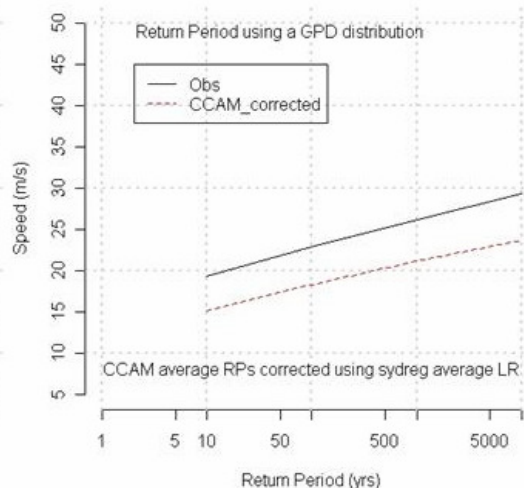


Figure 5b. Richmond obs. and CCAM (corrected) wind speeds.

Table 2 shows that the maximum error obtained in assessing wind hazard using CCAM wind speed is 21.2%, which occurs for RP of 10 years in Richmond. ‘CCAM’ in the table refers to CCAM speeds corrected using the algorithm discussed above.

Although the maximum error in the table can appear large in % terms, it represents only a few m/s in a 10-year RP. High-resolution climate models are still in development and there are large sources of uncertainties (apart from horizontal resolution) which can explain differences with observed and modelled results ( Déqué M. et al., 2007). Wind is highly variable both geographically and temporally (meteorological variable with highest variability). This variability persists over a wide range of scales, both in space and time.

Table 2. Summary of mean wind speed results for Bankstown and Richmond

-----Bankstown -----  -----Richmond -----								
RP	Obs	95% CI	CCAM	Error (%)	Obs	95% CI	CCAM	Error (%)
10	17.6	(16.5,21.0)	15.3	13.1	19.3	(18.0,22.0)	15.2	21.2
100	20.6	(17.8,26.0)	18.3	11.2	22.8	(19.8,26.6)	18.3	19.7
1000	23.4	(18.3,30.8)	21.2	9.4	26.1	(21.2,31.1)	21.2	18.8
10000	26.2	(18.5,35.5)	23.9	8.8	29.4	(23.2,35.4)	23.7	19.4

**(b) Correcting CCAM locations (gridpoints) outside the observed region**

A further analysis was carried out to observe the correction algorithm performance on data not used for development. Consider the wind speeds recorded at Williamtown, a RAAF station 142 km north of Sydney. The CCAM wind speeds for the 4 standard cases were extracted and the average RP for these 4 cases were calculated. Finally using the average LR expression from the Sydney Region, the RP of wind speeds for Williamtown as given by CCAM simulations were corrected and plotted. They are presented in Figure 6.

The max. error of CCAM-modelled wind speeds at this station is 18.2% at a RP of 10,000 years. This result is consistent with the previous results, and suggests that the algorithm is general enough to be used in stations close to the boundaries of the region used for correction.

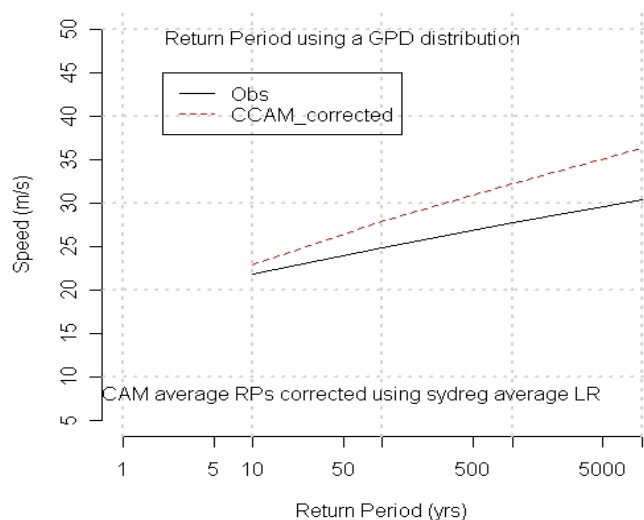


Figure 6. Williamtown observed and CCAM (corrected) mean wind speeds.

### **(c) CCAM gridpoints; consideration of gust wind speed**

The methodology allows the use of simulated data produced by a high resolution regional climate model (daily maximum mean “time-step” wind speed) to be used as a surrogate for an observed record. However, it is not the daily maximum mean wind speed that generally causes wind-related damage to infrastructure. It is the extreme wind speeds (3-second peak gusts) that cause the majority of the infrastructure and environmental damage.

RP peak gust wind speed estimates are produced by utilising empirical information regarding the gust factor (relationship between the peak gust speed and the 10-minute mean wind speed) obtained by considering the gust factor distribution derived only under elevated levels of wind hazard. This empirical data is sampled in a Monte-Carlo modelling approach (in association with the CCAM-modelled maximum daily mean wind speed distribution) to simulate the time-evolution of extreme peak gust mean wind speeds for each CCAM gridpoint considered (Sanabria & Cechet, 2007b).

## **Conclusions**

A method for wind hazard assessment based on high resolution climate model simulations has been presented. The model allows wind analysts to correct the wind speeds of climate simulation output over a given area in order to match the observed wind speeds. The correction expressions were developed by considering 4 standard cases (various spatial resolution) of extracted wind speed information from the climate model. Linear regression expressions between simulated and observed mean wind speeds were developed for the 4 cases. The simulated data can be corrected using the average of the linear regression of the 4 cases for a given area. Correction expressions for a number of regions in Australia can be developed using the algorithm discussed in this paper. The approach is suitable for application in areas where there are no recording stations (i.e. in these areas properly corrected wind speeds from climate simulation models can be used for wind hazard analysis).

## **References**

- AS/NZS 1170.2 (2002) Structural design actions, Part 2: Wind actions, *Australian/New Zealand Standard*, 2002.
- Brabson B.B. and Palutikof J.P. (2000). Test of the Generalized Pareto Distribution for Predicting Extreme Wind Speeds. *Journal of Applied Meteorology*, Vol. 39, 1627-1640.
- Chen, K., 2004. Relative risk ratings for Local Government Areas. *Risk Frontiers Quarterly Newsletter*, 3(3).
- Déqué M., Rowell D. P., Lüthi D., Giorgi F., Christensen J. H., Rockel B., Jacob D., Kjellström E., de Castro M. and van den Hurk B. (2007). An intercomparison of regional climate simulations for Europe: assessing uncertainties in model projections. *Climatic Change*, (2007) 81:53–70.
- Heckert N.A., Simiu E. and Whalen T. (1998). Estimates of Hurricane Wind Speeds by ‘Peaks over Threshold’ method. *Journal of Structural Eng.*, April 1998. 445-449.
- Holmes J.D. and Moriarty W.W. (1999). Application of the generalized Pareto distribution to extreme value analysis in wind engineering. *Journal of Wind Eng. and Industrial Aerodynamics*, 83 (1999) 1-10.
- Holmes J.D. (2002). A Re-analysis of Recorded Extreme Wind Speeds in Region A. *Australian Journal of Structural Engineering*. Vol. 4 No. 1, 29-40.
- Sanabria, L.A. and R.P. Cechet (2007a) A Statistical Model of Severe Winds. *Geoscience Australia Record*, 2007/12, 66p.
- Sanabria, L.A. and Cechet, R.P. (2007b) Monte-Carlo modelling of Severe Wind Gust. In: MODSIM 2007: proceedings of the Modelling and Simulation Society of Australia and New Zealand (MSSANZ), Queenstown NZ, December 2007. pp 1695-1701.

# High resolution modelling for the aviation weather service

R. Potts<sup>1</sup>, Y. Miao<sup>1</sup>, J. Bronsvoort<sup>2</sup> and G. McDonald<sup>2</sup>

1. *Centre for Australian Weather and Climate Research, a partnership between the Bureau of Meteorology and CSIRO, Melbourne, VIC, Australia*
2. *Airservices Australia, Melbourne, VIC, Australia*

## Introduction

Weather has a range of impacts on aviation operations from a safety perspective and an economic perspective. In the flight planning stage there is a need to consider fuel requirements, taking account of enroute winds and weather and the possibility that weather at the destination may cause delays or require a diversion. During the flight air traffic managers and airline flight operations groups must manage an increasingly congested airspace. Significant or hazardous weather at the departure airport, enroute or the destination airport can severely limit the number of aircraft that can operate through the airspace or into an airport. This can lead to delays, diversions and cancelled flights with a flow-on disruption that may extend around the country, last many hours and have large costs. In order that airline operations can be managed more effectively there is significant pressure to improve weather forecasting for the aviation industry.

Over the years the utility of NWP model output for the aviation weather service has increased significantly. Upper level wind and temperature forecasts are now used routinely by pilots, airlines and air traffic managers for flight planning and route optimization. Model output also provides valuable guidance to forecasters responsible for providing the aviation weather service. However many weather phenomena that have a significant impact on aviation operations are dependent on mesoscale factors that are not well represented or captured in current NWP models with resultant uncertainty in the available guidance. The implementation of high resolution modelling offers the potential for improvements in the representation of these mesoscale processes and an increase in the utility of NWP output for the aviation weather service.

In this paper we present two examples where high resolution modeling could provide increased benefit to the aviation weather service.

## Fog forecasting

A fog event at any major airport in Australia can cause major disruption with aircraft diversions, delays and cancelled flights. Although an aircraft can carry extra fuel in the event a diversion may be necessary this reduces carrying capacity and increases fuel burn. Airlines therefore rely on the terminal forecast to assess the likelihood of fog and reduce the unnecessary carriage of fuel. The accuracy in forecasting fog at a destination airport is therefore of great interest. Modern aircraft also have longer flight legs and with the additional time required for planning there is a need to improve the skill in forecasting fog at lead times of 24-30 hours.

The occurrence of fog is dependent on synoptic scale factors and also on local mesoscale factors that are often not well observed or understood. This introduces uncertainties in the forecasting of fog that can be very difficult to quantify. Forecast guidance may be available, including output from Numerical Weather Prediction (NWP) models and other techniques, but the utility of this guidance has been limited. Under these conditions the forecaster must make a categorical judgment based on observations, scientific knowledge, experience and available guidance. Although the forecaster aims to capture all fog events and at the same

time minimize false alarms the uncertainties do lead to unforecast fog events, false alarms and inconsistencies.

In recent years there has been work to develop a more structured fog forecasting process that aims to provide a more consistent forecast outcome. This includes the utilization of Bayesian Network techniques that deals with uncertainty in a more objective way (Newham et al, 2007; Weymouth et al, 2007). The result has been improved reliability in the forecast. One of the benefits of this approach is that guidance that may have some uncertainties can be integrated into this process and used more effectively.

Objective NWP guidance that is currently used includes hourly forecasts of basic weather elements from the Optimal Consensus Forecast (OCF) system (Engel, 2005) and a fuzzy logic model for Perth Airport. The fuzzy logic model uses a combination of observations and forecast weather elements from the Bureau's MESOLAPS model (Puri et al, 1998) and provides a forecast fog risk. The guidance has now been used operationally in Perth for 4 years and is an important component in the fog forecast process for Perth Airport. Figure 1 is a reliability diagram for the guidance provided by the fuzzy model and this shows an increase in the probability of fog with increasing risk category for cool season fog events although there is less skill for warm season events.

The current use of NWP model based guidance for fog forecasting is quite limited but with the implementation of high resolution models that include explicit microphysics and the possible use of single column models there is a potential for considerable improvement in the utility of guidance for fog forecasting.

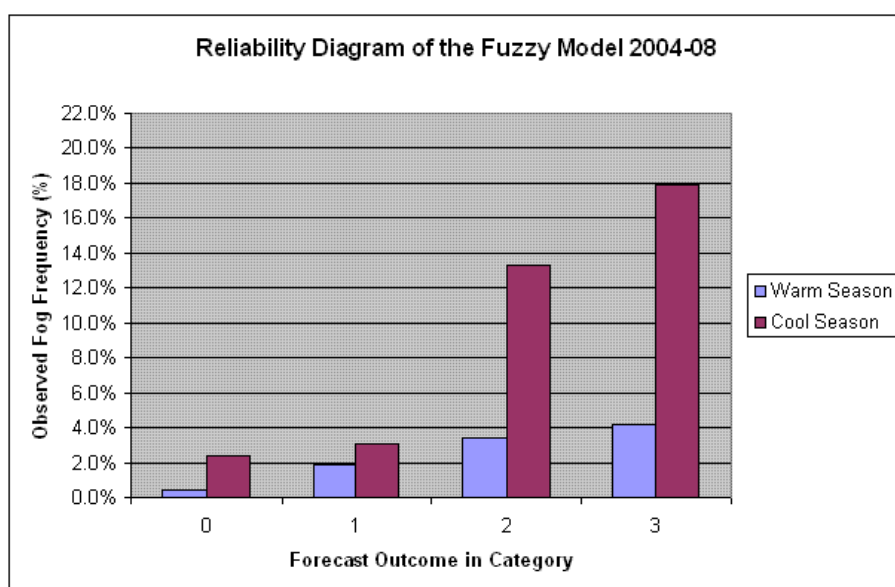


Figure 1. Reliability diagram for fuzzy logic fog forecast guidance for Perth Airport based on 00UTC MESOLAPS model run. This shows the observed frequency of fog for days when the forecast fog risk category was 0 (no risk), 1 (low), 2 (possible) or 3 (probable).

## Airport Tailored Arrivals

As aircraft with different airspeeds approach an airport from different directions and descend for a landing they are vectored by ATC to the approach for the operational runway. Typically the descent will be staged and in busy periods aircraft may be directed off-track or required to hold in order to set up aircraft in the correct sequence for the final approach. Staged descents

lead to increased fuel consumption and with increasing fuel prices, increasing traffic density and increasing concern about environmental impacts there is a demand for greater efficiency in air traffic management which includes the descent phase. Approaches where an aircraft can make a continuous descent at low power offer significant fuel savings, but to allow this in a dense traffic environment there must be confidence that aircraft meet their predicted arrival times at feeder fixes.

Airservices Australia has been conducting a trial with Tailored Arrivals at Melbourne Airport and experience has shown that estimated arrival times at way points on the descent are biased towards early arrivals. If Tailored Arrivals are to become operational there is a need to improve the accuracy of the arrival time estimates. Analysis has shown that inaccurate representation of the wind profile in the Flight Management System (FMS) is one of the primary factors contributing to this bias.

Due to design limitations the FMS only accepts 3 to 4 levels to represent wind conditions for the complete descent and currently most airlines provide their aircraft with fixed levels for the descent winds (eg FL100, FL200, FL330 and FL410), taken from the World Area Forecast System data. It has been hypothesised that a better representation of the wind profile for the descent can be provided if high resolution forecast wind data are used and there is a tailored selection of levels to load into the FMS. High resolution data from the Bureau of Meteorology's MESOLAPS model (Puri et al 1998) have been used in combination with a tool developed by Airservices Australia to determine the wind data which can be uploaded to the FMS and which most accurately represents the full wind profile for the descent.

Although the top of descent (TOD) for an approaching aircraft is typically around 100 NM from an airport, for this stage of the research the MESOLAPS data for a single point profile centred over the aerodrome reference point has been used. The Optimised Descent Winds tool developed by Airservices Australia is then used to determine the tailored levels (including height, wind direction, wind speed and temperature) that will most accurately represent the forecast wind profile for the full descent path.

## **Analysis**

The main objective in this stage of the research is to determine how well the MESOLAPS forecast and the tailored levels represent the winds observed by the aircraft. For all flights used in this analysis a meteorological report containing wind speed, wind direction and temperature was received every 2 minutes from the aircraft.

Thus for each flight the forecast descent winds provided and used by the airline, the winds from the MESOLAPS model and the ODW descent winds were each interpolated to 1000 ft increments and these were compared with the observed winds from the aircraft. This is illustrated in Fig 2 which shows the forecast and observed wind data for one arrival in the morning of 29 Jun 2008. It should be noted that the headwind and crosswind components apply to the aircraft track which varied in direction as the aircraft descended and turned to line up with the runway. Data from a total of 94 arrivals in the period 11 Apr to 23 Sep 2008 were collected and the mean absolute error for each wind component was calculated across all levels and for all flights (Fig 3).

Fig 3 shows little improvement between the descent wind data used by the airline and descent winds derived from the single point MESOLAPS data. In part this is considered to be a result of using single point MESOLAPS data only given that aircraft typically start the descent around 100 NM from the airport. Further analysis of these data will be undertaken to get a better understanding of the source of the errors. It is also expected that improvements in the resolution and accuracy of winds in the terminal area arising from NWP models will be of benefit for this application.

## Conclusions

In this study we have presented two examples where high resolution modeling data could offer benefits to the aviation weather service. There are a number of other areas where benefits could be provided including thunderstorm development, turbulence and atmospheric dispersion.

## References

- Engel C., 2005: Hourly Operational Consensus Forecasts (OCF). *BMRC Research Report* No. 115. Bureau of Meteorology Research Centre.
- Newham, P., T. Boneh, G.T. Weymouth, R. Potts, J. Bally, A. Nicholson, K. Korb, 2007: Fog forecasting at Melbourne Airport using Bayesian Networks. Proceedings of the Fourth International Conference on Fog, Fog Collection and Dew, 22-27 July, La Serena, Chile, [Pontificia Universidad Catolica de Chile], 291-294.
- Puri K., G.Dietachmayer, G.Mills, N.Davidson, R.Bowen, L.Logan and L.Leslie, 1998: The new BMRC Limited Area Prediction System, LAPS. *Australian Meteorological Magazine*, 47, 203-223.
- Weymouth, G.T., T. Boneh, P. Newham, J. Bally, R. Potts, A. Nicholson, K. Korb, 2007: Dealing with uncertainty in fog forecasting for major airports in Australia. Proceedings of the Fourth International Conference on Fog, Fog Collection and Dew. 22-27 July, La Serena, Chile, [Pontificia Universidad Catolica de Chile], 73-76.

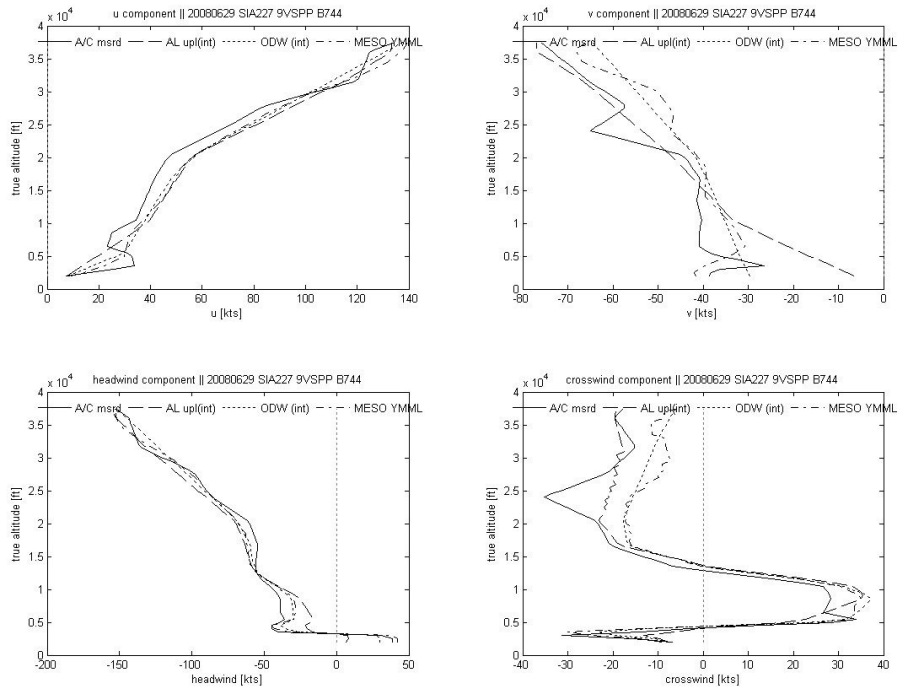


Figure 2. Forecast and observed wind data for flight of 29 Jun 2008 showing (a) u component, (b) v component, (c) headwind component and (d) crosswind component (+ve from right). Figures show winds observed by aircraft (A/C msrd), forecast winds uploaded by airline (AL upl), MESOLAPS forecast winds (MESO) and ODW winds derived from MESOLAPS data.

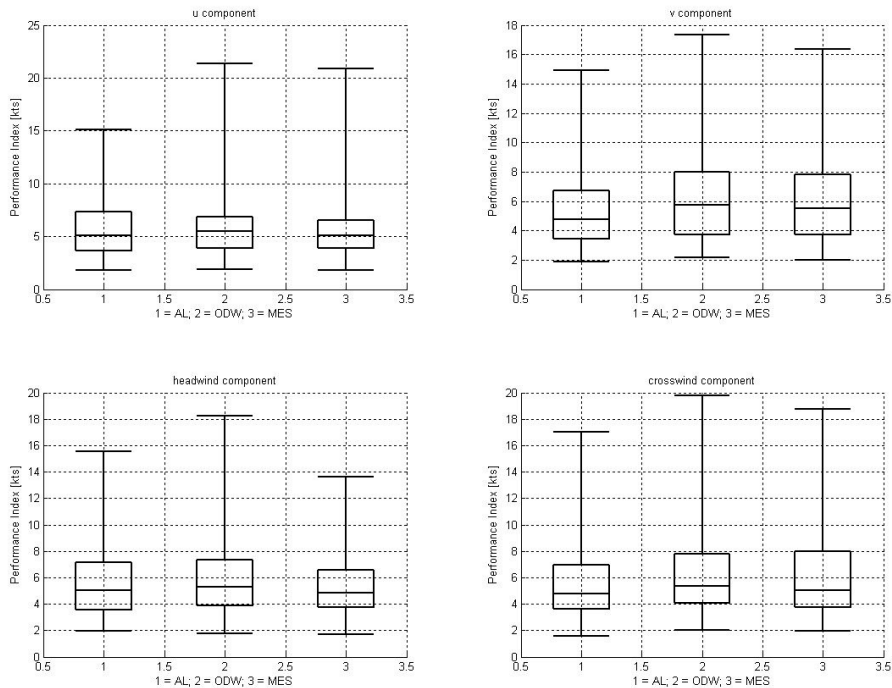


Figure 3. Box and whisker plot for mean absolute error between observed winds and forecast descent winds uploaded by airline (AL), MESOLAPS forecast winds (MES) and ODW winds across all levels and all flights.



# Modelling priorities in South Australia

John Nairn

*Supervising Meteorologist, South Australian Regional Office,  
Bureau of Meteorology*

## Rainfall prediction

Understanding rainfall regimes presented within models builds confidence over the predictability of an event. Forecasters have begun to experiment with phases of the Indian Ocean Dipole (sometimes focussing exclusively on NW Shelf SST anomalies) and phases of the Madden Julian Oscillation in order to better inform their decision as to whether warm sector rainfall or northwest rain band systems are possible. Goyder's line depicts typical precipitation distribution in the absence of NW cloud bands, or other warm process rain systems.

Interestingly, winter rainfall process can be poorly forecast in NWP. The stream shower process is frequently found in shallow layers of instability, with efficient accumulations critically linked to warm cloud depth associated with air mass trajectories over lower latitude water bodies. Longer air mass dwell time over warmer SST source regions contributes to higher shallow layer precipitable water. Experienced forecasters inferred these shallow processes to obtain estimates of shallow layer ingredients such as moisture and instability. This information is rarely evident in model guidance. High resolution layers in the boundary layer fed by high resolution SST data would be of great assistance in forecasting.

Forecasters also require greater assistance in defining the efficiency of the warm sector rainfall process. In the absence of NW cloud band rain processes, better totals accumulate on southwest land fall exposures. Typically northwest cloud bands provide marginal cropping regions with sustaining rainfall. Rainfall forecast for areas north of Goyder's line attract significant complaints when inaccurate. As noted above, any assistance in highlighting the ingredients feeding the NW cloud band process is very useful.

## Fire Weather

Land sea interactions are significant factors in wind evolution due to complex configuration of coastlines. Notably the 10 day fire event on Kangaroo Island is a good example of a complex wind event and unusual fire behaviour. To date, 5km resolution MesoLAPS has provided the best wind structure guidance to forecasters. Similar resolutions in ACCESS are required.

Greater emphasis by fire agencies placed upon early notification of approaching major fire weather days. Typically forecasters are experimenting with 4 day grass and forest fire danger charts. A climatology comparing the gradient of 850 temperature and maximum 850 temperature fields has shown early promise in identifying major events such as Ash Wednesday (1983) and Black Tuesday (Wangary 2005). More work is required to develop this climatology within the ACCESS model suite.

## Swell and Wave Forecasting

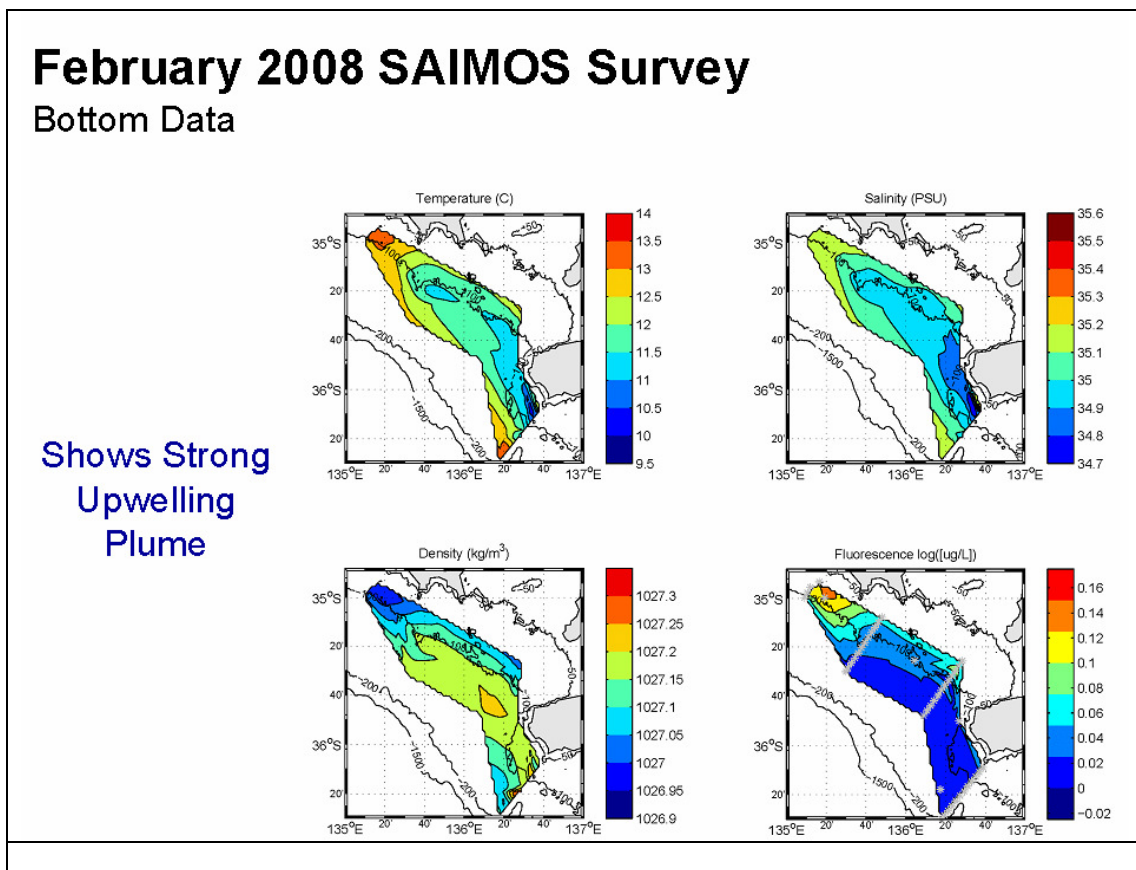
Preliminary results from SWAN (Simulating Waves Nearshore) indicates that high resolution modelling of swell and wave forecasting in the near-shore environment would be enhanced through access to real-time SWAN model runs. SWAN runs over the complex near-shore domain of the South Australian Gulf system show significant shallow water processes, including bottom friction and tidal currents, neither of which are well represented in Meso-WAM. High-resolution (1 Nm) model runs with and associated bathymetry show a complex swell propagation case with incident swell period and direction having a large effect on refraction and subsequent transmission of wave energy to the near-shore zone.

## Coastal Services

South Australian fisheries are estimated to be worth approximately \$370M per annum. Understanding the recruitment and food cycle within this marine resource is essential to its sustainable management. The nutrient cycle would appear to be heavily dependant upon periods of upwelling driven by sustained southeast wind stress. Seasonal variation in these events and resultant sea temperature variability (both surface and full column) impact fishery operations and productivity (see figures below). No less than their land counterparts, this primary industry would benefit from seasonal outlooks on factors affecting their industry.

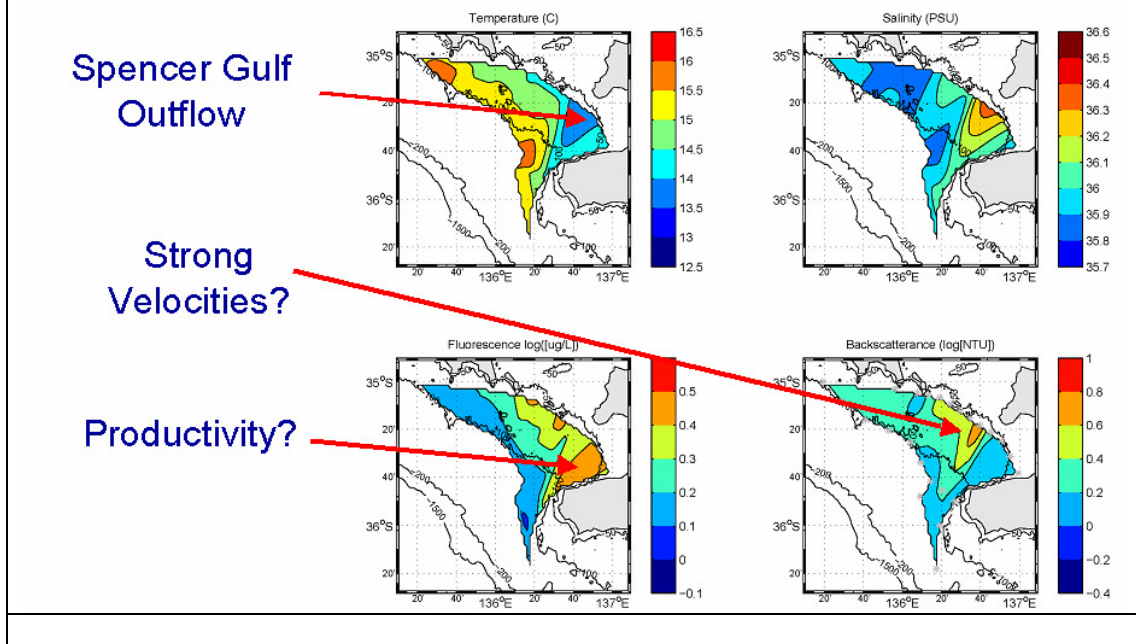
South Australian Coasts experience frequent sea level variability attributable to meteorological conditions, above and below levels determined by astronomical tides. The Southern Ocean effect experienced with the translation of cyclones regularly contributes 40 cm to sea height. It is not uncommon for an additional 60 to 70 cm to be added to sea height within Spencer Gulf and Gulf St Vincent when strong to gale force winds occur. Currently an empirical model is used quite successfully to predict storm surge at Outer Harbour (Adelaide). Irrespective of storm surge events (coincidence with highest astronomical tide), astronomical sea level predictions are meaningless when surges occur. A total sea level forecast service would meet the community's needs regardless of coincidence with high tide. Forecast sea level would be a routine service with storm surge featuring as a warning service, similar to current land service arrangements.

Marine wind forecast guidance from current NWP models is frequently found to be under strength for winds below 25 knots. Once GFE systems are introduced accuracy of these wind fields will offer significant efficiencies to the RFC allowing a reduced requirement to edit many grids along complex coastlines. Current gridded NWP model data would likely significantly increase RFC workload if GFE were introduced today.



# August 2008 SAIMOS Survey

## Bottom data



## Data Assimilation

New data types being assimilated into ACCESS bring NWP benefits to forecasters some 12 hours after the observations have become available, allowing for assimilation period, run time, transmission of NWP data into regional centres and forecaster model assessment. Clearly forecasters need to assess this data to maintain weather watch over current forecasts but to also build their expectations for potential evolution in the emerging NWP model runs. Without this facility there is immediate and real danger that critical analysis of model output will suffer.

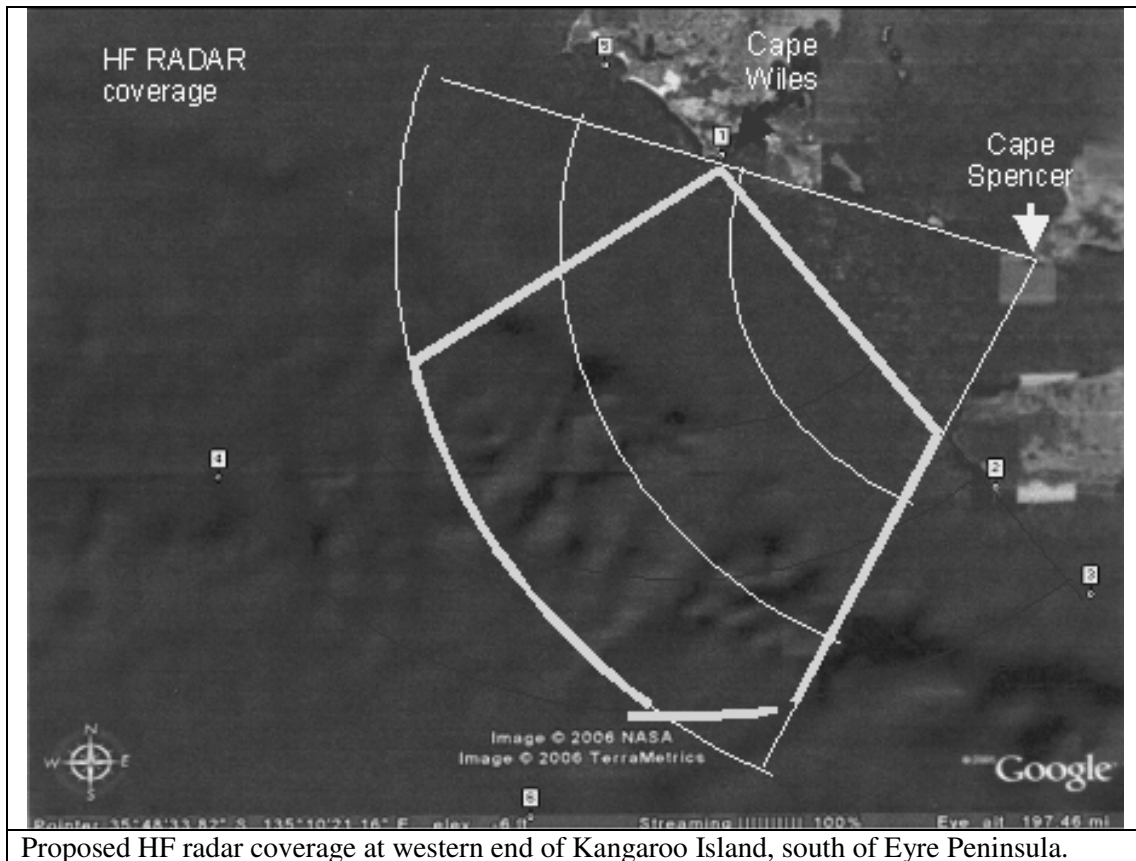
Most significant data types provide insights into vertical structure. These data are almost universally interrogated within separate platforms and applications (where developed).

To name a few of the data types:

Wind flights (rarer); Sondes; Doppler radar; AMDAR profiles (increasing); Wind Profilers (increasing); Ceilometers; Water Vapour (CGPS – coming); Satellite soundings; Cloud drift winds; Quikscat.

It is very difficult to build a case for a single bench data assessment environment in the Bureau of Meteorology. It is worth discussing the impact this may have on the effectiveness of cooperative ACCESS understanding and development, let alone the impact of not utilising this data in a more timely manner for operational forecasts.

New data types present other opportunities, such as that from HF radar scheduled for deployment by the SA Integrated Marine Observing System (SAIMOS) node at the western end of Kangaroo Island. Rapid updates of sea state and surface currents offer another source of surface wind data.



## Regional capacity to re-run ACCESS model

Forecasters quickly consume and discard NWP output. Forecasters need the capability to review model performance off line, after the events has been dealt with operationally. This invariably means that the data has been overwritten. The ability to rerun events, potentially with different model settings allows the forecasters to develop constructive criticism of model performance and a better appreciation of what the model can and cannot do. Apart from fostering better dialogue with developers there are likely to be more opportunities for joint research into interesting weather events.

## **NSW tidal anomaly – a tidal epoch review**

**B. Modra, S. Hesse, Peter Davidson and Edward Couriel**

*NSW Department of Commerce, Manly Hydraulics Laboratory, Sydney, NSW*

Oceanic circulation models can be a powerful tool for those operating in the ocean environment, however the vast majority of ocean users are concentrated at the land-sea interface - the boundary of ocean models. This boundary, perhaps the most problematic for models, is also the richest source of information from traditional data sources.

The DECC hydrographic and oceanographic network maintained by MHL is an extensive data collection program including offshore transducers, tide gauges, wave poles, waverider buoys, flood gauges and rain gauges recording for over 20 years. The reliable collection and dissemination of data has made MHL an invaluable source of coastal information for NSW coast users, and as such has an ongoing interest in developing the body of knowledge of coastal processes applicable to this region.

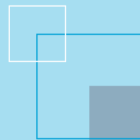
The occurrence abnormal ocean conditions cause severe damage on the densely populated NSW coast. An understanding of the frequency, duration, magnitude and causes of oceanographic and meteorological events provides the coastal, flood and estuary managers with essential information to better plan implement and provide warnings.

Strong public and political interest in climate change and coastal impact has driven further research into understanding the processes that impact the coast. Understanding the magnitude and recurrence of extreme sea levels is an essential component of risk analysis and in the development of effective risk management strategies for natural resource management and design of the built environment. These have driven a review of analytical techniques used, the knowledge about drivers for sea level variations, and a reduction in the error margins of the results.

As new users of BLUElink with a keen interest in understating the processes that affect our region, and providing our customers (the users of the NSW coastline) with an accurate interpretation of the ocean state, we see this model as having the potential to simplify the task of interpreting and forecasting oceanic conditions. Using a recent review of tidal anomalies as an example, this paper addresses the accessibility, accuracy and limitations of BLUElink model results for organisations operating on the coast, with comparison to currently employed instruments and techniques.







The Centre for Australian Weather and Climate Research is a partnership between CSIRO and the Bureau of Meteorology.